Table of Content

List of Tables

List of Figures

List of Schemes

Abbreviations

1D	One-dimensional
2D	Two-dimensional
3D	Three-dimensional
3DOM	Three-dimensionally ordered meso/macroporous carbons
acac	Acetylacetone
Al(O-i-Pr)$_3$	Aluminum isopropoxide
ALPO	Aluminophosphate
Al-ZSM-5(H)	Proton-exchanged ZSM-5 zeolite with Bronsted sites
APTES	(3-aminopropyl)triethoxysilane
APTMS	(3-aminopropyl)trimethoxysilane
ASTM	American society for testing and materials
BEA(H$^+$)	Proton-exchanged β-zeolite
BET	Brunauer-Emmett-Teller method
CBU	Composite building unit
CIT-5	California institute of technology number five
CMK-x	Carbon molecular sieves Korean advanced institute of science and technology number x
CTAB	Cetyltrimethylammonium bromide
CZA	Cu,ZnO,Al_2O_3 composite
DG	Diglycerides
DGC	Dry gel conversion techniques
DIR-MCFC	Direct internal reforming molten carbonate fuel cell
DLS	Dynamic light scattering
d_p	Pore size
DSC	Differential scanning calorimetry
DTG	Differential thermogravimetry
EDS	Energy-dispersive X-ray spectroscopy
FAME	Fatty acid methyl esters
FCC	Fluid catalytic cracking
FDU-x	Fudan University ordered mesoporous materials series
FFA	Free fatty acid
FID	Flame ionization detector
FSM	Folded Sheet Materials
FTC	Framework type code
GUM	Guide to the expression of uncertainty in measurement
HRSEM	High resolution scanning electron microscopy images
HT	Hydrothermal treatment
IMS	Isomorphous metal substitution
ITQ-x	Instituto de Tecnologıa Quımica zeolite series
IUPAC	International Union of Pure and Applied Chemistry
IZA	International Zeolite Association

KIT-6	Korea Advanced Institute of Science and Technology cubic ordered mesoporous silica
LBL	Layer-by-layer technique
M	Metal guest species (Ti, Co and Mn)
M41S	Generic term for Mobil composition of matter materials
MAPO	Metalloaluminophosphate
MAS	Magic angle spinning
MCM-x	Mobil composition of matter number x
MG	Monoglycerides
MOF	Metal-organic framework
MOR(H^+)	Proton-exchanged MOR zeolite
MSU-H	Michigan state university hexagonal material
$MTEA^+$	Methyltriethylammonium cation
MTEACl	Methyltriethylammonium chloride salt
MTEAOH	Methyltriethylammonium hydroxide
ND-1	University of Notre Dame number 1
NLDFT	Non-local density functional theory
NMR	Nuclear magnetic resonance
OMC	Ordered mesoporous carbons
OMM	Ordered mesoporous material
PBU	Primary building units
PDADMAC	Poly(diallyldimethylammonium chloride)
PDVB	Poly(divinylbenzene)
PEG	Polyethylene glycol
PMMA	Poly(methyl methacrylate)
PS	Polystyrene
PSS	Poly (styrenesulfonate, sodium salt)
RC	Relative crystallinity
RT	Room temperature
SAC	Steam-assisted technique
SAPO	Silicoaluminophosphates
SBA-x	Santa Barbara mesoporous silica series
SBU	Secondary building units
SDA	Structure-directing agent
SEM	Scanning electron microscopy
SG	Silica gel
SG20	Commercial silica gel spheres with particle diameter 20-45 μm
SG20(I)	SG20 spheres with d_p ~7nm
SG20(II)	SG20 spheres with d_p ~10 nm
SG3	Commercial silica gel spheres 3μm
Si/Al ratio	Silicon to aluminum ratio in zeolite framework
Si-BEA	Pure silica β-zeolite
TBAOH	Tetrabutylammonium hydroxide

TEA^+	Tetraethylammonium
TEABr	Tetraethylammonium bromide salt
TEAOH	Tetraethylammonium hydroxide
TEM	Transmission electron microscopy
TEOS	Tetraethyl orthosilicate
TGA	Thermogravimetric analysis
TG	Triglycerides
TMAOH	Tetramethylammonium hydroxide
TMB	Trimethylbenzene
TNBT	Titanium (IV) butoxide
TPA^+	Tetrapropylammonium cation
TPAOH	Tetrapropylammonium hydroxide
TS-1	Titanium silicalite-1
UTD-1	University of Texas at Dallas number one
VPI-5	Virginia Polytechnic Institute number five
VPT	Vapor phase transport
XPS	X-ray photoelectron spectroscopy
XRD	X-ray diffraction
ZSM-5(H^+)	Proton-exchanged ZSM-5 zeolite with Bronsted sites

Acknowledgments

My sincerest thanks and appreciation go to my advisors Prof. Freddy Kleitz, Prof. Serge Kaliaguine and Dr. Pablo M. Arnal.

I would like to express my deep appreciation and gratitude to my advisor, Prof. Kleitz, to whom I am indebted for granting me an opportunity to work in his group on an area I have been passionate about and for providing me with patient guidance, mentorship, unstinting support and freedom throughout my Ph.D. study.

I wish to express my gratitude to Prof. Kaliaguine who has been a great source of wisdom and encouragement for me. He was always willing to spend time discussing my research and helping me learn. I am very fortunate to have had the opportunity to work with him.

I would like to express my sincere gratitude to Dr. Arnal for his time, support and feedback on various aspects of this project.

I would also like to express my gratitude to my Ph.D. committee members, Prof. Kenneth J. Balkus, Prof. Trong-On Do and Dr. François Béland, for their time and efforts to go over my research work.

I would like to acknowledge the great assistance of Dr. Kyoungsoo Kim from Institute for Basic Science (IBS), South Korea for providing the HRSEM images.

I would like to thank professors, administrative staff, research professionals and technicians of the Department of Chemical Engineering and Department of Chemistry, Université Laval, for the kind help I received during my Ph.D. work. In particular, I would like to express my sincere gratitude to Mr. Pierre Audet, Mr. André Ferland, and Mr. Richard Janvier for their great assistance and training.

None of this work would have been possible without the support and help of the group members, both past and present. I would like to thank all my friends and colleagues at Laval University, especially, Dr. Jean-Luc Bridot, Meryem Bouchoucha, Karim Khadhraoui, Maëla Choime, Solange Schneider, Dr. Pablo Lebeld, Dr. Cao Thang-Dinh, Louis Lefrancois Perreault, Xu Wan, Thanh-Binh Nguyen, Fanny Silencieux, François Chalifour and Dr. John Dupont. It has been a real pleasure working with you all.

In particular, I wish to thank Dr. Hoang Yen, Dr. Justyna Florek, Dr. Remy Guillet-Nicolas, Dr. Simon Giret, Dr. Mahesh Nair, Estelle Juere and Maria Zakharova for their valuable discussion, support and friendship over the years.

Finally, I would like to thank my family for all their never-ending spiritual support and encouragement. I would like to thank my wife, the best friend of mine, Forough, for her endless support and innumerable sacrifices.

Foreword

This study aims at the design of more efficient zeolitic materials by either finding better-controlled conditions for traditional crystallization processes or designing and synthesizing high-quality structured zeolitic composites. In the first part, ZSM-12 was chosen as one of the most interesting large-pore 1D zeolites. Compared to other zeolites, such as ZSM-5, ZSM-12 has been scarcely studied. Considering the original verified synthesis method of ZSM-12 (published in the late 80s), most of the subsequent studies did not achieve significant improvements in terms of synthesis conditions (for instance, crystallization under less harsh conditions), the cost of the synthesis (shorter crystallization process, less-expensive SDAs, etc.) and controlling material properties, such as crystal size and shape, etc. On the other hand, using ZSM-12 has unfolded its versatility and efficacy in many applications. This has encouraged us to investigate various synthesis conditions to gain more insights into ZSM-12 crystallization behavior and hopefully attain better control of parameters that determine its performance in real practical applications, such as crystal morphology. The results of this study, recently published in the journal Microporous and Mesoporous Materials, are reported in Chapter two of the thesis.

Zeolitic core@shell materials have become popular in the past decade and used for many applications. In the second part of this study, the viability of complete encapsulation of mesoporous silica spheres using a microporous zeolitic shell was studied. Owing to exceptional properties of mesoporous silica spheres, such as high surface area and pore volume, synthesizing such a structure and the ability to tune its properties such as shell thickness, uniformity, activity, etc., will open new pathways in the field of catalysis and adsorption. Of course, this is not an easy task and it faces many problems including chemical incompatibilities with the zeolite crystallization conditions and pore network communication which have been brought up in the literature for similar materials (zeolite@zeolite). To address these issues, a thorough study of different synthesis parameters was performed and the results are reported in Chapters three and four of this thesis.

This dissertation is composed of five chapters. The first chapter starts with a brief introduction about classical zeolitic materials and describes the challenges which limit their application, especially the ongoing struggles with mass-transfer issues. This section is followed by reviewing the current state-of-the-art approaches which target those issues.

Chapters two, three and four of this dissertation report the experimental results, interpretations and discussions, in the form of three scientific articles of which the candidate is the primary author. These publications are outlined below:

Chapter 2: “Synergy between structure direction and alkalinity toward fast crystallization, controlled morphology and high phase purity of ZSM-12 zeolite”, Nima Masoumifard, Serge Kaliaguine and Freddy Kleitz, published in Microporous and Mesoporous Materials, 227 (2016) 258-271.

Chapter 3: “Synthesis of Microporous/Mesoporous Core-Shell Materials with Crystalline Zeolitic Shell and Supported Metal Oxide Silica Core”, Nima Masoumifard, Kyoungsoo Kim, Serge Kaliaguine, Pablo Arnal and Freddy Kleitz, published in CrystEngComm 18 (2016) 4452-4464.

Chapter 4: “Zeolitic Core@Shell Adsorbents for the Selective Removal of Free Glycerol from Crude Biodiesel”, Nima Masoumifard, Pablo Arnal, Serge Kaliaguine and Freddy Kleitz, published in ChemSusChem 8 (12) (2015) 2093-2105.

In these scientific papers, the candidate conducted the experimental works under the supervision of Prof. Freddy Kleitz, Prof. Serge Kaliaguine and Dr. Pablo Arnal. The high-resolution SEM images, presented in Chapter three, were taken by Dr. Kyoungsoo Kim from Institute for Basic Science (IBS), South Korea, who was also the co-author of this paper. The candidate who is the first author of the above papers has performed all of the experiments, collected the data and prepared the first drafts of all manuscripts. All the authors revised the manuscripts prior to publication.

Finally, chapter five completes this dissertation by providing overall conclusions along with some recommendations for future work.

Chapter 1- State-of-the-art

1.1 Introduction

The term "*engineered zeolitic materials*" refers to a class of material with rationally designed pore system and active site distribution. They are primarily made of crystalline microporous zeolites as the main building blocks which can be accompanied by other secondary components to form composite materials. The first section of the current chapter starts with providing general information about zeolite structure, properties and conventional synthesis methods, followed by discussing the motivating rationale behind the growing demand for structural alteration of the classical zeolitic materials. The main techniques that are currently available for such modifications are briefly reviewed in Section 1.3. Core@shell composites as one of the pathways toward creating a new generation of highly versatile and efficient engineered zeolitic substances are introduced in Section 1.4. Sections 1.5 and 1.6 summarize the synthesis approaches, developed so far, for making zeolitic core@shell and its analogues, yolk-shell and hollow materials. Section 1.7 reviews the findings around the performance of these materials, obtained from conducting laboratory-scale experiments.

1.2 Zeolites as Ordered Microporous Materials

The presence of the pores as tiny passages within a solid body has created a special class of substances with extraordinary characteristics, the so-called porous materials. The internal pore dimension (d_p) has initially been used, by IUPAC[1] organization, as a simple criterion to categorize all porous materials into three groups: microporous (d_p < 2 nm), mesoporous (d_p ~ 2-50 nm) and macroporous (d_p > 50 nm) materials [1, 2]. The term nanoporous has also been introduced to describe the materials which have pores in nanometer size range (d_p < 100 nm), however, it is mainly referring to microporous and mesoporous classes together (d_p < 50 nm).

[1]- International Union of Pure and Applied Chemistry.

Microporous materials, also known as molecular sieves, are the most important members of porous materials owing to their outstanding property of having size-discrimination capability at the molecular level. Despite the existence of various types of microporous materials, such as carbon-based materials, MOFs[1] and polymers, zeolites are still the most well-known and widely-used microporous solids. Zeolites are low-density, crystalline aluminosilicates with an ordered microporous structure, i.e., an extremely narrow and uniform pore size distribution [3-6].

1.2.1 Zeolite History

In 1756, A.F. Cronstedt, a Swedish mineralogist, discovered a special naturally-occurring crystalline aluminosilicate and described it as "*Zeolite*" since it released a significant amount of tiny bubbles upon heating [4]. The word "*Zeolite*" is actually a compound noun, made up of two separate ancient Greek words: "*zeo*" meaning "to boil" and "*lithos*" meaning "a stone". After then, various types of naturally occurring zeolites (around 50 so far) were found in rock, until about 200 years later in the 1940s, the first synthetic zeolite (ZK-5 (KFI)) was successfully made in hydrothermal conditions (high pressure and temperature) by R. M. Barrer [7]. Shortly after two industrially important synthetic zeolites, i.e., zeolite A and X, were synthesized by R. Milton [8, 9]. After these pioneering works, the field of zeolite science truly started and grew massively by finding several new structures every year. Over the last 70 years, over 200 synthetic zeolites and their isomorphic relatives, i.e., zeotypes[2], such as aluminophosphates (ALPOs), silicoaluminophosphates (SAPOs) and other metalloaluminophosphate (MAPO), have been identified as a separate group of minerals, synthesized and used on large-scale in many industrial processes [10].

However, the term zeolite was originally used for crystalline aluminosilicate materials, it has evolved and broadened to cover all newly-discovered structures and compositions including non-aluminosilicate zeotypes [10]. Today, the term "**zeolitic material"** is also used to denote

---

[1]- Metal Organic Framework

[2]- The term zeotype is widely used to name molecular sieves that show many structural similarities to typical aluminosilicate zeolites, but having elements other than Si and Al as the framework building units.

all classical zeolites, zeotypes and new compositions and structures [11]. Therefore, both zeolite and zeolitic materials will be used interchangeably here throughout the text.

1.2.2 Zeolite Structure

Zeolites are basically made of TO_4 tetrahedra, i.e., the primary building units (PBUs) in which the T atom, including Si, Al or some other elements like P, V, Ti, Ga, Ge, B, is covalently bonded to four oxygen atoms, e.g., $[SiO_4]^{4-}$ and $[AlO_4]^{5-}$ tetrahedra. These TO_4 building units are then linked together via covalent bonding to form the secondary building units (SBUs) and composite building units (CBUs). In contrast to CBUs, the SBU units which contain up to 16 T atoms, were found by assuming that the entire framework is made of one type of SBU only in a repetitive manner [12]. There are presently 23 observed SBUs as reported in [12, 13] (Figure 1.1). It is also possible to imagine that a single zeolitic framework is constructed from the attachment of various more complex units together, the CBUs, such as cages, chains, cavities and channels [12, 13]. Rings can be considered as the simplest building units (SBU or CBU), constructed from *n* TO_4 units where *n* is usually equal to 4, 5, 6, 8, 10 and 12 [14], forming transport windows of molecular dimensions with a maximum opening of about 0.7 nm in aluminosilicate zeolite. In zeotypes, however, larger windows can be formed, for instance, an extra-large window of thirty TO_4 tetrahedra (30-ring windows) has recently been reported for germanosilicate zeolite (ITQ-37[1]) [15] (Figure 1.1).

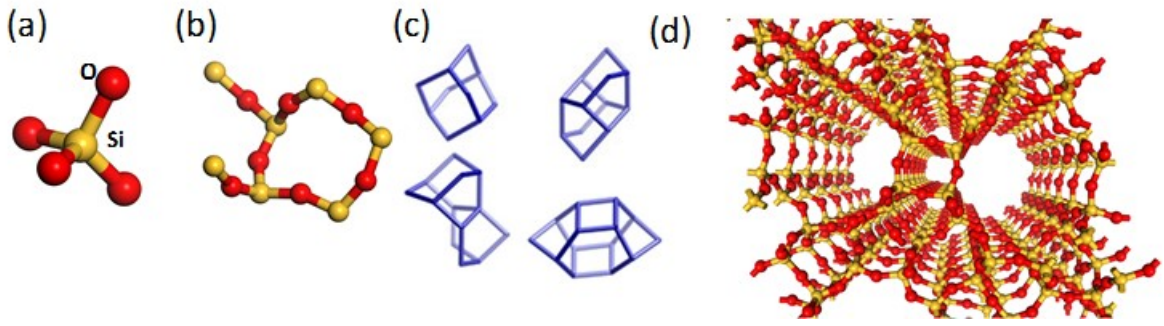

Figure 1.1- (a) PBU, (b) SBU, and (c) CBUs which build (d) the framework of ZSM-12.

[1]- ITQ-x: Instituto de Tecnologıa Quımica zeolite series

1.2.3 Zeolite Classification

Characteristic crystallographic data of zeolitic materials were initially used to identify the distinct types of the frameworks which were later documented by the structure commission of the International Zeolite Association (IZA) and published in “Atlas of Zeolite Framework Types” database [12] or on the regularly-updated IZA website [16]. A three letter Framework Type Code (FTC) is assigned by IZA to each unique identified zeolite topology, which has currently reached to over 230 framework types of zeolites and zeotypes. It should be noted that FTC just refers to the framework type, i.e., different zeolitic materials with various compositions can be called by the same code if they share a framework type.

The orderly perforated structure of the zeolites can also be categorized using other properties such as dimensionality of the micropore network, the size of the micropore opening (the window) and chemical compositions, as briefly discussed below.

Depending on micropore interconnectivity and dimensions, zeolites can be divided into three groups including one-, two-, or three-dimensional (1D, 2D and 3D). The micropore opening (size and topology) is directly related to the number of TO_4 units on the ring which forms the window. In this regard, aluminosilicate zeolites have been classified into small pore zeolites with eight-membered oxygen ring pore window (8-ring), medium pore zeolites with ten-membered oxygen ring pore window (10-ring) and large pore aluminosilicates with twelve-membered-ring pore window (12-ring). There is also an extra-large pore zeolite category with TO_4 units above 12 for phosphates and germanosilicates, e.g., ND-1 with 24 [17], ITQ-43 with 28 [18] and ITQ-37 with 30 elements [15] are the highest reported so far. This number of TO_4-elements on the ring leads to zeolites and zeotypes with various pore sizes, for instance, aluminosilicates with pores between 0.3 and 0.7 nm, and germanosilicates up to 2 nm [18]. In general, micropores are divided into two main groups: ultramicropores which are smaller than about 0.7 nm and supermicropores with the size range between 0.7 and 2 nm [2]. Regarding the pore sizes in each direction of a multidimensional zeolite, zeolitic materials were also classified into uni-modal micropore system such as zeolite Y and ZSM-5 and multi-modal micropore system such as MCM-22 [19].

The chemical composition of a zeolite is also a determinant parameter and can affect various zeolite properties. The chemical composition of a specific framework type can be altered by either changing the ratio between major building elements (Si, Al or P) within a limited range

or substituting those main elements with other (M^{III} and M^{IV}) such as B, Ti, V, Cr, Mn, Fe, Zn, Ga, Ge, and Zr, etc., [11, 20] via isomorphous substitution. These compositional variations have also been used to classify zeolitic materials into different groups, for instance, the Si/Al ratio in low silica zeolites is Si/Al= 1.0-1.5, in intermediate silica zeolites is Si/Al= 2.0-5.0 and in high silica ratio zeolites is Si/Al> 10 - which also includes all-silica zeolite with Si/Al> 100 [10, 21].

1.2.4 Zeolite Properties

As mentioned earlier, the chemical composition (T elements involved) and the way TO_4 tetrahedral units are linked to each other could provide various frameworks with different properties. According to the requirements imposed by various applications, these intrinsic properties, briefly discussed below, can be uniquely tuned, an opportunity that makes zeolites special compared to other inorganic oxide materials.

- *High internal surface area and pore volume:* All great properties of zeolitic materials are directly related to their porous structure, providing high surface area and voids which can host various type of species.

- *Shape selectivity characteristic*: Uniformly-sized and distributed micropores which are comparable to the size of a small molecule create a size/shape-selective adsorbent or catalyst. The molecular shape selectivity can have a significant influence on a reaction through various mechanisms such reactant, product or transition-state selectivity [22]. In addition, the existence of pore mouth and key-lock catalysis on selective distribution of the products have also been demonstrated [23]. In this case, reactants are more adsorbed on the pore mouth rather than diffusing into the zeolite bulk. Multidimensional microporous zeolite with various sizes in each direction (known as multi-modal micropore systems or simply multipore zeolite) could also provide a very selective network by favoring a guided diffusion of reactants and products through different channel systems depending on their size differences, known as “molecular traffic control” mechanism [24]. This property can lead to more advanced shape-selectivity by combining molecular traffic control feature with direction-dependent active site distribution within the pores, cavities and side pockets of a

multipore zeolite [24]. More details about multipore zeolites and their catalytic applications can be found elsewhere [19, 24].

- *Single-file diffusion*: Although multi-dimensional zeolites bring higher surface area and better accessibility to active sites, 1D zeolites can provide better trapping ability of molecules when strong adsorption is not feasible, i.e., efficient trapping of small molecules instead of adsorption and releasing them when it is needed [25].

- *Ion-exchange capacity*: The framework charge imbalance, e.g., caused by aluminum atoms as T-element in a zeolite, needs to be neutralized by a stoichiometric amount of extra-framework charge compensating counter-ions, such as H^+, Li^+, Na^+, K^+, Rb^+, Cs^+, Be^{2+}, Mg^{2+} and Ca^{2+} or transition metal elements. These cations are mobile and can be exchanged with another cation of interest from a solution in a reversible manner [26].

- *Internal acidity*: Exchanging the metal cation with proton (H^+) can create strong Bronsted acidic centers on the zeolite surface, especially in Si-rich aluminosilicates. Another interesting feature of these zeolitic acid sites is their even distribution throughout the surface of a zeolite. Lewis acid sites can also be generated within the porous structure of a zeolitic material via ion-exchange or isomorphic substitution of several isolated metal centers such as titanium, tin or zirconium [24].

- *Tunable chemical composition:* Tuning of the chemical composition of a zeolitic material directly controls its properties. For instance, an Al-rich zeolite provides huge exchange capacity which makes it an ideal separator of cations and polar impurities from a solution. A Si-rich zeolite, on the other side, if neutralized by a proton, is more favorable acid catalysts because of their higher thermal stability (required for high-temperature reactions and regeneration processes) and higher affinity toward adsorbing less polar molecules. In addition, optimum dispersion of acid sites with higher strength is ensured by their low Al content of the framework [27].

- *Isomorphous metal substitution (IMS)*: IMS refers to a situation that one of the major elements Si, Al and P in a zeolitic framework is replaced by a wide variety of heteroatoms such as Be, B, Ti, V, Cr, Mn, Fe, Co, Zn, Ga, Ge and Zr [11]. The presence of these elements can drastically change zeolite properties [28]. Moreover, this heteroatom substitution has

constantly helped to discover new zeolitic frameworks such as germanates and MAPOs with no zeolite or ALPO analogues [29].

- *High chemical, mechanical, thermal and hydrothermal stability*.

- *Easy regeneration:* Depending on the deactivation source, they can be easily regenerated with the minimum damage to the zeolitic structure *via* heat treatment (calcination), ion-exchange or pressure swing.

- *Supporting other guest species to make bi-functional catalysts*

- *Biocompatibility and low toxicity*

Due to all these exclusive properties, these materials have been massively used for industrial applications, e.g., adsorption, purification, separation, catalysis and ion-exchange [10, 30-33] and there are continuous efforts for improving the existing zeolitic materials and also finding new frameworks.

1.2.5 Zeolite Synthesis

The first step usually involves the preparation of a mixture consisting of all reagents, properly blended and conditioned toward the formation of an amorphous gel phase and/or precursor mixture. Silicates and aluminates species, a mineralizer (OH^- /F^-) and organic/inorganic structure-directing agents (SDA) are the main constituents of this gel which is homogeneously mixed together using mainly water as the solvent. Depending on the type of zeolite and gel composition, an aging step under specific conditions, mainly ambient, might be necessary before the final crystallization period starts.

Next step is the conversion of the as-prepared gel into zeolitic materials which mostly occurs by aging the mixture inside tightly closed (sealed) vessels, frequently at elevated temperatures and autogenous pressures. Depending on the chosen synthesis method, i.e., conventional hydrothermal treatment or dry gel conversion techniques (DGC), solvents can be partially or completely removed from the gel prior to high-temperature crystallization reaction. In DGC technique, a completely dried gel is placed on a support inside an

autoclave containing liquid phase in a way that direct mixing of two phase is avoided. The liquid phase in the bottom of the container can contain either an aqueous mixture of organic SDAs which can be later volatilized to reach the dried zeolite gel and promote zeolite formation, known as vapor phase transport (VPT) technique or, in case of non-volatile organic SDAs, simply pure water to produce required steam for zeolitization[1] of the dry gel, known as steam-assisted technique (SAC). In general, this technique has some beneficial aspect compared to conventional hydrothermal treatment including less SDA usage, higher yield and achieving higher metal incorporation into the framework (lower Si/Al). Moreover, it is found to be extremely helpful for proper implementation of the techniques proposed for hierarchical zeolite synthesis (discussed later in Section 1.3). This method has some disadvantages including non-uniform crystallization within the gel leading to amorphous impurities in the final product as well as scale-up issues [27]. The former is caused by a decrease in the mobility and interaction of the precursor species as a direct consequence of removing the solvent.

Finally, after washing and recovery of the product, a high-temperature calcination is mainly required to remove the organic templates from the pores, if any used. The calcination conditions (temperature and atmosphere) can also affect the properties of the product. In contrast to mesoporous silica (e.g., MCM-41 [34]), chemical extraction of the organic template is not viable unless some especially-designed organic template is used [35].

With slight modifications at different steps of the synthesis procedure, it is also possible to synthesize transition metal-containing (-exchanged, -substituted, and/or -impregnated) zeolites. A recent review by Li *et al.* [29] summarizes new synthesis strategies proposed over the last decade resulting in the discovery of new zeolitic materials.

1.2.5.1 Formation Mechanism and Key Synthesis Elements

Zeolite synthesis protocols were essentially discovered and optimized through trial and error approach. Therefore, understanding the mechanism and key elements can enormously enlighten the path toward rational design of new structures and optimization of the existing

[1]- The term usually used to describe the direct conversion of an amorphous solid phase to crystalline zeolite.

methods. There are ongoing efforts to gain more insights into the mechanism behind the crystallization of the zeolites from the gel which is still a matter of controversy. In general, zeolite crystals form during the crystallization process through various sequential steps including the pre-nucleation step, primary nucleation, the growth of the nuclei to larger sizes and finally the growth of the crystals which can sometimes be accompanied by simultaneous secondary nucleation. The driving force behind all these processes are related to supersaturation phenomenon, also occurring during the pre-nucleation step, a condition which is very difficult to study. In general, the pre-nucleation step includes complete/partial dissolution/hydrolysis of Si and Al sources followed by condensation of amorphous oligomeric silicate and aluminate species, also known as zeolite precursors and finally reaching a so-called supersaturation condition. Primary nucleation as a second step can occur either homogeneously within the solution gel and grow progressively by nourishing from dissolved species from liquid phase or heterogeneously within solid-like materials present in the gel and grow by solid-solid transformation. In the latter case, the gel can be entirely in the solid phase, i.e., an amorphous hydrogel. The last step is the crystal growth which small crystalline nuclei starts to rapidly grow by absorbing available Si-containing units from the gel through a layer-by-layer mechanism. Secondary nucleation may occur at this stage by these crystals. Most of the studies around zeolite formation mechanism were done for simple reaction system, however, the mechanisms of nucleation and crystal growth processes are generally governed by many factors and might be different from one framework type or even one synthesis condition of a specific type of zeolite to another. Such comprehensive understanding of the zeolite formation processes is something yet to be accomplished. More information about zeolite crystallization mechanisms can be found elsewhere [6, 36].

The major factors that influence the formation of zeolites are crystallization temperature, time, reagent sources, impurities and concentrations, seeding, SDAs and alkalinity. SDAs are highly vital for zeolite formation. Various chemicals in synthesis mixture can provide such an effect alone or in a cooperative manner [37]. They can be classified as one of the following groups: *charged molecules mainly cations (Organocations)*: they are also known as organic templates, primarily alkylammonium cations. They were first introduced by Barrer and Denny in 1961 [38]. Using this type of material was one of the key discoveries in the field of zeolite synthesis, leading to new synthesis routes, new frameworks and enhancing original properties such as widening the range of Si/Al ratio possible. Regarding their size

compared to pore dimensions, they can be considered as templates and pore-filling agents in some cases as well. They are the most popular SDAs. *Inorganic cations*, e.g., alkali and alkaline earth metal cations, which are mainly introduced to synthesis mixture in the forms of basic compounds to adjust the pH, can have significant effects on nucleation and crystal growth. In addition to this cationic species, *neutral molecules* such as water, amines, etc., and ionic pairs such as salts can also play templating roles by stabilizing a specific type of zeolitic framework. A list of newly developed pre-synthesized SDAs can be found in a recent review [29]. Other than its complex role in stabilizing the zeolitic structure and interactions with cationic SDAs (hydrating effect), water is also serving as the most popular solvent used in zeolite synthesis. Another key element is the alkalinity (OH^-) which affects the crystallization process in many ways. Under the influence of this parameter, the amorphous part of the gel is depolymerized to form oligomeric species in the solution. These solubilized species can provide supersaturation condition required for nucleation and crystal growth. It also plays a mineralizing role toward proper and faster condensation of aluminosilicate species into a more stable solid phase, the nuclei. These hydroxyl ions can also improve the crystal growth rates. The crystal phase, composition (Si/Al), morphology and crystallization yield are also other parameters which can be affected by alkalinity. Incorporation of other elements, especially aluminum can also have a great effect, not only on zeolite formation but also on the products properties such as morphology and physicochemical properties. Therefore, proper Al concentration should be adjusted within the synthesis gel, which requires many trials since the Si/Al ratio in the gel and the final product may differ. The reason is that Al incorporation might be controlled by some other factors such as alkalinity, counter ion concentration, type of framework, etc., rather than being proportional to the Al concentration.

For certain types of zeolites, it was shown that addition of already formed crystals (seed) with similar framework structures could speed up the crystallization process via either secondary nucleation phenomenon or eliminating the nucleation step by promoting faster (inter)growth of the seeds. Due to the structure-directing effect of the seeds in some cases, sometimes this technique, partially or completely, eliminates the need for organic SDAs [39]. In this way, environmental concerns in contact with the usage of organic SDAs can be avoided. More details about green routes of zeolite synthesis can be found in reference [40].

1.2.6 The Drawbacks of Classical Zeolites- Problem Description

Despite the extensive use of zeolitic materials in industry, their performances are negatively affected by the tiny microporous channel system. This is a highly restricting factor in zeolite application and can alter the catalytic activity of the zeolite by lowering the overall reaction rate and the accessibility of active sites, promoting undesirable side reactions and faster catalyst deactivation (coke formation and pore blockage), even if the molecules involved in the process are small enough to enter the micropores. This kind of hindered traffic is much more severe in zeolite with smaller pore size and lower dimensionalities. In addition, although size selectivity plays an important role in some applications, the classical zeolitic materials cannot be used in reaction systems which contain bulky reactants with molecular sizes larger than that of micropores [41, 42].

Owing to the importance of zeolitic materials, there have been a continuous endeavor in the field of zeolites, devoted to enhancing their performances via modifying various aspects of them. In the next sections, solutions which primarily target the mass transfer issue of the classical zeolites will be discussed. Other modification techniques can be found in the following references [20, 43, 44].

1.3 Proposed Solutions

In an optimal scenario, the proposed solutions should efficiently address the limitations and shortcomings of available classical zeolites while preserving all their advantages.

Let us first focus on the main issues, i.e., overall slow mass transport and lack of active-site accessibility for bulkier molecules in classical zeolites. There are two main solutions for this problem, derived from two distinct concepts, first, synthesis of new materials with expanded pore sizes and second, decreasing the micropore diffusion length. The latter is possible through two main approaches, crystal size reduction toward the nanoscale and creating a secondary pore system at meso/macro scale within zeolitic crystals.

The current section summarizes the main efforts toward achieving a new generation of porous materials over the last few years.

1.3.1 Large Pore Materials - Pros and Cons

Materials with larger pores than classical zeolites, which have so many intrinsic properties in common, i.e., ultra-large pore zeolitic materials and ordered mesoporous materials (OMMs), would not only avoid diffusion difficulties but also permit the application of these new classes as catalysts for reactions involving bulkier molecules [24, 32, 45-48].

Although the first synthesis of silica-based OMMs was reported back in the early 1970s [49], their remarkable properties have not been disclosed until beginning of the 1990s after discovery of FSM[1] type OMM by Japanese scientists in 1990 [50] and M41S family of OMMs by scientists in Mobil Research and Development Corporation [51, 52]. Introducing these silica-based OMMs, particularly MCM-41[2] with hexagonally arranged uniform mesopores has become a turning point in the field of OMMs syntheses. Supramolecular arrangements, formed by using cationic surfactants, i.e., a quaternary ammonium with different alkyl chain length, in MCM-41 synthesis permitted adjusting the pore size in a range of 2 to 10 nm. Subsequently, the concept of using organic templates as mesoporogen has been widely adapted to generate various ordered porous structures consisting of oxide and non-oxide materials [53, 54]. One of the outcomes in the area of ordered mesoporous silica materials was the introduction of several new classes of OMMs with various morphologies and symmetries such as MCM-48, MSU-H[3], KIT-6[4], SBA-x[5], FDU-x[6], etc. [45, 46, 53]. The majority of mesoporous materials are synthesized by a sol-gel process in the presence of ionic and non-ionic (neutral) amphiphilic organic templates. A detailed description of such a synthesis toward the formation of OMMs which basically falls into one of the two large synthesis pathways; i.e., the liquid-crystal templating and cooperative self-assembly processes, and the characterization of the final OMMs are not the topic of the present report and can be found elsewhere [53].

These surfactant-mediated methods have been thoroughly verified for the synthesis of silica-based OMMs. Although it is viable to extend these techniques for synthesizing non-siliceous OMMs [55], it is considered as a challenging route for some materials, especially the one

1- Folded Sheet Materials
2- Mobile Composition Matter No. 41
3- Michigan State University Hexagonal material
4- Korea Advanced Institute of Science and Technology cubic ordered mesoporous silica
5- Santa Barbara mesoporous silica series
6- Fudan University ordered mesoporous materials series

with crystalline atomic structures. Huge interest toward synthesizing OMMs from other materials than silica such as carbon, polymers, metals or metal oxides eventually led to the development of a facile technique, i.e., the hard templating (*nanocasting*). This method was realized by the use of the ordered network of silica as a hard template. The whole process is described in the pioneering work, initiated by Ryoo's group in 1999 [56] who synthesized ordered mesoporous carbons (OMC), i.e., CMK-x[1] materials, using this technique. A detailed description of the hard templating technique and related new findings can be found in [48, 54, 57, 58].

Regardless of the preparation method, silica-based OMMs have many advantages including a large and multi-dimensional pore system, fairly narrow pore size distribution, a tunable pore size in the range of 1.5-20 nm, high specific surface area and pore volume (on the order of 1000 m^2/g and 1 cm^3/g) and abundance of silanol surface groups. In contrast to classical zeolites, these pore-related properties facilitate the anchoring of wide variety of functional groups to the pore surfaces which not only allows to mimic the exact functionalities of zeolites but also opens a window toward a variety of new functionalities [53, 59]. The natural properties of these attached groups, mainly organofunctional groups, can be readily transferred to the surface of porous materials, yielding organic-inorganic hybrid mesoporous materials with superior activity in different applications [32, 45, 46, 48].

The majority of OMMs are basically amorphous which attributes to lower stability and acidity compared to the classical zeolites. Although chemical modifications of the OMMs' surface via grafting of functional groups could initially succeed in mimicking the active sites in classical zeolites, the limited hydrothermal/thermal stabilities of the amorphous walls of OMMs and grafted chemical groups are still challenging for their application as heterogeneous catalysts in many reaction systems [60].

The crystalline nature of zeolite framework characterizes its high stability and catalytic activity. In contrast to OMMs, this feature has been preserved through making ultra-large pore zeolites with a pore width of up to 2 nm. The pores of these materials are built from rings containing more than 12 T-atoms. Typically, common T-atoms, Si and Al, are not used to synthesize such a large pore crystalline structure, mainly due to the restriction imposed by low Si-O-Si bond angles. The discovery of ALPOs and new synthesis techniques such

[1]- Carbon Molecular Sieves Korean Advanced Institute of Science and Technology No. x

as solvothermal/ionothermal routes, pre-designed complex SDAs, various heteroatom substitutions, topotactical transformations and charge density mismatch allowed the creation of many new frameworks including some with ultra-large pores [29]. This class of materials was synthesized before silica-based OMM were found in 1992, starting with VPI-5 aluminophosphate with 18- rings that possesses pores as large as 1.2 nm [61]. Nonphosphate-based large pore crystalline materials were later synthesized by developing complex molecular SDAs, starting with the synthesis of 14-ring UTD-1[1] (FTC: DON) [62] and shortly after CIT-5[2] (FTC: CFI) [63]. These materials are first silicate-based molecular sieves all with a 1D micropore channel system containing rings with more than 12 T-atoms as pore entrance. Multidimensional ultra-large pore zeolites have also been synthesized with different channel sizes upon the discovery of germanosilicates ITQ-15 (FTC: UTL with 14- and 12-rings) [64], ITQ-33 (FTC: ITT with 18- and 10-rings) [65] and ITQ-43 (with 28-ring) [18]. Although this is an open research area, these materials suffer from some problems which hinder their application for industrial purposes such as using costly and complicated SDAs, precursors and zeolite preparation procedures, poor chemical/thermal/hydrothermal stability and weak surface acidity [27, 41, 62, 65-67]. Although the pores are larger than those in classical zeolites, they are still long and mainly 1D micropores which impose mass transfer difficulties and low micropore volume. The number of available extra-large pore zeolites is very limited as well.

It is also noteworthy that the OMMs and, somewhat, the ultra-large pore zeolite cannot provide the shape-selective property of classical zeolites, especially when small and medium size molecules are involved.

These problems are the main roadblocks toward making OMMs or ultra-large pore zeolites a suitable substitute for classical zeolites in many applications. Looking for alternative strategies that can preserve all beneficial features of zeolites, some new methods were introduced by the scientific community which mainly considers shortening the micropores rather than enlarging them. These methods which are briefly discussed in the next section not only remove the above-mentioned problems to an acceptable extent but also lead to

[1]- University of Texas at Dallas number one
[2]- California Institute of Technology number five

new properties, enhancing the efficacy of zeolites in classical applications and opening new windows toward using them in other areas [27].

1.3.2 Zeolitic Materials with Short Micropores

Narrowing down the microporous channel length is achievable through crystalline size reduction to nanosize, creating a secondary pore system (meso-macroporosity) within microporous zeolites and designing novel zeolitic architectures such as core@shell, yolk-shell and hollow zeolites. These materials offer all desirable features of classical zeolites along with some new aspects emerging from the physical changes. These techniques are providing opportunities to design a catalyst and adsorbent rationally rather than by the traditional trial and error method.

As stated in many review articles, the first two techniques have been recognized as the main viable methods to improve diffusional transport within zeolites [27, 68, 69]. Another direct consequence of such a change would be the increase of the external surface area, i.e., meso-/macropore surface area. The active sites residing in these places facilitate the conversion of bulkier molecules (> 1 nm), while a considerable amount of remaining micropores, which are now shorter, can (simultaneously) participate in faster conversion of smaller reactant/product molecules with less diffusion limitation, creating a perfect hybrid catalyst. The importance of the external surface area in some catalytic reactions which occur on or near the external surface was demonstrated by providing two practical examples in the recent review paper [68]. Moreover, the large external surface area can perfectly host new organic functional groups which are basically too large to be grafted on the internal micropore surfaces [27, 68, 69]. Owing to intrinsic differences, the third technique, i.e., designing novel zeolitic architectures, will be discussed in Sections 1.4 and 1.5.

1.3.2.1 Nanozeolites- Pros and Cons

Along with shortening the micropores, it is highly desirable to increase the extent of the accessible zeolite surface. The first feasible methodology to achieve these is the reduction of the particle size of zeolites to nanometer range. Synthesizing nanozeolite colloids with a

smaller diameter than 100 nm is of primary interest in many fields, and still a challenging task to accomplish. The first colloidally stable nanozeolite was synthesized in the early 1990s by using conventional hydrothermal treatment of a homogeneous gel [70]. After which several techniques were introduced to synthesize nanocrystals of different zeolite frameworks. These methods which allow the synthesis of nanosized zeolite crystals were reviewed in references [68, 69, 71]. These methods have been divided into two main groups: modified conventional techniques which try to achieve a highly controlled crystallization process toward favoring nucleation over crystal growth and alternative techniques, as summarized in Figure 1.2. Depending on the synthesis gel ingredients, the former group, i.e., modified conventional techniques, can be attained by using one of the following pathways: Organic template-assisted synthesis (clear gel method) or organic template-free synthesis (hydrogel technique). In both, abundant nucleation is the key to suppressing the crystal growth and reduce the final crystal size.

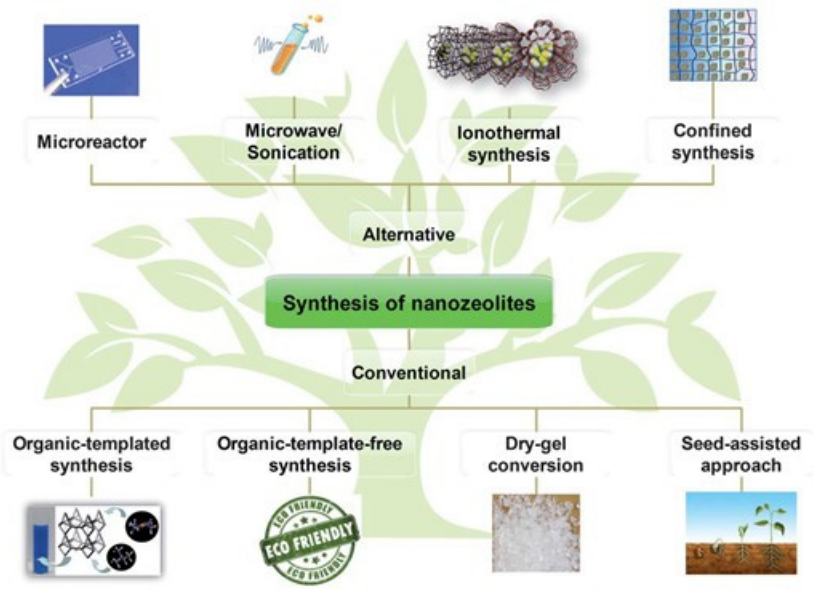

Figure 1.2- Nanozeolite synthesis routes (Reprinted with permission from [68]. Copyright 2013 RSC.).

Compared to the original conventional methods which are being used for micron-size crystal synthesis, nanozeolites are commonly synthesized using high quantities of organic templates, mainly in hydroxide form, mixed with other required chemicals and extra amount

of solvents. This gel composition will provide an optically transparent mixture (water-clear precursor gel) and guaranty high level of supersaturation for abundant homogeneous nucleation. Moreover, higher organic template concentration ensures the presence of excess template which can stabilize nanocrystals and hinder their aggregations by steric constraints. In addition to these two factors, there are some other parameters which can promote higher nucleation rates and increase the yield and cause less aggregation including using proper chemical sources of T-elements, additives (co-templates, growth inhibitors), gel aging, etc. Considering the activation energy difference between nucleation and crystal growth steps, lowering temperature is also playing a key role in limiting the crystal growth and other undesirable effects such as Ostwald ripening. Finding new templates can open new routes toward better crystallization of nanoparticles using clear gel technique, for example using metal complexes have successfully used to produce extremely small nanoparticles [68].

Due to environmental concerns, cost and low yield of organic-templated technique, lots of attention were recently drawn toward the synthesis of nanozeolite from an organic-template free hydrogel [68]. Hydrothermal treatment of an organic-template free hydrogel, made from proper chemical sources of T-elements and high alkali metal concentrations at moderate temperatures has produced high-quality discrete nanocrystals of the industrially important zeolite Y with high yield [72]. These methods usually provide higher crystallization rates and yields compared to clear gel technique. In contrast to clear gel technique, the main challenges for this technique are the intensive aggregation and intergrowth of formed nanocrystals within hydrogel and wide crystal size distribution of the final product. Factors like aging the hydrogel and finely adjusted chemical composition can improve the results [68].

In addition to conventional techniques, there are some specialized techniques such as microfluidic reactor synthesis, ionothermal synthesis, microwave and sonication synthesis approaches, confined space synthesis and top-down milling/recrystallization technique. All these methods were discussed in detail in recent review papers from Valtchev research group [68, 71].

Decreasing the size of a zeolite into the nanoregion (< 100 nm) can potentially provide many advantages other than short micropore diffusion distances and slightly higher external surface area. One of the impressive features is their usefulness in synthesizing structured

materials including uniform zeolitic coatings, membranes and zeolitic shells [68, 69], which will be discussed in Sections 1.4 to 1.6.

Although nano-zeolites are offering some beneficial properties, their industrial-scale applications have been hindered due to some main barriers as some listed below:

- Most of the methods discussed above cannot be easily generalized to various framework types, and if viable, an exhaustive trial and errors should be made to find an optimum synthesis procedure. Among all zeolitic frameworks discovered, only the crystal size of a few was successfully reduced to the nanoregion.

- Although zeolite nanoparticles under 40 nm have been reported for some frameworks [72], size reduction to smaller sizes is still challenging for the majority of zeolites.

- Difficult handling and recovery [41, 65, 69].

- Most of the discovered synthesis routes for nanozeolite synthesis suffer from low yield, long crystallization time, and high cost related to the pricey chemical sources, SDAs or hard templates used.

1.3.2.2 Hierarchical Zeolite - Pros and Cons

Hierarchy, in general, refers to "*certain ordering of individual elements relative to each other, often in combination with a certain degree of branching*" as stated in a recent review by Schwieger *et al.* [73]. From a material design point of view, such a property can be implemented on different aspects of a specific material which at the end usually emerges in one of the following forms: 1- structural hierarchy, 2- transport hierarchy and 3- compositional hierarchy [73]. Here, this term is used to describe the transport-related form within a zeolitic structure, i.e., the ordering with regards to pore structures, i.e., hierarchical porosity. A hierarchically-porous zeolitic material is actually single or polycrystalline (intergrown nanocrystals) zeolite which embodies pores in at least two different size scales, i.e., micropore and meso-macropores, within a single particle in a way that microporous and mesoporous networks are properly interconnected [27, 73, 74] (Figure 1.3). The way pores with different size scale are connected should lay on one of two interconnectivity patterns,

explained in Figure 1.3: Hierarchy type I and II (Figure 1.3). In other words, when defining a hierarchical zeolite, the transport properties should also be considered as an eligibility criterion along with the existence of secondary pores. In this case, the transport of substances within the newly designed network should be positively affected by the creation of the secondary pore system (meso-macropores) [73]. This kind of alteration also leads to shorter micropores and improved mass transfer in both single and polycrystalline zeolites.

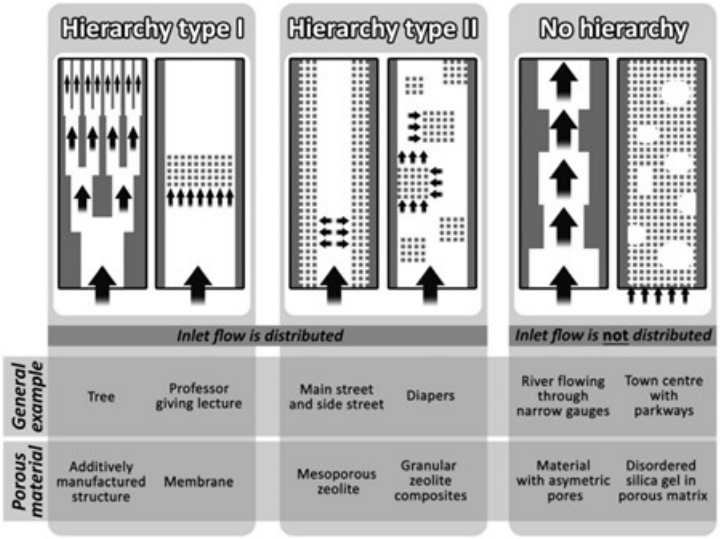

Figure 1.3- Different types of transport-related hierarchy (Reprinted with permission from [73]. Copyright 2015 RSC.).

It should be noted that ITQ-43, a multidimensional ultra-large pore zeolite (Section 1.3.1), can be considered as a true hierarchical zeolite since presenting pore as large as 2 nm connected to smaller pores (0.6 nm) [27]. The main difference between an ultra-large pore zeolite and a mesoporous zeolite is that the latter directly inherits beneficial properties of classical zeolites such as strong acidity and high thermal/hydrothermal stability since they share same crystalline structure with their original zeolites while earning all advantageous of mesoporous materials.

During the last decade, various approaches, mainly by adapting the templating concept used for OMMs synthesis, were introduced which will be briefly mentioned here. Further description regarding synthesis details, pros and cons, scale-up, effectiveness and yield, product properties and performance in real applications can be found elsewhere in

numerous review articles, published recently [19, 22, 27, 41, 43, 44, 67, 73-92]. In general, all the procedures and strategies toward hierarchical zeolite formation involve one or combination of the following processes; crystallization, aggregation and extraction (leaching) [73].

1.3.2.2.1 Hierarchical Zeolitic Structures - Synthesis Approaches

These preparation methods can be divided into two main categories. First, bottom-up techniques in which a secondary pore system forms either during zeolite crystallization period, i.e., in-situ techniques or *via* aggregation process of pre-synthesized crystals. The second category is the top-down techniques, also known as post-treatment methods. It should be noted that each one of the above-mentioned techniques can be used in a template-free or template-assisted fashions. The type of the secondary pore system, intracrystalline or intercrystalline, mainly depends on the method used and/or the intrinsic properties of the zeolite. Regarding the constituents, the final hierarchical product can also be either an all-zeolite material or a composite, made of zeolitic and non-zeolitic parts. Here, the most popular techniques for synthesizing hierarchical zeolites including leaching, templating and template-free techniques will be concisely reviewed (Figure 1.4).

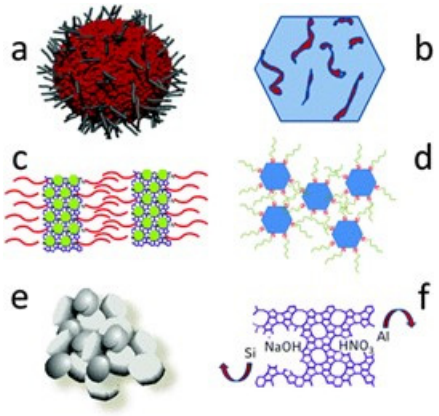

Figure 1.4- Overview of different strategies to implement mesoporosity in microporous zeolites: (a) inclusion of a secondary hard template in the form of rigid fibers, (b) incorporation of a secondary soft template, (c) application of a bifunctional template for micro-and mesostructuring, (d) covalent bonding of organosilane spacers to zeolite seeds, (e) formation of nanoparticle aggregates without secondary templates, and (f) post-synthetic leaching of alumina or silica species from premade zeolites (Reprinted with permission from [27]. Copyright 2013 RSC.).

Leaching of aluminum or silicon, so-called dealumination and desilication, from the framework of a pre-existing zeolite crystal by acid or alkali are two main post-treatments used for creating mesopores [41, 44, 81]. Dealumination of a zeolite framework can occur either by direct treatment of the zeolite with a concentrated acid or by first hydrolyzing the Si–O–Al using steam at high temperature, followed by a mild acid wash to remove extra-framework amorphous alumina. In contrast to steaming technique, the former method is usually applied for a zeolite with a more stable structure such as MOR. Due to the destructive effect of acid leaching, dealumination has also been reported with chemical treatments [83, 92]. In general, this method has some disadvantages as outlined in the following: 1- Removing Al from a framework directly affects the catalytic activity by changing the acidity of the catalyst, creating difficulties in investigating the real effect of mesoporosity on catalytic behavior of mesoporous zeolite. 2- Dealumination, especially through steaming, creates isolated cavities rather than a real hierarchical porous system. As a consequence, mass transfer issues in micropores persist and the inaccessibility of bulky molecules to the newly created meso-macropore surfaces still remains a problem. 3- Amorphous materials extracted from framework can easily block the micropores. 4- Dealumination is more applicable to high Al zeolites [73].

Desilication on the other side does not cause such issues, mainly because of higher Si concentration and more uniform dispersion than Al. Depending on the framework stability, this technique involves a quick treatment (30 min to some hours) of calcined samples with a dilute base such as NaOH at moderate temperatures (RT - 80 °C) [27, 90]. In general, desilication approach shows more versatility regarding its scalability and applicability for a wide variety of zeolites and zeotypes [27, 90]. Despite the apparent simplicity, the main challenge toward easy implementation of the desilication technique is a large number of controlling parameters. It is shown that this process is influenced by numerous factors such as Al gradient, Si/Al ratio, nature of the framework or extra-framework species, crystallographic properties, crystal morphology and degree of calcination (totally or partially de-templated zeolites) [27, 41, 44, 73]. It should be noted that this diversity has provided the possibility to apply this technique to various frameworks by adding different additives and, as expected, through time-consuming optimization process to control the reaction. For instance, desilication was initially restricted to zeolites with Si/Al ratios in the range of 20-50, which was later expanded to lower Si/Al and even Al-free zeolites by taking advantages of simultaneous acid-base treatment and partially passivated outer surface with organic

molecules, respectively [27, 73]. In conclusion, despite being simple and easy to perform, both dealumination and desilication methods cause some irreversible damage to the framework, such as loss of crystallinity and non-uniform composition changes, and as a consequence to zeolite catalytic activity, while the extent of improvement in mass transfer are highly restricted because of the lack in controlling mesopore morphology including pore shape, pore size distribution and interconnectivity.

Templating methods, i.e., using soft (secondary or bifunctional) and hard templates, are alternative techniques toward reaching a more tunable pore morphology. These methods, also called dual templating when a molecular organic template (SDA) is simultaneously used for directing the zeolite formation, are in-situ synthesis methods since templates as meso- or macro-porogens are directly introduced into the gel before starting the zeolite crystallization [27]. Crystallization is done using conventional hydrothermal or DGC methods. The DGC technique provides many advantages, some mentioned in Section 1.2.5. Another beneficial aspect, which can also be helpful in the synthesis of the novel zeolitic structures, is the diminished phase separation problem due to lower mobility of dry gel constituents. This can improve the inclusion of the secondary templates, especially the hydrophobic ones which do not interact well with the aqueous zeolite gel mixture and are susceptible to phase separation [27]. Major aspects of this templating technique have been comprehensively reviewed elsewhere [22, 27, 41, 76, 91].

Hard templates are rather rigid bodies, porous or non-porous, which can keep their initial form throughout the crystallization period. In a typical procedure, solid template and zeolite gel mixture, separately prepared, are properly mixed and subjected to a crystallization process. The solid template can later be eliminated from the meso-macropores *via* chemical or thermal treatments. This method presents several advantages such as the possibility of using purely inert substances with less/no effect on zeolites' acidity and fine control over meso-macropore sizes and shapes [73, 92]. This technique might be easily applied to the synthesis of various zeolitic frameworks. Polymeric material such as polystyrene beads, poly(methyl methacrylate) spheres (PMMA), resins, polyurethane foam, organic aerogels, inorganic materials such as silica, MgO and $CaCO_3$ particles, and biological materials are some examples, that have been successfully used as hard templates so far [27, 41, 73, 82]. However, carbon-based materials owing to their inert nature and easy elimination by calcination are by far the best candidates [75]. They were used in various forms such as commercial carbon black, carbon fibers, nanotubes, graphene oxide sheets, carbon aerogel

and finally, ordered meso-macroporous carbons (e.g., CMK-x and 3DOM[1]) [27, 73, 75]. The main problem of using carbon nanoparticles as the simplest carbon-based hard template was the formation of cavity like mesopores with broad pore size distribution. Although using other carbon-based hard templates such as 3DOM enabled the synthesis of zeolite with better-controlled pore morphology, the higher price, time-consuming preparation and difficulties in scale-up were highly discouraging [27]. Circumventing these issues, in-situ carbon templating technique by using non-expensive carbohydrates, e.g., sugar, was proposed. In-situ pyrolysis during the crystallization period could generate disordered mesoporosity in the zeolite [93, 94]. Another issue with carbon templates was the phase separation problem, arising from the hydrophobic nature of carbon hard templates. Formation of nanocrystals or single crystals with no mesoporosity and the creation of isolated internal mesopores which were not connected to the particle surface were some of the consequences. This problem has been mainly avoided by preliminary impregnation of the template with zeolite gel, drying and then crystallization through SAC process [27]. Using carbon-based templates dictates a high-temperature final calcination step. This unavoidable calcination step is believed to be a critical step in synthesizing high-quality mesoporous zeolites [27, 81]. To suppress the negative effect of the calcination step, the carbon templates were replaced by mesoporous amorphous siliceous materials, e.g., MCM-41, in their calcined or as-synthesized form [95-101]. These templates were converted to hierarchical composites or all-zeolite bodies through direct or seed-assisted transformation process. They can create some porosity in the final zeolitic products *via* either pseudomorphic crystallization[2] process or destructive crystallization into a mesoporous assembly of intergrown crystals. However, the so-called zeolitization process of their amorphous walls during hydrothermal process usually occurs partially, leaving behind a partly crystalline micro-mesoporous composite rather than all-zeolite materials [22, 98, 102]. This technique is called zeolitization [81]. CMK-x/mesoporous silica composite materials also provided the possibility of direct amorphous silica zeolitization along with avoiding the silica dissolution step in the mesoporous carbon preparation [60, 103].

Soft templating usually requires a supramolecular template to be added to the zeolite synthesis gel which might also contain a small organic molecular template (i.e., SDAs).

---

[1]- Monolithic three-dimensionally ordered meso/macroporous carbons (imprinted from colloidal silica)
[2]- In this type of transformation, the pore walls of the siliceous hard template crystallize into a zeolite without any damage to the initial pore system of the template.

Based on this concept, a zeolitic mesopore wall, rather than amorphous in the OMMs, forms around the supramolecular templates. Although the idea is adapted from surfactant templating of OMMs syntheses, due to the different chemistry of the prepared mixtures, synthesis conditions and presence of SDA, the mesoporous zeolites synthesis demands quite different types of organic templates, mesoporogens [104]. Using common templates used in OMMs synthesis such as CTAB[1] mainly leads to separate domains, i.e., microporous zeolite crystal in a physical mixture with amorphous mesoporous materials [73]. During the last few years, various approaches were introduced to solve this incompatibility issue which can be categorized into three different strategies [27, 73, 81]:

(I) Finding new organic templates, which can cooperate with SDAs and other components of zeolite precursor solution. The chemically reactive large silylating agents such as amphiphilic organosilanes or silane-functionalized polymers are some examples of these types of templates.

(II) Using a multi/single step synthesis route which allows using less complicated organic molecules such as commercially available organosilanes or even cationic polymers and surfactants as flocculating agent to assemble pre-synthesized zeolitic fragments (seeds) into a mesostructure. In contrast to other templating methods, this one is a top-down technique. The aggregation step can also be accompanied by a crystallization step to promote intergrowth between nanocrystals.

(III) Finally introducing more sophisticated bifunctional organic templates with the ability to act as directing agent for both zeolite formation and mesopore creation.

It should be noted that soft templates are mainly leading to the formation of mesopores rather than macropores, however, some successful attempts are reported which showed using emulsion agents could serve as macroporogens as well [105, 106].

DGC crystallization technique can improve the efficacy of soft templating by preserving more template within the crystallization region, increasing the mesopore volume of the final

[1]- cetyltrimethylammonium bromide

product. In general, the soft templating method suffers from using complex molecules which are mainly non-commercial and hard to prepare.

There are also some examples of mesoporous zeolite synthesis through a bottom-up strategy without using neither types of templates (No soft/hard templates used) [107-109]. The material can be produced following an either in-situ one step method *via* relying more on reaction conditions to eliminate the need to use a secondary template or multi-step procedures. The most common technique involves self-assembly or aggregation of randomly oriented nanozeolites, hardly aggregated forming a permanent intercrystalline mesopore network [107-109]. It should be mentioned that intercrystalline mesoporosity formed between nanozeolite aggregates is referring to a permanent situation created by partial condensed/sintered or intergrown nanoparticle assemblies and cannot be reversed [27]. In general, the products suffer from low stability [73] and lack of control in mesopore size distribution [75]. To improve the quality of these products, new synthesis approaches such as SAC technique, quasi-solid-state method, nano-fusion and using specific types of molecular SDAs have been used. Intergrown nanozeolites with intercrystalline mesoporosity, self-pillared nanosheets and layered aggregates formed based on repetitive twinning are some of the products with enhanced properties which are obtained by applying these techniques. Full descriptions of these specialized techniques can be found in review articles [27, 75].

The last technique is called delaminating and assembly which is restricted to a specific class of zeolitic material, so-called 2D or layered zeolites such as MCM-22 precursor (MCM-22(P)) [110]. This is a top-down strategy which involves swelling of the as-synthesized layer zeolite, followed by delamination or pillaring to create mesoporosity. This method is still facing a lot of challenges such as destructive swelling step and using high-cost surfactants for the post-treatment steps (swelling and pillaring) [73].

1.3.2.2.2 Macroscopic Structured Hierarchical Zeolites

Macroscopic structures are referring to shaped structures. The main part of the hierarchy in such system is related to the macroporosity which emerged from granulation or monolith formation processes. However, other meso-macropore networks can also be created within its zeolitic part using methods presented in the previous section such as desilication [73].

Similar to hard templating technique, the secondary pore system in a macroscopic composite is introduced with the use of a non-zeolitic material which can be itself either porous or non-porous. In contrast to previous techniques, most of the hard templates used here are non-sacrificial and do not need to be eliminated from the final product. Regarding the shape, size and porosity of the secondary materials, the composite morphology and porosity can be finely adjusted in wide ranges with less/no restrictions. The first generations of such structures were zeolitic pellets, beads, cylinders, etc., formed by compaction of the zeolite powders using a binder as a secondary material to glue the powdery zeolite microcrystals in a hierarchically porous network. The second type, structured monolith, however, is produced by coating of solid supports such as honeycomb monolith, sponge and even fibrous materials. Another difference of these supports to hard templates, mentioned in Section 1.3.2.2.1, is their size. These supports are at least some order of magnitudes larger than zeolite crystals while the other hard templates are comparable or smaller. Despite the granulation technique, the structured composites can provide some beneficial features such as improved mass and heat transfer, higher mechanical stability, lower pressure drop, better control of secondary pore system (shape, size, etc.). These aspects are mainly caused by the material and geometry-related properties of the supports.

Synthesizing granular zeolite composites *via* compaction techniques is not the focus of current study and will not be discussed here. However, due to the similarities in the formation mechanism and preparation techniques to zeolitic core@shell composite materials, macroscopic structured zeolitic material (also known as consolidated zeolite composite) are briefly discussed here and in Section 1.5.1. More details can be found in a recent review by Schwieger *et al.* [73].

The coating of the supports, known as surface zeolitization, can be performed using various techniques (Section 1.5.1). It is often important to keep the support and its physicochemical properties unchanged during the coating process [73]. Two common procedures for surface zeolitization are in situ coating in which the zeolite is directly coated on the support surface *via* hydrothermal treatment [111] or ex-situ coating which normally involves coating of some pre-synthesized crystals with the help of binder through a physical process. Depending on the nature of the support used in the first technique (in-situ), the support can be chemically reactive and participate in the process of zeolite coating formation by providing elements required for crystal growth. This kind of reactive supports, commonly made of silica or alumina, has a strong chemical interaction with the zeolitic layer caused by severe

intergrowth [73]. In some special cases which the complete continuity of the zeolitic film is desirable, the in-situ technique has been modified by seeding the support before the hydrothermal crystallization step. This technique is called seed-assisted secondary growth method (seeded growth technique), which will be discussed in Section 1.5.1.1.

There are some other techniques to make such macroscopic hierarchical zeolitic material. First one is the direct transformation of hierarchical macroscopic structure (monolith) having porous walls containing silica (porous silica, porous silica composite and porous glass) through a zeolitization process. Seed-assisted or direct transformation of the walls occurs during the hydrothermal process [73, 112]. This transformation is similar to the zeolitization process using silica-based OMMs as hard templates, as described in Section 1.3.2.2.1. The transformation of the supports can be complete or partial, leaving behind a composite or an all zeolite hierarchical macroscopic zeolitic material. Another technique, i.e., freeze casting technique, offers new opportunities for manufacturing of the hierarchically porous consolidated zeolite materials (comprehensively discussed in [73]).

1.3.2.3 Why Core@Shell and Hollow Zeolites?

Although all the techniques, discussed thus far, can completely or partially solve the diffusion problem of classical zeolites, none of them, neither pore enlargement techniques nor external surface area expansion, have achieved this without compromising the shape selectivity characteristic of the classical zeolites, as observed for instance in high-density polyethylene cracking using ZSM-5 nano-sheets [113]. The lack of shape-selectivity is also reported for the metal nanoparticles supported on a hierarchical zeolitic material since these active sites mainly reside on the external surface of the support (meso- and macropores surfaces) [114]. Even though this is somehow advantageous for the conversion of bulky molecules, sieving property of classical zeolites is still a must for many applications including separation and catalysis [115-117]. A uniquely designed core@shell material with a meso/microporous core and microporous zeolitic shell can present a spacious interior part to provide high adsorption capacity and to accommodate active sites larger than the size of the zeolite micropores while still providing high separation ability owing to the molecular sieving property donated by the microporous shell [118-121]. Moreover, these rationally designed materials can replace the classical zeolitic membranes in many applications since

the effective membrane area (membrane area per unit reactor volume) in these particle-level membrane reactors has enormously enhanced [122, 123]. It has to be noted that low surface area of classical membranes leads to low permeation fluxes and lower space velocities as compared to the conventional reactor systems which are one the main challenges facing the membrane reactor systems.

Diffusion problem of the microporous shell can also be addressed by manipulating the shell thickness [124-126]. In this way, the shell provides sieving properties while mass transfer limitation is reasonably alleviated. Also, new configurations of core@shell materials, i.e., yolk-shell, facilitates the accessibility of molecules to interior parts which might be negatively affected in some cases by direct contact between the shell and core components [127]. Moreover, a combination of different materials with zeolites, having various functionalities, in a single unit might also be interesting, especially in catalysis [99-101, 128-142]. This multi-functionality is critical to increasing the efficiency of a process which contains a multistep reaction; each step catalyzed by a part of the composite or hybrid catalysts. This also decreases the cost by eliminating several steps dedicated to separation, purification, storage and transportation of the intermediates after each step. It should be noted that the opportunity of having a multifunctional catalyst has also been feasibly provided by using multipore or hierarchical zeolitic catalysts after embedding various functional groups within their porous network, but not in an entirely shape-selective fashion.

Finally, this type of materials can be produced using techniques that are not destructive for zeolitic parts and usually, zeolite keeps all properties it has in its pristine forms.

1.4 Zeolitic Core@Shell Composites

Core@shell materials are composites, finely engineered at the microscopic level to ascertain the creation of new desirable features while keeping the majority of the original characteristics of each component intact. This kind of combination characterizes the whole assembly with more desirable properties than its original building parts individually or in a physical mixture, making this material a competent candidate in many areas including adsorption, catalysis, storage and biomedical applications [127, 143, 144].

1.4.1 Definition

A typical core@shell consists of at least two different materials in such a way that one, the shell, entirely encompasses the inner compartment, the core (Figure 1.5a). ***Core@shell*** terminology is a simplified form of the full name used to describe multi-layered materials, i.e., Core@Shell$_1$@Shell$_2$@...@Shell$_n$, introduced to describe layered composites. The "@" is used to separate different layers while various elements of each layer can be discriminated by using a "," separator [145].

In a layered material, the outer layer should be thick enough to be considered as a shell, usually, a few atomic monolayers are enough to efficiently restrict the exposure of the core compartment to the surrounding atmosphere [146]. In a multi-shell composite, one of the inner shells can be selectively removed from the structure. This creates a hollow inner space between the shell and the central part of the composite. This type of core@shell structures is termed as yolk-shell materials (Figure 1.5b). Hollow materials form if the core part is entirely removed from the assembly.

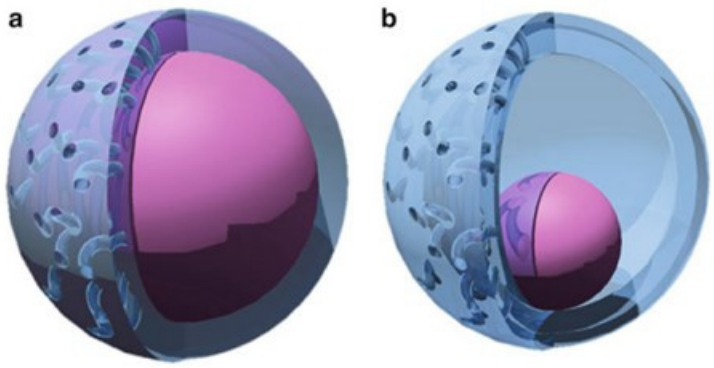

Figure 1.5- Schematic representations of (a) core@shell, and (b) yolk–shell (Reprinted with permission from [127]. Copyright 2014 Springer.).

The core may have various functionalities, among which the templating role is significantly important, i.e., the core acts as a hard template and determines the form and the size of the final composite.

1.4.2 History

More detailed studies on core@shell materials synthesis and applications were started in the 1980s [147, 148], although encapsulated materials were known since the 1920s [145]. Following this, the concept of core@shell composite has been widely used by researchers for designing new materials including core@shell, yolk-shell and hollow materials with various compositions, size and porosities in interior and exterior parts [127, 143, 144]. These composites have solved many problems, for instance, in the field of catalysis, the engineered catalysts showed not only high thermal stability (resistance to sintering at elevated reaction/regeneration temperatures) [149-151] but also an enhanced catalytic performance (i.e., activity) [127, 152-155].

A wide variety of materials were used for making the shell such as silica [151, 155, 156], metal oxides such as zirconia [149, 150, 153, 154], titania [157], ceria [152], iron oxide [158], carbon [153], etc. Most of them were unable to provide true shape selectivity for small molecules, except Pt particles covered with mesoporous silica to forming a yolk-shell structure, used for Suzuki coupling reaction involving large molecules [156]. This example confirms the importance of shape selectivity of the shell in such catalytic reactions, a requirement which is mostly met when zeolitic materials are involved. There are some examples of providing such selectivity by using microporous metal-organic frameworks (MOF) [159, 160] as the shell. These studies are not discussed here.

In general, a zeolitic core@shell material is a typical core@shell with at least one part made of zeolites. According to the definition, zeolitic core@shell materials can be classified into two main groups: composite with a non-zeolitic shell and composite with a zeolitic shell. Most of the research in the first group is dedicated to the synthesis of zeolites which are covered with a mesoporous shell, mainly silica-based OMMs [161-164]. These hierarchical composite assemblies have provided numerous features. From shape-selectivity point of view, these materials do not show any fundamental difference to classical zeolites due to the true hierarchy in their porous network. This class of core@shell materials is not within the scope of the current chapter.

Because of the growing interest, remarkable properties and challenging synthesis approaches, the second group, i.e., materials with a zeolitic shell which are referred as zeolitic core@shell materials throughout the text, will be comprehensively addressed in the

next sections. It should be noted that depending on the functionality and the purpose of having such a structure, these zeolitic core@shell materials can also be considered as a type of zeolite membrane. In this regards, they have been denoted by various names, such as “zeolite capsuled catalyst particles” , “micro-membrane reactors” , “microscopic structured membrane reactors” or “permselective membrane-coated catalyst particles (PLMR)” [123].

1.4.3 Zeolitic Core@Shell with Zeolite as Shell (Core@Zeolite)

Among all types of possible building materials for core@shell composites, crystalline zeolites seem ideal for forming the shell of a core@shell sphere owing to their high thermal/hydrothermal stability, excellent resistance under corrosive conditions, highly ordered pore structure, large specific surface area and micropore volume, shape selectivity, encapsulation properties and intrinsic chemical activity. This class of material includes all-zeolite core@shell composites (zeolite@zeolite) as well as core@shell composite with zeolitic shell and non-zeolitic cores. Yolk-shell and hollow zeolitic materials as their close relatives mainly form by applying some changes on the core part of a pre-synthesized zeolitic core@shell composite. Synthesis techniques for all these materials will be discussed in Sections 1.5 and 1.6, respectively.

It should be mentioned that zeolitic core@shell materials may or may not be regarded as an alternative for hierarchical meso-macroporous zeolites. According to the definition presented earlier for hierarchical materials, such composites do not provide expected mass transport pattern as regular meso-macroporous zeolitic materials do. In spite of this discrepancy, some reviewers have considered this class of zeolitic core@shells as hierarchical zeolites [41]. The recent review by Schwieger *et al.* has assigned the hierarchy within these examples as compositional, but not transport-related, i.e., hierarchical porosity [73]. Although having a mesoporous zeolitic shell can establish a real hierarchy system in these materials, it should be remembered that one of the main reasons for using core@shell material is their shape-selective property which is guaranteed by having an entirely microporous zeolitic shell.

In contrast to appealing features provided by a zeolitic core@shell material, some challenges are hindering the successful production of such materials. Firstly, achieving 100% shell coverage which can entirely encapsulate the core part with a highly crystalline zeolitic shell is a challenging task. Moreover, one of the biggest concern of forming a composite from porous constituents is the pore network connectivity. This problem is much severe when one of the compartments has very tiny pores, especially with less dimensionality. Randomly oriented crystals in the shell are used as a solution to partially overcome this problem when multidimensional microporous material are used as building blocks [165, 166]. Finally, regarding the complexity of the zeolite formation process which mainly occurs in a highly destructive environment, there is a huge concern about the permanent harm done to the core and its functionalities during this indispensable step. All these factors can profoundly affect the performance of a zeolitic core@shell material.

1.5 Synthesis of Core@Zeolite Materials

Synthesis of zeolitic core@shell has been historically initiated by coating macroscopic supports with zeolite which has been briefly discussed in Section 1.3.2.2.2 from hierarchical porosity point of view. In this section, their physical structure and their early synthesis techniques will be reviewed as the initial stage of the zeolitic core@shell evolution path.

1.5.1 Zeolitic Coatings on Macroscopic Structures

Conventional zeolite synthesis protocols usually produce zeolitic microcrystals and/or their micron-sized aggregates. Not long after zeolite application in chemical industry, it was realized that using these powdery zeolites imposes many limitations including high pressure drop, fast plugging of the bed and inefficient heat and mass transfer, etc. Therefore, along with improving other properties of zeolites such as stability, acidity, particle size and morphology and modifying the porous structure in microscopic level by creating macro/mesopores, designing stable macrostructures of the zeolites have also become a top priority. As discussed in Section 1.3.2.2.2, this type of structural engineering may introduce a secondary pore system and create a macroscopic structured hierarchical zeolite.

Compacting the zeolite crystals in a millimeter size amorphous matrix by using inorganic binder was one of the first zeolitic macrostructures introduced. These agglomerates were produced in a variety of shapes including beads, rings, pellets, cylindrical extrudates, and flakes [73]. However, this method suffered from a couple of issues including lower activity and selectivity of zeolites by diluting the active site concentrations and imposing mass transfer limitations, faster deactivation (shorter catalyst life span), attrition, low heat transfer rate, non-regular flow pattern and high pressure drop [112, 132, 167]. For dealing with this issues, elimination of the binder from synthesis protocol of such structures was aimed at through either modifying classical zeolites synthesis mixture to directly crystallize into macroscopic zeolitic bodies [168] or direct transformation of pre-structured Si-containing materials (porous silica, glass or densified aluminosilicate gels, etc.) into self-bonded zeolite assemblies [73, 132]. Although no binder was used, binderless self-standing macrostructure products could not significantly solve the above-mentioned problems.

Formation of zeolitic coats and thin films mounted on a highly accessible supporting substrate were found to form zeolitic structures (monoliths) with adequate thermal/mechanical stability and mass transfer rate inside their well-defined porous structure [73, 132, 169, 170]. Such a technique was quite versatile allowing customization of the structural properties such as the shape, porosity (pore size and distribution) and mechanical stability based on their envisioned applications [132]. Moreover, by developing in-situ techniques to make such structures and complete elimination of binders (used in ex-situ methods), problems such as dilution of active-site concentration, dust presence, mass/heat transfer issues were also pretty solved [120, 167, 171, 172]. It should be noted that the macroscopic support used in this approach does not present any catalytic activity, a frequently happening case [167]. Carefully adjusting the orientation of the zeolitic crystal layer deposition and their growth and continuity on a catalytically-active substrate can provide a special type of catalyst with shape-selective property or membranes [120, 173, 174]. If the zeolite layer is catalytically active, this material benefits from bifunctionality and if not, the external surface will be effectively passivated hindering any undesirable side reactions. For example, such a classical zeolitic composite system with shape selectivity capability, designed and implemented by van der Puil *et al.* [119], is schematically shown is Figure 1.6. The presence of some crystals with improper orientations and some pinholes were observed, however, it was claimed that these defects cannot affect the shape selectivity of the whole assembly [120].

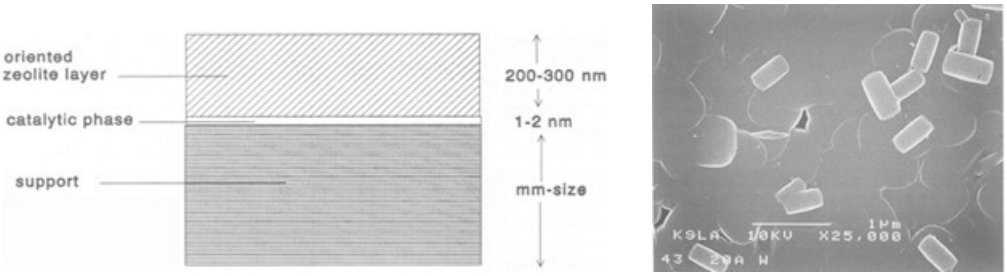

Figure 1.6- (a) Schematic representation of the composite system. In the case of laterally oriented silicalite-1, the straight channels are perpendicular to the support. Silicalite-1 was directly synthesized on the metal oxide coated support using conventional hydrothermal treatment in a gel containing TPAOH, TEOS and water at 150 °C for 3h, (b) HRSEM photograph of silicalite-1 crystals grown with 200 nm of thickness and the average size of the laterally oriented intergrown crystals is 0.6 μm on a continuous layer of Fe_2O_3 (Reprinted with permission from [119]. Copyright 1995 Elsevier.).

Although many long-lasting problems of powder catalysts were solved by this designed zeolitic macroscopic structure, this approach suffers from some drawbacks itself: the amount of zeolite that these monolithic structures can accommodate per unit volume is very low which may affect the activity or create some difficulties in reactor design [112]. In addition, the difference in thermal properties such as conductivity and expansion coefficient between substrate and zeolite may lead to a short lifetime of the whole structure, especially in processes with frequent temperature changes [112, 167, 171, 172]. These monolithic membrane-like macroscopic structures and the roadblocks toward their proper implementation are not the topics of the current report. They have been briefly discussed here since the synthesis approaches used for such structures, later became a source of inspiration for developing micron-sized core@shell catalysts. More details about the synthesis techniques and applications, especially in the field of zeolite membrane, can be found in recent reviews [123, 175-177].

1.5.1.1 Synthesis of Macroscopic Coated Zeolitic Structures

Supported zeolite coatings (monoliths, thin films, membranes, etc.) are synthesized by placing a film on a substrate with different shapes and porosity such as metals, oxides, stainless steel, mullite, mica, glass, SiC, etc., and used as membranes, catalysts and sensors [178]. To make such a thin film on substrates, conventional techniques such as vapor deposition, radio frequency sputtering, and laser beam deposition, etc., cannot be implemented [170]. As mentioned in Section 1.3.2.2.2, in-situ or ex-situ techniques are used to make such structured zeolitic materials. Ex-situ techniques such as wash-coating the substrate with crystals or by co-extruding zeolite crystals with ceramic paste have also been used [169]. However, these methods were unable to provide a firmly attached zeolitic coats to the substrate and sufficient mechanical stability of the whole assembly (due to lowered sintering temperature) [169].

The first widely used method was in-situ crystal growth on the support by immersing the substrate in the zeolite synthesis clear gel (mainly at high pH) and then hydrothermal treatment at high temperatures [179]. The mechanism is based on heterogeneous nucleation on the substrate solid surface. The nuclei which are preferably formed and chemically bonded to the solid surface at the early stages of the crystallization process, later grow to form the film during crystallization [169]. The in-situ growth of zeolite has also been used to cover the non-flat surface of fibrous materials. However, the surface was not perfectly covered with crystals, as can be seen in Figure 1.7.

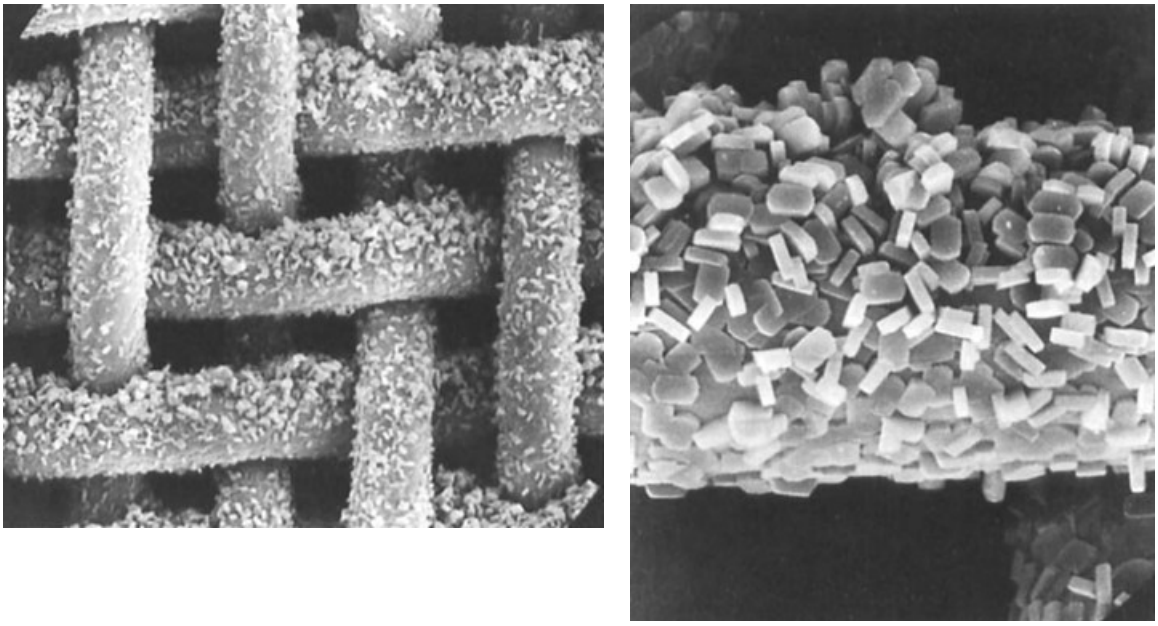

Figure 1.7- SEM images of the ZSM-5 zeolite coated on stainless steel wire gauze using the in-situ method. The wire diameter is 35 μm (Reprinted with permission from [169]. Copyright 2009 Wiley.).

As can be seen in Figure 1.7, the coverage of zeolitic layer using in-situ technique was not continuous, i.e., the crystals were not uniformly intergrown to cover the entire surface. The formation of a thin continuous layer of molecular sieve was later realized using a multistep procedure [132, 180, 181]. The method starts with coating the support with pre-synthesized discrete colloidal crystals, known as seeds and then hydrothermal crystallization using zeolite synthesis mixture to grow the seeds into a continuous film. This method, also called seeded (secondary) growth technique, has been successfully implemented for synthesizing thin films on flat and fibrous substrates (Figure 1.8) [112, 132, 134, 137, 167, 171, 172, 180, 182-186] and later successfully adapted to synthesize microscopic zeolitic core@shell, yolk-shell and hollow materials which will be discussed in the next sections. A review of new findings about macroscopic structured zeolites, especially with the use of fibrous supports can be found in review articles [88, 178, 187].

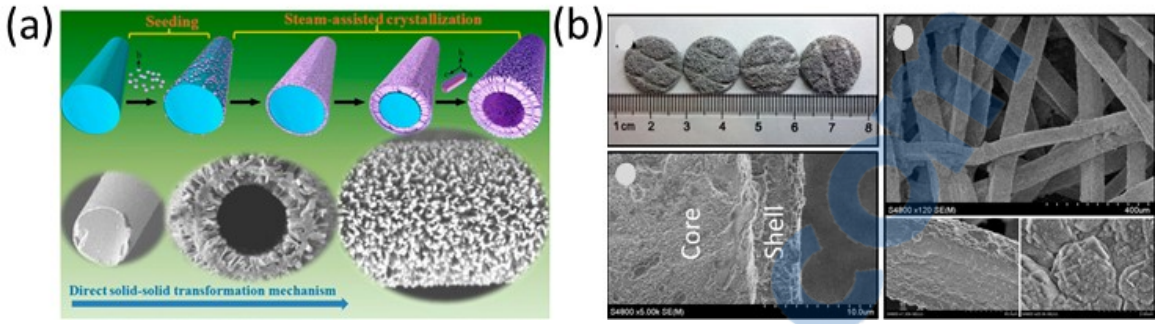

Figure 1.8- Using controlled seeded growth technique to synthesize: (a) macroscopic c-axis oriented ZSM-5 hollow fibers (Reprinted with permission from [112]. Copyright 2013 ACS.), and (b) monolithic Al-fiber@ZSM-5(H^+) (Reprinted with permission from [171]. Copyright 2015 Elsevier.).

1.5.2 Synthesis of Zeolitic Core@Shell

The idea of having a zeolitic layer on a large-size support has inspired material scientists to synthesize zeolitic core@shell reactors which combine numerous desirable properties in a single unit (Discussed in Section 1.7). Zeolitic core@shell materials are composites formed from crystalline zeolite layer coated on a support in a way that the zeolitic shell totally covers the outer surface of the support. Over the past 15 years, a variety of core materials, porous or non-porous, such as polymers, [99, 100, 129, 131, 133, 188], amorphous silica, [134, 137, 140, 189] and metals, alloys and metal oxides, [128, 171, 172, 190] and even different types of zeolites [118, 141, 166, 190-192] have been used to synthesize either core@shell or hollow materials with a zeolitic shell. Typically, zeolitic core@shell materials are synthesized using one of three different techniques, i.e., seeded growth technique, in-situ method and physical coating.

1.5.2.1 Seeded Growth Technique

Owing to its versatility and simplicity, the seeded growth technique has been widely used in zeolitic core@shell synthesis. As mentioned earlier, this technique was first introduced for coating flat and fibrous substrates with zeolitic materials [132, 180]. Not long after, this

method, with slight modifications, has been successfully applied for making zeolitic core@shell or hollow zeolites [133].

1.5.2.1.1 History

Layer-by-layer technique (LBL) was successfully utilized for the synthesis of hollow silica spheres assembled from silica nanoparticles in 1998 [193]. Shortly after, this technique was adapted to effectively deposit nanozeolite crystals around the outer surface of discrete polystyrene spheres (PS) [131, 141, 142]. The method simply used multilayers of surface modifiers (surfactant or cationic polymers) and as-prepared zeolitic nanocrystals in a repetitive manner (at least three times). After recovering, drying and removing the core, self-standing hollow assemblies of nano-zeolites were produced, entirely replicating the spherical shape of PS particles. Dissolution or thermal treatment methods were used to eliminate the core or both the core and polyelectrolyte layers, respectively, leaving behind a hierarchical hollow zeolite with intercrystalline mesoporosity [129]. Repeating similar procedure, Yang *et al.* [129] studied the effect of various parameters on coating quality. They found that the zeta potential of the colloidal nanozeolite solution, which is highly controlled by the pH and salt concentration in synthesis media, framework type and composition of nanozeolite, is the most important parameter and should be carefully adjusted to provide required attraction between core@shell components.

The mechanical stability of these loosely packed spherical nano-assemblies was improved by a secondary hydrothermal treatment in a zeolite synthesis gel (Figure 1.9a) [133, 188]. At the same time, a similar technique, i.e., seeded growth method, has been used to synthesize hollow zeolitic spheres using mesoporous silica as the core (Figure 1.9b) [101].

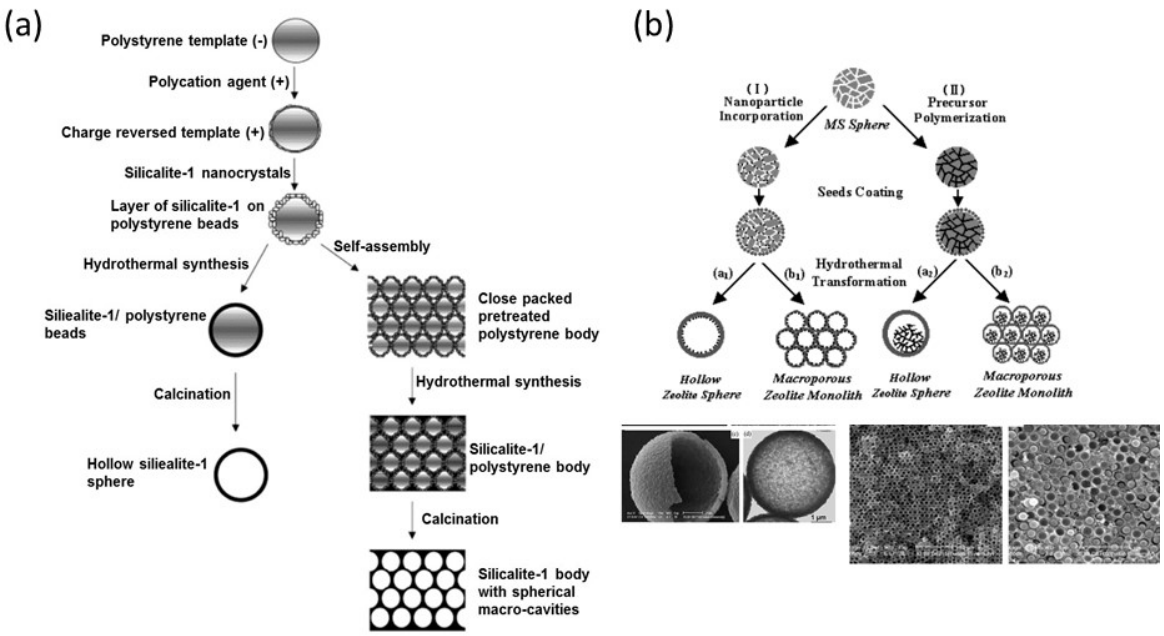

Figure 1.9- Schematic representation of the seeded growth technique to synthesize the core@shell and hollow zeolites using (a) PS beads [133, 188] (Reprinted with permission from [133]. Copyright 2002 ACS.), and (b) mesoporous silica spheres [99, 100] (Reprinted with permission from [99]. Copyright 2003 Wiley.).

Table 1.1 summarizes all studies using this technique, sometimes with slight modifications, to produce core@shell with a wide variety of core templates.

Table 1.1- Core@shell materials, synthesized using the seeded growth technique.

Ref.	Year	Product	Core				Pre-treatment	Surface modifier	Crystallization	Post-treatment	Application
			Core	Shape	Porosity	Size					
[194]	2016	Fe,Cu,β-zeolite @Ni,β-zeolite	β-zeolite (Si-BEA)	Truncated bi-pyramidal	Microporous	15-20 μm	Fe & Cu loading	PDADMAC	Conventional HT @ 140 °C	Ni loading	Ethanol steam reforming
[195]	2015	Pt,Al_2O_3@silicalite-1	Al_2O_3	Pellet	Porous	2-2.3 mm	Pt loading	TPAOH	Conventional HT @ 170 °C, 3d, rotation	-----	Shape-selective Xylene hydrogenation
[196]	2015	SiO_2@silicalite-1	SiO_2	Sphere	Mesoporous	1.5, 3, 20-45 μm	-----	PDADMAC	2 x (Conventional HT @ 200 °C, 45 min)	-----	Shape-selective adsorptive separation-biodiesel purification
[197]	2015	ɣ-Fe_2O_3@TS-1	ɣ-Fe_2O_3 (Magnetic core)	Sphere	-----	~ 100 nm	-----	PDADMAC	Conventional HT @ 100 °C, 20h & 130/170 °C, 36h	-----	Photocatalytic degradation of phenol
[198]	2014	Ni/Al_2O_3@silicalite-1	ɣ-Al_2O_3	Spherical Beads	Porous	0.8-2.2 mm	Ni loading (Route a)	APTMS	Conventional HT	Ni loading, water & toluene soaking (Route c)	Methane steam reforming
[199]	2013	β-zeolite@silicalite-1	β-zeolite (Si-BEA)	Truncated bi-pyramidal	Microporous	25 μm	-----	PDADMAC	2 x (Conventional HT @ 200 °C, 45min)	-----	Shape-selective adsorptive separation of branched paraffin isomers

[200]	2013	Fused iron@MOR(H^+)	Fused iron	Pellet	-----	0.85-1.7 mm	-----	APTMS	Conventional HT @ 180 °C, 2d, rotation	-----	Shape-selective modified Fischer-Tropsch synthesis (syngas to i-paraffin)
[201]	2013	SiO_2@silicalite-1	SiO_2	-----	Mesoporous	25-50 µm	-----	PDADMAC, PSS	Conventional HT @ 175 °C, 1d, rotation	-----	Shape-selective adsorptive separation of Xylene isomers
[202]	2013	β-zeolite@silicalite-1	β-zeolite (BEA(H^+))	-----	Microporous	<1-2 µm	-----	PDADMAC	Conventional HT @ 200 °C, 15-180min	-----	Shape-selective Racemization of (S)-1-phenylethanol
[203]	2013	Fe_3O_4@Au,SiO_2 @silicalite-1	Fe_3O_4 (Magnetic core)	Sphere	-----	0.4-0.5 µm	SiO_2 coating, Au loading & SiO_2 coating	PDADMAC	VPT HT @ 180 °C, 3d	-----	Reduction of 4-nitrophenol by $NaBH_4$
[204]	2012	13X@silicalite-1	13X	-----	Microporous	<4-5 µm	-----	PDADMAC	Conventional HT @ 80 °C, 24h	-----	-------
[205]	2011	Ni,SiO_2@ silicalite-1, Ni/Al_2O_3@ silicalite-1	SiO_2, Al_2O_3	Beads	Porous	0.8-1.7, 0.8-2.2 mm	Ni loading	APTMS	Conventional HT @ 150/175 °C, 2-72h	-----	Alkali-resistant catalyst for DIR-MCFC[18]
[206]	2011	SiO_2@TS-1	SiO_2	Beads	Mesoporous	3 mm	-----	APTMS	Conventional HT @ 175 °C, 48h, rotation	-----	Styrene oxidation

[18]- Direct internal reforming molten carbonate fuel cell

[207]	2011	ZSM-5(H^+) @ silicalite-1	ZSM-5(H^+) extrudate	Cylindrical	Hierarchical	OD: 2 mm, L= 4-5 mm	-----	PDADMAC	Conventional HT @ 180 °C, 24h	-----	Toluene disproportionation
[208]	2011	Fe,SiO_2@silicalite-1	SiO_2	Pellet	Mesoporous	1.81-2.36 mm	Fe loading	APTMS	Conventional HT @ 175 °C, 24h	-----	Shape-selective Fischer-Tropsch synthesis
[191] [128]	2010	β-zeolite@Y & Ru,β-zeolite@Y	β-zeolite	-----	Microporous	1-2 µm	Ru loading	-------	Conventional HT @ 90 °C, 12-36h	-----	Liquid-phase hydrogenation of benzene
[209]	2010	Ni,SiO_2@silicalite-1	SiO_2	-----	Mesoporous	50 µm	Ni loading	PDADMAC, PSS	Conventional HT @ 175 °C, 24h, rotation	-----	Shape-selective gas phase hydrogeneation of 1-hexene and 3,3-dimethyl-1-butene
[210]	2009	TiO_2@silicalite-1 ZnO@silicalite-1	TiO_2 ZnO	Sphere	-------	1 µm, 0.2-0.8 µm	-----	PDADMAC, PSS	Conventional HT @ 100 °C, 12h, Rotation	-----	-----
[211]	2009	Ni,SiO_2@silicalite-1, Ni,Al_2O_3@ Silicalite-1	SiO_2 Al_2O_3	Beads	Porous	0.85-1.7, 1.5-2.8 mm	Ni loading	APTMS	Conventional HT @ 175 °C	-----	Alkali-resistant catalyst for DIR-MCFC[1]
[190]	2009	Fe_3O_4 @silicalite-1	Fe_3O_4	Sphere	-------	400 nm	-------	PDADMAC	VPT HT @ 180 °C, 3d	-------	Microwave-Assisted Protein Digestion
[212]	2009	Y(Na^+)@β-zeolite	Y(Na^+)	-----	Microporous	1-2 µm	Ion-exchange	TEAOH loading	Conventional HT @ 140 °C	-------	Catalytic cracking of n-octane
[192]	2007	β-zeolite@silicalite-1	β-zeolite	Beads	Hierarchical	300- 500 µm	-------	PDADMAC	Conventional HT @ 200 °C, 30-60min	-------	-------
[165]	2006	MOR@silicalite-1	MOR	Single crystal	Microporous	20-35 µm	-------	PDADMAC	Conventional HT @ 150 &	-------	-------

									200 °C, 30-240min		
[166]	2006	ZSM-5@silicalite-1, ZSM-5@β-zeolite	ZSM-5	Single crystal	Microporous	20 μm	-------	PDADMAC	Conventional HT	-------	-------
[118]	2005	β-zeolite@silicalite-1	β-zeolite (Al- & Si-BEA)	Single crystal	Microporous	15 μm	-------	PDADMAC	3 x (Conventional HT @ 200 °C, 15-120min)	-------	Shape-selective adsorptive separation of butane, toluene, and trimethylbenzene
[213]	2004	Pt,TiO_2@silicalite-1	TiO_2	Sphere	Mesoporous	0.5 mm	Pt loading	Polyethyleneimine	Conventional HT @ 180 °C, 24h		Shape-selective hydrogenation of 1-hexene and dibranched 3,3-dimethylbut-1-ene
[188]	2002	PS@zeolite A	PS	Sphere	-------	8-15 μm	-------	Redifloc	Conventional HT @ 60 °C, 2h	-------	-------

1.5.2.1.2 Notes on Synthesis Steps

The whole process of the seeded growth technique involves several steps, starting with the building blocks selection and preparation, i.e., the core material and zeolite seeds. Depending on the desired functionalities and textural and morphological properties of the final product, the proper type of cores has to be rationally chosen and modified with pre-treatments such as guest species loading and ion-exchange.

The surface of the core particles should be conditioned to easily adsorb the nanocrystals. Surface modification is found to be a critical step for the formation of a uniform zeolitic shell by creating required infrastructure, essential for an effective interaction between seeds and the core surface. Surface modification facilitates the interactions between the core material and shell primary building blocks (i.e., zeolite seeds or precursors) *via* grafting of chemical species on the external surface, multi-layer coverage with polyelectrolytes and some other treatment such as mild basic/acidic treatment. The type of treatment depends on the nature of the core material. For example, carbon fiber support was treated first with oxidizing H_2O_2 and HCl aqueous solution and then with a cationic polymer [132], metal foil support was treated with strong base and acids [170] and silica support was chemically modified *via* APTMS grafting [206]. Using polyelectrolytes is the most common technique *via* single layer or multilayer coating of differently charged soluble polymers [210]. It should be mentioned that there are some studies which did not use surface modification prior to seeding [128, 191, 206, 214]. Despite the simplicity, this often yields a non-uniform coating.

The next step is the core seeding. Seeds on the external surface of the core induce faster shell formation which is hindering core dissolution in the harsh conditions of secondary growth step. This seeding step is essential for vulnerable core particles such as siliceous materials which show a restricted chemical compatibility with the secondary growth conditions [118, 166]. Washing cycles should be done excessively to remove all free un-adsorbed polyelectrolyte or nanoparticles from the media. A repetitive procedure of surface modification and seeding steps, i.e., LBL, might also be needed which is to ensure an effective and uniform coverage of the core surface or to make multilayered structures.

Secondary growth is the next step which can be done using a conventional hydrothermal method or dry gel conversion (DGC) technique. Treatment conditions such as duration, temperature, gel composition need to be finely optimized. It has been reported that

secondary growth of the seed under rotation can improve the uniformity and integrity of the zeolite shell, especially in the case of large millimeter-sized core templates [195]. This step might need to be repeated several times to ensure the shell coverage and integrity when shape-selectivity is desired.

1.5.2.1.3 Pros and Cons

The main advantages of this technique are outlined below:

- This method is applicable to a wide variety of core materials, as can be seen in Table 1.1. This freedom in core selection allows avoiding the collapse of the core particles by choosing more stable materials for different secondary growth conditions.

- The presence of the seed on the core surface improves the core@shell formation in many ways such as faster shell formation, suppressing bulk zeolite nucleation within the secondary growth gel, controlling the shell thickness over a certain size range, assuring a uniform and continuous shell [215].

This technique also suffers from some drawbacks:

- Minimum achievable shell thickness is limited to the size of the nanoparticles used and the crystal growth extent. Reducing the size of nanozeolites to few tens of nanometer (smaller than 40 nm) might be highly difficult and has not been achieved for many framework types. It means that, even with highly controlled seed growth, synthesizing a core@shell material with shell thickness finer than 100 nm is very challenging.

- Chemical incompatibility is an issue. Although it was shown that the presence of the seeds can hinder core dissolution [118], the secondary growth conditions should be managed in a way that the dissolution rate becomes extremely slow in comparison with crystal growth rate. Such rapid growth of the shell, induced by the presence of the nanoseeds, was observed for a limited number of frameworks such as silicalite-1. Otherwise, core dissolution, even if very little, can lead to seed detachment and bulk crystals formation. Despite negative effects of core dissolution, there are some cases such as certain types of zeolitic cores with Al gradient, in which the desilication during the seeded growth process can be used to create

zeolitic double shells or mesoporous zeolite@zeolite [191]. In this type of zeolite, desilication leaves behind an Al-rich rim in the core which can provide enough support for the seeds, while desilication from interior parts is in progress.

- In the case of using Si-containing cores, dissolution of the core changes the chemical composition of the secondary gel and therefore, affects the composition of the zeolitic shell and may change the zeolitic shell properties such as acidity [166, 191, 216].

1.5.2.2 In-Situ Technique

There are several examples of the formation of zeolitic shell on a support without using seeds, generally called in-situ techniques (Table 1.2). In the first step a non-crystalline macroscopic core template, non-pretreated or pretreated, is immersed in a zeolite solution and undergoes a hydrothermal crystallization step. This coating process is probably favored by simultaneous formation, adsorption and growth of seeds on the external surface of the core, all in a one-pot synthesis route or direct heterogeneous nucleation on the support surface. The intercrystalline spaces between shell crystals create hierarchical systems and increase the core accessibility in a non-shape-selective way. This type of hierarchy is desirable in some applications. Combining different catalytically-active elements in a form of core@shell architecture is the best technique for making more efficient composite catalysts which may or may not present shape-selective property [217-220].

Table 1.2- Core@shell materials, synthesized using one-step (in-situ) zeolitic shell growth over the non-crystalline core.

Ref.	Year	Product	Core				Pre-treatment	Crystallization	Post-treatment	Application
			Core	Shape	Porosity	Size				
[221]	2015	(CuO,ZnO,Al_2O_3) @ ZSM-5(H^+)	CuO,ZnO,Al_2O_3 composite nanoparticles	Aggregates	-------	-------	-------	Conventional HT @ 180 °C, 48h, rotation	-------	Bifunctional catalyst for CO_2 hydrogenation to dimethyl ether
[222]	2015	Fe,SiO_2@ZSM-5(H^+)	SiO_2	-------	Mesoporous	-------	Fe loading	SAC HT @ 160 °C, 18h	-------	Bifunctional catalyst for modified Fischer-Tropsch synthesis (syngas to i-paraffin)
[223]	2015	Fe,SiO_2@silicalite-1@ ZSM-5(H^+)	SiO_2	Pellet	Porous	0.85-1.7 mm	Fe loading	2 x (Conventional HT @ (1) 180 °C, 24h and (2) 180 °C, 24h, rotation)	-------	Bifunctional catalyst for modified Fischer-Tropsch synthesis (syngas to i-paraffin)
[224]	2013	Ru,Al_2O_3@Pd,silicalite-1	ɣ-Al_2O_3	Pellet	Porous	1.66 mm	Ru loading	Conventional HT @ 180 °C, 24h, rotation	Pd loading	Bifunctional catalyst for liquid-phase tandem reaction of glycerol conversion
[225]	2013	Co,SiO_2@silicalite-1@ ZSM-5(H^+)	SiO_2	Pellet	Porous	0.85-1.7 mm	Co loading	2 x (Conventional HT 180 °C, 24h)	-------	Bifunctional catalyst for modified Fischer-Tropsch synthesis (syngas to i-paraffin)
[226]	2013	Co,SiO_2@ZSM-5(H^+); Co,SiO_2@silicalite-1, Co,SiO_2,TiO_2 @ZSM-5(H^+)	SiO_2 & SiO_2,TiO_2	Sphere	Porous	300-500 µm	Co loading	Conventional HT @ 180 °C, 24h, rotation	-------	Bifunctional catalyst for modified Fischer-Tropsch synthesis (syngas to i-paraffin)
[227]	2012	Pd,SiO_2@silicalite-1@ ZSM-5(H^+)	SiO_2	Pellet	Porous	0.85-1.7 mm	Pd loading	2 x (Conventional HT @ 180 °C, 24h)	-------	Bifunctional catalyst for tandem reaction

										(syngas to dimethyl ether)
[228]	2012	Co,SiO_2@β-zeolite	SiO_2	Pellet	Porous	0.85-1.7 mm	Co loading	Modified VPT HT @ 150 °C, 96h, rotation	-------	Shape-selective modified Fischer-Tropsch synthesis (syngas to i-paraffin)
[229]	2012	Raney Fe@ZSM-5(H^+)	Raney Fe (Fe 50 Al 50 Alloy)	Ground ribbon	-------	40-80 mesh	-------	Conventional HT @ 180 °C, 2d	-------	Shape-selective modified Fischer-Tropsch synthesis (syngas to i-paraffin)
[230]	2011	Cr/ZnO@silicalite-1@ ZSM-5(H^+)	Cr,ZnO	Pellet	Mesoporous	0.85-1.7 mm	-------	2 x (Conventional HT @ 180 °C, 24h, rotation)	-------	Bifunctional catalyst for CO_2 hydrogenation to dimethyl ether
[231]	2011	Fused iron@ZSM-5(H^+)	Fused iron	Pellet	-------	0.85-1.7 mm	-------	2 x (Conventional HT @ 180 °C, 24, rotation)	-------	Shape-selective modified Fischer-Tropsch synthesis (syngas to i-paraffin)
[232]	2011	Co,Zr@ZSM-5(H^+)	Co-precipitated Co and Zr catalyst	-------	-------	200-400 mesh	Treating with TPAOH @ 110°C, 4h & soaking in ethanol	Conventional HT @ 180 °C, 5, 7d, rotation	-------	Bifunctional catalyst for modified Fischer-Tropsch synthesis (syngas to i-paraffin)
[233]	2010	CZA@ZSM-5(H^+) & CZA@silialite-1	Cu,ZnO,Al_2O_3 composite (CZA)	Pellet	-------	0.85-1.7 mm	-------	Conventional HT @ 180 °C, 24h, rotation	-------	Bifunctional catalyst for CO_2 hydrogenation to dimethyl ether
[234]	2010	SiO_2@ZSM-5	SiO_2	Spherical	Mesoporous	200-300 μm	-------	Conventional HT @ 170 °C, 1h-7d	-------	-------

[235] [236]	2010	Rh,activated carbon@silicalite-1, Pd,Co,activated carbon@silicalite-1	activated-carbon	-------	Mesoporous	0.45-0.9 mm	Rh loading	2 x (Conventional HT @ 180 °C, 2d, rotation)	Silica deposition in shell macropores	Shape-selective hydroformylation of 1-hexene
[237]	2008	Ru,SiO_2@ZSM-5(H^+)	SiO_2	Pellet	Porous	0.85-1.7, 0.5-0.85, 0.38-0.5 mm	Ru loading	Conventional HT @ 180 °C, 24h, rotation	-------	Bifunctional catalyst for modified Fischer-Tropsch synthesis (syngas to i-paraffin)
[238]	2008	Co,Al_2O_3@β-zeolite (BEA(H^+))	γ-Al_2O_3	Pellet	Porous	0.35-0.83 mm	Co loading, treating with TEAOH @ 114°C, 4h	Conventional HT @ 155 °C, 3d, rotation	-------	Bifunctional catalyst for modified Fischer-Tropsch synthesis (syngas to i-paraffin)
[239]	2008	Co,SiO_2@ZSM-5(H^+)	SiO_2	Pellet	Porous	0.85-1.7 mm	Co loading	Conventional HT @ 180 °C, 1,2,7d, rotation	-------	Bifunctional catalyst for modified Fischer-Tropsch synthesis (syngas to i-paraffin)
[240]	2007	Co,SiO_2@ZSM-5(H^+)	SiO_2	Pellet	Porous	0.85-1.7, 0.5-0.85, 0.38-0.5 mm	Co loading	Conventional HT @ 180 °C, 1,2,7d, rotation	-------	Bifunctional catalyst for modified Fischer-Tropsch synthesis (syngas to i-paraffin)
[241]	2006	Pt,γ-Al_2O_3@ Zeolite A (Na^+)	Pt,γ-Al_2O_3	Sphere	Porous	1.5 mm	Pt loading, Treating with NaOH	Conventional HT @ 180 °C, 3h		Shape-selective oxidation reaction of a mixture of CO and n-butane
[242] [243]	2006, 2005	Co,SiO_2@ZSM-5(H^+)	SiO_2	Pellet	Porous	0.85-1.7, 0.38-0.50 mm	Co loading	Conventional HT @ 180 °C, 1,2,7d, rotation	-------	Bifunctional catalyst for modified Fischer-Tropsch synthesis (syngas to i-paraffin)
[126]	2005	Pt/TiO_2@silicalite-1	TiO_2	Sphere	Mesoporous	0.5 mm	Pt loading	2 x (Conventional HT @ (1) 180 °C,	-------	Shape-selective hydrogenation of 1-hexene and

								2h, rotation, and (2) 180 °C, 2d)		dibranched 3,3-dimethylbut-1-ene
[122]	2001	SiO_2,Al_2O_3@silicalite-1	SiO_2,Al_2O_3	-------	Porous	~ 1 mm	-------	Conventional HT @ 180 °C, 1d	-------	Shape-selective toluene disproportionation

Epitaxial nucleation and growth of a new crystalline phase over the external surface of another zeolitic support have also permitted the formation of all-zeolite core@shell material. Structural similarities between the zeolitic support (core) and the targeted zeolitic shell promote the intergrowth of the two elements under specific synthetic conditions [244]. By taking advantage of this property, one can easily form a zeolitic shell of a certain type of zeolite over a support with similar structure. Although the properties such as acidity can be managed differently in each compartment [245], zeolites with structural similarities usually provide similar characteristics, especially the ones which are related to the pore structures. Some examples of zeolitic core@shell formed using this technique are presented in Table 1.3.

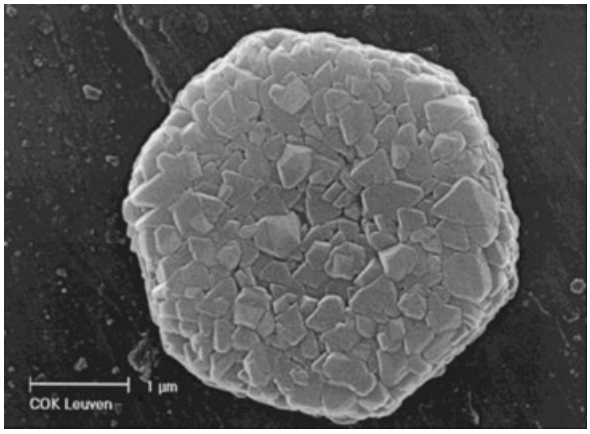

Figure 1.10- EMT@FAU all zeolite composite, formed by crystal overgrowth (Reprinted with permission from [246]. Copyright 1999 Wiley.).

Although this technique seems to be simpler than the seeded growth technique, some shortcomings need to be taken into account: One of the biggest concerns in this method is the chemical compatibility of the core in the crystallization conditions of the zeolitic shell. This problem prevents using different core materials to synthesize a core@shell through a one-pot synthesis procedure [118, 165, 166, 192]. The competition between nucleation centers in the bulk gel and on the core surface which leads to abundant bulk crystal formation is another challenge which has to be addressed [247, 248]. However, the core@shell crystals can be simply separated from the bulk crystals through sedimentation/centrifugation process when their sizes are sufficiently different.

In addition to the techniques, summarized in Table 1.3, which all require the addition of pre-synthesized zeolitic core crystals to the synthesis mixture, there are few reports on the synthesis of zeolite@zeolite synthesis without any pre-synthesized cores [249, 250]. For instance, ZSM-5 microcrystals covered with a hierarchical ZSM-5 shell (vesicular or lamellar ZSM-5 zeolite shell) were recently synthesized from a homogeneous zeolite gel mixture using a dual-templating technique [250].

Table 1.3- Core@shell materials, synthesized using zeolite overgrowth over the crystalline zeolitic shell.

Ref.	Year	Product	Core				Pre-treatment	Crystallization	Post-treatment	Application
			Core	Shape	Porosity	Size				
[251]	2016	ZSM-5(H^+)@silicalite-1	ZSM-5(H^+)	Single crystal	Hierarchical	2-3 μm	Desilication using NaOH	Conventional HT @ 140 °C, 24h	Ion-exchange	Methanol conversion into gasoline and diesel
[252]	2016	ZSM-5(H^+)@silicalite-1	ZSM-5(H^+)	Single crystal	Microporous	-------	-------	2 x (Conventional HT @ 180 °C, 24h, rotation)	-------	Xylene isomerization
[253]	2015	C,Y@Y(H^+)	Y(Na^+)	Single crystal	Microporous	2-6 μm	-------	Conventional HT @ 140 °C, 6h	Ion-exchange	Dehydrations of 1-phenylethanol
[125]	2015	ZSM-5(Na^+)@silicalite-1	ZSM-5	Single crystal	Microporous	<100 nm	Annealing @ 170 °C, 12d	Conventional HT @ 100 °C, 20h	Annealing @ 170 °C, 12d, & Ion-exchange	Ketonization and Cracking reactions
[254]	2015	Ga,Al-ZSM-5@silicalite-1	Ga,Al-ZSM-5	Sphere	Microporous	10 μm	-------	Conventional HT @ 180 °C, 24h	Ion-exchange	Aromatization of propane and n-butane & Cracking of 1,3,5-triisopropylbenezene
	2015	ZSM-5(H^+)@silicalite-1 (*b*-oriented)	ZSM-5(H^+)	Single crystal	Microporous	-------	Treatment with 20% NH_4OH for 5h	Conventional HT @ 180 °C, 24h	-------	Alkylation of toluene with methanol
[255]	2014	Fe-ZSM-5@silicalite-1	ZSM-5	Single crystal	Microporous	200 nm	PDADMAC	Conventional HT @ 200 °C, 1h	-------	Selective catalytic reduction (SCR) with ammonia

[220]	2014	Ni,Mo,Y(H^+)@hierarchical β-zeolite (BEA(H^+))	Y(Na^+)	Single crystal	Microporous	-------	-------	Conventional HT @ 140 °C, 108-216h	Ion-exchange & Ni, Mo loading	Hydrocracking
[256]	2013	ZSM-5@SAPO-5	ZSM-5	Single crystal	Microporous	-------	-------	Conventional HT @ 180 °C, 24h	-------	FCC
[247]	2013	Al-TON@Si-TON	Al-TON	Needle	Microporous	30 μm	-------	Conventional HT @ 160 °C, 5d	-------	Skeletal isomerization of tetradecane
[257]	2013	ZSM-5(H^+)@silicalite-1, Mo,ZSM-5(H^+)@silicalite-1	ZSM-5	Polycrystalline	Microporous	>1 μm	Mo loading	Conventional HT @ 180 °C, 1d	-------	Methane dehydroaromatization
[258]	2011	Al-ZSM-5@silicalite-1	ZSM-5	Single crystal	Microporous	10-20 μm	-------	Conventional HT @ 180 °C, 90h	-------	Methylation of toluene with methanol
[259]	2011	Al-MWW(H^+)@B-MWW	Al-MWW or MCM-22	Platelet	Microporous	20 nm thickness	-------	Conventional HT @ 170 °C, 4h-5d	Ion-exchange	Toluene disproportionation to para-xylene
[260]	2011	ZSM-5(H^+)@silicalite-1	ZSM-5(H^+)	Single crystal	Microporous	50 x15x15 μm	-------	Conventional HT using F^-	-------	oligomerization of styrene, methanol-to-olefin conversion & aromatization of light naphtha derivatives
[261]	2010	ZSM-5(H^+)@silicalite-1	ZSM-5(H^+)	Single crystal	Microporous	-------	-------	Conventional HT @ 180 °C, 15d using F^-	-------	
[248]	2010	Pt,FAU@LTA	FAU	Single crystal	Microporous	60-90 μm	Ion-exchange	Conventional HT @ 85 °C, 12-72h	Ion-exchange	CO chemisorption
[262]	2010	LTL(K^+)@LTL(Ba^{2+})	LTL(K^+)	Needle & cylindrical	Microporous	<5 μm	-------	Conventional HT @ 85 °C, 2d	-------	-------
[216]	2009	β-zeolite@MOR	as-synthesized β-zeolite	Single crystal	Microporous	<5 μm	-------	Conventional HT @ 170 °C, 21h	-------	Methanol dehydration to dimethyl ether

[263]	2009	ZSM-5@silicalite-1	ZSM-5(H^+)	Single crystal	Microporous	10 μm	-------	Conventional HT @ 180 °C, 24h, rotation	-------	Alkylation of toluene with methanol
[264]	2009	MOR@ZSM-5	MOR	-------	Microporous	-------	TPAOH loading	Conventional HT @ 130 °C, 48h	-------	-------
[265]	2008	β-zeolite@SAPO-11	β-zeolite (BEA(H^+))	Single crystal	Microporous	<2 μm	-------	Conventional HT @ 200 °C, 35h	-------	Cracking of 2-butylene
[266]	2008	ZSM-5(H^+)@silicalite-1	ZSM-5(H^+)	Single crystal	Hierarchical	1-2 μm	-------	4 x (Conventional HT @ 170 °C, 24h, rotation)	Ion-exchange	Methanol to gasoline
[267]	2008	ZSM-5(H^+)@silicalite-1	ZSM-5(H^+)	Single crystal	Microporous	5 μm	-------	3 x (Conventional HT @ 180 °C, 24h, agitation)	-------	Alkylation of toluene with methanol
[268]	2006	EMT@MAZ	EMT	Single crystal	Microporous	2-3 μm	-------	Conventional HT @ 100 °C, 6d	-------	-------
[269]	2006	ZSM-5(H^+)@silicalite-1	ZSM-5(H^+)	Single crystal	Microporous	10 μm	-------	2 x (Conventional HT @ 180 °C, 24h)	-------	Alkylation of toluene with methanol
[270]	2006	ZSM-5@SAPO-11	ZSM-5(H^+)	Single crystal	Microporous	<5 μm	-------	Conventional HT @ 185 °C, 24h	-------	FCC gasoline hydro-upgrading catalyst
[245]	2005	ZSM-5(H^+)@silicalite-1	ZSM-5(H^+)	Single crystal	Microporous	3 μm	-------	Conventional HT @ 180 °C, 24h	-------	Alkylation of toluene with methanol
[246]	2001	EMT@FAU	EMT	Single crystal	Microporous	2-3 μm	-------	Conventional HT @ 100 °C, 72h	-------	-------

1.5.2.3 Physical Coating Technique

As mentioned in Section 1.5.2.1.1, self-assembly of colloidal nanoparticles around the micron-sized core, as the first physical technique proposed, suffers from mechanical instability and hierarchical shell porosity issues (Figure 1.8). By using a modified physical procedure, more stable zeolitic shells were recently formed around a macroscopic catalyst. In this method, as-prepared zeolitic crystals are coated around a hard template using a binder. Using this technique, some of the main disadvantages of the previously mentioned techniques such as core dissolution, the negative effect of crystallization steps on the active sites within the core part and bulk crystal formation, can be circumvented (Table 1.4).

Figure 1.11- Preparation of CuZnAl@SAPO-11 catalyst by physical coating method (Reprinted with permission from [271]. Copyright 2015 Elsevier.).

Using a binder imposes some problems such as dilution effect, i.e., reducing active sites concentration, and active site accessibility. Moreover, this technique is mainly applicable for macroscopic supports rather than small micron-sized cores.

Table 1.4- Core@shell materials, synthesized using the physical coating technique.

Ref.	Year	Product	Core				Surface modifier	Binder (Adhesive)	Application
			Core	Shape	Porosity	Size			
[271]	2015	(Cu/ZnO/Al_2O_3)@SAPO-11	CuZnAl composite	Pellet	-------	0.85-1.7 mm	-------	Silica sol	Syngas to dimethyl ether
[272]	2015	(1.6%Ni,1.2%Mg, $Ce_{0.6}Zr_{0.4}O_2$)@ β-zeolite (BEA(H^+))	Ce,Zr, Ni,Mg composite	Pellet	-------		-------	Silica sol	Steam reforming of toluene and methane
[225]	2013	Co,SiO_2@ZSM-5(H^+)	SiO_2	Pellet	Mesoporous	0.85-1.7 mm	-------	Silica sol	Modified Fischer-Tropsch synthesis (syngas to i-paraffin)
[273]	2013	(Cr/ZnO)@SAPO-46	Cr,ZnO	Pellet	-------	0.85-1.7 mm	-------	Silica sol	Syngas to dimethyl ether
[141]	2001	PS@shell (shell: A, Y, β and silicalite-1 zeolites)	PS	Sphere	-------	4-8 µm	Redifloc	-------	-------
[131]	2000	PS@silicalite-1, PS@β-zeolite	PS	Sphere	-------		PDADMAC, PSS	-------	-------
[142]	2000	PS@silicalite-1	PS	Sphere	-------	640 nm	PDADMAC, PSS	-------	-------

1.6. Synthesis of Hollow and Yolk-Shell Zeolitic Material

As discussed earlier, in the early stages of synthesizing zeolitic core@shell materials, zeolitic thin films were placed around fibrous materials, leading to composites (Figure 1.7). The inner compartment was an inert support, causing several problems including decreasing the concentration of the active sites, lowering the specific surface area and creating mass/heat transfer problems, etc. Soon after, it was realized that these inner supports could easily be removed if a stable self-standing zeolitic film covers them, leaving behind an all-zeolite hollow fiber with improved mass transfer property [132]. Moreover, these hollow zeolitic shells have a high specific surface area and low density and provide encapsulation properties. Therefore, zeolitic yolk-shell and hollow materials were being started to develop in parallel with their zeolitic core@shell relative, sometimes by a simple post-treatment such as calcination or extraction (Figure 1.9).

The formation of hollow and yolk-shell materials possessing a porous shell made of an inorganic oxide (mainly mesoporous silica) or carbon and their application have been extensively studied [127, 274, 275]. However, as mentioned previously, because of the fundamental differences, those methods cannot be extended for fabricating materials with the zeolitic shell. Hollow zeolitic spheres have been synthesized applying two main methods: templating method, post-treatment method or a combination of both.

The yolk-shells, however, are mainly formed by synthesizing a core@shell using techniques outlined in Section 1.5, followed by selective partial removal of one of the components or both at their interface through chemical extraction (etching) method. An alternative method is to first synthesize a multilayer core@shell material with at least three different layers and then selectively remove the middle layer(s) using a chemical extraction or calcination techniques [127, 149]. The former method can be considered as a post-treatment method while the second can be somehow categorized as the templating technique. The templating technique is similar to core@shell synthesis process, discussed in Section 1.5 and will not be reviewed here. Yolk-shell materials have recently been synthesized using a method initially used for hollow zeolites, called dissolution-recrystallization, which will be discussed in Section 1.6.2.2.

1.6.1 Templating Technique - Seeded Growth Technique

In Section 1.3, various types of templates which can be used to create meso-macroporous (hierarchical) network within zeolitic structures were reviewed. Using discrete micron-sized hard templates provides the possibility of creating macrostructured materials with extremely large cavities and hollow domains [276, 277]. Discrete hollow zeolitic materials, however, need a more controlled synthesis procedure, such as self-assembly of nanocrystals around a hard template using a multi-step LBL technique (Figure 1.9) [129, 131, 141, 142]. Due to the interstitial pores created between deposited nanocrystals, such assembly of nano-zeolites around a template produces core@shell or hollow zeolitic spheres with meso-microporous shells. This hierarchical porosity of the shell can be advantageous for some applications [217-220]. Seeking an entirely microporous hollow zeolite, this technique needs, however, to be usually merged with seeded growth technique, as described in Section 1.5.2.1.2. This technique was initially used to synthesize a self-standing hollow fiber with an entirely microporous wall [132] and later hollow spheres [99, 100, 133, 188]. Over the last decade, this technique has been widely adapted to synthesize hollow zeolitic materials with various encapsulated species in their interiors, as summarized in Table 1.5. The hollow zeolitic material has also been synthesized using in-situ seed-free crystallization method [234, 249, 278-283]. However, this method has mostly led to low-quality hollow spheres with mechanically-weak and non-uniform meso-macroporous shell.

Table 1.5- Hollow and yolk-shell zeolitic materials, synthesized using the seeded growth technique.

Ref.	Year	Product	Core				Pre-treatment	Surface modifier	Crystallization	Application
			Core	Shape	Porosity	Size				
[214]	2016	Hollow ZSM-5 & ZnO, silicalite-1 (Bayberry-like)	SiO_2	Sphere	Porous	15 μm	-------	-------	SAC HT @ 180 °C, 1d	Methanol to aromatics
[284, 285]	2012	Hollow Pt,silicalite-1	SiO_2	Sphere	Mesoporous	1-2 μm	Pt loading	APTES	Conventional HT @ 170 °C, 72h	Racemization reaction, Tandem Reaction
[286]	2011	Hollow silicalite-1	SiO_2	Sphere	Mesoporous	3-4 μm	-------	PDADMAC	Conventional HT @ 175 °C, 12h	Mixed matrix membranes for gas separation
[287]	2011	Hollow silicalite-1	Oil/water emulsion	Sphere	-------	20-50 μm	-------	-------	Conventional HT @ 85 °C, 3d	-------
[135]	2010	Hollow silicalite-1	SiO_2	Sphere	Mesoporous	1 μm	-------	PDADMAC, PSS	Conventional HT @ 90 °C, 8h	------
[128]	2010	Hollow FAU	β-zeolite	Single crystal	Microporous	1-2 μm	-------	-------	Conventional HT @ 90 °C, 22h	-------
[288]	2009	Hollow silicalite-1	SiO_2	Sphere	Mesoporous	2-4 μm	-------	PDADMAC	Conventional HT @ 175 °C, 2-24h	Selective gas adsorption
[289]	2008	Hollow Ni,ZSM-5 (magnetic)	PS	Sphere	-------	3 μm	Ni loading	PDADMAC	Conventional HT @ 80 °C, 24-54h	-------
[137]	2008	Hollow: Silicalite-1/ ZSM-5/ Va, Cu,ZSM-5(H^+)/ APTES,Silicalite-1/ Cu,ZSM-5/ V, ZSM-5	SiO_2	Sphere, Tube	Mesoporous	------	Guest species loading (Metal/APTES)	PDADMAC	VPT HT @ 160 °C, 2d	-------
[217, 290]	2007	Hollow Pt,silicalite-1, Hollow Ag,silicalite-1	SiO_2	Sphere	Mesoporous		NH_2-modification, and Pt/Ag loading	PDADMAC	2 x (Conventional HT @ (1) 100 °C, 1h, and (2) 100 °C, 8h)	Oxidation of aromatic/aliphatic alcohols in liquid/gas phase [217] & Heck coupling for various substrates [290]

[130]	2005	Hollow ZSM-5	SiO_2	Sphere	Mesoporous	------	------	Seeding (Pulse Laser deposition)	VPT HT @ 145 °C, 3-7d	-------
[99, 100]	2003	<u>Hollow:</u> silicalite-1/ Ag,silicalite-1/ Fe_2O_3,silicalite-1/ PdO,silicalite-1 <u>Yolk-shell:</u> Carbon,silicalite-1 / PDVB,silicalite-1	SiO_2	Sphere	Mesoporous	3-6 μm	Guest species loading (Metal, oxide, C, polymer)	PDADMAC & PDADMAC, PSS	VPT HT @ 140 °C, 48h & Conventional HT @ 100 °C, 24h	-------
[101]	2002	Hollow silicalite-1/ Hollow Fe_2O_3, silicalite-1	SiO_2	Sphere	Mesoporous	3-6 μm		PDADMAC	VPT HT @ 140 °C, 48h	-------
[133]	2002	Hollow silicalite-1	PS	Sphere	-------	10, 260 μm	-------	Redifloc	Conventional HT @ 95 °C, 48h	-------

The types of the template used can generally be divided into two main groups; siliceous and non-siliceous. Non-siliceous hard templates such as PS beads can be selectively removed after crystallization and shell formation through chemical treatments or calcination [131, 141, 142].

Siliceous templates, usually mesoporous silica materials, are of great importance since this type of template is consumed during the secondary growth step by providing Si for growing crystals [99-101, 137, 138, 291]. This phenomenon might eliminate the need for final calcination in some cases when no molecular organic SDA is used. Moreover, various shapes of the mesoporous siliceous template can be easily prepared and used for synthesizing hollow zeolites with different shapes and morphology such as spheres and tubes [132, 291]. The highly porous network of this template can also be infiltrated with inorganic guest species which after crystallization will be encapsulated inside a microporous shell [99, 100]. Although most of the siliceous templates used were amorphous silica, it is observed that some crystalline cores would also be dissolved or consumed by the growing shell if the secondary growth step is long enough [165], leading to hollow zeolite formation [128, 191].It was shown that by using this technique, the seed growth orientation could also be controlled using quartz fibers [112] (Figure 1.7).

This technique suffers from some drawbacks mainly related to its long preparation procedure. Moreover, the templates cannot often be recovered. The hollow products are normally polycrystalline and thick (> 200-300 nm), causing mass transfer limitations due to long diffusion path and pore blocking.

1.6.2 Post Treatment

This technique is used to synthesize both hollow and yolk-shell materials, starting from an already prepared zeolite.

1.6.2.1 Dissolution (Selective Desilication)

As mentioned earlier, desilication is one of the widely-used techniques to create mesoporosity in a zeolite crystal. Proper desilication can be achieved by simple treatment of a zeolite, in its as-prepared or calcined form, with a basic solution at a moderate temperature for a short period of time. It was initially found that the hierarchy formation based on desilication process is much more favorable in the zeolites with low Al concentration (20< Si/Al <50), however, later this restriction have been circumvented by taking advantages of the many controlling parameters (such as Al gradient [140, 292, 293], Si/Al ratio, nature of the framework [140, 189, 294-296] or extra-framework species [292, 297-299]). This opportunity has also been exploited to create hollow zeolites (Table 1.6).

In this regard, controlled mild desilication in some specific cases of zeolites led to hollow zeolites [140, 189, 300-302]. As shown in Figure 1.12, the hollow spheres are created by selective extraction of silicon from the core of a crystal when in a single crystal, inner parts are richer in Si [140]. However, this technique cannot be applied to the majority of zeolites and might lead to extremely heterogeneous structures. It means that if the Al-gradient within a crystal does not follow the above-mentioned trend, i.e., Al-poor interior and Al-rich exterior (Al zoning [302]), this technique leads to different porous structures than hollow zeolites. β-zeolite@Y double shell and hollow Y zeolites have also been produced by taking advantage of this Al-zoning property [191].

The beneficial point of this technique is the ability to decrease the shell thickness to few nanometer, which is critical for many applications. However, this method is just applicable to a limited number of zeolites with certain properties such as Al-zoning. This method might also create mesopores on the hollow shell [140, 218].

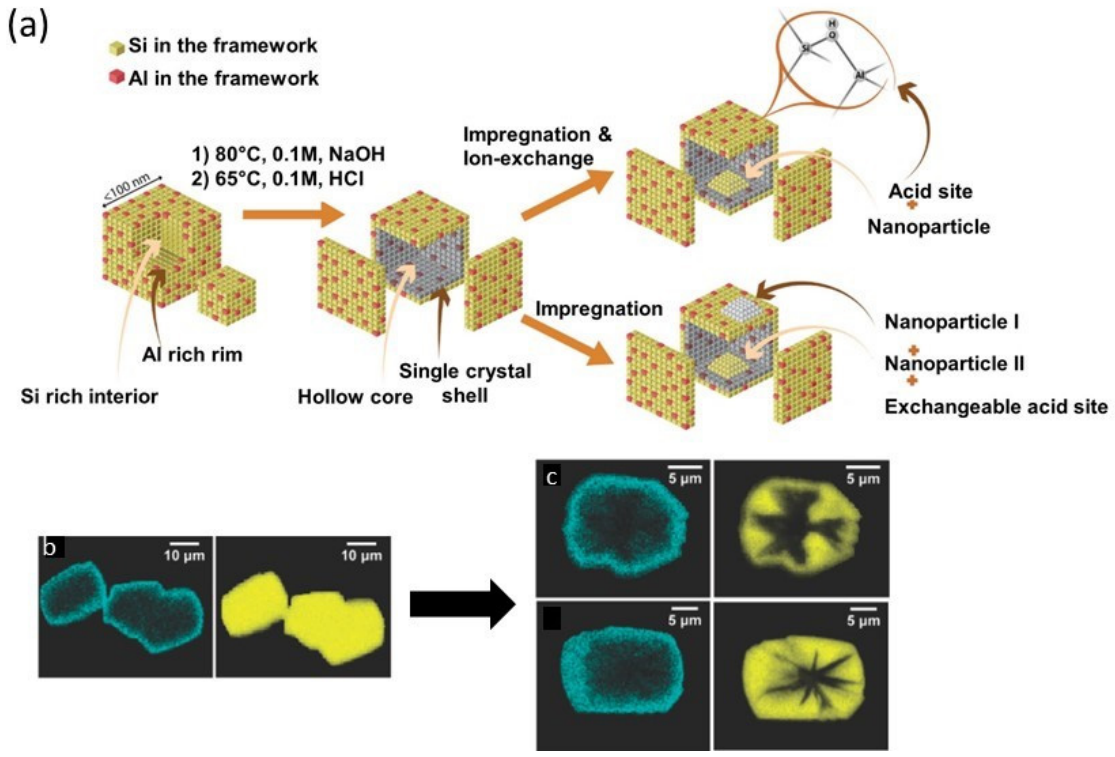

Figure 1.12- (a) Scheme of making multifunctional nanoreactors by selective desilication (Reprinted with permission from [303]. Copyright 2015 Wiley.), and (b,c) SEM-EDS images of large crystal ZSM-5: (b) before alkaline treatment, (c) after alkaline treatment (Blue and yellow colors represent aluminum and silicon, respectively) (Reprinted with permission from [140]. Copyright 2005 ACS.).

Table 1.6- Hollow and yolk-shell zeolitic materials, synthesized by using post treatment – Desilication.

Ref.	Year	Product	Starting Materials		Pre-treatment	Desilication		Post-treatment	Application
			Core	Size		Condition	Base		
[218]	2015	Hollow Pt, ZSM-5	ZSM-5	~200 nm	Pt loading	Stirring @ 80 °C, 12h	Na_2CO_3	-------	hydrogenation of toluene and trimethylbenzene
[303]	2015	Hollow Fe, ZSM-5, Hollow Fe,Pt,ZSM-5, Hollow Co,ZSM-5	ZSM-5	~100 nm	-------	Stirring @ 80 °C, 10h	NaOH	Acid wash & Fe, Fe/Pt or Co loading	-------
[304]	2015	Hollow ZSM-5	ZSM-5	~100 nm	-------	Stirring @ 80 °C, 2, 5, 10, 20, and 30min; 1, 2, 4, and 10h	NaOH	Acid wash	-------
[300]	2014	Hollow ZSM-5	ZSM-5	~100 nm	-------	Stirring @ 80 °C, 10h	NaOH	Acid wash	-------
[305]	2011	Hollow mesoporous zeolite	ZSM-5 (Mesoporous)	<1 µm	-------	Stirring @ 60 °C, 3h	Na_2CO_3	-------	Methylene blue adsorption
[140]	2005	Hollow ZSM-5	ZSM-5	20 µm	-------	Stirring @ 65 °C, 15-30min	NaOH	Ion-exchange	-------

1.6.2.2 Dissolution-Recrystallization Technique

Dissolution-recrystallization method involves simultaneous processes of selective dissolution of Si species from the interior part of a zeolite and consumption by the exterior part, forming a fully microporous shell at the end [306, 307]. In contrast to desilication technique, the Al gradient (Al-zoning) is not the driving force for such dissolution. It is shown that the area of a crystal which contains higher concentrations of defect sites starts dissolving and providing Si for more crystalline part to grow [308]. This method has been used to synthesize hollow zeolitic materials with encapsulated guest species for various reactions [121, 124, 218, 219, 308]. In this method, pre-synthesized bulk single crystals of silicalite-1 were initially impregnated with metal precursors, followed by hydrothermal treatment at high temperature in the presence of the corresponding zeolite SDA in its hydroxide form, i.e., TPAOH, and final calcination [114]. Such treatment led to the formation of metal nanoparticles entrapped in a thin shell, made of fully microporous silicalite-1 zeolite. All these procedures promoted by high-temperature and pH of the secondary hydrothermal process [114].

The same concept has also been used to synthesize large hollow aggregates of zeolites. The process is described based on the Ostwald ripening phenomenon, in such a way that larger crystals grow by consuming more soluble smaller ones [281]. Within the primitive aggregates, the smaller crystals dissolve into the liquid phase and serve as nutrients for recrystallization on the surface of larger crystals. Voids gradually form and grow in the cores of large aggregates, and in the meantime, the shell thickness increases [281]. In general, this method offers many advantages. It was found extremely efficient and less destructive, in comparison to simple desilication. This approach applies to the zeolites without Al gradient within the crystal. If all the dissolved species go back to the crystalline hollow structure *via* recrystallization process, the composition of the starting gel and final product does not severely change and no material will be wasted. The shell seems to be more uniform and complete due to recrystallization over the outer shell. Finally, the shell thickness can be finely tuned [114].

Table 1.7- Hollow and yolk-shell zeolitic materials, synthesized using post treatment – Dissolution- Recrystallization.

Ref.	Year	Product	Starting Materials		Pre-treatment	Dissolution Recrystallization		Post-treatment	Application
			Core	Size		Conditions	Base		
[219]	2015	Cu/Ni/Co,silicalite-1/ ZSM-5 yolk-shell	ZSM-5, silicalilite-1	200 × 150 × 140 nm	Metal (Cu, Ni & Co) loading	Conventional HT @ 170 °C, 24h	TPAOH	Reduction at high temperature	Shape-selective hydrogenation of toluene and trimethylbenzene
[309]	2015	Hollow ZSM-5, Double shells (Hollow ZSM-5@silicalite-1, Hollow ZSM5 @Hollow@ZSM-5), Hollow Fe_2O_3,C nanotube, ZSM-5 & Hollow CuO,Pd, ZSM-5	ZSM-5, Hollow ZSM-5@silicalite-1@ZSM-5	120 × 180 nm	Metal (Fe, Cu or Pd) loading	Conventional HT @ 170 °C, 3d	TPAOH	Carbonization	Biphenyl methylation with methanol
[310]	2015	Hollow Pd, silicalite-1 & Hollow Pd, CuO, silicalite-1	Silicalite-1	~ 100-150 nm	Metal (Pd, Pd-CuO) loading	Conventional HT @ 170 °C, 3d	TPAOH	-------	Shape-selective Suzuki – Miyaura reaction
[121]	2014	Hollow Pt, silicalite-1	Silicalite-1	<200 nm	Pt loading	Conventional HT @ 170 °C, 24h	TPAOH	-------	Shape-selective hydrogenation of toluene and trimethylbenzene
[124]	2014	Hollow Pt, silicalite-1	Silicalite-1	<200 nm	Pt loading	Conventional HT @ 170 °C, 24h	TPAOH	-------	Shape-selective oxidation of CO in the Presence of Propylene
[311]	2014	Hollow phosphotungstic acid, silicalite-1	Silicalite-1	~100 nm		Conventional HT @ 170 °C, 3d	TPAOH	Phosphotungstic acid formation	Esterification reaction

[308]	2013	Hollow Au,silicalite-1	Silicalite-1	<200 nm	Au loading	Conventional HT @ 170 °C, 24h	TPAOH	-------	
[307]	2013	Hollow silicalite-1	Silicalite-1	150 nm	-------	Conventional HT @ 170 °C, 24h	TPAOH	NH_4F treatment	-------
[312]	2013	Hollow ZSM-5	-------	-------	-------	Conventional HT @ 140 °C, 2d => Conventional HT @ 120 °C, 3d	-------	-------	Alkylation of toluene with benzyl chloride, Acetalization of cyclohexanone
[313]	2013	Hollow silicalite-1, Hollow Ag,silicalite-1	Silicalite-1	150-500 nm	Ag loading	Conventional HT @ 175 °C, 3d	TPAOH / TPAOH + NaOH	-------	-------
[139]	2011	Hollow sodalite spheres	Zeolite A	-------	High- pressure aging of the gel	Conventional HT @ 90 °C in a closed bottle for 3d and in the open bottle for 4d	-------	-------	-------
[314]	2008	Hollow ZSM-5 Hollow silicalite-1	Silicalite-1	100-200 nm / 0.5-1 µm	-------	Conventional HT @ 170 °C, 1-24h	TPAOH/ TBAOH/ TMAOH	-------	-------

1.7 Applications

Zeolites showed exceptional performance in many applications such as ion-exchange, adsorption, catalysis, separation. Zeolites, especially the synthetic ones, became one of the most popular heterogeneous catalysts in the chemical industry (petrochemical, oil refinery and fine chemical synthesis) upon the discovery and application of zeolite X (and Y) in the 1960s and ZSM-5 in the 1970s [10]. Water and waste-water treatments, drying agent especially for the gas streams, shape-selective separation such as separation of branched hydrocarbons from linear ones and more recently biomedical applications, i.e., imaging, wound healing and drug delivery, chemical sensors, ion-exchanged electrodes, low dielectric constant materials, micro fuel cells and bio-refinery, i.e., catalyzing the conversion of biomass to chemicals and fuels and others are all showing the diverse capability and versatility of zeolitic materials [19, 24, 27, 31-33, 67, 68, 80]. They have earned their reputation because of their outstanding and unique properties, as summarized in Section 1.2.4. The structured zeolitic materials, with or without hierarchical porosity, have significantly enhanced their effectiveness in traditional applications, and also opened windows toward finding novel applications. For example, zeolite membranes, as macroscopic planar counterparts of zeolitic core@shell materials, are one of these rationally designed zeolitic structures, which have proven their competence in many applications (some mentioned above) [123, 175-177, 315].

This report is not dealing with macroscopic structured hierarchical zeolites, especially the fibrous ones, a detailed review of which can be found in [187]. Here, we chose to focus on zeolitic core@shell or hollow materials with a zeolitic shell. These rationally designed novel zeolitic architectures can boost the classical zeolite performances in previously developed or new application processes due to their custom-made properties [122, 211, 233, 239]. These properties have mainly emerged from highly synergetic combinations of at least two parts which can be intrinsically different. In this type of structure, one of the most important characteristics of zeolites, i.e., being selective at the molecular level, is mainly aimed to be inherited. From catalytic and separation viewpoints, such a composite, in which the accessibility of the active sites is governed by the microporous shell, can be a material with ultimate desirable properties [119, 120]. In addition, efficient confinement of the core compartment inside a shell of microporous crystalline zeolite creates highly stable microcapsules [99, 100, 133, 188, 217, 290]. The applications of these novel core@shell,

yolk-shell and hollow zeolitic materials, mostly at lab-scale, are summarized in Tables 1.1-1.7. Most of the applications are related to the field of catalysis and adsorptive separation. Some of the important achievements are discussed in this section.

1.7.1 Adsorptive Separation

Zeolites have been long identified as excellent materials for adsorption and separation purposes, especially Al-rich ones (Si/Al ≈ 1) which provide high exchange capacities. It was shown that in addition to surface properties (hydrophilicity and hydrophobicity) which directly depend on Al content [316], the separation power of a zeolite is directly related to its pore size, i.e., for the high separating ability the pore size should match the molecular size of the adsorptive. This characteristic might sometimes, depending on molecular size, reduce the adsorption capacity of the zeolite used. For instance, zeolites with 10-membered rings were found as the most efficient separators of branched and linear hydrocarbons, while 12-membered ring zeolites were found to be more proper storage materials. Therefore, rationally structured composites could serve as more efficient candidates (Figure 1.13).

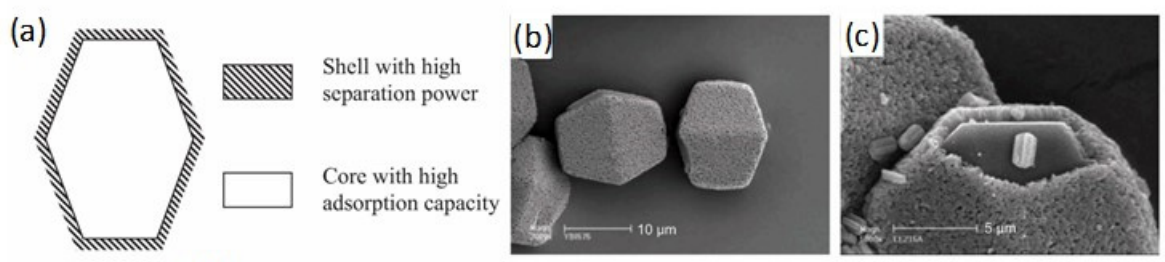

(d)

Sample	Loading [mg g^{-1}]		
	Butane	Toluene	TMB
Silicalite-1	93.8	75.4	5.3
β-Zeolite	112.2	94.4	99.8
Core–shell [a]	96.4	80.3	2.6

Figure 1.13- (a) Schematic representation of a core@shell adsorbent, (b,c) SEM images of β-zeolite@silicalite-1 composite, and (d) adsorption of butane, toluene, and trimethylbenzene (TMB) on β-zeolite@silicalite-1 (Reprinted with permission from [118]. Copyright 2005 Wiley.).

The performance of micron size zeolitic core@shell materials has been demonstrated by using the β-zeolite@silicalite-1 material in selective adsorption of small hydrocarbons, e.g.,

butane and toluene from a mixture also containing a bulkier molecule, i.e., 1,3,5-trimethylbezene (TMB) [118]. Matching with theoretical expectations, the smaller hydrocarbons have been efficiently separated from the large one by the shape-selective silicalite-1 shell (Figure 1.13d). Since then, this class of materials, core@shell and hollow zeolites, has been used for many gas or liquid phase adsorptive separation processes [196, 199, 201, 288], as listed in Tables 1.1-1.7. The importance of the film thickness, quality (fewer defects, pinholes and cracks) and the orientation of the crystals in determining the separation performance of zeolitic membranes was discussed in many publications [123, 317-319]. For example, a silicalite-1 membrane with a *b*-preferred orientation showed high separation and flux in xylene isomer separations, while *c*-oriented was performing better in separating linear hydrocarbons from branched one [317, 318]. Film thickness has crucial effects on the zeolite membrane as well. Thick zeolite membranes often crack during calcination for the removal of SDAs and exhibit low fluxes in most separations [126, 319]. A similar situation holds true for zeolitic core@shell materials, i.e., a finely customized shell in terms of crystal growth orientation and shell thickness and quality is believed to enhance the performance of the material.

1.7.2 Catalysis

After proving their merit in separation processes, core@shell, yolk-shell and hollow materials have been used in the field of catalysis [122, 198, 202, 203, 208, 209, 320]. The presence of a zeolitic microporous shell can enhance the catalyst efficacy in many ways. Not only the main intrinsic core and zeolitic shell properties will be inherited by the composite, but some new synergetic properties will also emerge [155]. In general, these catalysts present many properties among which six have often been highlighted in the field of catalysis (Tables 1.1-1.7).

1.7.2.1 Shape Selectivity

By having a microporous shell, these materials present shape selectivity mainly for reactants. This property is critically important when the active sites cannot be conveniently accommodated within microporous channels of zeolites and a mixture of molecules with

different sizes are used as feed [122, 126, 132, 202, 213, 230, 231, 233, 235, 237, 241, 320, 321]. Figure 1.14 shows some of these practically-implemented shape-selective catalysts in various reactions. It should also be mentioned that molecules with the sizes smaller than the size of the micropores can still be selectively differentiated by the zeolite membrane based on their diffusion rate into the tiny pores of the zeolitic shell [124].

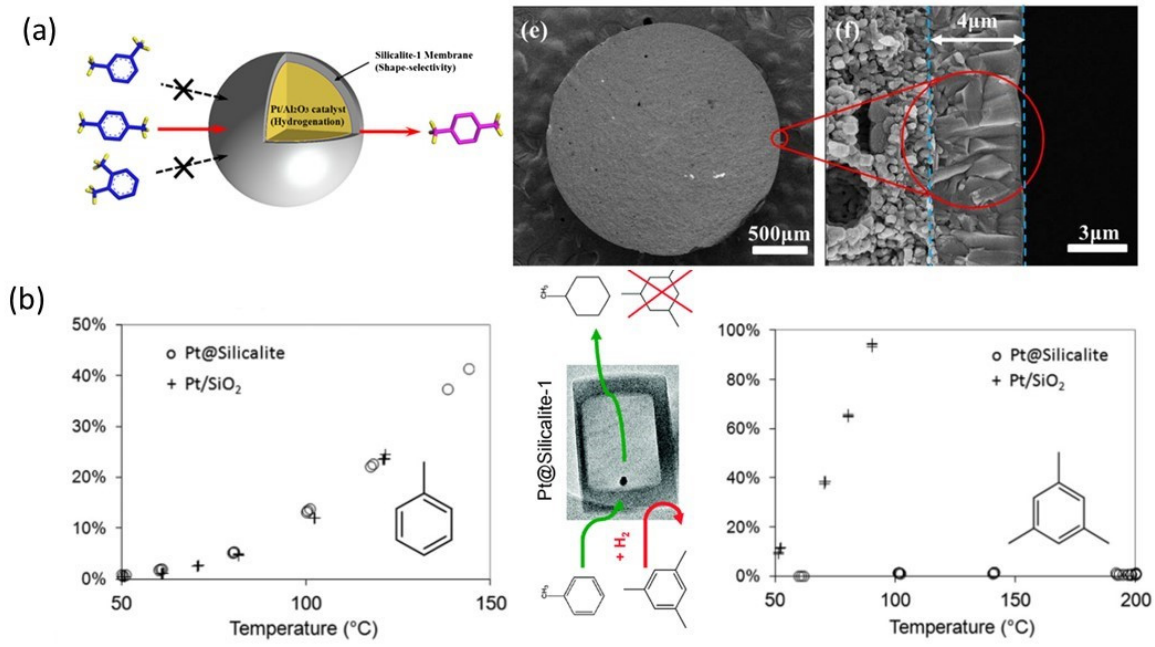

Figure 1.14- Selective hydrogenation model of (a) xylene isomers over Pt,alumina@silicalite-1 (Reprinted with permission from [195]. Copyright 2015 Elsevier.), and (b) toluene and TMB over hollow Pt,silicalite-1 (Reprinted with permission from [121]. Copyright 2013 RSC.).

One of the main issues with such a design is the proximity of the metal active site to the zeolitic framework which might be important in some applications due to the beneficial synergetic effect emerged from an efficient contact between the metal nanoparticles and the zeolite framework [114, 226]. In this regard, using mesoporous zeolitic cores with metal nanoparticles positioned on their external (mesopore) surface area might be helpful.

1.7.2.2 Bi-functionality

By placing a zeolitic shell with acidic sites, active for such reactions as cracking, isomerization and dehydration, over a catalytically active core material, a composite catalyst with bi-functional characteristics forms. This is necessary for catalyzing multistep reactions in a single unit such as direct conversion of synthesis gas to isoparaffins using modified Fischer-Tropsch synthesis [112, 208, 230, 231, 233, 235, 237, 320] or to dimethyl ether [221, 230, 233, 271, 273]. In addition to shape-selectivity, core@shell catalysts benefit from a unique design which can inhibit loss of intermediate products in a cascade reaction, as demonstrated in Figure 1.15.

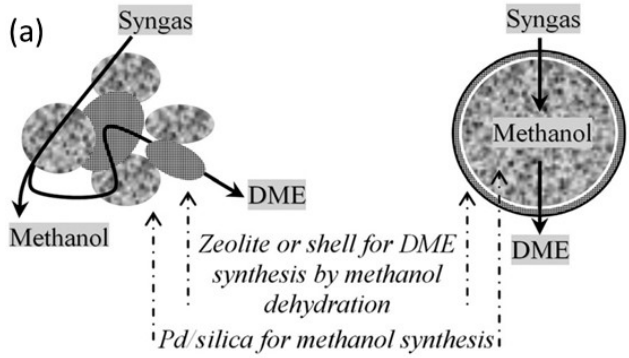

(b)

	Conv. (%)		Selectivity (%, C-mol)			
Catalysts	CO	CO_2	CH_4	C_{2+} [b]	MeOH	DME
Pd/silica	9.88	3.87	0.62	0.42	98.53	0.43
Pd/silica–M[c]	12.84	4.15	1.47	33.62	16.51	48.40
Pd/silica–SZ[d]	9.48	3.45	16.80	9.74	4.76	68.70

[a] Reaction conditions: 523 K, 5.0 MPa, $W_{Pd/silica}/F_{Syngas}$ = 20 g h mol^{-1}; syngas: Ar 3.02%, CO 32.6%, CO_2 5.16%, H_2 59.22%; [b] "C_{2+}" means the summary of alkanes/alkenes with carbon number more than 2; [c] "M" means the mixture of Pd/silica with H-ZSM-5 zeolite and the zeolite content is the same as the zeolite capsule catalyst; [d] "SZ" stands for zeolite capsule catalyst by using the dual-layer method.

Figure 1.15- (a) Illustration of tandem reaction process on general hybrid and capsule catalysts, and (b) catalysts performance in terms of activity and products distribution in tandem catalysis reaction (Reprinted with permission from [227]. Copyright 2011 RSC.).

Figure 1.15b shows that although a physical mixture of catalysts led to a higher conversion, the core@shell configuration of the catalysts enhanced the selectivity of the desired product, achieved by efficient mixing pattern between reactants, intermediate and active sites.

1.7.2.3 Protecting Layer

Active sites can be chemically attacked or poisoned by many destructive elements present within a chemical process, leading to deactivation or permanent destruction. A crystalline zeolitic shell, however, might effectively shelter the active sites from harsh reaction

conditions and keep them away from the reach of poisoning elements [124, 213, 217, 290]. For instance, Zhang *et al.* [198, 205, 211] showed that Ni/Al_2O_3 core as methane steam reforming catalyst equipped with the silicalite-1 shell could be protected from the alkali vapor and electrolyte solution in the DIR-MCFC[19]. Shi *et al.* [284, 285] have also reported an enhanced performance for encapsulated Pt particles by a silicalite-1 hollow shell (hollow Pt, silicalite-1) due to an effective role played by the shell in hindering deactivation of reaction elements (enzyme and Pt) and reducing the by-products. In conclusion, such a protective layer hinders deactivation by either stopping the poisonous chemicals from reaching the active site or preventing the dissolution of active sites which reside in the core section, all leading to a more stable, re-usable and durable catalysts [217, 290]. It is shown that the presence of a crystalline layer can also enhance the hydrothermal stability of the composite catalyst [203].

In addition to providing useful properties for catalysis, the protective property of the silicalite-1 shell has also been exploited for the synthesis of more robust composite catalysts. For instance, dual shell bi-functional catalysts were synthesized by first placing a silicalite-1 shell around the core under less-destructive synthesis condition (close-to-neutral synthesis condition), followed by covering with an acidic ZSM-5 outer layer. This structural silicalite-1 membrane has not only alleviated the damaging effect caused by harsh crystallization conditions of acidic ZSM-5 but also favored the in-situ growth of ZSM-5(H^+) zeolite membrane [223, 227, 230].

1.7.2.4 Sintering Resistance

In many reactions involving high temperature and pressure, catalytic nanoparticles dispersed on an oxide support are doomed to be deactivated by aggregation and sintering. The presence of a hollow zeolitic shell encapsulating tiny single metal nanoparticles can effectively reduce the chance of sintering by restricting their mobility [127]. Such a unique structure, as depicted in Figure 1.14b, has recently been reported by Li *et al.* [121, 219, 308] using dissolution/recrystallization process (Table 1.7). They have also synthesized a ZSM-5 shell, hosting uniformly dispersed Pt nanoparticles, which has significantly resisted

[19]- direct internal reforming-molten carbonate fuel cell

sintering [218]. ZSM-5 shell benefits from hierarchical porosity, created by the mild desilication method used, which facilitates the accessibility of the reactant, especially bulky ones, to the active sites.

1.7.2.5 Passivation of External Surface Area

In order to stop side reactions which are catalyzed by active site sitting on the external surface of a zeolite and increase the reaction selectivity, various passivation techniques were introduced including epitaxial growth of a pure Si zeolitic shell over the external surface of zeolitic catalyst [125, 245, 247, 258, 267, 269]. Figure 1.16 provides an example of passivation of the external surface of an aluminum-containing TON-type zeolite using crystal overgrowth of an aluminum-free TON-type zeolite shell.

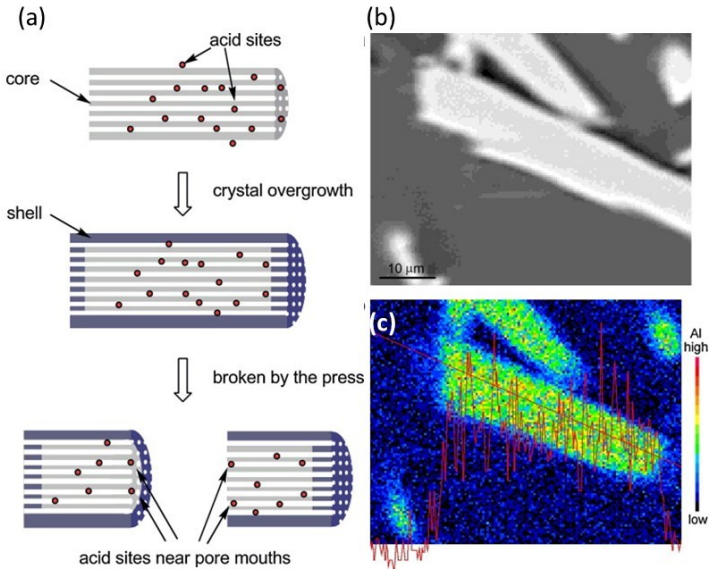

Figure 1.16- (a) Scheme for the preparation of Al-TON@Si-TON zeolites, and (b,c) aluminum distribution in a cross section of the core@shell zeolite: (b) A back-scattered electron image, and (c) map of the aluminum concentration measured by using WDS[20] (Reprinted with permission from [247]. Copyright 2013 Elsevier.).

[20]- wavelength dispersive spectrometer

1.7.2.6 Easy Recovery

In addition to catalytic effect, encapsulation of magnetic species within a zeolitic catalyst facilitates the recovery of the catalyst from solution [197, 289, 322].

1.8 Organization of the Thesis

Two different approaches were used to modify the classical zeolitic materials and enhance their performance; first, via exploring new synthesis conditions and second, via using zeolitic materials as a building block to form structured composites with a core@shell structure.

In the first part of the current chapter, Chapter one, a brief introduction about zeolites as ordered microporous crystalline materials was provided, followed by discussing their main problems and remedies. These remedies are mainly discussed and examined for the major framework types such as MFI, FAU or LTA. In contrast to its exceptional performance in many applications, ZSM-12 zeolite, its structure and crystallization behavior have not been sufficiently studied. Chapter two provides a brief review of the literature, dedicated to this framework type. This is followed by presenting some results, obtained in the present work which was aiming at the control of the size and morphology of ZSM-12 by exploring new synthesis conditions (new chemical sources, compositions, gel preparation techniques, etc.).

Also, in the current chapter, Chapter one, a comprehensive review about the zeolitic core@shell architectures was presented. Among all different methods, seeded growth technique as the most reliable technique was chosen to study the synthesis of mesoporous silica@zeolite core-shell materials. The effect of various parameters including the core size, coating technique, and the presence of various metallic guest species within the mesoporous silica core on the quality of the zeolitic shell were investigated. The results are presented in Chapter three. In Chapter four, we have tested the performance of these core@shell materials in a model application process, i.e., biodiesel purification.

Chapter five highlights the main findings and conclusions of the work presented in this thesis, followed by providing some recommendations and proposals for the continuation and the application of the results obtained in this work.

1.9 References

[1] K.S.W. Sing, D.H. Everett, R.A.W. Haul, L. Moscou, R.A. Pierotti, J. Rouquerol, T. Siemieniewska, *Pure Appl. Chem.* **1985**, *57*, 603-619.

[2] M. Thommes, *Chem. Ing. Tech.* **2010**, *82*, 1059-1073.

[3] R. Barrer, Hydrothermal Chemistry of Zeolites, Academic Press, **1982**.

[4] E.M.F. H. van Bekkum, P.A. Jacobs and J.C. Jansen, ed. Introduction to Zeolite Science and Practice, Vol. 137, **2001**, Elsevier.

[5] J.A.M. P.A. Jacobs, ed. Synthesis of High-Silica Aluminosilicate Zeolites, Vol. 33, **1987**, Elsevier, Amsterdam.

[6] C.S. Cundy, P.A. Cox, *Microporous Mesoporous Mater.* **2005**, *82*, 1-78.

[7] R.M. Barrer, *Journal of the Chemical Society (Resumed)* **1948**, 127-132.

[8] R.M. Milton, Molecular sieve adsorbents, US2882243 A, Union Carbide Corp, **1959**.

[9] R.M. Milton, Molecular sieve adsorbents, US2882244 A, Union Carbide Corp, **1959**.

[10] E.M. Flanigen, R.W. Broach, S.T. Wilson, Introduction, Zeolites in Industrial Separation and Catalysis, Wiley-VCH Verlag GmbH & Co. KGaA, **2010,** pp. 1-26.

[11] D.P. Serrano, R. van Grieken, *J. Mater. Chem.* **2001**, *11*, 2391-2407.

[12] C. Baerlocher, L.B. McCusker, D.H. Olson, Atlas of Zeolite Framework Types (Sixth Edition), Elsevier Science B.V., Amsterdam, **2007,** pp. 232-233.

[13] H. van Koningsveld, Compendium of Zeolite Framework Types: Building Schemes and Type Characteristics, Elsevier Science, **2007**.

[14] R.F. Lobo, Introduction to the Structural Chemistry of Zeolites, Handbook of Zeolite Science and Technology, CRC Press, **2003**.

[15] J. Sun, C. Bonneau, A. Cantin, A. Corma, M.J. Diaz-Cabanas, M. Moliner, D. Zhang, M. Li, X. Zou, *Nature* **2009**, *458*, 1154-1157.

[16] http://www.iza-structure.org/databases/, 2014

[17] G.-Y. Yang, S.C. Sevov, *J. Am. Chem. Soc.* **1999**, *121*, 8389-8390.

[18] J. Jiang, J.L. Jorda, J. Yu, L.A. Baumes, E. Mugnaioli, M.J. Diaz-Cabanas, U. Kolb, A. Corma, *Science* **2011**, *333*, 1131-1134.

[19] J. Shi, Y. Wang, W. Yang, Y. Tang, Z. Xie, *Chem. Soc. Rev.* **2015**, *44*, 8877-8903.

[20] C.-Y. Chen, S.I. Zones, Post-Synthetic Treatment and Modification of Zeolites, Wiley-VCH Verlag GmbH & Co. KGaA, **2010**, pp. 155-170.

[21] P.M. Visakh, M.J.M. Morlanes, Nanomaterials and Nanocomposites: Zero- to Three-Dimensional Materials and Their Composites, Wiley, **2016**.

[22] S. Mintova, J. Cejka, Micro/mesoporous composites, in: Jirí Cejka, Herman van Bekkum, A. Corma, F. Schüth (Eds.) Studies in Surface Science and Catalysis, Elsevier, **2007,** pp. 301-326.

[23] J.A. Martens, G. Vanbutsele, P.A. Jacobs, J. Denayer, R. Ocakoglu, G. Baron, J.A. Muñoz Arroyo, J. Thybaut, G.B. Marin, *Catal. Today* **2001**, *65*, 111-116.

[24] M. Moliner, C. Martínez, A. Corma *Angew. Chem. Int. Ed.* **2015**, *54*, 3560-3579.

[25] A. Iliyas, Z. Sarshar, H. Zahedi-Niaki, M. Eić, S. Kaliaguine, *Top. Catal.* **2009**, *52*, 1860-1867.

[26] D.W. Breck, Zeolite Molecular Sieves: Structure, Chemistry, and Use, Wiley-Interscience, **1974**.

[27] K. Moller, T. Bein, *Chem. Soc. Rev.* **2013**, *42*, 3689-3707.

[28] J. B.Nagy, R. Aiello, G. Giordano, A. Katovic, F. Testa, Z. Kónya, I. Kiricsi, Isomorphous Substitution in Zeolites, in: H.G. Karge, J. Weitkamp (Eds.)

Characterization II, Springer Berlin Heidelberg, Berlin, Heidelberg, **2007,** pp. 365-478.
[29] J. Li, A. Corma, J. Yu, *Chem. Soc. Rev.* **2015**, *44*, 7112-7127.
[30] B. Smit, T.L.M. Maesen, *Chem. Rev.* **2008**, *108*, 4125-4184.
[31] A. Corma, *Chem. Rev.* **1995**, *95*, 559-614.
[32] A. Corma, *Chem. Rev.* **1997**, *97*, 2373-2419.
[33] V. Sebastián, C. Casado, J. Coronas, Special Applications of Zeolites, Zeolites and Catalysis, Wiley-VCH Verlag GmbH & Co. KGaA, **2010**, pp. 389-410.
[34] S. Hitz, R. Prins, *J. Catal.* **1997**, *168*, 194-206.
[35] H. Lee, S.I. Zones, M.E. Davis, *Nature* **2003**, *425*, 385-388.
[36] P. Cubillas, M.W. Anderson, Synthesis Mechanism: Crystal Growth and Nucleation, Zeolites and Catalysis, Wiley-VCH Verlag GmbH & Co. KGaA, **2010**, pp. 1-55.
[37] J. Pérez-Pariente, R. García, L. Gómez-Hortigüela, A.B. Pinar, Co-Templates in Synthesis of Zeolites, Zeolites and Catalysis, Wiley-VCH Verlag GmbH & Co. KGaA, **2010**, pp. 107-129.
[38] R.M. Barrer, P.J. Denny, *Journal of the Chemical Society (Resumed)* **1961**, 971-982.
[39] K. Iyoki, K. Itabashi, T. Okubo, *Microporous Mesoporous Mater.* **2014**, *189*, 22-30.
[40] X. Meng, F.-S. Xiao, *Chem. Rev.* **2014**, *114*, 1521-1543.
[41] J. Perez-Ramirez, C.H. Christensen, K. Egeblad, C.H. Christensen, J.C. Groen, *Chem. Soc. Rev.* **2008**, *37*, 2530-2542.
[42] M. Hartmann, *Angew. Chem. Int. Ed.* **2004**, *43*, 5880-5882.
[43] R. Szostak, Secondary synthesis methods, in: H. van Bekkum, E. M. Flanigen, P. A. Jacobs, J.C. Jansen (Eds.) Studies in Surface Science and Catalysis, Elsevier, **2001,** pp. 261-297.
[44] V. Valtchev, G. Majano, S. Mintova, J. Perez-Ramirez, *Chem. Soc. Rev.* **2013**, *42*, 263-290.
[45] U. Ciesla, F. Schüth, *Microporous Mesoporous Mater.* **1999**, *27*, 131-149.
[46] X.S. Zhao, G.Q. Lu, G.J. Millar, *Ind. Eng. Chem. Res.* **1996**, *35*, 2075-2090.
[47] J. Jiang, J. Yu, A. Corma, *Angew. Chem. Int. Ed.* **2010**, *49*, 3120-3145.
[48] H. Tüysüz, F. Schüth, *Adv. Catal.* **2012**, *55*, 127-239.
[49] C. Vincent, R.J. E, V.C. D, Process for producing low-bulk density silica, US 3556725 A, Sylvania Electric Prod, **1971**.
[50] T. Yanagisawa, T. Shimizu, K. Kuroda, C. Kato, *Bull. Chem. Soc. Jpn.* **1990**, *63*, 988-992.
[51] C.T. Kresge, M.E. Leonowicz, W.J. Roth, J.C. Vartuli, J.S. Beck, *Nature* **1992**, *359*, 710-712.
[52] J.S. Beck, J.C. Vartuli, W.J. Roth, M.E. Leonowicz, C.T. Kresge, K.D. Schmitt, C.T.W. Chu, D.H. Olson, E.W. Sheppard, S.B. McCullen, J.B. Higgins, J.L. Schlenker, *J. Am. Chem. Soc.* **1992**, *114*, 10834-10843.
[53] F. Kleitz, Ordered Mesoporous Materials, Handbook of Heterogeneous Catalysis, Wiley-VCH Verlag GmbH & Co. KGaA, **2008,** pp. 178-219.
[54] Y. Shi, Y. Wan, D. Zhao, *Chem. Soc. Rev.* **2011**, *40*, 3854-3878.
[55] G.S. Attard, P.N. Bartlett, N.R.B. Coleman, J.M. Elliott, J.R. Owen, J.H. Wang, *Science* **1997**, *278*, 838-840.
[56] R. Ryoo, S.H. Joo, S. Jun, *J. Phys. Chem. B* **1999**, *103*, 7743-7746.
[57] A.H. Lu, F. Schüth, *Adv. Mater.* **2006**, *18*, 1793-1805.
[58] A. Thomas, F. Goettmann, M. Antonietti, *Chem. Mater.* **2008**, *20*, 738-755.
[59] G.J.A.A. Soler-Illia, O. Azzaroni, *Chem. Soc. Rev.* **2011**, *40*, 1107-1150.

[60] Y. Fang, H. Hu, *J. Am. Chem. Soc.* **2006**, *128*, 10636-10637.
[61] M.E. Davis, C. Saldarriaga, C. Montes, J. Garces, C. Crowdert, *Nature* **1988**, *331*, 698-699.
[62] C.C. Freyhardt, M. Tsapatsis, R.F. Lobo, K.J. Balkus, M.E. Davis, *Nature* **1996**, *381*, 295-298.
[63] P. Wagner, M. Yoshikawa, K. Tsuji, M. E. Davis, M. Lovallo, M. Taspatsis, *Chem. Commun.* **1997**, *0*, 2179-2180.
[64] A. Corma, M.J. Diaz-Cabanas, F. Rey, S. Nicolopoulus, K. Boulahya, *Chem. Commun.* **2004**, 1356-1357.
[65] A. Corma, M.J. Diaz-Cabanas, J.L. Jorda, C. Martinez, M. Moliner, *Nature* **2006**, *443*, 842-845.
[66] A. Corma, M.S. Grande, V. Gonzalez-Alfaro, A.V. Orchilles, *J. Catal.* **1996**, *159*, 375-382.
[67] M.E. Davis, *Nature* **2002**, *417*, 813-821.
[68] S. Mintova, J.-P. Gilson, V. Valtchev, *Nanoscale* **2013**, *5*, 6693-6703.
[69] L. Tosheva, V.P. Valtchev, *Chem. Mater.* **2005**, *17*, 2494-2513.
[70] B.J. Schoeman, J. Sterte, J.-E. Otterstedt, *J. Chem. Soc., Chem. Commun.* **1993**, 994-995.
[71] V. Valtchev, L. Tosheva, *Chem. Rev.* **2013**, *113*, 6734-6760.
[72] H. Awala, J.-P. Gilson, R. Retoux, P. Boullay, J.-M. Goupil, V. Valtchev, S. Mintova, *Nat Mater* **2015**, *14*, 447-451.
[73] W. Schwieger, A.G. Machoke, T. Weissenberger, A. Inayat, T. Selvam, M. Klumpp, A. Inayat, *Chem. Soc. Rev.* **2016**, *45*, 3353-3376
[74] M. Kustova, K. Egeblad, C.H. Christensen, A.L. Kustov, Hierarchical zeolites: progress on synthesis and characterization of mesoporous zeolite single crystal catalysts, in: Z.G. R. Xu, J. Chen and W. Yan (Ed.) Studies in Surface Science and Catalysis, Elsevier, **2007,** pp. 267-275.
[75] Y. Wei, T.E. Parmentier, K.P. de Jong, J. Zecevic, *Chem. Soc. Rev.* **2015**, *44*, 7234-7261.
[76] J. Čejka, S. Mintova, *Catal. Rev.: Sci. Eng.* **2007**, *49*, 457-509.
[77] K. Li, J. Valla, J. Garcia-Martinez, *ChemCatChem* **2014**, *6*, 46-66.
[78] J. Vernimmen, V. Meynen, P. Cool, *Beilstein J. Nanotechnol.* **2011**, *2*, 785-801.
[79] S. Lopez-Orozco, A. Inayat, A. Schwab, T. Selvam, W. Schwieger, *Adv. Mater.* **2011**, *23*, 2602-2615.
[80] J. Čejka, G. Centi, J. Perez-Pariente, W.J. Roth, *Catal. Today* **2012**, *179*, 2-15.
[81] D.P. Serrano, J.M. Escola, P. Pizarro, *Chem. Soc. Rev.* **2013**.
[82] L.-H. Chen, X.-Y. Li, J.C. Rooke, Y.-H. Zhang, X.-Y. Yang, Y. Tang, F.-S. Xiao, B.-L. Su, *J. Mater. Chem.* **2012**, *22*, 17381-17403.
[83] R. Chal, C. Gerardin, M. Bulut, S. van Donk, *Chemcatchem* **2011**, *3*, 67-81.
[84] L. Zhang, A.N.C. van Laak, P.E. de Jongh, K.P. de Jong, Textural Characterization of Mesoporous Zeolites, Zeolites and Catalysis, Wiley-VCH Verlag GmbH & Co. KGaA, **2010**, pp. 237-282.
[85] F.-S. Xiao, X. Meng, Zeolites with Hierarchically Porous Structure: Mesoporous Zeolites, Hierarchically Structured Porous Materials, Wiley-VCH Verlag GmbH & Co. KGaA, **2011,** pp. 435-455.
[86] D.P. Serrano, J. Aguado, J.M. Escola, J.M. Rodríguez, Á. Peral, *Chem. Mater.* **2006**, *18*, 2462-2464.
[87] Y. Tao, H. Kanoh, L. Abrams, K. Kaneko, *Chem. Rev.* **2006**, *106*, 896-910.

[88] C. Boissiere, E. Prouzet, D. Grosso, C. Sanchez, Hierarchically Structured Porous Coatings and Membranes, Hierarchically Structured Porous Materials, Wiley-VCH Verlag GmbH & Co. KGaA, **2011,** pp. 335-361.
[89] Y.-H. Zhang, L.-H. Chen, Y. Tang, X.-Y. Yang, B.-L. Su, Micro-Macroporous Structured Zeolite, Hierarchically Structured Porous Materials, Wiley-VCH Verlag GmbH & Co. KGaA, **2011,** pp. 457-479.
[90] D. Verboekend, J. Perez-Ramirez, *Catal. Sci. Technol.* **2011**, *1*, 879-890.
[91] K. Egeblad, C.H. Christensen, M. Kustova, C.H. Christensen, *Chem. Mater.* **2007**, *20*, 946-960.
[92] S. van Donk, A.H. Janssen, J.H. Bitter, K.P. de Jong, *Catal. Rev.: Sci. Eng.* **2003**, *45*, 297-319.
[93] A.H. Janssen, A.J. Koster, K.P. de Jong, *Angew. Chem. Int. Ed.* **2001**, *40*, 1102-1104.
[94] M. Kustova, K. Egeblad, K. Zhu, C.H. Christensen, *Chem. Mater.* **2007**, *19*, 2915-2917.
[95] M.B. Yue, L.B. Sun, T.T. Zhuang, X. Dong, Y. Chun, J.H. Zhu, *J. Mater. Chem.* **2008**, *18*, 2044-2050.
[96] A.G. Machoke, A.M. Beltrán, A. Inayat, B. Winter, T. Weissenberger, N. Kruse, R. Güttel, E. Spiecker, W. Schwieger, *Adv. Mater.* **2015**, *27*, 1066-1070.
[97] A.A. Campos, L. Dimitrov, C.R. da Silva, M. Wallau, E.A. Urquieta-González, *Microporous Mesoporous Mater.* **2006**, *95*, 92-103.
[98] D. Trong On, S. Kaliaguine, *Angew. Chem. Int. Ed.* **2001**, *40*, 3248-3251.
[99] A. Dong, N. Ren, W. Yang, Y. Wang, Y. Zhang, D. Wang, J. Hu, Z. Gao, Y. Tang, *Adv. Funct. Mater.* **2003**, *13*, 943-948.
[100] A. Dong, Y. Wang, D. Wang, W. Yang, Y. Zhang, N. Ren, Z. Gao, Y. Tang, *Microporous Mesoporous Mater.* **2003**, *64*, 69-81.
[101] A. Dong, Y. Wang, Y. Tang, N. Ren, Y. Zhang, Z. Gao, *Chem. Mater.* **2002**, *14*, 3217-3219.
[102] Y. Liu, W. Zhang, T.J. Pinnavaia, *J. Am. Chem. Soc.* **2000**, *122*, 8791-8792.
[103] S.I. Cho, S.D. Choi, J.H. Kim, G.J. Kim, *Adv. Funct. Mater.* **2004**, *14*, 49-54.
[104] N. Petkov, M. Hölzl, T.H. Metzger, S. Mintova, T. Bein, *J. Phys. Chem. B* **2005**, *109*, 4485-4491.
[105] H. Li, J. Jin, W. Wu, C. Chen, L. Li, Y. Li, W. Zhao, J. Gu, G. Chen, J.-l. Shi, *J. Mater. Chem.* **2011**, *21*, 19395-19401.
[106] F. Hasan, R. Singh, P.A. Webley, *Microporous Mesoporous Mater.* **2012**, *160*, 75-84.
[107] Z. Wang, C. Li, H.J. Cho, S.-C. Kung, M.A. Snyder, W. Fan, *J. Mater. Chem. A* **2015**, *3*, 1298-1305.
[108] Y. Fang, H. Hu, G. Chen, *Chem. Mater.* **2008**, *20*, 1670-1672.
[109] A. Petushkov, G. Merilis, S.C. Larsen, *Microporous Mesoporous Mater.* **2011**, *143*, 97-103.
[110] W.J. Roth, P. Nachtigall, R.E. Morris, J. Čejka, *Chem. Rev.* **2014**, *114*, 4807-4837.
[111] D. Trong On, S. Kaliaguine, *J. Am. Chem. Soc.* **2003**, *125*, 618-619.
[112] K. Shen, W. Qian, N. Wang, C. Su, F. Wei, *J. Am. Chem. Soc.* **2013**, *135*, 15322-15325.
[113] M. Choi, K. Na, J. Kim, Y. Sakamoto, O. Terasaki, R. Ryoo, *Nature* **2009**, *461*, 246-249.
[114] D. Farrusseng, A. Tuel, *New J. Chem.* **2016**, *40*, 3933-3949.

[115] C.P. Canlas, J. Lu, N.A. Ray, N.A. Grosso-Giordano, S. Lee, J.W. Elam, R.E. Winans, R.P. Van Duyne, P.C. Stair, J.M. Notestein, *Nat Chem* **2012**, *4*, 1030-1036.
[116] N. Chen, T. Degnan, C. Smith, Molecular Transport and Reaction in Zeolites: Design and Application of Shape Selective Catalysis, John Wiley & Sons, **1994**.
[117] E.G.D. A. W. Chester, ed. Zeolite Characterization and Catalysis: A Tutorial, Zeolite Characterization and Catalysis, ed. E.G.D. Arthur W. Chester, **2009**, Springer
[118] Y. Bouizi, I. Diaz, L. Rouleau, V. Valtchev, *Adv. Funct. Mater.* **2005**, *15*, 1955-1960.
[119] N. van der Puil, E.W. Kuipers, H. van Bekkum, J.C. Jansen, Composite catalysts of supported zeolites, in: G. Poncelet, J. Martens, B. Delmon, P.A. Jacobs, P. Grange (Eds.) Studies in Surface Science and Catalysis, Elsevier, **1995,** pp. 1163-1171.
[120] N. van der Puil, E.C. Rodenburg, H. van Bekkum, J.C. Jansen, Novel model catalysts containing supported MFI-type zeolites, in: L. Bonneviot, S. Kaliaguine (Eds.) Studies in Surface Science and Catalysis, Elsevier, **1995,** pp. 377-384.
[121] S. Li, T. Boucheron, A. Tuel, D. Farrusseng, F. Meunier, *Chem. Commun.* **2014**, *50*, 1824-1826.
[122] N. Nishiyama, M. Miyamoto, Y. Egashira, K. Ueyama, *Chem. Commun.* **2001**, 1746-1747.
[123] R. Dragomirova, S. Wohlrab, *Catalysts* **2015**, *5*, 2161-2222.
[124] S. Li, C. Aquino, L. Gueudré, A. Tuel, Y. Schuurman, D. Farrusseng, *ACS Catal.* **2014**, *4*, 4299-4303.
[125] A. Ghorbanpour, A. Gumidyala, L.C. Grabow, S.P. Crossley, J.D. Rimer, *ACS Nano* **2015**, *7*, 4006-4016.
[126] N. Nishiyama, K. Ichioka, M. Miyamoto, Y. Egashira, K. Ueyama, L. Gora, W. Zhu, F. Kapteijn, J.A. Moulijn, *Microporous Mesoporous Mater.* **2005**, *83*, 244-250.
[127] S.H. Joo, J.Y. Cheon, J.Y. Oh, Core–Shell Nanoarchitectures as Stable Nanocatalysts, in: Y.J. Park (Ed.) Current Trends of Surface Science and Catalysis, Springer New York, New York, NY, **2014,** pp. 93-119.
[128] J. Zheng, Q. Zeng, J. Ma, X. Zhang, W. Sun, R. Li, *Chem. Lett.* **2010**, *39*, 330-331.
[129] W. Yang, X. Wang, Y. Tang, Y. Wang, C. Ke, S. Fu, *J. Macromol. Sci., Part A: Pure Appl.Chem.* **2002**, *39*, 509-526.
[130] C. Xiong, D. Coutinho, K.J. Balkus Jr, *Microporous Mesoporous Mater.* **2005**, *86*, 14-22.
[131] X.D. Wang, W.L. Yang, Y. Tang, Y.J. Wang, S.K. Fu, Z. Gao, *Chem. Commun.* **2000**, 2161-2162.
[132] V. Valtchev, B.J. Schoeman, J. Hedlund, S. Mintova, J. Sterte, *Zeolites* **1996**, *17*, 408-415.
[133] V. Valtchev, *Chem. Mater.* **2002**, *14*, 4371-4377.
[134] W. Song, R. Kanthasamy, V.H. Grassian, S.C. Larsen, *Chem. Commun.* **2004**, 1920-1921.
[135] J. Shi, N. Ren, Y.-H. Zhang, Y. Tang, *Microporous Mesoporous Mater.* **2010**, *132*, 181-187.
[136] Li, Shi, Hua, Chen, Ruan, Yan, *Nano Lett.* **2003**, *3*, 609-612.
[137] R. Kanthasamy, K. Barquist, S.C. Larsen, *Microporous Mesoporous Mater.* **2008**, *113*, 554-561.
[138] R. Kanthasamy, Characterization and applications of mesoporous silica and hollow zeolite structures, 3323433, University of Iowa, **2008**.
[139] W. Ji, M. Li, C. Zeng, J. Yao, L. Zhang, *Microporous Mesoporous Mater.* **2011**, *143*, 189-195.

[140] J.C. Groen, T. Bach, U. Ziese, A.M. Paulaime-van Donk, K.P. de Jong, J.A. Moulijn, J. Pérez-Ramírez, *J. Am. Chem. Soc.* **2005**, *127*, 10792-10793.
[141] V. Valtchev, S. Mintova, *Microporous Mesoporous Mater.* **2001**, *43*, 41-49.
[142] K.H. Rhodes, S.A. Davis, F. Caruso, B. Zhang, S. Mann, *Chem. Mater.* **2000**, *12*, 2832-2834.
[143] H. Wang, L. Chen, Y. Feng, H. Chen, *Acc. Chem. Res.* **2013**, *46*, 1636-1646.
[144] R. Ghosh Chaudhuri, S. Paria, *Chem. Rev.* **2011**, *112*, 2373-2433.
[145] P.M. Arnal, The synthesis of monodispersed colloidal core@shell spheres and hollow particles, Ph.D. Thesis, Ruhr University Bochum, **2006**.
[146] X. Peng, M.C. Schlamp, A.V. Kadavanich, A.P. Alivisatos, *J. Am. Chem. Soc.* **1997**, *119*, 7019-7029.
[147] B. Aiken, E. Matijević, *J. Colloid Interface Sci.* **1988**, *126*, 645-649.
[148] A. Garg, E. Matijević, *J. Colloid Interface Sci.* **1988**, *126*, 243-250.
[149] P.M. Arnal, M. Comotti, F. Schüth, *Angew. Chem.* **2006**, *118*, 8404-8407.
[150] R. Guttel, M. Paul, F. Schüth, *Chem. Commun.* **2010**, *46*, 895-897.
[151] C. Wu, Z.-Y. Lim, C. Zhou, W. Guo Wang, S. Zhou, H. Yin, Y. Zhu, *Chem. Commun.* **2013**, *49*, 3215-3217.
[152] J. Qi, J. Chen, G. Li, S. Li, Y. Gao, Z. Tang, *Energy Environ. Sci.* **2012**, *5*, 8937-8941.
[153] C. Galeano, R. Güttel, M. Paul, P. Arnal, A.-H. Lu, F. Schüth, *Chem. - Eur. J.* **2011**, *17*, 8434-8439.
[154] R. Guttel, M. Paul, F. Schüth, *Catal. Sci. Technol.* **2011**, *1*, 65-68.
[155] S.H. Joo, J.Y. Park, C.-K. Tsung, Y. Yamada, P. Yang, G.A. Somorjai, *Nat Mater* **2009**, *8*, 126-131.
[156] Z. Chen, Z.-M. Cui, P. Li, C.-Y. Cao, Y.-L. Hong, Z.-y. Wu, W.-G. Song, *J. Phys. Chem. C* **2012**, *116*, 14986-14991.
[157] I. Lee, J.B. Joo, Y. Yin, F. Zaera, *Angew. Chem. Int. Ed.* **2011**, *50*, 10208-10211.
[158] Z. Wei, Z. Zhou, M. Yang, C. Lin, Z. Zhao, D. Huang, Z. Chen, J. Gao, *J. Mater. Chem.* **2011**, *21*, 16344-16348.
[159] L. Lin, T. Zhang, H. Liu, J. Qiu, X. Zhang, *Nanoscale* **2015**, *7*, 7615-7623.
[160] C.-H. Kuo, Y. Tang, L.-Y. Chou, B.T. Sneed, C.N. Brodsky, Z. Zhao, C.-K. Tsung, *J. Am. Chem. Soc.* **2012**, *134*, 14345-14348.
[161] A. Guerrero-Martínez, J. Pérez-Juste, L.M. Liz-Marzán, *Adv. Mater.* **2010**, *22*, 1182-1195.
[162] M. Enterría, F. Suárez-García, A. Martínez-Alonso, J.M.D. Tascón, *J. Alloys Compd.* **2013**, *583*, 60-69.
[163] X.F. Qian, B. Li, Y.Y. Hu, G.X. Niu, D.Y.H. Zhang, R.C. Che, Y. Tang, D.S. Su, A.M. Asiri, D.Y. Zhao, *Chem. - Eur. J.* **2012**, *18*, 931-939.
[164] X.F. Qian, J.M. Du, B. Li, M. Si, Y.S. Yang, Y.Y. Hu, G.X. Niu, Y.H. Zhang, H.L. Xu, B. Tu, Y. Tang, D.Y. Zhao, *Chem. Sci.* **2011**, *2*, 2006-2016.
[165] Y. Bouizi, L. Rouleau, V.P. Valtchev, *Microporous Mesoporous Mater.* **2006**, *91*, 70-77.
[166] Y. Bouizi, L. Rouleau, V.P. Valtchev, *Chem. Mater.* **2006**, *18*, 4959-4966.
[167] X. Wang, M. Wen, C. Wang, J. Ding, Y. Sun, Y. Liu, Y. Lu, *Chem. Commun.* **2014**, *50*, 6343-6345.
[168] T. Sano, Y. Kiyozumi, M. Kawamura, F. Mizukami, H. Takaya, T. Mouri, W. Inaoka, Y. Toida, M. Watanabe, K. Toyoda, *Zeolites* **1991**, *11*, 842-845.
[169] H.P. Calis, A.W. Gerritsen, C.M. Vandenbleek, C.H. Legein, J.C. Jansen, H. Vanbekkum, *Can. J. Chem. Eng.* **1995**, *73*, 120-128.

[170] S.P. Davis, E.V.R. Borgstedt, S.L. Suib, *Chem. Mater.* **1990**, *2*, 712-719.
[171] J. Ding, L. Han, M. Wen, G. Zhao, Y. Liu, Y. Lu, *Catal. Commun.* **2015**, *72*, 156-160.
[172] M. Wen, J. Ding, C. Wang, Y. Li, G. Zhao, Y. Liu, Y. Lu, *Microporous Mesoporous Mater.* **2016**, *221*, 187-196.
[173] H.-K. Jeong, J. Krohn, K. Sujaoti, M. Tsapatsis, *J. Am. Chem. Soc.* **2002**, *124*, 12966-12968.
[174] Z. Lai, M. Tsapatsis, J.P. Nicolich, *Adv. Funct. Mater.* **2004**, *14*, 716-729.
[175] J. Gascon, J.R. van Ommen, J.A. Moulijn, F. Kapteijn, *Catal. Sci. Technol.* **2015**, *5*, 807-817.
[176] N. Rangnekar, N. Mittal, B. Elyassi, J. Caro, M. Tsapatsis, *Chem. Soc. Rev.* **2015**, *44*, 7128-7154.
[177] N. Kosinov, J. Gascon, F. Kapteijn, E.J.M. Hensen, *J. Membr. Sci.* **2016**, *499*, 65-79.
[178] A. Julbe, Chapter 6 - Zeolite Membranes – Synthesis, Characterization and Application, in: H.v.B.A.C. Jiří Čejka, S. Ferdi (Eds.) Studies in Surface Science and Catalysis, Elsevier, **2007,** pp. 181-219.
[179] I.M. Lachman, M.D. Patil, Method of crystallizing a zeolite on the surface of a monolithic ceramic substrate, US4800187 A, Corning Glass Works, **1989**.
[180] V. Valtchev, J. Hedlund, B.J. Schoeman, J. Sterte, S. Mintova, *Microporous Mater.* **1997**, *8*, 93-101.
[181] J. Sterte, S. Mintova, G. Zhang, B.J. Schoeman, *Zeolites* **1997**, *18*, 387-390.
[182] M. Wen, X. Wang, L. Han, J. Ding, Y. Sun, Y. Liu, Y. Lu, *Microporous Mesoporous Mater.* **2015**, *206*, 8-16.
[183] Y. Jiao, X. Yang, C. Jiang, C. Tian, Z. Yang, J. Zhang, *J. Catal.* **2015**, *332*, 70-76.
[184] J. Shao, Z. Zhan, J. Li, Z. Wang, K. Li, Y. Yan, *J. Membr. Sci.* **2014**, *451*, 10-17.
[185] T.C.T. Pham, H.S. Kim, K.B. Yoon, *Science* **2011**, *334*, 1533-1538.
[186] T.C.T. Pham, T.H. Nguyen, K.B. Yoon, *Angew. Chem. Int. Ed.* **2013**, *52*, 8693-8698.
[187] E. Reichelt, M.P. Heddrich, M. Jahn, A. Michaelis, *Appl. Catal., A* **2014**, *476*, 78-90.
[188] V. Valtchev, *Chem. Mater.* **2002**, *14*, 956-958.
[189] J.C. Groen, J.C. Jansen, J.A. Moulijn, J. Pérez-Ramírez, *J. Phys. Chem. B* **2004**, *108*, 13062-13065.
[190] Y. Deng, C. Deng, D. Qi, C. Liu, J. Liu, X. Zhang, D. Zhao, *Adv. Mater.* **2009**, *21*, 1377-1382.
[191] J. Zheng, Q. Zeng, Y. Zhang, Y. Wang, J. Ma, X. Zhang, W. Sun, R. Li, *Chem. Mater.* **2010**, *22*, 6065-6074.
[192] Y. Bouizi, G. Majano, S. Mintova, V. Valtchev, *J. Phys. Chem. C* **2007**, *111*, 4535-4542.
[193] F. Caruso, R.A. Caruso, ouml, H. hwald, *Science* **1998**, *282*, 1111-1114.
[194] Z. Zheng, D. Yang, T. Li, X. Yn, S. Wang, X. Wu, X. An, X. Xie, *Catal. Sci. Technol.* **2016**, *6*, 5427-5439.
[195] Y. Wu, Y. Chai, J. Li, H. Guo, L. Wen, C. Liu, *Catal. Commun.* **2015**, *64*, 110-113.
[196] N. Masoumifard, P.M. Arnal, S. Kaliaguine, F. Kleitz, *ChemSusChem* **2015**, *8*, 2093-2105.
[197] Q. Lv, G. Li, H. Lu, W. Cai, H. Huang, C. Cheng, *Microporous Mesoporous Mater.* **2015**, *203*, 202-207.
[198] J. Zhang, T. Zhang, X. Zhang, W. Liu, H. Liu, J. Qiu, K.L. Yeung, *Catal. Today* **2014**, *236*, 34-40.
[199] G.D. Pirngruber, C. Laroche, M. Maricar-Pichon, L. Rouleau, Y. Bouizi, V. Valtchev, *Microporous Mesoporous Mater.* **2013**, *169*, 212-217.

[200] Q. Lin, G. Yang, X. Li, Y. Yoneyama, H. Wan, N. Tsubaki, *ChemCatChem* **2013**, *5*, 3101-3106.
[201] E.A. Khan, A. Rajendran, Z. Lai, *Chem. Eng. Res. Bull.* **2013**, *16*, 1-15.
[202] J. Wang, D.-M. Do, G.-K. Chuah, S. Jaenicke, *ChemCatChem* **2013**, *5*, 247-254.
[203] X. Wang, Y. Cui, Y. Wang, X. Song, J. Yu, *Inorg. Chem.* **2013**, *52*, 10708-10710.
[204] L. Liu, R. Singh, G. Li, G. Xiao, P.A. Webley, Y. Zhai, *Mater. Chem. Phys.* **2012**, *133*, 1144-1151.
[205] J. Zhang, X. Zhang, M. Tu, W. Liu, H. Liu, J. Qiu, L. Zhou, Z. Shao, H.L. Ho, K.L. Yeung, *J. Power Sources* **2011**, *198*, 14-22.
[206] X. Wang, X. Zhang, Y. Wang, H. Liu, J. Wang, J. Qiu, H.L. Ho, W. Han, K.L. Yeung, *Chem. Eng. J.* **2011**, *175*, 408-416.
[207] H. Teng, J. Wang, D. Chen, P. Liu, X. Wang, *J. Membr. Sci.* **2011**, *381*, 197-203.
[208] N. Jiang, G. Yang, X. Zhang, L. Wang, C. Shi, N. Tsubaki, *Catal. Commun.* **2011**, *12*, 951–954.
[209] E.A. Khan, A. Rajendran, Z. Lai, *Ind. Eng. Chem. Res.* **2010**, *49*, 12423-12428.
[210] E.A. Khan, E. Hu, Z. Lai, *Microporous Mesoporous Mater.* **2009**, *118*, 210-217.
[211] J. Zhou, X. Zhang, J. Zhang, H. Liu, L. Zhou, K. Yeung, *Catal. Commun.* **2009**, *10*, 1804-1807.
[212] J. Zheng, X. Zhang, Y. Wang, Y. Bai, W. Sun, R. Li, *J. Porous Mater.* **2009**, *16*, 731-736.
[213] N. Nishiyama, K. Ichioka, D.-H. Park, Y. Egashira, K. Ueyama, L. Gora, W. Zhu, F. Kapteijn, J.A. Moulijn, *Ind. Eng. Chem. Res.* **2004**, *43*, 1211-1215.
[214] N. Wang, W. Qian, K. Shen, C. Su, F. Wei, *Chem. Commun.* **2016**, *52*, 2011-2014.
[215] P.K. Dutta, J. Bronic, *Zeolites* **1994**, *14*, 250-255.
[216] J. Zheng, J. Ma, Y. Wang, Y. Bai, X. Zhang, R. Li, *Catal. Lett.* **2009**, *130*, 672-678.
[217] N. Ren, Y.-H. Yang, J. Shen, Y.-H. Zhang, H.-L. Xu, Z. Gao, Y. Tang, *J. Catal.* **2007**, *251*, 182-188.
[218] S. Li, A. Tuel, F. Meunier, M. Aouine, D. Farrusseng, *J. Catal.* **2015**, *332*, 25-30.
[219] S. Li, A. Tuel, D. Laprune, F. Meunier, D. Farrusseng, *Chem. Mater.* **2015**, *27*, 276-282.
[220] Q. Zhao, B. Qin, J. Zheng, Y. Du, W. Sun, F. Ling, X. Zhang, R. Li, *Chem. Eng. J.* **2014**, *257*, 262-272.
[221] R. Liu, H. Tian, A. Yang, F. Zha, J. Ding, Y. Chang, *Appl. Surf. Sci.* **2015**, *345*, 1-9.
[222] C. Xing, J. Sun, Q. Chen, G. Yang, N. Muranaka, P. Lu, W. Shen, P. Zhu, Q. Wei, J. Li, J. Mao, R. Yang, N. Tsubaki, *Catal. Today* **2015**, *251*, 41-46.
[223] Y. Jin, G. Yang, Q. Chen, W. Niu, P. Lu, Y. Yoneyama, N. Tsubaki, *J. Membr. Sci.* **2015**, *475*, 22-29.
[224] G. Yang, H. Kawata, Q. Lin, J. Wang, Y. Jin, C. Zeng, Y. Yoneyama, N. Tsubaki, *Chem. Sci.* **2013**, *4*, 3958-3964.
[225] G. Yang, C. Xing, W. Hirohama, Y. Jin, C. Zeng, Y. Suehiro, T. Wang, Y. Yoneyama, N. Tsubaki, *Catal. Today* **2013**, *215*, 29-35.
[226] S. Sartipi, J.E. van Dijk, J. Gascon, F. Kapteijn, *Appl. Catal., A* **2013**, *456*, 11-22.
[227] G. Yang, D. Wang, Y. Yoneyama, Y. Tan, N. Tsubaki, *Chem. Commun.* **2012**, *48*, 1263-1265.
[228] C. Li, H. Xu, Y. Kido, Y. Yoneyama, Y. Suehiro, N. Tsubaki, *ChemSusChem* **2012**, *5*, 862-866.
[229] B. Sun, G. Yu, J. Lin, K. Xu, Y. Pei, S. Yan, M. Qiao, K. Fan, X. Zhang, B. Zong, *Catal. Sci. Technol.* **2012**, *2*, 1625-1629.

[230] G. Yang, M. Thongkam, T. Vitidsant, Y. Yoneyama, Y. Tan, N. Tsubaki, *Catal. Today* **2011**, *171*, 229-235.
[231] J. Bao, G. Yang, C. Okada, Y. Yoneyama, N. Tsubaki, *Appl. Catal., A* **2011**, *394*, 195-200.
[232] X. Huang, B. Hou, J. Wang, D. Li, L. Jia, J. Chen, Y. Sun, *Appl. Catal., A* **2011**, *408*, 38-46.
[233] G. Yang, N. Tsubaki, J. Shamoto, Y. Yoneyama, Y. Zhang, *J. Am. Chem. Soc.* **2010**, *132*, 8129-8136.
[234] Z. Wang, Y. Liu, J.-g. Jiang, M. He, P. Wu, *J. Mater. Chem.* **2010**, *20*, 10193-10199.
[235] X. Li, Y. Zhang, M. Meng, G. Yang, X. San, M. Takahashi, N. Tsubaki, *J. Membr. Sci.* **2010**, *347*, 220-227.
[236] X. Li, Y. Zhang, F. Meng, X. San, G. Yang, M. Meng, M. Takahashi, N. Tsubaki, *Top. Catal.* **2010**, *53*, 608-614.
[237] G. Yang, Y. Tan, Y. Han, J. Qiu, N. Tsubaki, *Catal. Commun.* **2008**, *9*, 2520-2524.
[238] J. Bao, J. He, Y. Zhang, Y. Yoneyama, N. Tsubaki, *Angew. Chem. Int. Ed.* **2008**, *47*, 353-356.
[239] G. Yang, J. He, Y. Zhang, Y. Yoneyama, Y. Tan, Y. Han, T. Vitidsant, N. Tsubaki, *Energy Fuels* **2008**, *22*, 1463-1468.
[240] G. Yang, J. He, Y. Yoneyama, Y. Tan, Y. Han, N. Tsubaki, *Appl. Catal., A* **2007**, *329*, 99-105.
[241] Y. Zhong, L. Chen, M. Luo, Y. Xie, W. Zhu, *Chem. Commun.* **2006**, 2911-2912.
[242] J. He, Z. Liu, Y. Yoneyama, N. Nishiyama, N. Tsubaki, *Chem. - Eur. J.* **2006**, *12*, 8296-8304.
[243] J. He, Y. Yoneyama, B. Xu, N. Nishiyama, N. Tsubaki, *Langmuir* **2005**, *21*, 1699-1702.
[244] T. Okubo, T. Wakihara, J. Plévert, S. Nair, M. Tsapatsis, Y. Ogawa, H. Komiyama, M. Yoshimura, M.E. Davis, *Angew. Chem. Int. Ed.* **2001**, *40*, 1069-1071.
[245] M. Miyamoto, T. Kamei, N. Nishiyama, Y. Egashira, K. Ueyama, *Adv. Mater.* **2005**, *17*, 1985-1988.
[246] A.M. Goossens, B.H. Wouters, V. Buschmann, J.A. Martens, *Adv. Mater.* **1999**, *11*, 561-564.
[247] M. Okamoto, L. Huang, M. Yamano, S. Sawayama, Y. Nishimura, *Appl. Catal., A* **2013**, *455*, 122-128.
[248] X. Zou, K.-L. Wong, S. Thomas, T.H. Metzger, V. Valtchev, S. Mintova, *Catal. Today* **2011**, *168*, 140-146.
[249] G.-R. Xu, J.-N. Wang, C.-J. Li, *RSC Advances* **2013**, *3*, 12985-12992.
[250] D. He, D. Liu, *RSC Advances* **2015**, *5*, 5438-5441.
[251] J. Zheng, X. Sun, Y. Du, B. Qin, Y. Zhang, H. Zhang, M. Pan, R. Li, *J. Mater. Res.* **2016**, 1-15.
[252] K. Miyake, Y. Hirota, K. Ono, Y. Uchida , N. Nishiyama, *ChemistrySelect* **2016**, *1*, 967-969.
[253] D. Mochizuki, R. Sasaki, M.M. Maitani, M. Okamoto, E. Suzuki, Y. Wada, *J. Catal.* **2015**, *323*, 1-9.
[254] M. Miyamoto, K. Mabuchi, J. Kamada, Y. Hirota, Y. Oumi, N. Nishiyama, S. Uemiya, *J. Porous Mater.* **2015**, *22*, 769-778.
[255] T. Du, H. Qu, Q. Liu, Q. Zhong, W. Ma, *Chem. Eng. J.* **2014**, *262*, 1199-1207.
[256] Q. Zhang, C. Li, S. Xu, H. Shan, C. Yang, *J. Porous Mater.* **2013**, *20*, 171-176.
[257] Z. Jin, S. Liu, L. Qin, Z. Liu, Y. Wang, Z. Xie, X. Wang, *Appl. Catal., A* **2013**, *453*, 295-301.

[258] M. Okamoto, Y. Osafune, *Microporous Mesoporous Mater.* **2011**, *143*, 413-418.
[259] Y.-J. Ji, B. Zhang, L. Xu, H. Wu, H. Peng, L. Chen, Y. Liu, P. Wu, *J. Catal.* **2011**, *283*, 168-177.
[260] D. Mores, E. Stavitski, S.P. Verkleij, A. Lombard, A. Cabiac, L. Rouleau, J. Patarin, A. Simon-Masseron, B.M. Weckhuysen, *PCCP* **2011**, *13*, 15985-15994.
[261] A. Lombard, A. Simon-Masseron, L. Rouleau, A. Cabiac, J. Patarin, *Microporous Mesoporous Mater.* **2010**, *129*, 220-227.
[262] R. Brent, S.M. Stevens, O. Terasaki, M.W. Anderson, *Cryst. Growth Des.* **2010**, *10*, 5182-5186.
[263] D. Van Vu, M. Miyamoto, N. Nishiyama, Y. Egashira, K. Ueyama, *Catal. Lett.* **2009**, *127*, 233-238.
[264] D. Kong, J. Zheng, X. Yuan, Y. Wang, D. Fang, *Microporous Mesoporous Mater.* **2009**, *119*, 91-96.
[265] X. Zhang, J. Wang, J. Zhong, A. Liu, J. Gao, *Microporous Mesoporous Mater.* **2008**, *108*, 13-21.
[266] M. Kustova, M.S. Holm, C.H. Christensen, Y.-H. Pan, P. Beato, T.V.W. Janssens, F. Joensen, J. Nerlov, Synthesis and characterization of mesoporous ZSM-5 core-shell particles for improved catalytic properties, in: P.M. Antoine Gédéon, B. Florence (Eds.) Studies in Surface Science and Catalysis, Elsevier, **2008,** pp. 117-122.
[267] D.V. Vu, M. Miyamoto, N. Nishiyama, S. Ichikawa, Y. Egashira, K. Ueyama, *Microporous Mesoporous Mater.* **2008**, *115*, 106-112.
[268] A.L. Yonkeu, G. Miehe, H. Fuess, A.M. Goossens, J.A. Martens, *Microporous Mesoporous Mater.* **2006**, *96*, 396-404.
[269] D. Van Vu, M. Miyamoto, N. Nishiyama, Y. Egashira, K. Ueyama, *J. Catal.* **2006**, *243*, 389-394.
[270] Y. Fan, D. Lei, G. Shi, X. Bao, *Catal. Today* **2006**, *114*, 388-396.
[271] R. Phienluphon, K. Pinkaew, G. Yang, J. Li, Q. Wei, Y. Yoneyama, T. Vitidsant, N. Tsubaki, *Chem. Eng. J.* **2015**, *270*, 605-611.
[272] U. Cimenler, B. Joseph, J.N. Kuhn, *Appl. Catal., A* **2015**, *505*, 494-500.
[273] K. Pinkaew, G. Yang, T. Vitidsant, Y. Jin, C. Zeng, Y. Yoneyama, N. Tsubaki, *Fuel* **2013**, *111*, 727-732.
[274] J. Hu, M. Chen, X. Fang, L. Wu, *Chem. Soc. Rev.* **2011**.
[275] X. Lai, J.E. Halpert, D. Wang, *Energy Environ. Sci.* **2012**, *5*, 5604-5618.
[276] S. Vaudreuil, M. Bousmina, S. Kaliaguine, L. Bonneviot, *Adv. Mater.* **2001**, *13*, 1310-1312.
[277] S. Vaudreuil, M. Bousmina, S. Kaliaguine, L. Bonneviot, *Microporous Mesoporous Mater.* **2001**, *44-45*, 249-258.
[278] N. Chu, J. Wang, Y. Zhang, J. Yang, J. Lu, D. Yin, *Chem. Mater.* **2010**, *22*, 2757-2763.
[279] J. Jiang, Y. Yang, C. Duanmu, Y. Xu, L. Feng, X. Gu, J. Chen, *Microporous Mesoporous Mater.* **2012**, *163*, 11-20.
[280] T.A. Vereshchagina, S.N. Vereshchagin, N.N. Shishkina, O.A. Mikhaylova, L.A. Solovyov, A.G. Anshits, *Microporous Mesoporous Mater.* **2013**, *169*, 207-211.
[281] S. He, Y. Wang, C. Yang, Y. Li, Z. Zhou, X. Tian, *Microporous Mesoporous Mater.* **2016**, *225*, 365-370.
[282] J. Cheng, S. Pei, B. Yue, L. Qian, C. He, Y. Zhou, H. He, *Microporous Mesoporous Mater.* **2008**, *115*, 383-388.
[283] L. Han, J. Yao, D. Li, J. Ho, X. Zhang, C.-H. Kong, Z.-M. Zong, X.-Y. Wei, H. Wang, *J. Mater. Chem.* **2008**, *18*, 3337-3341.

[284] J. Shi, X. Li, Q. Wang, Y. Zhang, Y. Tang, *J. Catal.* **2012**, *291*, 87-94.
[285] J. Shi, L. Chen, N. Ren, Y. Zhang, Y. Tang, *Chem. Commun.* **2012**, *48*, 8583-8585.
[286] B. Zornoza, O. Esekhile, W.J. Koros, C. Téllez, J. Coronas, *Sep. Purif. Technol.* **2011**, *77*, 137-145.
[287] N.L. Yue, M. Xue, S.L. Qiu, *Inorg. Chem. Commun.* **2011**, *14*, 1233-1236.
[288] C. Casado, J. Bosque, N. Navascués, C. Téllez, J. Coronas, *Microporous Mesoporous Mater.* **2009**, *120*, 69-75.
[289] J. Jiang, J. Yao, C. Zeng, L. Zhang, N. Xu, *Microporous Mesoporous Mater.* **2008**, *112*, 450-457.
[290] N. Ren, Y.-H. Yang, Y.-H. Zhang, Q.-R. Wang, Y. Tang, *J. Catal.* **2007**, *246*, 215-222.
[291] G. Schulz-Ekloff, J. Rathouský, A. Zukal, *Int. J. Inorg. Mater.* **1999**, *1*, 97-102.
[292] J.C. Groen, W. Zhu, S. Brouwer, S.J. Huynink, F. Kapteijn, J.A. Moulijn, J. Pérez-Ramírez, *J. Am. Chem. Soc.* **2007**, *129*, 355-360.
[293] J.C. Groen, L.A.A. Peffer, J.A. Moulijn, J. Pérez-Ramírez, *Chem. - Eur. J.* **2005**, *11*, 4983-4994.
[294] B. Gil, L. Mokrzycki, B. Sulikowski, Z. Olejniczak, S. Walas, *Catal. Today* **2010**, *152*, 24-32.
[295] J.C. Groen, T. Sano, J.A. Moulijn, J. Pérez-Ramírez, *J. Catal.* **2007**, *251*, 21-27.
[296] X. Wei, P.G. Smirniotis, *Microporous Mesoporous Mater.* **2006**, *97*, 97-106.
[297] B. Sulikowski, J. Datka, B. Gil, J. Ptaszynski, J. Klinowski, *J. Phys. Chem. B* **1997**, *101*, 6929-6932.
[298] J.C. Groen, J.A. Moulijn, J. Pérez-Ramírez, *Microporous Mesoporous Mater.* **2005**, *87*, 153-161.
[299] D. Verboekend, J. Perez-Ramirez, *Chem. - Eur. J.* **2011**, *17*, 1137-1147.
[300] D. Fodor, L. Pacosova, F. Krumeich, J.A. van Bokhoven, *Chem. Commun.* **2014**, *50*, 76-78.
[301] C. Mei, Z. Liu, P. Wen, Z. Xie, W. Hua, Z. Gao, *J. Mater. Chem.* **2008**, *18*, 3496-3500.
[302] R.M. Dessau, E.W. Valyocsik, N.H. Goeke, *Zeolites* **1992**, *12*, 776-779.
[303] D. Fodor, T. Ishikawa, F. Krumeich, J.A. van Bokhoven, *Adv. Mater.* **2015**, *27*, 1919-1923.
[304] D. Fodor, F. Krumeich, R. Hauert, J.A. van Bokhoven, *Chem. - Eur. J.* **2015**, *21*, 6272-6277.
[305] J. Zhou, Z.L. Hua, W. Wu, Z.C. Liu, Y. Zhu, Y. Chen, J.L. Shi, *Dalton Trans.* **2011**, *40*, 12667-12669.
[306] Y. Wang, M. Lin, A. Tuel, *Microporous Mesoporous Mater.* **2007**, *102*, 80-85.
[307] L. Burel, A. Tuel, *Microporous Mesoporous Mater.* **2013**, *174*, 90-99.
[308] S. Li, L. Burel, C. Aquino, A. Tuel, F. Morfin, J.-L. Rousset, D. Farrusseng, *Chem. Commun.* **2013**, *49*, 8507-8509.
[309] C. Dai, A. Zhang, M. Liu, X. Guo, C. Song, *Adv. Funct. Mater.* **2015**, *25*, 7479-7487.
[310] C. Dai, X. Li, A. Zhang, C. Liu, C. Song, X. Guo, *RSC Advances* **2015**, *5*, 40297-40302.
[311] C. Dai, A. Zhang, J. Li, K. Hou, M. Liu, C. Song, X. Guo, *Chem. Commun.* **2014**, *50*, 4846-4848.
[312] H. Tao, J. Ren, X. Liu, Y. Wang, G. Lu, *J. Solid State Chem.* **2013**, *200*, 179-188.
[313] C. Dai, A. Zhang, L. Li, K. Hou, F. Ding, J. Li, D. Mu, C. Song, M. Liu, X. Guo, *Chem. Mater.* **2013**, *25*, 4197-4205.
[314] Y. Wang, A. Tuel, *Microporous Mesoporous Mater.* **2008**, *113*, 286-295.

[315] M.P. Pina, R. Mallada, M. Arruebo, M. Urbiztondo, N. Navascués, O. de la Iglesia, J. Santamaria, *Microporous Mesoporous Mater.* **2011**, *144*, 19-27.
[316] J.A. van Bokhoven, N. Danilina, Aluminum in Zeolites: Where is it and What is its Structure?, Zeolites and Catalysis, Wiley-VCH Verlag GmbH & Co. KGaA, **2010**, pp. 283-300.
[317] M.A. Snyder, M. Tsapatsis, *Angew. Chem. Int. Ed.* **2007**, *46*, 7560-7573.
[318] Z. Lai, G. Bonilla, I. Diaz, J.G. Nery, K. Sujaoti, M.A. Amat, E. Kokkoli, O. Terasaki, R.W. Thompson, M. Tsapatsis, D.G. Vlachos, *Science* **2003**, *300*, 456-460.
[319] H.-K. Jeong, Z. Lai, M. Tsapatsis, J.C. Hanson, *Microporous Mesoporous Mater.* **2005**, *84*, 332-337.
[320] Y. Yoneyama, X. San, T. Iwai, N. Tsubaki, *Energy Fuels* **2008**, *22*, 2873-2876.
[321] J. Zhang, X. Zhang, W. Liu, H. Liu, J. Qiu, K.L. Yeung, *J. Power Sources* **2014**, *246*, 74-83.
[322] Z. Sun, S. Kaliaguine, *Int. J. Chem. React. Eng.* **2016**, *14*, 667-684.

Chapter 2- Synergy between Structure Direction and Alkalinity toward Fast Crystallization, Controlled Morphology and High Phase Purity of ZSM-12 Zeolite

Nima Masoumifard,[a,b,c] Serge Kaliaguine*[b] and Freddy Kleitz*[a,c]

[a] Department of Chemistry, Université Laval, Quebec City, G1V 0A6, QC, Canada,
[b] Department of Chemical Engineering, Université Laval, Quebec City, G1V 0A6, QC, Canada,
[c] Centre de Recherche sur les Matériaux Avancés (CERMA), Université Laval, Québec, G1V 0A6, QC, Canada,

Published in

Microporous and Mesoporous Materials

Volume 227, Pages 258-271

2016

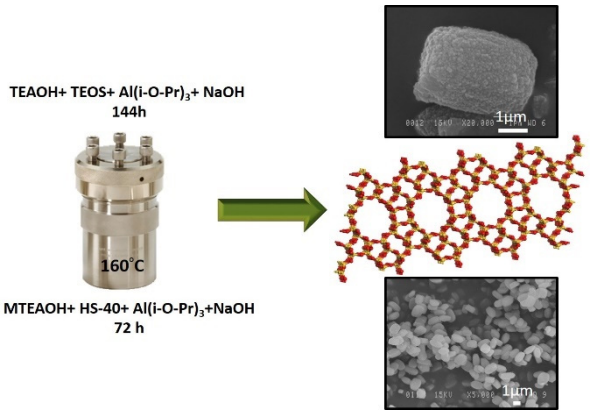

* Corresponding author:

Prof. Freddy Kleitz, E-mail: freddy.kleitz@chm.ulaval.ca, TEL: +1-418-656-7812

Prof. Serge Kaliaguine, E-mail: serge.kaliaguine@gch.ulaval.ca, TEL: +1-418-656-2708

Résumé

Visant un contrôle de la morphologie et de la pureté de phase du produit final, deux gabarits organiques disponibles dans le commerce, fournissant les cations de tetraethylammonium (TEA^+) et de methyltriethylammonium ($MTEA^+$) dans le mélange de synthèse, ont été utilisés pour la synthèse hydrothermale de la zéolithe ZSM-12. En tant que facteurs clés, l'alcalinité, le rapport eau/silicium du mélange réactionnel et les types de sources d'aluminium, ont été étudiées de manière approfondie avec ces deux gabarits organiques. Tous les produits obtenus ont été caractérisés par diffraction de rayons X (DRX), microscopie électronique à balayage (MEB), physisorption d'azote, spectroscopie RMN du ^{29}Si et ^{27}Al à l'état solide et l'analyse thermogravimétrique (ATG). À l'aide du gabarit organique TEA^+ sous forme d'hydroxyde, des sources en Si et Al organiques ainsi que le bon ajustement des teneurs en eau et d'hydroxyde de sodium dans le mélange réactionnel, des particules polycristallines de tailles identiques de ZSM-12 ont été synthétisées avec une haute cristallinité et une grande pureté. Pour contourner les inconvénients liés à l'utilisation du TEA^+, le $MTEA^+$ sous sa forme d'hydroxyde (MTEAOH) a été utilisé et a conduit à la formation de monocristaux de ZSM-12 de tailles identiques. Lors de l'utilisation MTEAOH comme agent structurant organique, l'ion hydroxyde, la teneur en Na^+ et le type de source d'aluminium ont joué un rôle majeur dans la nucléation et la croissance des cristaux de ZSM-12. En raison de l'augmentation de l'alcalinité du mélange de synthèse, le MTEAOH a également favorisé une cristallisation plus rapide sur une large gamme de rapport Si / Al (de 30 à l'infini). Les cristaux monodisperses synthétisés possèdent une morphologie cubique bien définie et sans impuretés.

Abstract

Aiming for a control of the morphology and phase purity of the final product, two commercially available organic templates, supplying tetraethylammonium (TEA^+) and methyltriethylammonium ($MTEA^+$) cations in the synthesis mixture, were used for the hydrothermal synthesis of ZSM-12 zeolite. As key factors, alkalinity and water content of the synthesis mixture and silicon and aluminum source types were comprehensively studied using these two organic templates. All the products obtained were characterized by powder XRD, SEM, N_2 physisorption, ^{29}Si and ^{27}Al-MAS solid state NMR and TGA techniques. Using TEAOH organic template and organic Si and Al sources along with the proper adjustment of water and sodium hydroxide contents in synthesis mixture, mono-sized polycrystalline particles of ZSM-12 with high crystallinity and purity were synthesized. Alleviating TEAOH drawbacks, $MTEA^+$ organocation in the hydroxide form was used which led to the formation of mono-sized ZSM-12 single crystals. When using MTEAOH organic template, hydroxide ion and Na^+ contents and the type of Al source were found to be playing major roles toward nucleation and growth of ZSM-12 crystals. Owing to increased alkalinity of the synthesis mixture, MTEAOH also promoted faster crystallization over a wide-range of Si/Al ratio (30 to ~infinity). The discrete mono-dispersed synthesized crystals possessed a well-defined cubic morphology with no impurities.

Keywords:

Hydrothermal Crystallization, ZSM-12 Zeolite, Alkalinity, Organic Template, Morphology Control

2.1 Introduction

The growing demands for zeolites as one of the best available porous catalysts and adsorbents [1] have encouraged many researchers to either introduce new types of zeolitic material or innovate and optimize the synthesis conditions of the existing frameworks [2, 3]. To date, more than 200 frameworks are known [4, 5] among which some, such as ZSM-12, have recently attracted more attention due to their exceptional pore topologies. ZS**M**-**TW**elve (MTW) is a high-silica zeolite (Si/Al >10) which was first invented by Mobil Research and Development scientists, Rosinski and Rubin in 1974 [6]. Later on, using more sophisticated techniques, the structural characteristics of ZSM-12 were discovered [7, 8]. In general, ZSM-12 framework owns a mono-dimensional non-interpenetrated pore structure with well-defined 12-membered ring channels run in the [0 1 0] direction. The framework topology has monoclinic symmetry (C2/m) with unit cell parameters of a= 2.4863 nm, b= 0.5012 nm, c= 2.4328 nm and β= 107.7° [9]. The elliptic ring opening has free diameters of ~ 5.6×6 Å, which is very narrow for a zeolite with 12-membered ring, for instance FAU-type aperture is almost 7.5 Å wide [10]. This exceptional pore size is more comparable to that of 10-membered ring zeolites, such as MFI and TON zeolites, which are extensively used in chemical industries. Searching alternatives for 10-membered ring catalysts with higher catalytic performances, ZSM-12, as a most interesting candidate, presents surface properties similar to those zeolites with medium-size pores along with many other features. First, the slightly larger pore size allows ZSM-12 to accommodate bulky intermediate species, enhancing catalytic efficacy in some applications, as discussed by Wang *et al.* [11] in a publication entitled "0.3 Å makes the difference". Second, single file diffusion within the 1D straight channels of ZSM-12 provides trapping ability of small molecules between strongly adsorbed large molecules. This appealing property was exploited to capture small un-burned hydrocarbons along with larger ones from automotive exhaust during the cold-start period [12]. Finally, non-interconnecting linear channels of ZSM-12 hinder catalyst deactivation by carbonaceous deposits, providing superior catalytic stability in a variety of hydrocarbon conversion reactions [13-16]. Regarding all these beneficial properties, ZSM-12 is becoming the focus of numerous catalytic studies searching for an optimized shape-selective catalyst, especially for reactions occurring in petroleum refining such as isomerization, alkylation, hydroisomerization, hydrocracking and oligomerization [15-28].

The great performance of ZSM-12, provided by its intricate channel system, can be further improved by optimizing other characteristics of the zeolite, besides its textural properties,

including framework acidity, phase-purity and crystal size and morphology. Especially, crystal size and morphology are of great importance in controlling selectivity and deactivation of a zeolite catalyst [29, 30]. It was demonstrated for many zeolite catalysts other than ZSM-12 that larger crystals suffer from faster deactivation [28, 31-33]. Furthermore, zeolites with 1D channel system, including ZSM-12, have a high crystal aspect ratio (length-to-width ratio) which creates mass transfer issues inside their long micropores. Therefore, controlling the size and morphology of ZSM-12 crystals promises improved catalytic performances [28]. The pivotal role of ZSM-12 size and morphology was recently demonstrated for the hydroisomerization of n-hexadecane [29]. This study showed that the ZSM-12 microcrystals with small dimensions exhibited higher isomer yield and selectivity towards mono-branched products. Moreover, considering the importance of nanozeolite in catalysis and separation [34], further size reduction of ZSM-12 is believed to immensely enhance their performance. Despite numerous reported works on ZSM-12 synthesis, [35-38], there are still no routes toward synthesizing nano-ZSM-12 particles from organic template-containing or template-free gels.

Morphological modification of a zeolite can be achieved by either modifying the classical solvothermal synthesis routes upon varying synthesis parameters, such as aging of the gel, introducing new organic templates, sources of silicon and aluminum, adjusting the synthesis temperature and composition of the starting gel [39, 34] or post-treatment [40, 41]. Looking for new methods, crystal-growth modifiers [42-45] and microemulsion techniques [46, 47] are also proposed to control the size and morphology of a crystalline zeolite. These chemicals can be solvents, surfactants or polymers [48-51]. In contrast to other types of zeolite, controlling the size and morphology of ZSM-12 crystals has rarely been studied. For instance, the crystal growth behavior of ZSM-12 was recently investigated using various co-solvents and growth-modifier chemicals (e.g., PEG, Brij 35) [52, 53]. Although these studies could successfully introduce a broader synthesis window for faster ZSM-12 crystallization, the size and morphology of the products did not show considerable improvements, compared to original synthesis using TEA^+ organocation and all led to the formation of large aggregates of intergrown nanocrystals. Moreover, the micro-emulsion technique might not be extended to the ZSM-12 synthesis conditions due to emulsion thermal stability issue at the high temperature used in the hydrothermal synthesis of ZSM-12 [47, 54]. Therefore, modifying the classical hydrothermal synthesis routes upon varying the synthesis parameters with no extra-additives would be a much more appealing technique to control

the ZSM-12 morphology. This technique was implemented for widely used zeolites, especially silicalite-1, leading to a full knowledge of its crystallization mechanism [55-57]. Unfortunately, the proposed size reduction methodology used for silicalite-1 zeolite, for instance, by using TEOS/organic template/water clear gel cannot be generalized and extended for other high silica zeolites, specifically ZSM-12 (TEOS: tetraethyl orthosilicate). Using six different organic templates, Cheng *et al.* [58] showed that such a synthesis mixture does not produce ZSM-12, not only at low temperatures (<100 °C) but also, at the conventional synthesis temperature, i.e., 160 °C.

High-silica zeolites such as ZSM-12 are mainly synthesized through hydrothermal treatment of an as-prepared gel. Using this classical technique, ZSM-12 microcrystals with different morphologies such as cubic, spherical, hexagonal, needle, rice-shaped crystals were reported [9, 35, 37, 38, 59, 60]. This diversity is mainly attributed to the types of organic molecular templates used for the synthesis [61] which act as either structure-directing or pore-filling agents. Although organic template-free seed-assisted synthesis, proposed by Okubo and coworkers, has successfully produced ZSM-12 microcrystals with rod-like morphology, the final product suffered from pore blocking, aggregation and intergrowth and wide particle size distribution [36, 62]. Moreover, it is not possible to synthesize pure silica zeolite using inorganic structure-directing agents [34]. All these show the pivotal role played by organic templates in ZSM-12 hydrothermal synthesis affecting the crystallization products in terms of crystalline phase, size and morphology [56, 63, 64].

In literature, there are many reports on the synthesis of ZSM-12 zeolites using various organic templates, starting with the work of Rosinski and Rubin who synthesized ZSM-12 zeolite using either a mixture of diethylsulphate and triethylamine or tetraethylammonium ions (hydroxide and bromide forms), all resulted in pure crystalline ZSM-12 [6]. Later on, several quaternary ammonium molecules, in the forms of hydroxides or halides of simple alkylammonium [29, 35, 37, 38, 65-67] and complex molecules such as cyclic and polycyclic N-heterocycles [68-77] were utilized. Because of the commercial availability and lower cost, simple quaternary ammonium molecules, i.e., $MTEA^+$ and TEA^+ cations, have extensively been used for ZSM-12 synthesis. Using methyltriethylammonium bromide (MTEABr) and tetraethylammonium hydroxide (TEAOH), ZSM-12 crystallization was thoroughly studied by Ernst *et al.* [37] and Gopal et al [38], respectively. Initially, MTEABr was introduced as the best candidate, allowing faster crystallization at higher Si contents along with reaching lower Si/Al ratios (22.5 to infinity) while TEA^+-based templates (at Si/Al<60) was leading to some

impurities such as ZSM-5 [37]. Reducing the cost of organic templates, two other forms of these organocations, i.e., MTEACl [66] and TEABr [35], were also proposed. Using one of these simple organic templates, the morphology of the final ZSM-12 product was also shown to be affected. For instance, ZSM-12 with an elongated cuboidal geometry (rice shaped) of crystallites with an average length of 5 μm and a diameter of 1.5 μm were obtained using MTEABr [37, 61] whereas cuboidal geometry of crystallites of a size smaller than 2 μm was produced using TEABr organic template [35, 61]. Such crystallization behavior was found to be highly reproducible by other researchers, even with slight changes [29].

Although zeolites such as ZSM-12 are highly selective to the type of organic templates being used, synthesis conditions are also playing a delicate role, i.e., one organic template, dedicated to ZSM-12 synthesis, may result in zeolites with different structures upon alternating the synthesis conditions. In addition to crystal phase, there is a strong correlation between the size and morphology of a specific zeolite and chemical sources and alkalinity of a synthesis mixture which can be controlled by an organic template, water content and the base [37, 78].

Considering all these facts, focusing on the composition of the classical gel mixtures of ZSM-12 and using new chemical sources seem to be a rational strategy to tailor the size and morphology of ZSM-12. In this contribution, the significant role of organic templates and the complementary effects between these species and other important parameters, such as alkalinity and chemical sources, will be discussed. In our study, we have tried to use commercially available inexpensive organic templates and adjust other important synthesis parameters aiming to optimize ZSM-12 particle size and morphology.

2.2 Experimental

2.2.1 Chemicals

Two types of commercially available quaternary ammoniums, tetraethylammonium hydroxide solution (TEAOH, Sigma, 40 wt% in water) and methyltriethylammonium chloride salt (MTEACl, Sigma, ≥97.0%), were used as molecular organic templates. LUDOX HS-40 colloidal silica (Sigma, 40 wt %,), sodium silicate solution (Fisher scientific, technical grade, 28.5 wt% SiO_2, 8.8 wt% Na_2O, 62.7 wt% H_2O) and tetraethyl orthosilicate (TEOS, Sigma, 98%) were used as the silicon sources. Various aluminum sources including sodium aluminum oxide (40 wt% Na_2O and 54 wt% Al_2O_3, Alfa Aesar, technical grade), aluminum nitrate nonahydrate ($Al(NO_3)_3.9H_2O$, Sigma) and aluminum isopropoxide ($Al(O\text{-}i\text{-}Pr)_3$, Sigma, >98%) were used. Sodium hydroxide pellet (NaOH, Fisher, 98.1%) was used to adjust the alkalinity and provide the required counter-ion for zeolite synthesis. Distilled water was the only solvent used for the gel preparation and washing steps. Organic salt was converted to hydroxide using Amberjet 4400 (OH) ion-exchange resin (Sigma).

2.2.2 Zeolite Preparation

All samples were prepared via hydrothermal treatment of a gel mixture at 160 °C in a Parr Teflon-lined autoclave which was firstly cleaned using dilute HF solution. Samples are numbered in the order of their appearance in the present contribution and reported in Tables 2.1 and 2.2.

2.2.2.1 Benchmark Syntheses

Based on the seminal works in the area of ZSM-12 synthesis, two different synthesis procedures were adapted to synthesize reference materials: one proposed by Ernst *et al.* [37] and another proposed by Gopal *et al.* [38]. The main difference is associated to the type of organic template used in each protocol. The former group used MTEABr, while the latter used TEAOH solution. The typical preparation methods of the benchmark samples are

briefly outlined in 2.6 supporting information. Replicating the synthesis proposed by Ernst *et al.* [37], MTEABr organic template was replaced by chloride salt, i.e., MTEACl [66].

2.2.2.2 Proposed Synthesis:

Depending on the type of organic templates used for ZSM-12 syntheses, the starting recipe was adapted from either Ernst *et al.* [37] or Gopal *et al.* [38], which was then further optimized to reach a protocol with controlled morphology and phase purity. Typical sample preparation methods are described below.

2.2.2.2.1 TEA^+ as Organic Template

TEAOH solution, water, $Al(O\text{-}i\text{-}Pr)_3$ and NaOH were all mixed in 100 ml round-bottom flask, capped and stirred until all solids were dissolved. TEOS was added drop-wise under vigorous stirring and the mixture was stirred overnight. Adjusting the H_2O/Si ratio, a part of the obtained clear solution was removed using a vacuum rotary evaporator at a temperature around 50 °C. The clear gel was then transferred into a 125 ml capacity Parr Teflon-lined stainless steel autoclave and crystallization was carried out statically at 160 °C under autogenous pressure in a convection oven. After 5.5 days, the autoclave was removed from the oven and cooled down to ambient temperature in air. After each synthesis, the resulting product was filtered, washed with copious amount of distilled water until neutralization and dried for at least 12 h at 100 °C in an oven. The organic template was removed by heating under air from room temperature to 600 °C with a heating rate of 1 °C min^{-1} and holding at 600 °C for 5 h.

2.2.2.2.2 $MTEA^+$ as Organic Template

MTEACl salt was ion-exchanged once by using 5-fold excess ion-exchange resin. The obtained dilute solution of methyltriethylammonium hydroxide (MTEAOH) was then concentrated using a rotary evaporator operating at 50 °C and vacuum of 50 mbar. Hydroxide concentration in the remaining solution was measured by titration with 0.1N HCl

standard solution using a VWR online pH-meter. The concentration of organic template solution was then adjusted to approximately 25 wt% using distilled water.

MTEAOH solution, water, $Al(O\text{-}i\text{-}Pr)_3$ and NaOH were mixed in 100 ml round-bottom flask, capped and stirred until a water-like solution was obtained. HS-40 colloidal silica was added drop-wise under vigorous stirring which continued for 12h. The clear gel was transferred into a 125 ml capacity Parr Teflon-lined stainless steel autoclave, followed by addition of NaOH 2M to increase the Na/Si molar ratio to desirable values. The gel was homogenized using a spatula and heated to 160 °C under autogenous pressure for 3 days. Similar procedure as TEA^+-samples was repeated for recovery, washing and calcination.

2.2.3 Characterization

Powder X-ray diffraction (XRD) patterns of all samples were recorded using two different instruments. For the qualitative study, quick scans were performed from 5-35 degree of 2θ with 2s dwell time and 0.1° step size using a Siemens powder diffractometer (40kV, 40mA) with CuK_α radiation (λ= 1.54059 Å). Evaluating the relative crystallinity (RC), a Siemens D5000 powder diffractometer with CuK_α radiation (λ= 1.54059 Å) was used. The diffractograms were collected between 2θ values of 5 and 35° with a step width of 0.02° and a step time of 1.2s. RC values for all samples were calculated using the sum of integral intensities of the six main diffraction peaks from the base-line corrected XRD pattern of each sample in the 7-25° 2θ range, corresponding to (200), (002), (-202), (310), (006) and (-406) atomic planes, divided by the corresponding intensities obtained for a benchmark sample. In this way, some samples presented higher sum of intensities than the corresponding benchmark, leading to RC values higher than 1. All samples used for relative crystallinity calculation were calcined prior to XRD measurements.

$$Relative\ crystallinity\ (\%) = \frac{\sum Area_{sample}}{\sum Area_{benchmark}} \times 100 \quad (1)$$

Scanning electron microscopy (SEM) studies were performed using a JEOL JSM-840A scanning electron microscope. To prepare the sample, a small quantity of the powder sample was placed onto the SEM sample holder and then coated two times with gold and palladium to attain adequate conductivity. Thermogravimetric analysis (TGA)

measurements were performed using a Netzsch STA 449C thermogravimetric analyzer under air purge flow of 20 ml/min with a heating ramp rate of 10 °C/min. Nitrogen adsorption/desorption isotherms were measured at liquid nitrogen temperature (-196 °C), using a Quantachrome Autosorb-1 adsorption analyzer. Prior to the measurements, the samples were evacuated at 200 °C for at least 12h on the outgassing station of the instrument. Total pore volume was estimated from the amount of nitrogen adsorbed at P/P_0= 0.95. The linear part of Brunauer-Emmett- Teller (BET) plot was used to calculate the specific surface area from adsorption data. Micropore BET assistant option provided in Quantachrome ASiQwin software was used to find the appropriate range of relative pressure for this calculation which mainly occurred at P/P_0 between 0.005 and 0.05. Micropore surface area and volumes were determined using non-local density functional theory (NLDFT) method applying the NLDFT metastable adsorption branch kernel and considering sorption of nitrogen at -196 °C in silica as a model adsorbent and cylindrical pores as a pore model. A Bruker DRX300 MHz spectrometer (7.00T) was used for recording ^{27}Al and ^{29}Si MAS NMR spectra in a standard zirconia rotor with a diameter of 4 mm at the spinning speed of 12 and 8 kHz, respectively. The ^{29}Si MAS NMR spectra were measured at a resonance frequency of 59.60 MHz. A total of 2000 scans were acquired with 3.05 μs pulse width and 30s recycle delays. ^{27}Al MAS NMR spectra were measured at a resonance frequency of 78.17 MHz, a pulse width of 1.55 μs, a recycle delay of 1s and a total number of scans of 2000. Prior to NMR measurements, all samples were finely ground and kept at room temperature for a long period of time. The same amounts of sample were used for all NMR tests. The chemical shifts, reported in ppm, were externally referenced relative to tetramethylsilane (TMS) for ^{29}Si and relative to aluminum nitrate solution-1M for ^{27}Al (δ= 0 ppm). Mnova V10.1 software was used to interpret the signals. Assuming similar sensitivities for Al in tetrahedral and octahedral coordination states, the percentages of Al in each state were calculated by dividing the corresponding peak area by the total area of all detectable ^{27}Al NMR signal.

2.3 Result and Discussion

Among all verified compositions for ZSM-12 synthesis, discussed in the literature [35, 37, 38, 66], two were chosen here as benchmarks for using TEAOH and MTEACl. The synthesis procedures of these benchmark samples are briefly described in 2.6 supporting information and summarized in Tables 2.1 and 2.2. These two common types of organocations, i.e., $MTEA^+$ and TEA^+ were further used as organic templates in modified conditions to synthesize ZSM-12 with controlled morphology. Regarding the hydrothermal treatment temperature, 160 °C was chosen here as an optimized temperature for all syntheses [37, 38]. High temperature (T> 140 °C) is necessary for ZSM-12 crystallization within a week, which at lower temperatures (T~ 100 °C) would take longer than three months [6]. The chemical compositions of the initial gel, the synthesis conditions and the crystalline phase of the final products are summarized in Tables 2.1 and 2.2. Reference samples using TEAOH and MTEACl organocations are designated as benchmarks, whereas all other products are indicated with a sample number which corresponds to their appearance in the text.

2.3.1 TEA^+ as Organic Template

TEA^+ is the most common organic template used to synthesize ZSM-12. In its hydroxide form, it provides wider synthesis window for ZSM-12 zeolites than the halide forms, e.g., TEABr [35]. Moreover, using TEAOH as the organic template in a dilute condition, the resulting synthesis mixture would be a clear solution with low viscosity, compared to synthesis gels prepared from other available organic templates. This is a beneficial gel property which can be exploited for controlling the size and morphology of zeolite crystals using confined space synthesis [79-81]. Regarding the positive effects of reduced gel viscosity, choosing the right sources of the T elements (T: Si, Al) such as TEOS or sodium silicate and $Al(O\text{-}i\text{-}Pr)_3$ with the ability of producing monomeric silicate and aluminate species is also of great importance. Using such sources in a finely controlled alkalinity can directly affect the nucleation and crystal growth kinetics and consequently, the crystallite size and shape, making them very popular in nanozeolite syntheses [34]. In contrast to molecular silicon sources, amorphous polymeric silicon sources such as fumed silica and colloidal silica solution, result in either the formation of large and intergrown crystals [49,82, 83] or

single crystals with wide size distribution [49, 55, 82]. In the case of sodium silicate, despite providing silicate oligomers, large zeolite crystals are usually produced probably owing to its high Na^+ cation content [49, 83-84]. In conclusion, although TEOS and $Al(O\text{-}i\text{-}Pr)_3$ are high-cost reagents, they can readily yield monomeric silicate species upon hydrolysis and contribute more effectively to viscosity reduction and size and morphology control [55]. Therefore, these two chemical sources were proposed as alternative sources for silicon and aluminum, respectively.

Replacing aluminum nitrate by $Al(O\text{-}i\text{-}Pr)_3$ while other conditions remained identical, led to the same result as the benchmark (Benchmark-TEA^+), however, the crystallization becomes more rapid, which is attributed to the increased alkalinity (Sample 1, Table 2.1). Using TEOS, however, as the silicon source in the benchmark to provide equimolar silicon in the gel as colloidal silica, with other chemicals and conditions kept similar, has led to the formation of a thick gel at the end of the crystallization period and did not form any ZSM-12 crystals (Sample 2, Table 2.1). Similar results are reported by Cheng *et al.* [58] who were trying to synthesize ZSM-12 from TEOS/organic template/water mixture. The lack of alkali cations in the synthesis mixture was initially assumed to be the reason for failed synthesis. Adding however NaOH while the $[OH^-]$ was kept constant, did not enhance the formation or growth of ZSM-12 at lower temperatures using 4,4′-trimethylenebis(1,1′-dimethylpiperidinium) dihydroxide as the organic template. They did not report the result for 160 °C for any organic templates in the presence of NaOH [58]. Similar to $Al(O\text{-}i\text{-}Pr)_3$, using TEOS as silicon source can possibly change the composition of the initial gel mixture in terms of alkalinity and water content and consequently hinders the nucleation of ZSM-12 zeolite.

Table 2.1- ZSM-12 synthesis conditions using TEAOH as the organic template[a]. The temperature was set to 160 °C for all the syntheses.

Name	Si Source	Organic template	Na Source	Al Source	Time (h)	(Si/Al)	(TEA^+/Si)	(Na/Si)	(H_2O/Si)	(OH^-/Si)[b]	Crystalline phase	RC[c]
Benchmark-TEA^+	HS-40	TEAOH	NaOH	$Al(NO_3)_3.9H_2O$	144	61	0.245	0.019	15	0.21	ZSM-12	1
Sample 1	HS-40	TEAOH	NaOH	Al(O-i-Pr)$_3$	98	61	0.25	0.02	14	0.26	ZSM-12	0.95
Sample 2	TEOS	TEAOH	NaOH	$Al(NO_3)_3.9H_2O$	132	61	0.25	0.019	14	0.22	Amorphous	-----
Sample 3	TEOS	TEAOH	$Al_2O_3.Na_2O$	$Al_2O_3.Na_2O$	168	86	0.22	0.0146	9.5	0.22	ZSM-5	-----
Sample 4	TEOS	TEAOH	$Al_2O_3.Na_2O$	$Al_2O_3.Na_2O$	156	87	0.23	0.0144	18	0.23	ZSM-5 +ZSM-12	-----
Sample 5	TEOS	TEAOH	$Al_2O_3.Na_2O$	$Al_2O_3.Na_2O$	120	87	0.22	0.0144	31	0.22	Amorphous + Zeolite	-----
Sample 6	TEOS	TEAOH	$Al_2O_3.Na_2O$	$Al_2O_3.Na_2O$	192	84	0.22	0.0148	35	0.22	Amorphous + Zeolite	-----
Sample 7	TEOS	TEAOH	$Al_2O_3.Na_2O$	$Al_2O_3.Na_2O$	168	86	0.22	0.0145	40	0.22	Amorphous + Zeolite	-----
Sample 8	TEOS	TEAOH	NaOH	Al(O-i-Pr)$_3$	144	85	0.22	0.029	19	0.24	~ ZSM-12	0.63
Sample 9	TEOS	TEAOH	NaOH	Al(O-i-Pr)$_3$	144	85	0.22	0.029	13.5	0.24	ZSM-12	1.24
Sample 10	TEOS	TEAOH	NaOH	Al(O-i-Pr)$_3$	168	84	0.22	0.056	13.5	0.27	ZSM-12	1.04
Sample 11	TEOS	TEAOH	NaOH	Al(O-i-Pr)$_3$	144	84	0.56	0.029	16	0.58	ZSM-5	-----

[a] Molar ratios are calculated based on initial gel composition after evaporating the solvent. The chemical loss during evaporation is neglected.

[b] Hydroxide concentration is calculated based on the protocol provided in Ref. [89].

[c] RC: relative crystallinity using a benchmark as a reference.

It is believed that one of the important factors in the gel preparation is the initial water content of the gel. Zeolite crystallization rate and the promoted crystalline phase over all competing phases depend on the water content of the reaction mixture [37, 85]. Moreover, finely adjusted water content plays a critical role on complete dissolution/hydrolysis of the chemicals present in any given gel composition. As reported, the consumption of two water molecules per TEOS has to be considered when adjusting the important H_2O/Si molar ratio of the final synthesis mixture [85]. The effect of H_2O/Si on our synthesis mixture was investigated by repeating the benchmark synthesis, using TEOS and sodium aluminum oxide and adjusting the water content. In order to avoid gelation in synthesis mixture (observed for Sample 2, Table 2.1), high quantity of water was initially added to synthesis mixture. After hydrolysis of TEOS, a certain amount of water was removed from gel to adjust the H_2O/Si ratio to desired values. Table 2.1 summarizes the synthesis conditions with various H_2O/Si ratios ranging from 9 to 40 (Samples 3-7, Table 2.1). After each synthesis, the synthesized zeolite was identified and its relative crystallinity was measured by powder XRD as depicted in Figure S 2.1. It is obvious that none of the syntheses resulted in pure phase ZSM-12; amorphous material formed when using a very dilute gel, and by decreasing the water, large crystals of pure ZSM-5 were formed. Figure S 2.2 shows the SEM images of the formed crystals and amorphous material. Using colloidal silica, Gopal *et al.* [38] did not observe any significant impact of water content on ZSM-12 purity, only a longer crystallization time upon decreasing the water content. Using the same silica source, Wei *et al.* [79] found that fine adjustment of H_2O/Si close to 10 is necessary for ZSM-12 formation under relatively low Si/Al ratios (Si/Al~ 40) and a small deviation lead to the formation of amorphous material. Less sensitivity to H_2O content was observed by increasing the Si/Al ratio to 60 and ZSM-12 were synthesized in a broader range of H_2O/Si ratios, even as high as 30. This conclusion is in contrast with what was observed here for TEOS as a silicon source which led to amorphous material at even higher Si/Al ratio (84) at H_2O/Si of 30.

For Sample 4 in Table 2.1 and the corresponding XRD pattern, i.e., Figure S 2.1c, ZSM-12 was partially formed at H_2O/Si ratio of 18, but lower values led to the formation of ZSM-5 (Sample 3). In addition to water content, partial evaporation could probably decrease the pH of the final mixture below the value required for ZSM-12 formation [86]. In order to promote ZSM-12 formation over other competing phases, Na^+ concentration and alkalinity were adjusted by simply doubling the NaOH content of the gel for two different H_2O/Si ratios, as reported in Table 2.1 (Samples 8-9). The major role of alkali ions to overcome the activation

barriers can also be deduced from the unsuccessful attempt for synthesizing ZSM-12 from TEOS/organic template/water mixture [58]. $Al(O\text{-}i\text{-}Pr)_3$ has been used for the new syntheses since its advantage over inorganic aluminum sources were demonstrated in Sample 1 by favoring ZSM-12 formation in a shorter time.

The XRD patterns of the products (Samples 8-9, Table 2.1) are depicted in Figure 2.1b,c along with the XRD data of the benchmark (Figure 2.1a) and the simulated XRD pattern for MTW zeolite [87]. Interestingly, Sample 8 with higher water content (ratio= 20) contained ZSM-5 and amorphous contaminations, even after 6 days, even though the NaOH content was doubled. This confirms that water plays a crucial role in stabilizing ZSM-12 framework under the proposed synthesis conditions. Higher reduction of water content (ratio= 13) eliminated the impurities by favoring complete crystallization of ZSM-12 zeolite in the synthesis gel (Sample 9). All the high intensity peaks associated to the structure of ZSM-12 zeolite and occurring at 2θ values of 7.4, 7.6, 8.9, 20.9, 23 and 23.1 are present in both benchmark and Sample 9 (Figure 0.3a,c), revealing that the synthesized material is highly crystallized and phase-pure ZSM-12 [37, 38]. Higher increase in NaOH content (Na/Si around 0.056), however, resulted in ZSM-12 with small ZSM-5 impurities as evidenced by a small shoulder peak at 7.9° (Figure 2.1d), although MTW phase is dominant (Sample 10, Table 2.1). This shows that there is an optimum NaOH content in which sufficient alkalinity and the Na^+ cations, required for ZSM-12 formation, are provided, and going beyond that optimal concentration may favor the nucleation of other competing zeolites.

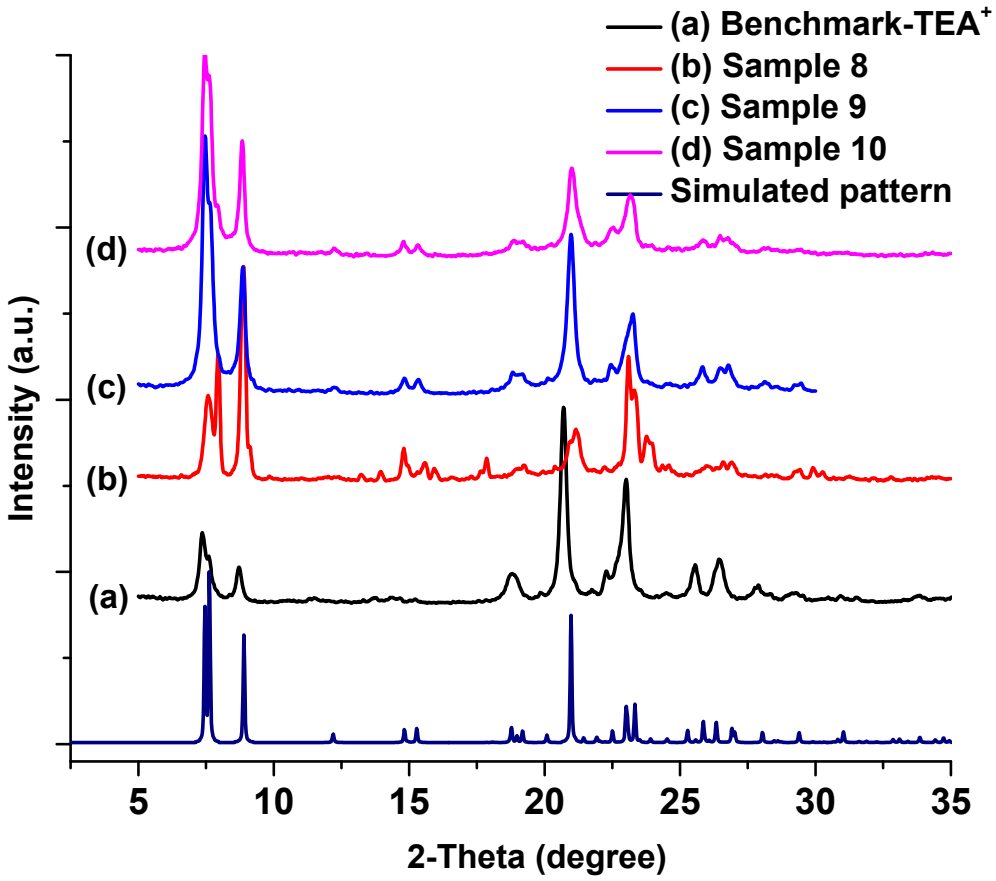

Figure 2.1- XRD patterns for (a) noncalcined TEA^+-based benchmark (Benchmark-TEA^+), (b,c) calcined ZSM-12 synthesized using TEOS and different water contents (Sample 8: H_2O/Si= 19 and Sample 9: H_2O/Si= 13), and (d) effect of NaOH/Si on modified TEA^+-ZSM-12 (Sample 10).

Comparing the crystallinity of the produced ZSM-12 to the benchmark, the relative crystallinity (RC) values for the pure ZSM-12 samples were evaluated and reported in Table 2.1. The RC value for these ZSM-12 samples has a strong correlation with water and alkaline contents. The samples synthesized by a gel with optimum water contents and enough NaOH are more crystalline than the synthesized benchmark and showed RC value higher than 100 %. It should be noted in all the synthesis attempts without water partial evaporation, crystalline zeolites had never been obtained even by adjusting Na/Si as high as 0.056 and prolonged heating time.

In order to study the size and morphology of the synthesized crystals, the SEM imaging technique was used. Figure 2.2a shows the scanning electron micrograph of the ZSM-12

benchmark synthesized using colloidal silica and aluminum nitrate as silicon and aluminum sources, respectively. The benchmark-TEA^+ particles are cube-shaped intergrown aggregates of nanocrystals and slightly smaller than a micron, as also reported by Gopal [38]. Figure 0.4b,c show the SEM micrographs of the materials synthesized using the modified gel (Samples 9 and 10). As can be seen, the shape of particles is more uniform than for the benchmarks, however, they were still polycrystalline particles, composed of intergrown nanocrystals.

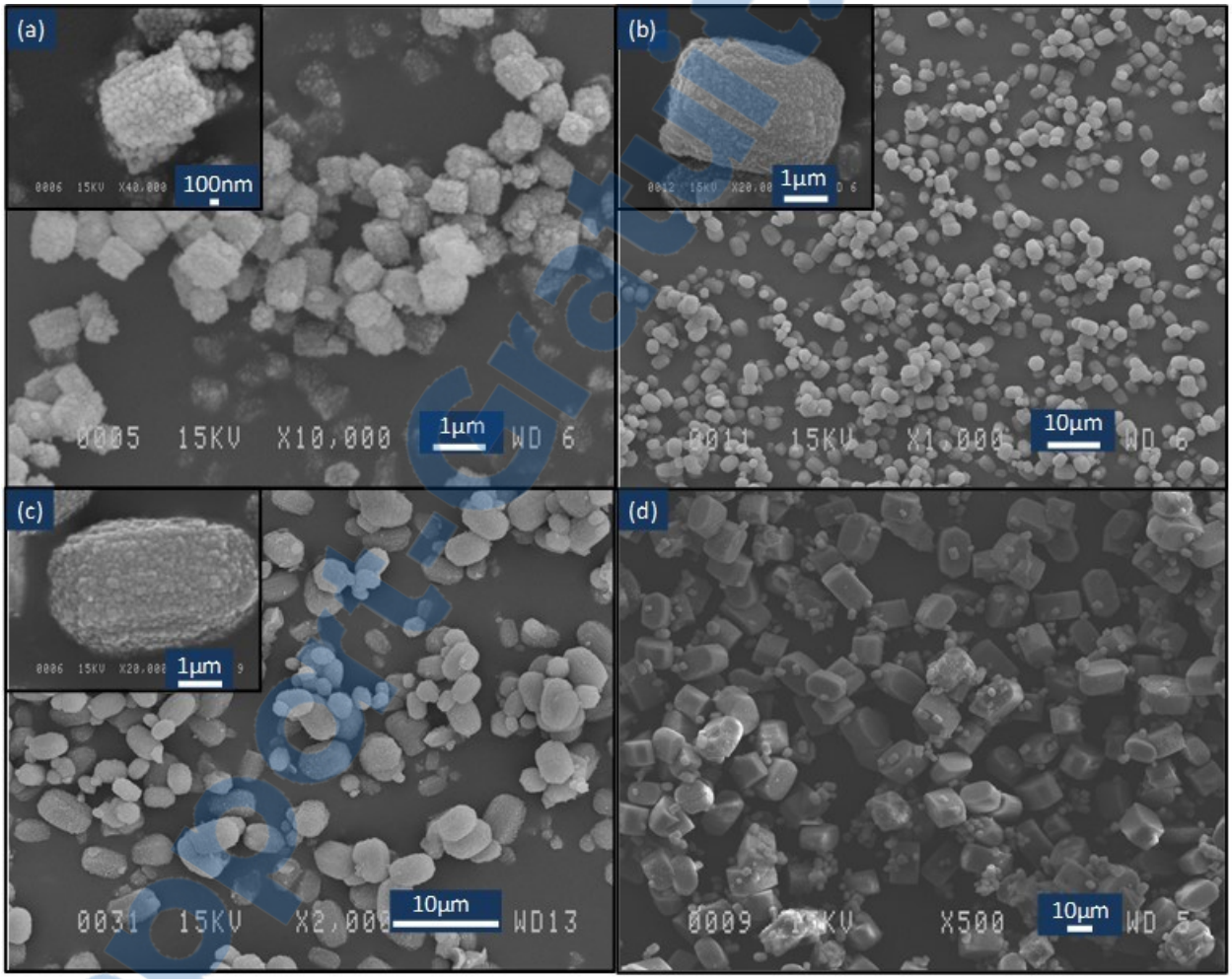

Figure 2.2- SEM images of (a) TEA^+-based benchmark (Benchmark-TEA^+), (b) calcined ZSM-12 synthesized using TEOS and H_2O/Si= 13 (Sample 9), (c,d) effect of NaOH/Si and TEA^+/Si on modified TEA^+-ZSM-12 (Sample 10 and Sample 11, respectively).

Regarding the textural properties of the synthesized ZSM-12 using TEA^+, Table 2.3 reports the data, extracted from N_2 sorption measurements (shown in Figure S 2.3). The product of modified syntheses showed results comparable to benchmark. Due to slightly larger crystals and lower interstitial spaces between intergrown crystals, the external surface area and mesopore volume decreased.

2.3.1.1 Issues with the Use of TEA^+- Why $MTEA^+$?

Although TEAOH is widely used for ZSM-12 synthesis, it suffers from some drawbacks, leading to a search for more reliable organic templates for ZSM-12, which are listed below.

1- Competing phases: Depending on TEA^+/Si and Si/Al ratio, TEAOH eventually favors one of several competing phases. For instance, depending on Si/Al ratio, at high TEA^+/Si (i.e., 0.25), zeolite Beta forms along with ZSM-12: the higher the Al content, the higher the concentration of Beta zeolite is [38]. On the other hand, when TEA^+/Si is low (i.e., 0.1), ZSM-5 impurities form together with ZSM-12 [37, 38]. This also means that adjusting Si/Al ratio for the synthesis of Al-rich ZSM-12 highly depends on the TEA^+/Si ratio. The effect of organic template concentration was studied by repeating the modified synthesis with three times higher TEAOH (Sample 11, Table 2.1). Figure 2.2d shows large crystals of ZSM-5, which is consistent with the XRD pattern of this sample (Figure S 2.1g). This shows that the optimized ratio for Na^+/Si and H_2O/Si strictly depends on organic template concentration, i.e., higher template at constant Si/Al ratio promotes the formation of other zeolites like ZSM-5, and lower TEAOH lowers the alkalinity, causing synthesis mixture gelation and/or amorphous impurities. This is in accordance with the findings that TEA^+ template for ZSM-12 has a more pore-filling role while for ZSM-5 it has a structure-directing effect [37, 38]. All these observations show a close relation between the final product phase and the gel composition in terms of Si/Al and TEA^+/Si. Although this tight relation can be slightly altered by controlling the alkalinity of the mixture toward ZSM-12 formation [37, 38], proper adjustment of [TEA^+], [OH^-] and water in a process with partial evaporation can be problematic and cause irreproducibility issues [86].

2- *Heterogeneous nature of the crystallization*: Another undesirable aspect of using TEA^+ as the organic template for ZSM-12 synthesis is that an amorphous transparent thick gel forms

even after a short hydrothermal treatment (less than 2h at 160 °C) using all sorts of silicon sources. This phenomenon can be attributed to highly uncontrolled polymerization reaction between silica and alumina precursor species [34], indicating the heterogeneous nature of ZSM-12 nucleation from a gel-mediated environment. The inhomogeneous hydrogel with significant chemical gradients hinders an abundant and uniform nucleation within the precursor gel mixture [34]. As a consequence of this non-uniform nucleation, it is very difficult to control the crystal growth rate, being a major barrier toward synthesizing ZSM-12 nano-crystals, which remains a challenging task to be addressed.

3- Large stacking faults and defect groups: Using TEA^+ organocations as a template normally leads to polycrystalline particles; consisting of strongly packed intergrown aggregates. Many grain and twin boundaries may form within the intergrown polycrystalline particles introducing a considerable number of defect sites into the zeolite framework. This was confirmed for ZSM-12 samples using $BMAN^{2+}$ (2,7-dibenzyl-2,7-dimethyl-2,7-diazoniaspiro[4.4]nonane cation) [9] and TEA^+ cation [61] organic templates. This is mostly attributed to the simultaneous creation of nucleation centers, spread at various locations within the hydrogel, ultimately leading to the simultaneous growth of small domains and twinning [9]. Material properties, especially the micropores accessibility of ZSM-12 with 1D channel system can be negatively affected by the occurrence of these stacking defects [36, 88].

4- TEAOH reagent tends to precipitate upon storage at ambient conditions which may change the chemical composition of the solution used in synthesis.

All these issues encouraged us to find new synthesis conditions for high-quality crystals of ZSM-12, especially with the use of available, easy to access organic templates such as $MTEA^+$.

2.3.2 $MTEA^+$ as the Organic Template

$MTEA^+$ possesses a relatively small and flexible molecule which weakly interacts with the framework during the synthesis and acts more as a pore-filling agent rather than structure-directing agent [9, 37]. It is also believed that the strong directing role of Na^+ in the nucleation and growth of ZSM-12 crystals may additionally weaken the structure-directing effect of this

organocation [9]. This type of interaction would result in smooth single crystals of ZSM-12 with rather perfect framework structure extending over a large domain [9]. Moreover, it is shown that $MTEA^+$ organocation enlarges the crystallization window of ZSM-12, favors aluminum incorporation into its framework and reduces the number of required moles of organocation in the hydrogel in comparison to TEA^+ template [61]. Considering all these studies, $MTEA^+$ can be identified as a more specific template for the synthesis of more regular ZSM-12 crystals with fewer defects.

Although it is proven that $MTEA^+$-based templates used so far, i.e., MTEABr and MTEACl, provide some advantages for ZSM-12 synthesis, there are still some important issues and concerns to be addressed such as long diffusion path in elongated 1D crystals [28] and long crystallization time. Using $MTEA^+$ in halide form has resulted into large elongated crystals of ZSM-12 with an average length of 5 μm [37] and 20 μm [9]. Using various compositional mixtures of TEA^+ and $MTEA^+$ while keeping the total number of moles for organic template constant, Katovic *et al.* [61] showed when the $MTEA^+$ moles in the synthesis gel exceeds that of TEA^+, the crystals become rice-shaped and larger, until, at pure $MTEA^+$-containing gel, it reaches the average crystal size eight times larger than those in the synthesis with sole TEA^+. Inspired by size-reduction strategy applied for nano-ZSM-5 synthesis, Ernst *et al.* [37] tried to reduce the product size by increasing the template concentration, however, this decreased the ZSM-12 crystallization yield and led to the formation of amorphous species without considerable change in crystal size.

This demands more studies on ZSM-12 crystallization in the presence of $MTEA^+$ to establish the important parameters controlling the crystallization behavior toward adjusting morphology and size in shorter crystallization period.

2.3.2.1 Using MTEAOH as Organic Template

A proper adjustment of the alkalinity in the synthesis mixture seems a viable way to solve $MTEA^+$-related issues by accelerating the crystallization (faster nucleation and growth), controlling the crystallization yield, crystal morphology and size and at the same time, preventing the nucleation of competing phases [37, 78]. Ernst *et al.* [37] introduced an optimum value for OH^- concentration (OH^-/Si ~ 0.3), adjusted by using NaOH, initial

increasing to a certain level (OH^-/Si ~ 0.2) led to a drastic acceleration in crystallization, however, any further increase did not show considerable enhancement in crystallization rate. In contrast to the great effect of OH^- on crystallization rate, the morphology has not been affected much by this ratio in their work. All these OH^- related findings encourage more study on such an important parameter. The alkalinity of a synthesis mixture can be controlled through various ways; i.e., the concentration of base ($NaOH/Na_2O$) and OH^- introduced by organic template in hydroxide form, aluminum source and water content.

In order to further study the effect of such an important parameter, the synthesis proposed by Ernst *et al.* [37] was repeated using the different chemical as Al source, i.e., $Al(O\text{-}i\text{-}Pr)_3$ (Sample 12- Table 2.2). Inorganic sources of aluminum such as alumina, sodium aluminate and aluminum nitrate or sulfate consume hydroxide ions (e.g., alumina acts as 2 moles of acid) upon Al incorporation into a zeolite framework as aluminate ion [89]. This leads to a lower alkalinity of the synthesis mixture compared to the gel prepared using $Al(O\text{-}i\text{-}Pr)_3$. Being able to compare the results, a benchmark was synthesized, adapted from Araujo *et al.* [66], using MTEACl as the organic template (Benchmark-$MTEA^+$- Table 2.2). Powder X-ray diffractograms of ZSM-12 benchmark and Sample 12 are depicted in Figure 2.3, showing all the peaks exclusively attributed to the structure of the ZSM-12 zeolite. These results confirm the production of pure phase ZSM-12 in shorter time upon using $Al(O\text{-}i\text{-}Pr)_3$ as Al source (around 96 h).

Table 2.2- ZSM-12 synthesis conditions using MTEAOH as the organic template[a]. The temperature was set to 160 °C for all the syntheses.

Name	Si Source	Organic template	Na Source	Al Source	Time (h)	(Si/Al)	($MTEA^+$/Si)	(Na/Si)	(H_2O/Si)	(OH^-/Si)[b]	Crystalline phase	RC[c]
Benchmark-$MTEA^+$	$Na_2Si_3O_7$	MTEACl	$Na_2Si_3O_7$	$Al(NO_3)_3.9H_2O$	156	94	0.4	0.597	37.8	0.32	ZSM-12	1
Sample 12	HS-40	MTEACl	NaOH	$Al(O\text{-}i\text{-}Pr)_3$	96	99	0.38	0.575	36	0.575	ZSM-12	1.22
Sample 13	HS-40	MTEACl	NaOH	$Al(O\text{-}i\text{-}Pr)_3$	120	87	0.34	0.217	23	0.217	ZSM-12+ZSM-5	----
Sample 14	HS-40	MTEAOH	NaOH	$Al(O\text{-}i\text{-}Pr)_3$	72	88	0.33	0.23	22	0.56	ZSM-12	1.23
Sample 15	HS-40	MTEAOH	NaOH	$Al(NO_3)_3.9H_2O$	72	89	0.3	0.23	22	0.5	Amorphous	----
Sample 16	HS-40	MTEAOH	NaOH	$Al(O\text{-}i\text{-}Pr)_3$	120	85	0.35	0.19	30	0.54	Amorphous	----
Sample 17	TEOS	MTEAOH	NaOH	$Al(O\text{-}i\text{-}Pr)_3$	144	90	0.3	0.23	23	0.53	ZSM-5	----
Sample 18	TEOS	MTEAOH	NaOH	$Al(O\text{-}i\text{-}Pr)_3$	84	90	0.31	0.23	12	0.54	ZSM-5	----
Sample 19	TEOS	MTEAOH	NaOH	$Al(O\text{-}i\text{-}Pr)_3$	96	87	0.15	0.24	19.5	0.38	ZSM-5	----
Sample 20	HS-40	MTEAOH	NaOH	$Al(O\text{-}i\text{-}Pr)_3$	84	30	0.32	0.23	22.4	0.55	ZSM-12	0.71
Sample 21	HS-40	MTEAOH	NaOH	$Al(O\text{-}i\text{-}Pr)_3$	144	33	0.3	0.235	22.3	0.54	ZSM-12	0.98
Sample 22	HS-40	MTEAOH	NaOH	-------	72	inf.	0.34	0.23	22	0.57	ZSM-12+ ZSM-5	1.04

[a] Molar ratios are calculated based on initial gel composition.
[b] Hydroxide concentration is calculated based on the protocol provided in Ref. [89].
[c] RC: relative crystallinity using a benchmark as a reference.

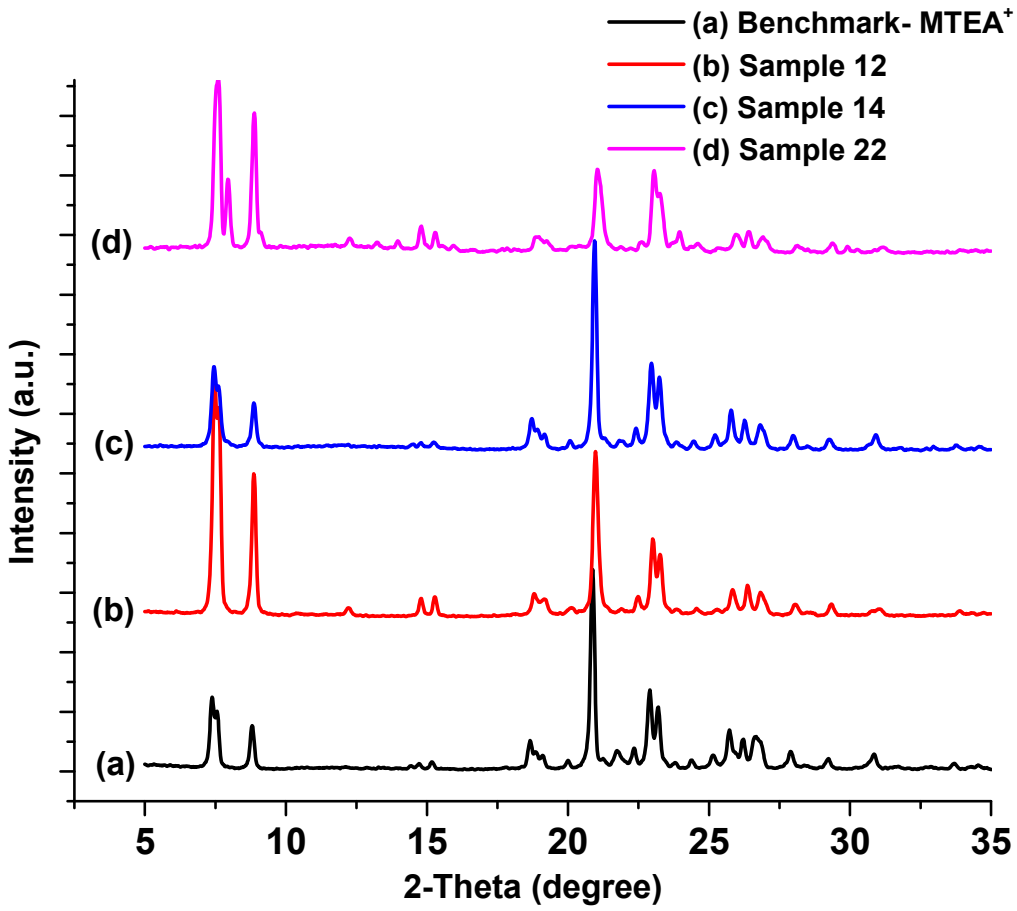

Figure 2.3- XRD patterns for (a) noncalcined $MTEA^+$-ZSM-12 benchmark (Benchmark-$MTEA^+$), (b) calcined ZSM-12 using $Al(O\text{-}i\text{-}Pr)_3$ (Sample 12), (c) noncalcined ZSM-12 using $Al(O\text{-}i\text{-}Pr)_3$ and MTEAOH (Sample 14), and (d) effect of Si/Al on modified $MTEA^+$-ZSM-12 (Sample 22).

Studying the morphology of the synthesized material, SEM images were obtained and depicted against the ZSM-12 benchmark in Figure 2.4. Benchmark-$MTEA^+$ (Figure 2.4a) consists of cubic crystals along with intergrown crystals or sheet-like impurities, however, Ernst *et al.* [37] reported rice-shaped ZSM-12 crystals of length 4-6 μm and ~ 1 μm diameter when the synthesis was carried out using MTEABr. Replacing Al source, cubic intergrown crystals with smaller sizes were formed (Figure 2.4b). The formed aggregates were quite large and very difficult to break.

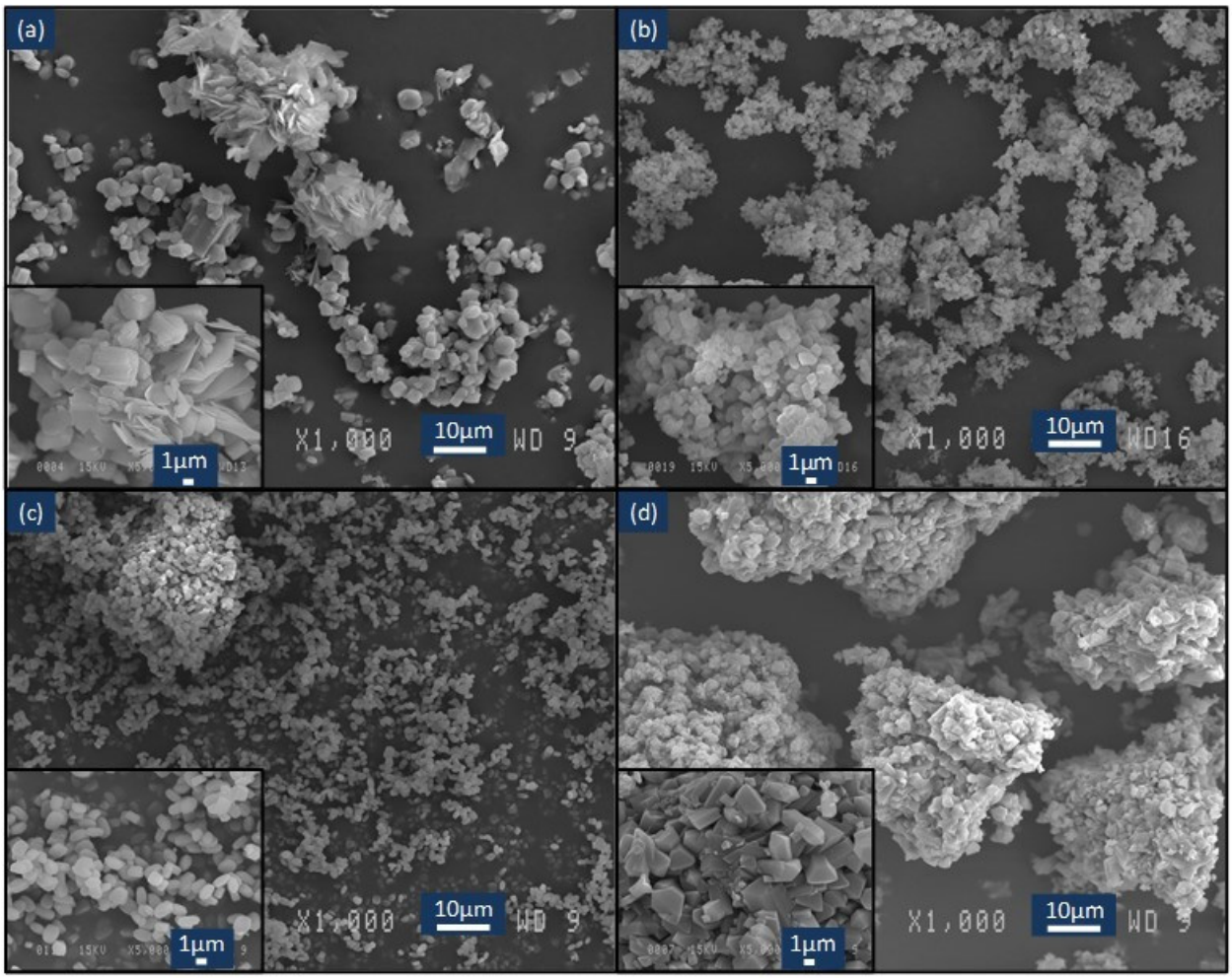

Figure 2.4- SEM images of (a) $MTEA^+$-ZSM-12 benchmark (Benchmark-$MTEA^+$), (b) ZSM-12 using $Al(O\text{-}i\text{-}Pr)_3$ (Sample 12), (c) ZSM-12 using $Al(O\text{-}i\text{-}Pr)_3$ and MTEAOH (Sample 14), and (d) effect of Si/Al on modified $MTEA^+$-ZSM-12 (Sample 22).

In contrast to rapid crystallization of ZSM-12, promoted by $Al(O\text{-}i\text{-}Pr)_3$, the intense aggregation and intergrowth of the crystals is undesirable and might be caused by the large Na^+ content of the gel proposed by Ernst *et al.* [37]. The drastic decrease in the Na^+ content of the starting gel led to the formation of ZSM-5 large crystals along with ZSM-12, most probably due to a decrease in alkalinity (Sample 13, Table 2.2 and Figure S 2.5a- XRD). Large crystals of ZSM-5 zeolite can be clearly seen in Figure S 2.6a. Organic templates can be exploited here, not only to act as structure-directing/pore-filling agent but also as a donor of hydroxyl ion and to balance the framework charge. Organic templates in hydroxide form ensure the high alkalinity and supersaturation level needed in the precursor solutions for

uniform and abundant nucleation [34]. In order to provide the OH^-/Si concentration required for the formation of high-quality ZSM-12 single crystals, OH^- exchanged MTEACl is considered as one of the best choices to compensate the reduced alkalinity. As expected, using MTEAOH led to the formation of pure phase ZSM-12 (Sample 14- Table 2.2). The XRD analysis of the product (Figure 2.3c) showed well-defined Bragg diffraction peaks with slightly higher intensities compared to those of the benchmark (Figure 2.3a), confirming the formation of highly crystalline, pure MTW-type zeolite after 72 h of the hydrothermal treatment. Figure 2.4c shows the SEM images of monodispersed cubic single crystals of ZSM-12. Using MTEAOH and $Al(O\text{-}i\text{-}Pr)_3$ provides opportunities to increase the alkalinity (OH^-/Si) of the gel mixture from 0.3 in the benchmark to around 0.55 in proposed sample (Table 2.2, sample 14), without adding more NaOH. Two interesting features of the proposed synthesis route will be discussed in the following sections:

2.3.2.1.1 Crystallization Time- Rapid Crystallization

ZSM-12 synthesis is quite long (~ week) and accelerating the crystallization process by increasing synthesis temperature may increase the impurities such as cristobalite [37] as well as Hofmann elimination of the template, as reported for $MTEA^+$ [9]. As can be seen in Table 2.2, one of the advantages of using MTEAOH is the rapid crystallization. It is economically important to reach a condition (temperature, chemical reagents and composition) that could lead to a shorter crystallization time without compromising the quality of the synthesized material in terms of purity, crystallinity, size and morphology. Ernst *et al.* [37] have tried to enhance the rate of crystallization by adjusting Na^+ content, however, they found a slight decrease in crystallization time at its optimum concentration (Na^+/MTEABr ratio ~ 1.5). Studying the crystal formation versus hydrothermal treatment time, similar synthesis gel as the benchmark was used by Cejka *et al.* [65], finding that only X-ray amorphous materials form up to about 80h of hydrothermal treatment. The first diffraction lines of ZSM-12 appeared after 96h, and finally, well-crystalline zeolite material was synthesized after at least 144h. Using the gel of Sample 14, the evolution of ZSM-12 versus time was followed by X-ray powder diffraction. The XRD results depicted in Figure S 2.4, show that crystallization had already taken place after 24h hydrothermal treatment. As time elapses, there is a slow increase in crystallinity. It is clear that after about 72h at 160 °C, a highly crystalline sample was obtained. Longer crystallization time did not improve the

crystallinity of the final product (Figure S 2.4d). Considering the fact that the proposed gel composition has a high alkalinity while the Na^+ content was reduced to medium quantities, the great effect of OH^- concentration over other synthesis parameters on enhancing the rate of crystallization is evident.

2.3.2.1.2 Controlled Size and Morphology

Another advantage of using the proposed gel is the control of size and morphology, as evident from Figure 2.4c. As mentioned in the introduction section, the mutual effect of size and crystalline structure are contributing to better activity and higher catalytic performance of zeolites. Up to now, using TEA^+ has led to the smallest polycrystalline ZSM-12 crystals [59, 60]. This small size can improve the diffusion of reactants and products, as shown by Mehla *et al.* [29]. However, using TEABr leads to aggregates of nanocrystals which might produce lots of grain boundaries and as consequent difficulties in diffusion [9, 36, 88]. Using MTEABr or organic-template free syntheses also results in rod-like crystals which are mostly intergrown with each other [9, 36, 37, 62]. Therefore, having ZSM-12 single crystals with controlled morphology and lower aspect ratio, as Sample 14, may promisingly contribute to enhancing the ZSM-12 catalyst performance.

2.3.2.2 Effect of Al Source

In order to study the effect of inorganic sources for Al on the proposed gel, $Al(NO_3)_3.9H_2O$ was used which has led to amorphous material after 72h of hydrothermal treatment (Sample 15, Table 2.2 and Figure S 2.5b- XRD). This can be attributed to a decreased alkalinity and complex interaction between silica and alumina precursor species which might dramatically alter the crystallization behavior of the hydrogel, however, because of the high-silica nature of ZSM-12, such strong sensitivity to Al source was not expected.

2.3.2.3 Effect of Water Content

Adjusting the water content of the gel, Ernst *et al.* [37] showed that the lower the H_2O/OH^- ratio, the faster and more complete the crystallization. In addition, water content presents a significant effect on the morphology of ZSM-12 as well; higher water led to more elongated crystals, increasing the length from around 1 to 5 µm [37]. In our case, increasing the water content of the modified gel resulted in the formation of amorphous materials, even after a long hydrothermal treatment (Table 2.2, Sample 16 and Figure S 2.5c- XRD).

2.3.2.4 Effect of Si Source

As previously discussed, zeolite precursor formation which occurs during the synthesis mixture preparation and hydrothermal treatment could highly affect the crystallization behavior including the crystallization rate and the framework type obtained [90, 91]. Different chemical sources for silicon and aluminum can control the creation of these aluminosilicate precursors under certain conditions such as high alkalinity and temperature. For instance, Toktarev and Ione [92] found that the synthesis of ZSM-12 with TEA^+ is sensitive to the nature of silicon source and pure ZSM-12 could be obtained only with silica gel, while other silicon sources produced analcime and ZSM-5. Aiming to synthesize ZSM-12 with smaller size, the silicon source was changed to TEOS at various key synthesis parameters such as water and organic template contents (Table 2.2, Sample 17-19). The X-ray pattern (Figure S 2.5d-f) showed only characteristic reflections of MFI-type zeolite, which is in accordance to the SEM data (Figure S 2.6b) showing the formation of large ZSM-5 microcrystals.

2.3.2.5 Effect of Al Content

2.3.2.5.1 Al-Rich ZSM-12

In the original patent, Rosinski and Rubin showed that ZSM-12 can preferentially be synthesized at high Si/Al ratios (>42.5). Afterward, there were just a few successful published works, attempting to reach lower Si/Al ratio (< 30) for ZSM-12. Depending on the organic template used, the minimum limit obtained for Si/Al ratio in different studies are

summarized based on their chronological order; 30 using MTEABr by Ernst *et al.* [37], 31 using TEAOH by Gopal *et al.* [38], 20 using MTEABr by Katovic *et al.* [16], 37-40 using MTEABr by Cejka *et al.* [65] and 33 using MTEACl by Araujo *et al.* [66]. Kamimura *et al.* [36] introduced an organic-template-free method to produce seed-assisted ZSM-12 samples with the minimum Si/Al ratio of 10.4–14.6, however, the pores were blocked and crystals were intergrown aggregates. Li *et al.* [23] have recently synthesized Al-rich ZSM-12 (Si/Al= 8-23) using a non-commercial organic template, which is claimed to be the lowest Si/Al composition among all published studies on ZSM-12. Reviewing this literature, Si/Al ratio of 30 was chosen to put the proposed composition, Sample 14, in test. It is believed that the obtained higher alkalinity can facilitate the incorporation of Al into the ZSM-12 framework, as confirmed in the case of Al-rich zeolites, such as high-silica Y zeolite and low-silica zeolite X [93]. Increasing aluminum content of the gel resulted in ZSM-12 formation (Samples 20 & 21), as confirmed by XRD (Figure 2.5a,b), and there was no competition between the ZSM-12 framework and other possible types of zeolites. It is reported that by lowering Si/Al ratio the gel crystallizes into other frameworks depending on the type of organic templates used such as β-zeolite [6, 38], ZSM-5 [37] and some unidentified crystalline contaminant [66]. None of the aforementioned crystalline impurities were observed in our synthesis (Figure 2.5a,b).

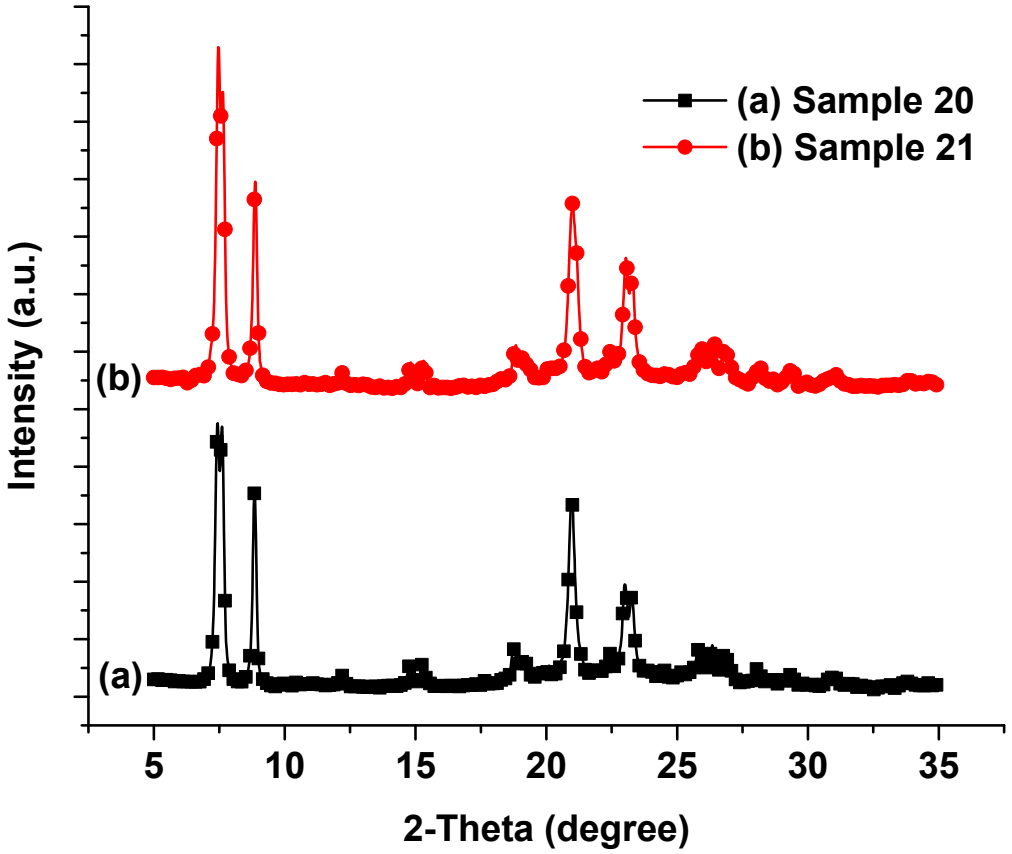

Figure 2.5- XRD patterns for calcined $MTEA^+$-ZSM-12 at Si/Al= 30 and hydrothermal treatment duration of (a) 84h (Sample 20), and (b) 144h (Sample 21).

In addition to competing impurities, it was also shown that increasing Al content of the gel negatively affects the quality of crystallization process by slowing down the rate of crystallization and lowering the synthesis yield and diminishing the crystallinity of the final product [37, 38, 65]. Similar behavior was observed in our modified synthesis route for producing Al-rich ZSM-12 (Samples 20 and 21). Decreasing the Si/Al ratio to 30, time-wise XRD measurements showed, in contrast to Sample 14, 72h of hydrothermal treatment was not long enough to reach the highest crystallinity for Al-rich zeolite (Figure 2.5a). This was previously explained by Lowenstein's rule which demonstrates, in contrast to silicon, none of the aluminate ions from solution can form an Al–O–Al bridges and they are only allowed to react with silicate groups on the growing crystal surface. Increasing the duration of the crystallization period to 144h enhanced the crystallinity (Figure 2.5b); however, it remained less crystalline than Sample 14. This confirms although longer crystallization time would be

required upon increasing the Al concentration in synthesis gel mixture, the poorer quality of the final product than the high Si zeolite might not be further improved after certain crystallization time, which is pretty consistent with the data obtained for ZSM-12 using different organic templates [37, 38, 65]. By visual inspection of low Si/Al samples, Figure S 2.7, large quantities of tiny contaminants were confirmed, especially at shorter crystallization times (Figure S 2.7a). Longer crystallization period decreased the amount of these contaminants; however, the surface of large crystals is still covered with tiny particles (Figure S 2.7b). Since XRD pattern showed the formation of ZSM-12 crystals with reasonable quality, the formation of small crystals over large ones can be due to the occurrence of secondary nucleation during hydrothermal treatment. These small particles might be less rich in Al than the large ones [94].

Depending on the type of organic template used, Si/Al ratio can also affect the crystal size and morphology of the final product [37, 65, 66, 78]. Using MTEACl as the organic template, Araujo *et al.* [66] found an increase in Si/Al ratio of the gel causes a decrease in the size of the ZSM-12 particles. Other researchers found an opposite trend [37, 65]. In general, by increasing the Al content of the gel mixture, smaller crystals are expected, but this size reduction is restricted by contaminating phases at very low Si/Al ratios. According to the SEM results of the synthesized samples (Figures 0.6 and S 0.8), reducing the Si/Al ratio from 90 to 30 did not make a significant change in the particle size and morphology, however, the monodispersity of the crystals was decreased.

Proper aluminum incorporation from the gel into the ZSM-12 framework was studied for selected samples using ^{29}Si MAS NMR and ^{27}Al MAS NMR characterization techniques (Figures 0.8 and 0.9). The ^{29}Si MAS NMR spectrum of all samples is a superposition of various signals. In the ^{29}Si NMR spectrum of benchmark-MTEA^{+} and sample 14 (Figure 2.6a,b), there are two main signals with chemical shifts at -111/-112 ppm and -109 ppm and a shoulder signal at around -104/-105 ppm, corresponding to Si-atoms in different tetrahedral sites of the ZSM-12 crystal structure [92]. According to literature, signals with chemical shifts at -112 to -109 ppm can be assigned to the Si(0Al) groups (Q^4 0Al) [95]. At lower Si/Al ratio, these two overlapping peaks merge into one rather broad peak, centered at -111 ppm, showing the crystals become less regular and contain more defects at high aluminum contents [61]. In addition to Si(0Al) dominating peaks, the shoulder signal at around -104/-105 ppm can be attributed to either Si(1Al) positions (Q^4 (1Al)) or SiOH defects groups (Q^3 (0Al)) located on the external surface of a single crystal [61, 86, 96]. Katovic *et*

al. [61] calculated the amount of Si(1Al) and SiOH groups contributing to this weak peak at -104ppm for ZSM-12 with Si/Al ~ 34-39 and reported quite similar shares for these two possibilities. Considering the spectrum of pure silica sample, Sample 22, the shoulder at -104 ppm was significantly dampened, showing that although it is believed that the defect sites concentration in Al-deficient ZSM-12 decreases, the shoulder peak might be mainly related to Si(1Al) compared to SiOH in our aluminum-containing samples. Another weak peak below -100 ppm was observed in Sample 20 spectrum, attributed to Si(2Al) and SiOH sites [95]. The comparable relative intensity for the Si(0Al) signal was recorded for the samples with close Si/Al ratio, especially at around -112 ppm, however, noncalcined and Al-rich samples showed lower intensities due to Si concentration.

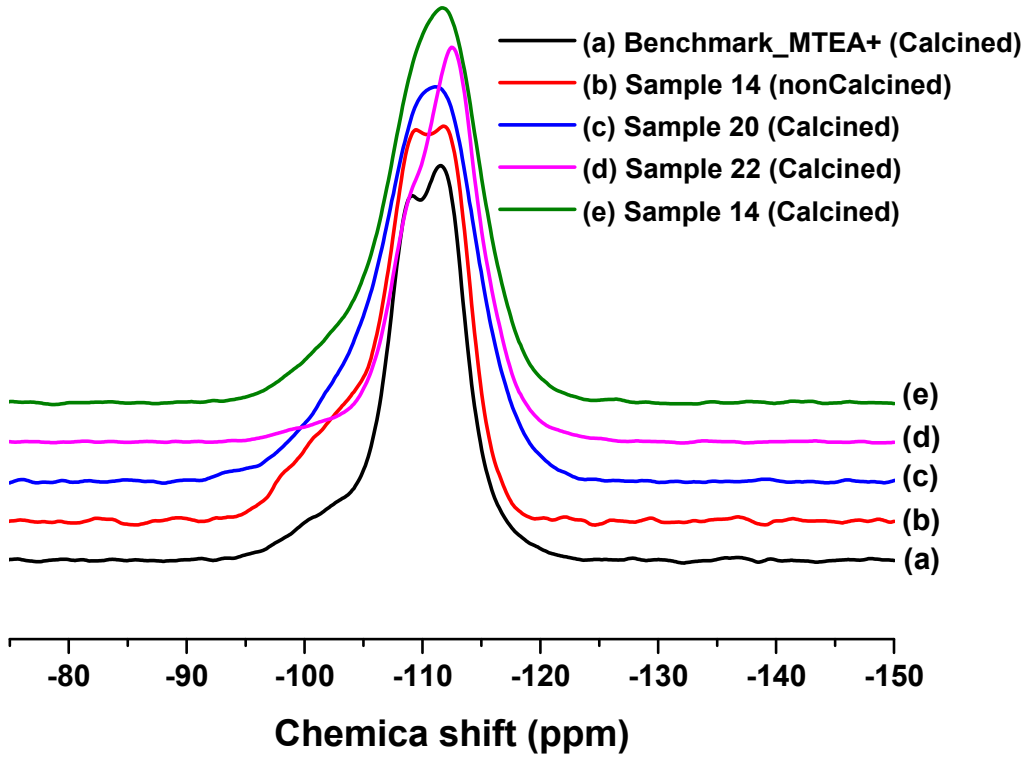

Figure 2.6- ^{29}Si MAS-NMR curves of (a) MTEA$^+$-ZSM-12 benchmark (Benchmark-MTEA$^+$) and modified MTEA$^+$-ZSM-12, (b) Si/Al= 90 (Sample 14- noncalcined), (c) Si/Al= 30 (Sample 20, calcined), (d) Si/Al~ inf. (Sample 22-calcined), and (e) Si/Al= 90 (Sample 14- calcined). The signal intensities were normalized by the maximum intensity in each curve.

^{27}Al MAS solid state NMR spectra were recorded for selected samples in order to determine the effect of Si/Al ratio on the aluminum atom environments in the sample. The ^{27}Al MAS NMR spectrum of calcined Samples 14 and 20, with different Si/Al ratios, along with the benchmark are shown in Figure 2.7. The benchmark spectrum exhibits only one symmetric resonance peak centered at δ= 56 ppm, while Samples 14 and 20 showed a slight shift to δ= 54. According to the literature, both of these symmetric chemical shifts correspond to tetrahedrally coordinated aluminum [16, 61, 62]. For the samples with higher Si/Al ratios, calcined or noncalcined, no signal peak at around δ= 0 ppm was observed, Figure 2.7a-c, which confirms the absence of octahedrally coordinated extra-framework aluminum [62]. However, the Al rich sample, Sample 20, exhibited another weak signal at around 0 ppm (Figure 2.7d), indicating the presence of a small number of octahedrally coordinated Al sites in the sample, probably formed by dealumination during the post-synthesis calcination processes [16, 62]. Calculating the peak area at 0 ppm and dividing by total peaks area at 56 and 0 ppm, the concentration of octahedral sites was estimated to be less than 2%. Repeating the test for as-synthesized Al-rich ZSM-12, Figure 2.7e, the peak around 0 ppm was eliminated which shows that all Al atoms prior to final calcination are properly positioned in ZSM-12 framework tetrahedral sites. It is shown that these octahedral sites, generated during the calcination process, can be reversibly transformed back into their original tetrahedral state by treatment of calcined solids in ammonium nitrate [97]. It can also be seen that ^{27}Al NMR spectra of some calcined samples are negligibly skewed toward upfield, making slightly asymmetric peaks. This may be attributed to distorted tetrahedral sites with chemical shift around 45 ppm. In total, high quality and catalytic performance of all synthesized samples can be concluded from the negligible number of distorted tetrahedral and octahedral Al sites, proved by ^{27}Al NMR technique [24].

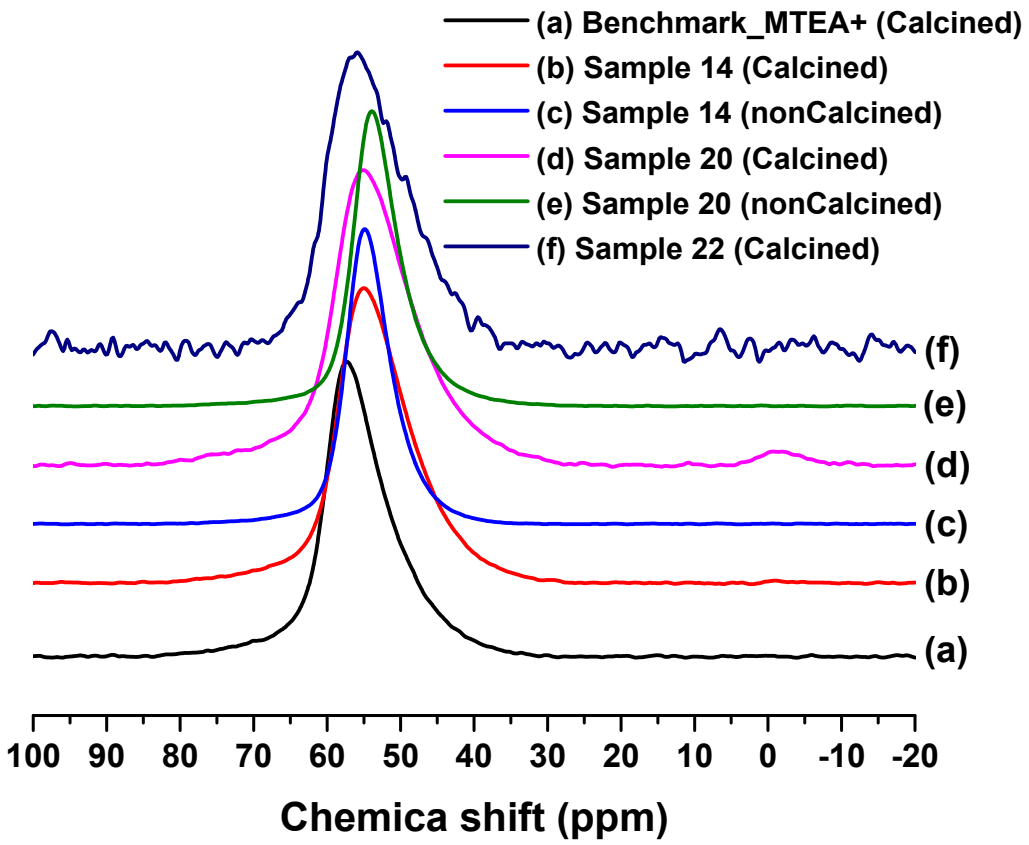

Figure 2.7- ^{27}Al MAS-NMR curves of (a) MTEA^{+}-ZSM-12 benchmark (Benchmark-MTEA^{+}) and modified MTEA^{+}-ZSM-12 zeolites: (b) Si/Al= 90 (Sample 14- calcined), (c) Si/Al= 90 (Sample 14-noncalcined), (d) Si/Al= 30 (Sample 20, calcined), (e) Si/Al= 30 (Sample 20, noncalcined), and (f) Si/Al~ inf. (Sample 22-calcined). The signal intensities were normalized by the maximum intensity in each curve.

2.3.2.5.2 Pure Silica ZSM-12

At the other extreme, synthesizing pure silica ZSM-12 zeolites is not easily achievable unless using non-commercial large complex organic templates and /or fluoride medium in an extended crystallization process [72, 73, 85, 98, 99]. Both these conditions remain as major constraints for scaling-up the synthesis of pure-silica ZSM-12 zeolite. Using simple organic template TEAOH, there is only one report on pure silica ZSM-12 synthesis by Mitra *et al.* [90], who proposed a two silicon sources method. However, other studies showed that at high Si/Al ratio (Si/Al > 200) of the synthesis gel mixture containing simple organic

templates, the formation of cristobalite is much favored during the hydrothermal synthesis of ZSM-12 at elevated temperatures [36, 37, 62, 78].

Using MTEAOH organic template, pure silica ZSM-12 was synthesized upon repeating the modified gel synthesis, Sample 14, without adding any Al source (Table 2.2, Sample 22). XRD data (Figure 2.3d) confirms the formation of ZSM-12 crystals in a shorter time, slightly contaminated with MFI type impurities. Eliminating Al source from synthesis mixture led to large aggregates of small crystals (Figure 2.4d). These firmly aggregated chunks are indeed intergrown crystals, showing not only $Al(O\text{-}i\text{-}Pr)_3$ affects the crystallization rate of ZSM-12, but also ensures the discreetness of the formed crystals. ^{29}Si MAS NMR spectrum of pure silica ZSM-12 (Figure 2.6d) showed a slight shift of the main peaks from -111 to -112 ppm, compared to Al-containing samples. It is also worth mentioning that the intensity of the peak at -104/105 ppm, assigned to Q^3 (0Al) sites, has dramatically diminished. Figure 2.7f, however, reveals a very weak peak for tetrahedral coordinated Al, which is likely introduced to the synthesis mixture via silicon source impurities [90, 100].

Figure 2.8 provides the N_2 adsorption- desorption isotherms of ZSM-12 synthesized using $MTEA^+$ with various Si/Al ratios, after burning off the organic template. All N_2 sorption isotherms showed an abrupt uptake below P/P_0= 0.02, followed by a plateau (Type I isotherm) which suggests the existence of micropores. In contrast to $MTEA^+$-based samples, the benchmark-TEA^+ exhibits a Type-IV isotherm with a hysteresis loop, which shows the presence of mesopores along with micropores (Figure S 2.3a). Textural properties including BET surface areas, micropore volumes, mesopore volumes and external surface area are summarized in Table 2.3. Even though the application of BET model for microporous materials is disputed, the surface areas are derived from the sorption isotherm at linear range of BET plot, i.e., P/P_0= 0.005 to 0.05, and used as *apparent* surface area for zeolite characterization [101, 102]. The highest BET surface area of around 380 m^2/g was observed for TEA^+-based samples. All the synthesized samples, except the aluminum rich one, Sample 21, showed high micropore surface area. It is worth mentioning that the micropore surface area is proportional to the degree of crystallinity and may be used as an indicative parameter to evaluate the purity of a zeolite sample [66]. From the pore volume data in Table 2.3, micropores (~ 0.12 cm^3/g) can be identified as the main contributor to total available pore volume compared to mesopores. Porosity measurements showed a considerable reduction in pore volume and surface area for Al-rich ZSM-12 (Sample 21). The Al-NMR results showed the formation of extra-framework Al species after calcination, which might

have whittled the textural properties of Al-rich samples. Moreover, higher Al amount means the higher content of counter-ion which can partially block the 1D pores in some localized sites [36, 88, 103, 104]. High stacking faults and structural defects may have occurred at Al rich sample, leading to pore blocking as investigated by Ritsch *et al.* [9] for ZSM-12 using two different types of organic template.

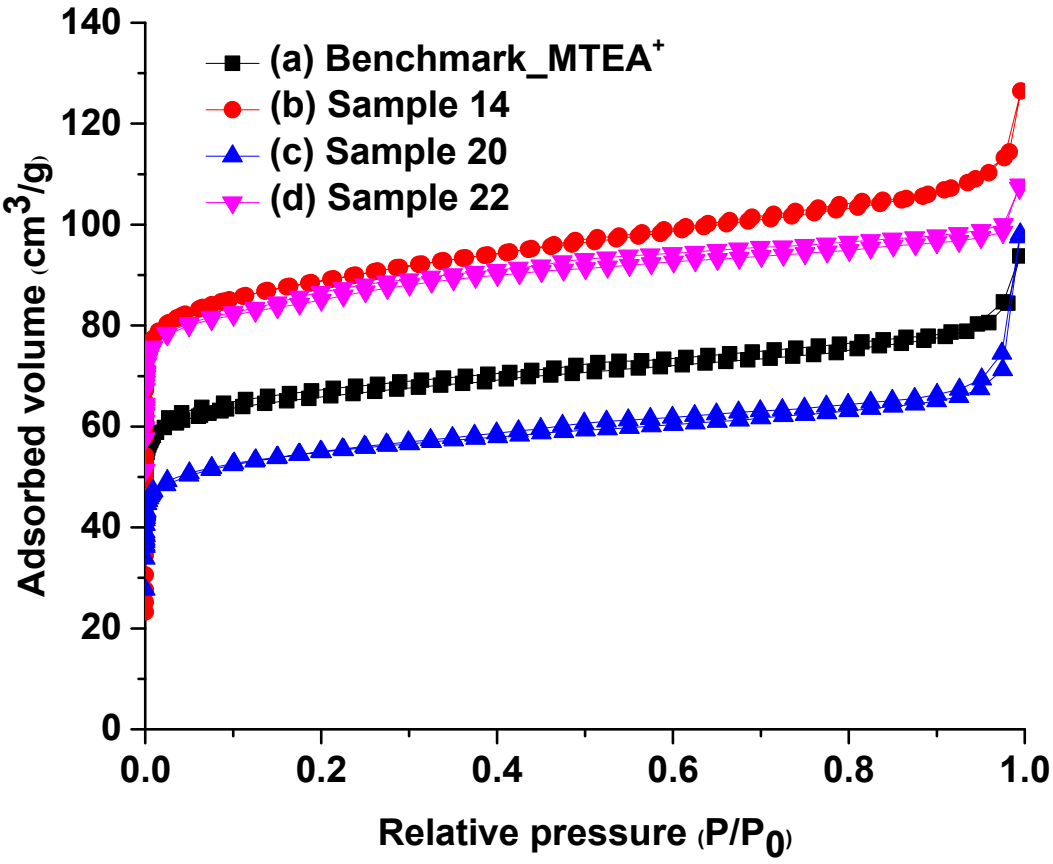

Figure 2.8- Nitrogen adsorption/desorption isotherms (-196 °C) for (a) $MTEA^+$-ZSM-12 benchmark (Benchmark-$MTEA^+$) and modified $MTEA^+$-ZSM-12 zeolites: (b) Si/Al= 90 (Sample 14), (c) Si/Al= 30 (Sample 20), (d) Si/Al~ inf. (Sample 22).

Table 2.3- Textural properties of ZSM-12 samples.

	Surface area (m^2/g)			Pore volume (cm^3/g)		
Sample name	**BET**	**Micro**	**External**	**Total**	**micro**	**meso**
Benchmark-$MTEA^+$	258	223	35	0.12	0.085	0.035
Benchmark-TEA^+	380	312	68	0.23	0.12	0.11
Sample 9	381	324	57	0.19	0.13	0.06
Sample 14	344	302	42	0.17	0.12	0.05
Sample 21	211	188	23	0.11	0.075	0.03
Sample 22	334	305	29	0.15	0.12	0.03

The amount of organic retained in the pore system of synthesized zeolites was determined by TG measurements (Figure S 2.8). Mass losses corresponding to different temperature ranges are reported in Table 2.4. Mass loss steps were differentiated for each sample into four main steps using corresponding DTG curve, as plotted in Figure S 2.8, and the maximum upper limit for each step is reported in Table 2.4. Mass loss below 250 °C is attributed to desorption of physically adsorbed/intracrystalline water. Al-rich samples, such as Sample 21, adsorbed the highest amount of water due to hydrophilic nature, while the pure silica sample, Sample 22, kept a little number of water molecules in its crystalline microporous system. The high-temperature mass-loss, below 600 °C, can be assigned to either decomposition/removal of trapped organic template, decomposition of charge compensating organocations, the combustion of organic residues strongly adsorbed on the acid sites or condensation of silanol groups [36, 38, 58, 62, 66]. Two distinct mass-loss steps in DTG curve were identified within different temperature ranges, 250-430 and 430-600 °C. The corresponding mass-losses were assigned to total organic template content (Step II+III) and the charge compensating TEA^+/$MTEA^+$ content (Step III), as reported in Table 2.4. Sample 21, as the richest sample in aluminum, showed the highest weight loss at step III, attributed to charge compensating organic template in ionic form. For a pure siliceous sample, however, the main mass-loss occurred at a lower temperature (Step II), with the highest value among all $MTEA^+$-based ZSM-12 zeolites. In addition, the total organic template content, obtained by summation of the mass loss in Step II and III slightly differs

depending on Si/Al ratio, i.e., the lower the Si/Al ratio, the lower the organic template retained in solid. This might be due to strict charge compensating effect of sodium ions in Al-rich zeolites [35]. Same results were obtained by Araujo *et al.* [66] using MTEACl, however, such a behavior is in contradiction with what was observed with organic templates such as diethyldimethyl ammonium ion, i.e., more Si results in less organics in the zeolite, even when higher concentration organic template in synthesis mixture was used [94]. In general, considering the data presented in Table 2.4, although the organocation content (organic template/Si) and Si/Al ratio of the gel for modified samples were different from those of the benchmarks, the total organic content of all as-synthesized ZSM-12 crystals is comparably similar, proving the pore-filling role of simple organic templates in ZSM-12 synthesis [9, 37, 38].

Table 2.4- Thermogravimetric data for benchmarks as well as modified samples.

Temperature range (°C)	<250	<430	<600	<700	250-600	50-700
	Mass loss %					
Sample Name	**Step I**	**Step II**	**Step III**	**Step IV**	**Step II+III**	**Total**
Benchmark-$MTEA^+$	1.2	3.5	2.9	1.5	6.4	9.1
Benchmark-TEA^+	1.3	7.9	1.2	1.2	9.1	11.6
Sample 9	1.6	7.8	1.7	0.6	9.5	11.7
Sample 14	1.2	4.3	2.8	1.7	7.1	10
Sample 20/21	1.6	3.3	3.5	1.5	6.8	9.9
Sample 22	0.5	6.9	2.7	0.5	9.6	10.6

2.4 Conclusions

Owing to intrinsic properties and usefulness of ZSM-12 in a variety of applications, there is a re-emerging interest toward better understanding its structure and crystallization aspects. In this regards, the effect of different parameters such as alkalinity and chemical source types were studied using two commercial organic templates. Using TEAOH as the organic template, TEOS and $Al(O\text{-}i\text{-}Pr)_3$ were used as Si and Al sources. Although higher initial water

content was necessary to avoid gelation and form initial water-clear solution, extra-water and other volatile impurities, have to be carefully evaporated to reach pure-phase ZSM-12 crystals. In this way, a clear gel is obtained which can be used for different applications. Depending on the organic template and water contents of the gel, it is required to adjust the alkalinity and Na^+ concentrations to get rid of impurities such as ZSM-5 crystals or amorphous materials. Pure ZSM-12 zeolite has also been obtained by using MTEAOH over a wide range of Si/Al ratio. MTEAOH has provided some advantages such as faster crystallization of highly pure product, perfectly controlled size and morphology, the formation of defect-free single crystals. Moreover, it does not require to adjust the pH (using H_2SO_4). All this being said, using MTEAOH organic template may promisingly contribute to enhancing the ZSM-12 catalyst performance, produced within an efficient and easy-to-scale-up synthesis procedure.

2.5 Acknowledgement

The authors acknowledge financial support from the National Science and Engineering Research Council (Canada) and the Fonds québécois de la recherche sur la nature et les technologies (FRQNT).

2.6 Supporting Information

2.6.1 Experimental Section

2.6.1.1 $MTEA^+$-Based ZSM-12 Benchmark

Benchmark-$MTEA^+$ ZSM-12 zeolite was synthesized according to the method proposed by Ernst et al [37]. Solution A was prepared by adding sodium silicate solution with half of total distilled water and stirred for 10 min. Preparing solution B, MTEACl salt was dissolved in 30 wt% of total distilled water upon stirring for about 10 min. Solution B was added to solution A drop-by-drop, followed by addition of well-dissolved $Al(NO_3)_3.9H_2O$ in rest of total distilled water to the mixture. The resulting composition of the gel was: $24Na_2O$: $0.42Al_2O_3$: $80SiO_2$: 32MTEABr: $3040H_2O$. Finally, given amount of H_2SO_4 were added under vigorous stirring to adjust the pH. After 5 min the gel was transferred into a 125 ml Parr Teflon-lined stainless steel autoclave, and crystallization was carried out at 160 °C without agitation for 5.5 days. The final products were separated by filtration and then repeatedly washed with distilled water until neutral pH was reached. The sample was dried in air at 70 °C overnight. Finally, calcination at 600 °C was carried out for 5h under air atmosphere.

2.6.1.2 TEA^+-Based ZSM-12 Benchmark

Benchmark-TEA^+ ZSM-12 zeolite was synthesized according to the method proposed by Gopal et al [38]. TEAOH solution was first diluted with half of total distilled water. Sodium hydroxide and aluminum nitrate were subsequently added to TEAOH mixture and stirred to produce a water-clear solution. Ludox HS-40 and the rest of water were then added to the above solution and stirred until a uniform gel was obtained. The chemical composition of the resulting gel was: $0.8Na_2O$: $1Al_2O_3$: $80SiO_2$: 20TEAOH: $1040H_2O$. The gel was transferred into a 125 ml Parr Teflon-lined stainless steel autoclave and crystallization was carried out at 160 °C under autogenous pressure. After 5.5 days, the autoclave was removed from the oven and the product was recovered using filtration and washed thoroughly with distilled water and dried at 70 °C. The template was removed by heating under air atmosphere from room temperature to 600 °C with a heating rate of 1 °C min^{-1} and holding at 600 °C for 5 h.

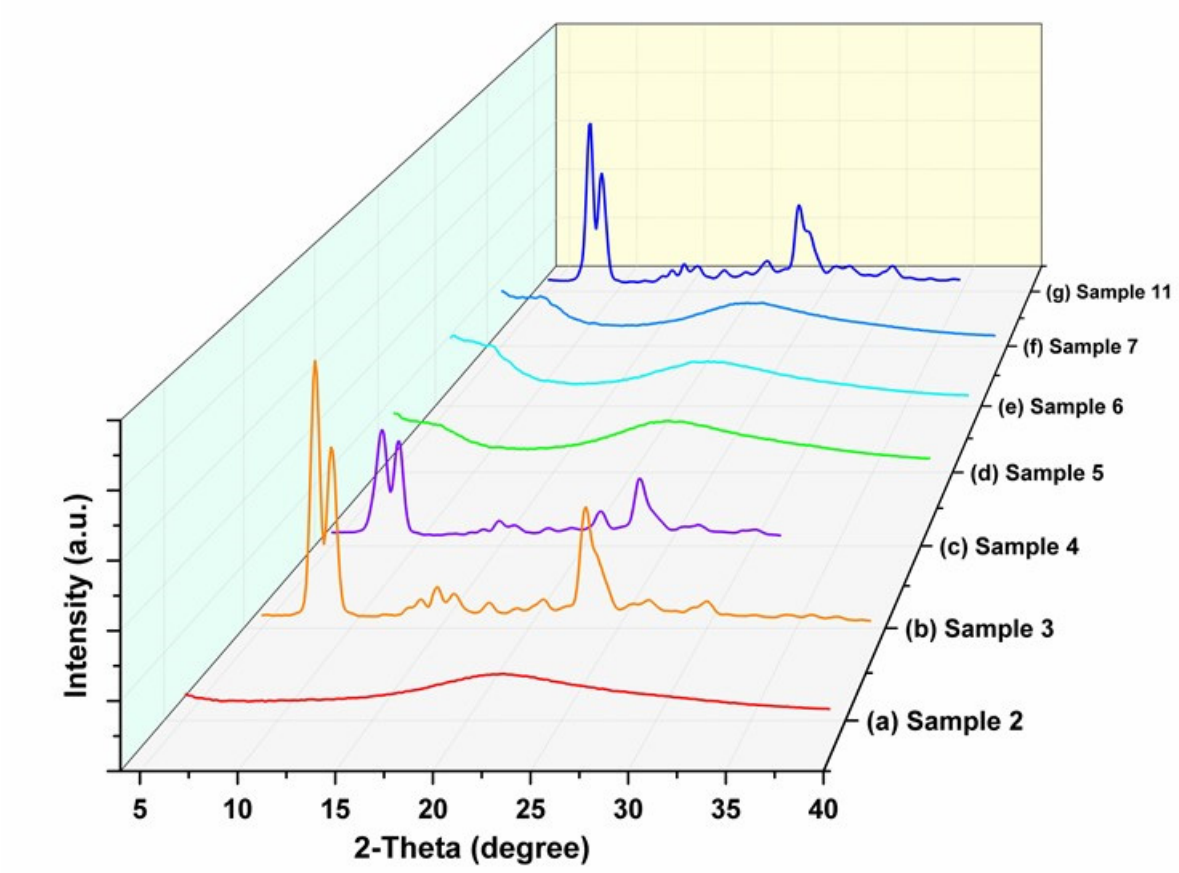

Figure S 2.1- XRD patterns (effects of water content (S-1a- S-1f), and TEAOH content (S-1g) in the ZSM-12 synthesis using TEOS and TEAOH reagents).

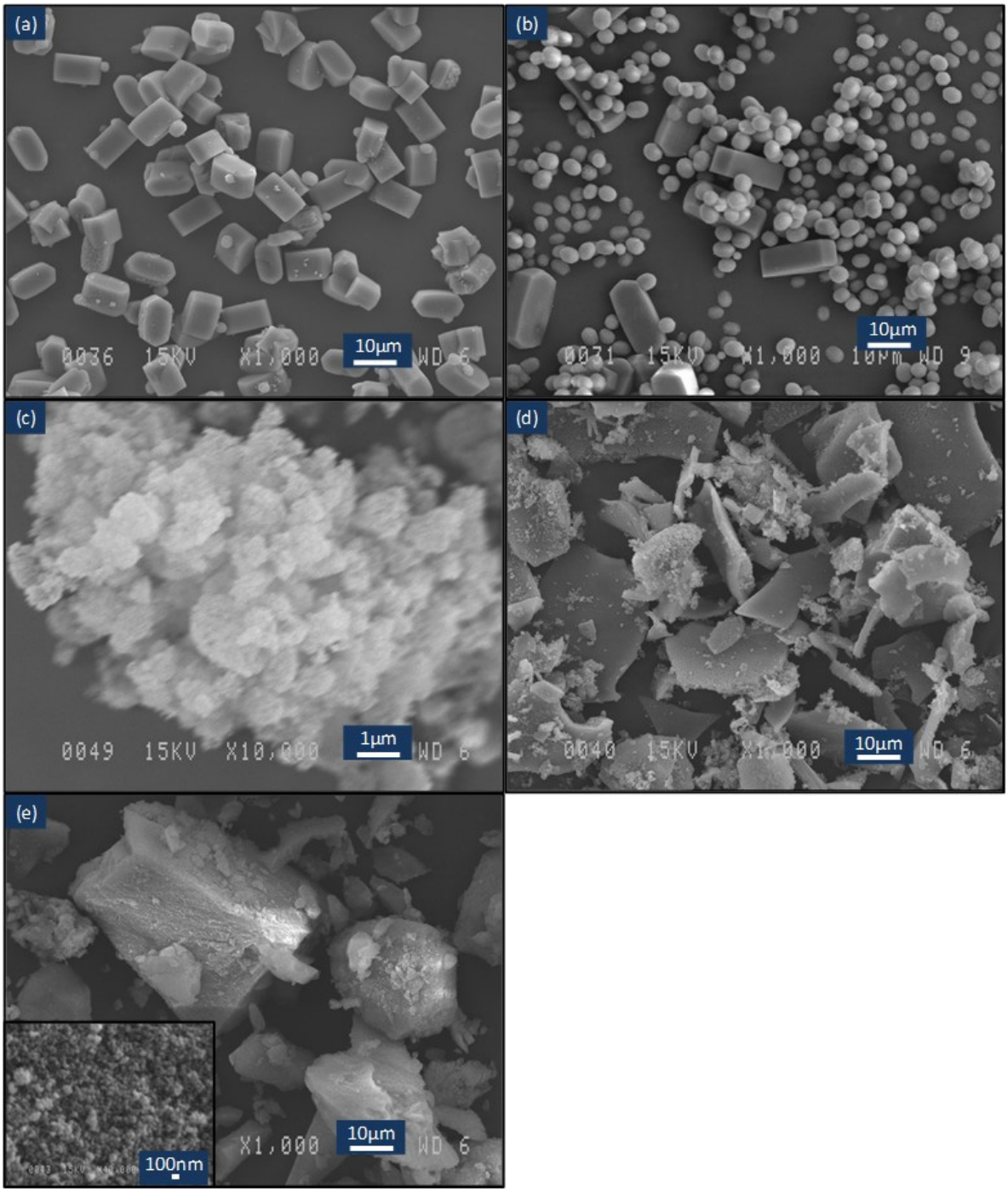

Figure S 2.2- SEM images: effect of water content on products obtained after hydrothermal treatment of the gels produced using TEOS and TEAOH reagents (a-e: Sample 3-7).

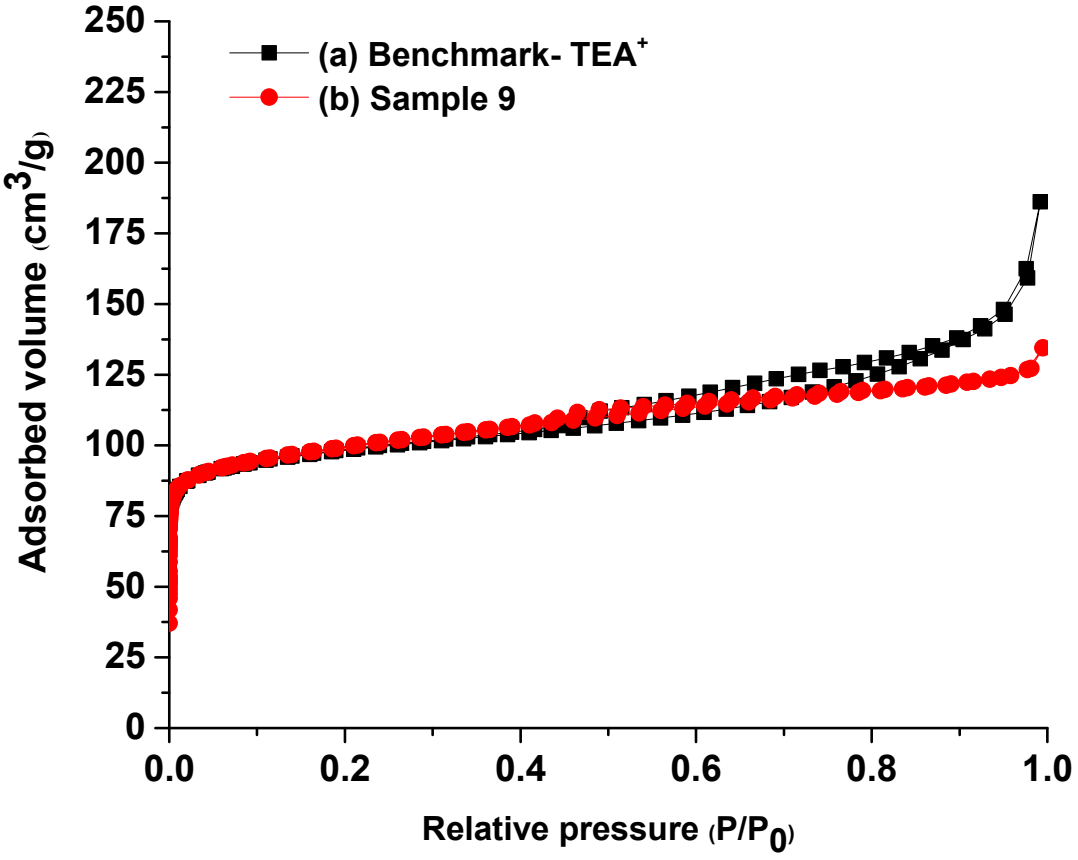

Figure S 2.3- Nitrogen adsorption/desorption isotherms (-196 °C) for (a) benchmark-TEA^+ sample, and (b) modified TEA^+-ZSM-12 (Sample 9).

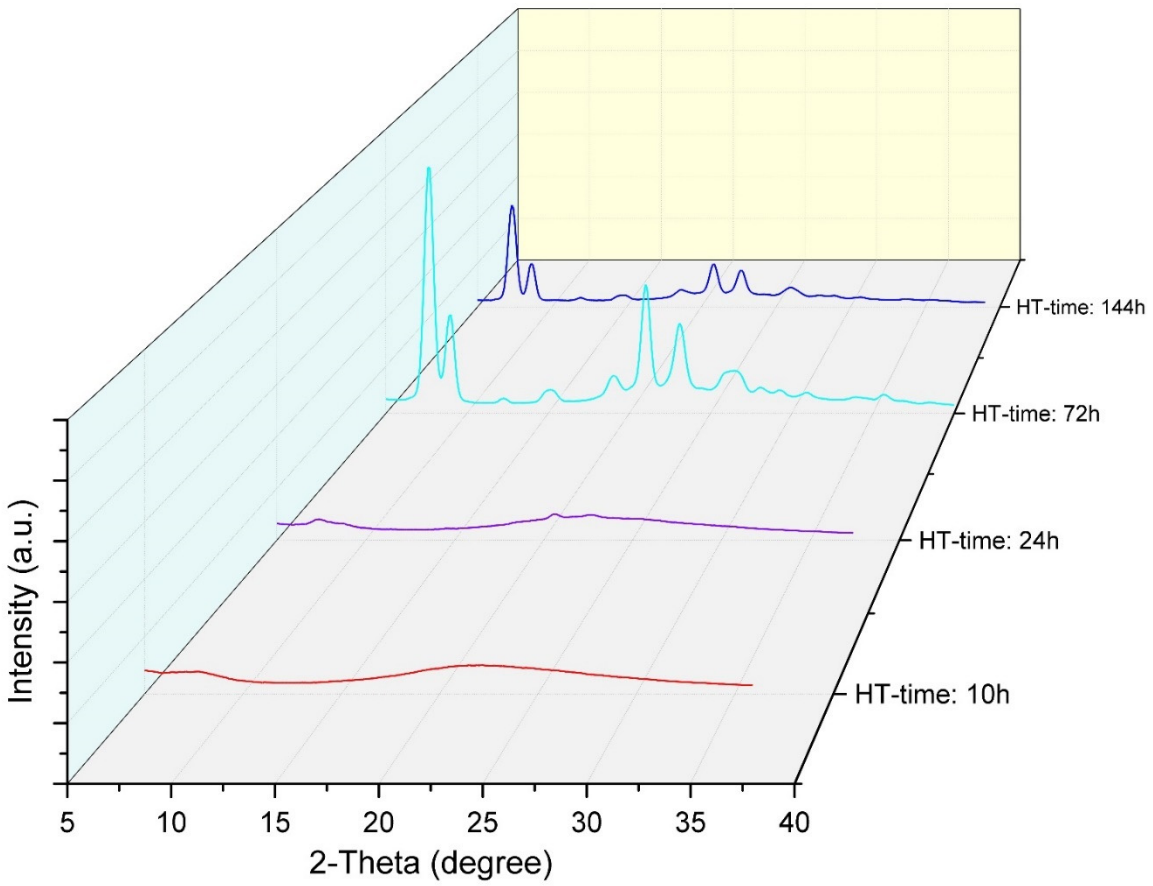

Figure S 2.4- The evolution of crystalline ZSM-12 phase versus hydrothermal treatment time using MTEAOH as the organic template (Si/Al= 87).

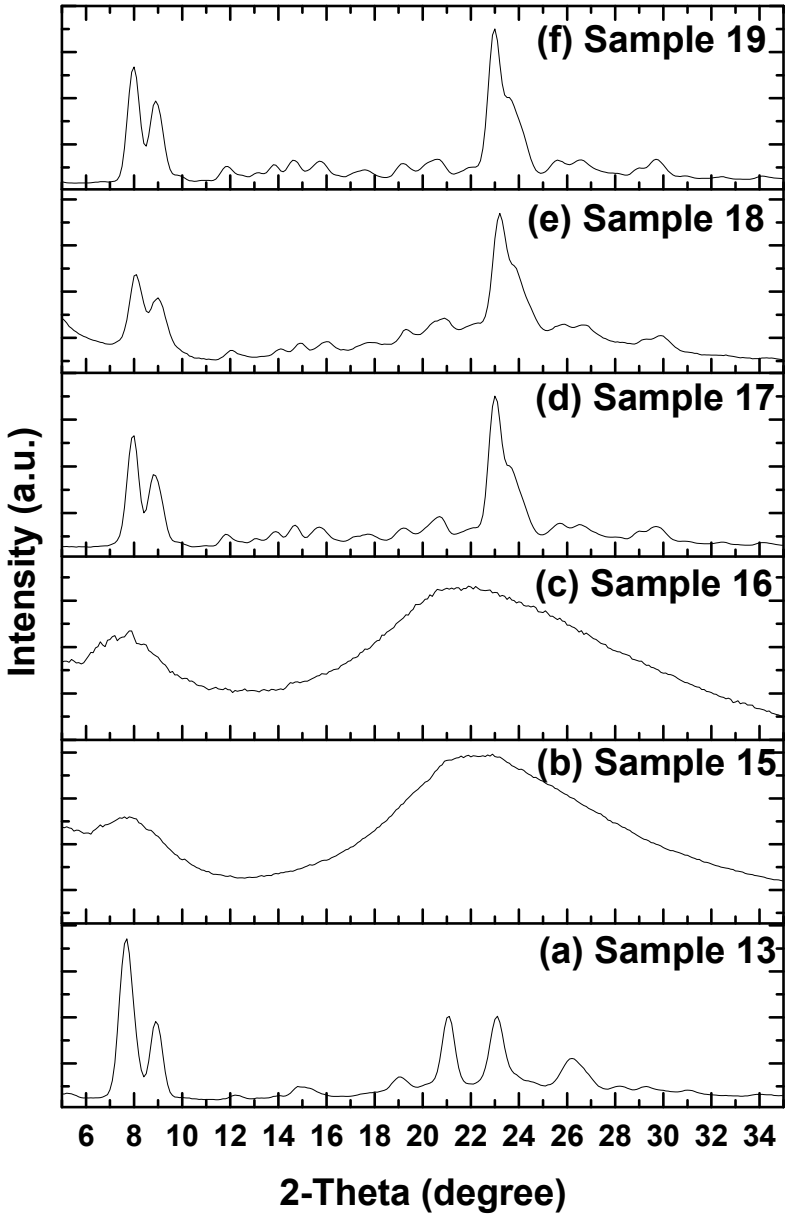

Figure S 2.5- XRD patterns of the samples, synthesized using $MTEA^+$ as organic template to study the effect of (a) Na concentration on $MTEA^+$- benchmark, (b) using $Al(NO_3)_3.9H_2O$ as Al source, (c) water content and (d-f) using TEOS as Si source on modified gel (Sample 14).

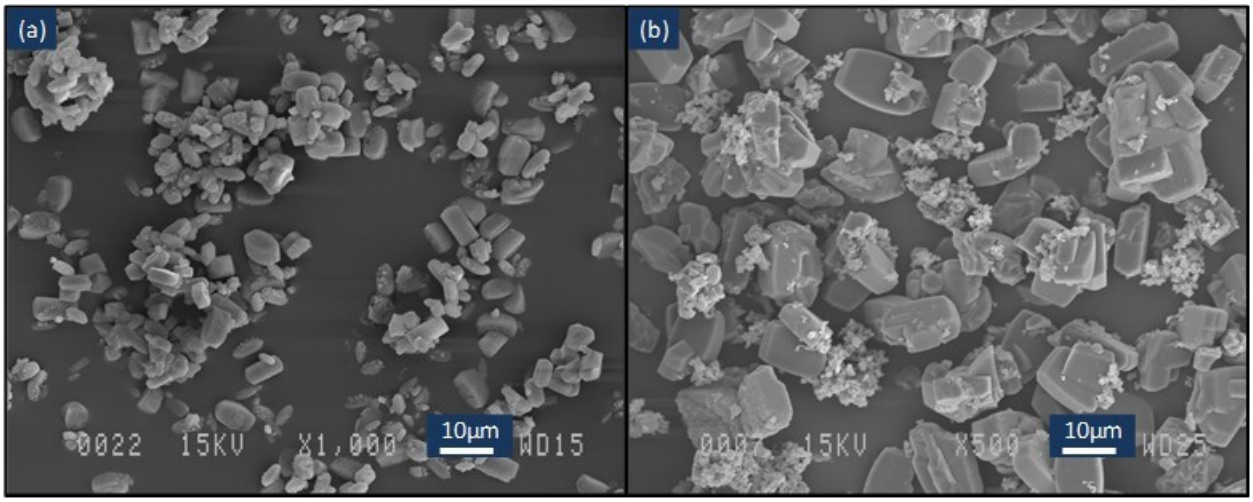

Figure S 2.6- SEM images showing the effects of (a) reducing Na content and using $Al(O\text{-}i\text{-}Pr)_3$ (Sample 13), and (b) using TEOS (Sample 17).

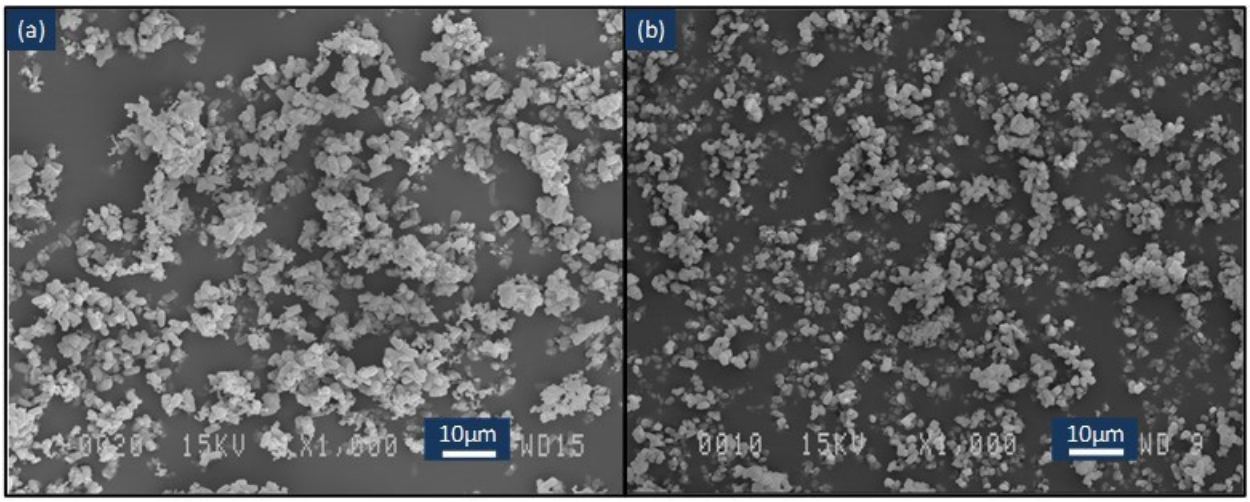

Figure S 2.7- SEM images of modified $MTEA^+$-ZSM-12 samples, synthesized at Si/Al= 30 and hydrothermal treatment duration of (a) 84h, and (b) 144h.

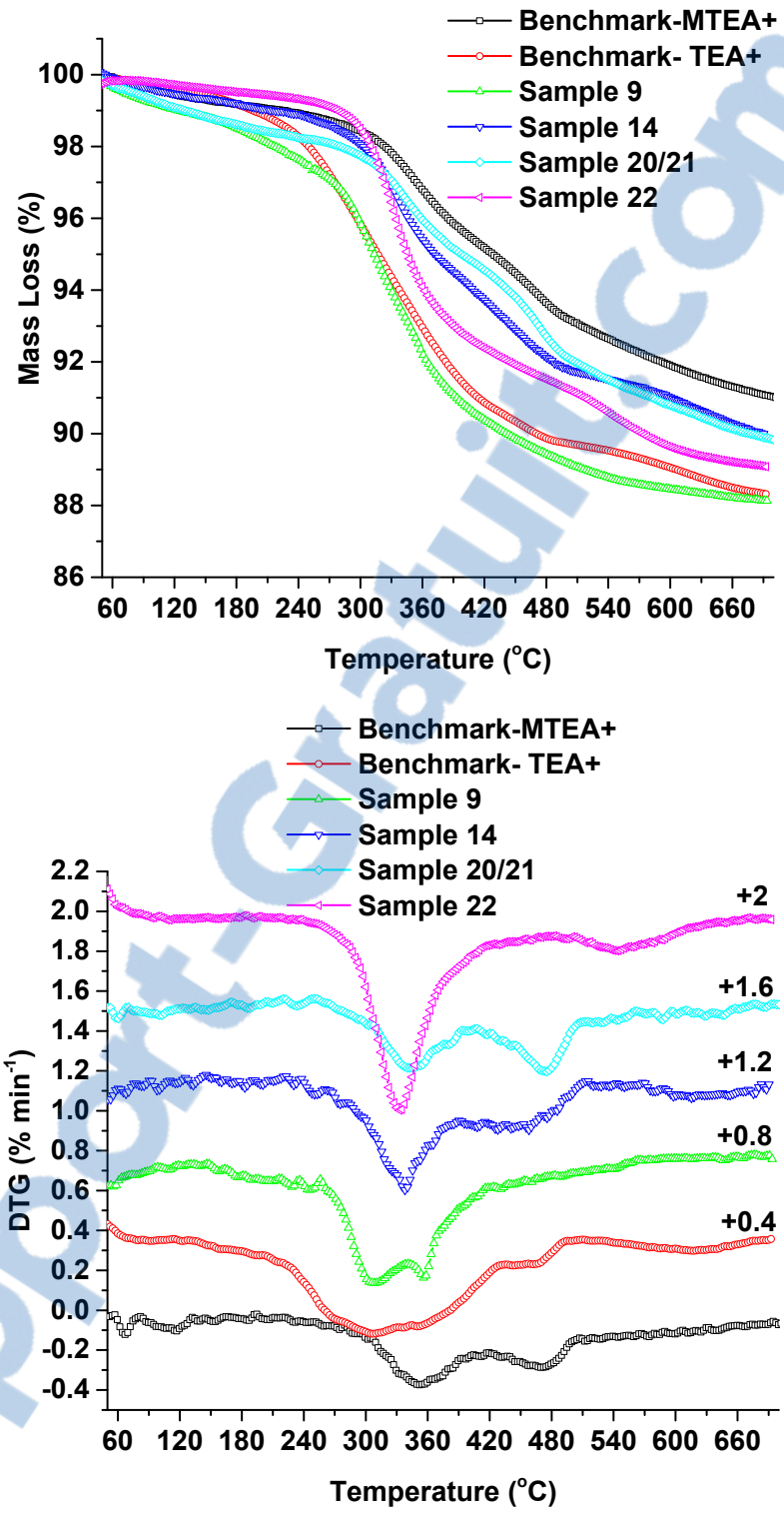

Figure S 2.8- Thermogravimetric (TG) and the corresponding first derivative (DTG) profiles obtained for benchmarks as well as modified ZSM-12 samples using both TEA^+ and $MTEA^+$ organic templates.

2.7 References

[1] A. Corma, *Chem. Rev.* **1997**, *97*, 2373-2419.
[2] X. Meng, F. S. Xiao, *Chem. Rev.* **2014**, *114*, 1521-1543.
[3] M. Moliner, C. Martínez, A. Corma, *Angew. Chem. Int. Ed.* **2015**, *54*, 3560-3579.
[4] C. Baerlocher, L. B. McCusker, D. H. Olson, Atlas of Zeolite Framework Types, Elsevier, Amsterdam, Netherlands, **2007**.
[5] http://www.iza-structure.org/databases/, **2014**.
[6] E. J. Rosinski, M. K. Rubin, Crystalline Zeolite ZSM-12, US3832449, Mobil Oil Corp.,**1974**.
[7] R. B. LaPierre, A. C. Rohrman, J. L. Schlenker, J. D. Wood, M. K. Rubin, W. J. Rohrbaugh, *Zeolites* **1985**, *5*, 346-348.
[8] C. A. Fyfe, H. Gies, G. T. Kokotailo, B. Marler, D. E. Cox, *J. Phys. Chem.* **1990**, *94*, 3718-3721.
[9] S. Ritsch, N. Ohnishi, T. Ohsuna, K. Hiraga, O. Terasaki, Y. Kubota, Y. Sugi, *Chem. Mater.* **1998**, *10*, 3958-3965.
[10] S. Rabl, Ring Opening of Decalin on Iridium- and Platinum- Containing Zeolite Catalysts of the FAU-, MTW- and MWW-Type, PhD dissertation, Institut für Technische Chemie, University of Stuttgart, **2011**.
[11] Q. Wang, Z. M. Cui, C. Y. Cao, W. G. Song, J. *Phys. Chem. C* **2011**, *115*, 24987-24992.
[12] Z. Sarshar, M. H. Zahedi-Niaki, Q. Huang, M. Eic, S. Kaliaguine, *Appl. Catal., B* **2009**, *87*, 37-45.
[13] W. Zhang, P. G. Smirniotis, *Catal. Lett.* **1999**, *60*, 223-228.
[14] K. Yoo, P. G. Smirniotis, *Appl. Catal., A* **2003**, *246*, 243-251.
[15] S. Gopal, P. G. Smirniotis, *Appl. Catal., A* **2003**, *247*, 113-123.
[16] A. Katovic, B. H. Chiche, F. Di Renzo, G. Giordano, F. Fajula, *Stud. Surf. Sci. Catal.* **2000**, *130*, 857-862.
[17] C. W. Jones, S. I. Zones, M. E. Davis, *Appl. Catal., A* **1999**, *181*, 289-303.
[18] W. Zhang, P. G. Smirniotis, *J. Catal.* **1999**, *182*, 400-416.
[19] S. Gopal, W. Zhang, P. G. Smirniotis, *Ind. Eng. Chem. Res.* **2003**, *43*, 2950-2956.
[20] K. Yoo, E. C. Burckle, P. G. Smirniotis, *J. Catal.* **2002**, *211*, 6-18.
[21] K. Yoo, E. C. Burckle, P. G. Smirniotis, *Catal. Lett.* **2001**, *74*, 85-90.
[22] N. G. Grigor'eva, R. R. Talipova, L. P. Korzhova, S. V. Bubennov, B. I. Kutepov, U. M. Dzhemilev, *Pet. Chem*. **2010**, *50*, 129-134.
[23] J. Li, L. L. Lou, C. Xu, S. Liu*, Catal. Commun.* **2014**, *50*, 97-100.
[24] L. Dimitrov, M. Mihaylov, K. Hadjiivanov, V. Mavrodinova, *Microporous Mesoporous Mater.* **2011**, *143*, 291-301.
[25] A. Chokkalingam, H. Kawagoe, S. Watanabe, Y. Moriyama, K. Komura, Y. Kubota, J. H. Kim, G. Seo, A. Vinu, Y. Sugi, *J. Mol. Catal. A: Chem.* **2013**, *367*, 23-30.
[26] C. Li, L. Li, W. Wu, D. Wang, A. V. Toktarev, O. V. Kikhtyanin, G. V. Echevskii*, Procedia Eng.* **2011**, *18*, 200-205.
[27] W. Wu, W. Wu, O. V. Kikhtyanin, L. Li, A. V. Toktarev, A. B. Ayupov, J. F. Khabibulin, G. V. Echevsky, J. Huang, *Appl. Catal., A* **2010**, *375*, 279-288.
[28] O. Muraza, *Ind. Eng. Chem. Res.* **2015**, *54*, 781-789.
[29] S. Mehla, K. R. Krishnamurthy, B. Viswanathan, M. John, Y. Niwate, S. A. Kishore Kumar, S. M. Pai, B. L. Newalkar, *Microporous Mesoporous Mater.* **2013**, *177*, 120-126.

[30] J. A. Martens, P. A. Jacobs, *Stud. Surf. Sci. Catal*. **2001**, *137*, 633-671.
[31] A. Corma, C. Martínez, E. Doskocil, *J. Catal.* **2013**, *300*, 183-196.
[32] J. K. Reddy, K. Motokura, T. Koyama, A. Miyaji, T. Baba, *J. Catal.* **2012**, *289*, 53-61.
[33] N. Batalha, A. Soualah, L. Pinard, Y. Pouilloux, F. Lemos, T. Belin, *J. Chromatogr. A* **2012**, *1260*, 206-214.
[34] S. Mintova, J. P. Gilson, V. Valtchev, *Nanoscale* **2013**, *5*, 6693-6703.
[35] K. Yoo, R. Kashfi, S. Gopal, P. G. Smirniotis, M. Gangoda, R.N. Bose, *Microporous Mesoporous Mater.* **2003**, *60*, 57-68.
[36] Y. Kamimura, K. Itabashi, T. Okubo, *Microporous Mesoporous Mater.* **2012**, *147*, 149-156.
[37] S. Ernst, P. A. Jacobs, J. A. Martens, J. Weitkamp, *Zeolites*, **1987**, *7*, 458-462.
[38] S. Gopal, K. Yoo, P. G. Smirniotis, *Microporous Mesoporous Mater.* **2001**, *49*, 149-156.
[39] H. van Bekkum, E. M. Flanigen, P. A. Jacobs, J.C. Jansen (Eds.), Introduction to Zeolite Science and Practice, Stud. Surf. Sci. Catal., Elsevier, Amsterdam, 2001.
[40] T. Wakihara, A. Ihara, S. Inagaki, J. Tatami, K. Sato, K. Komeya, T. Meguro, Y. Kubota, A. Nakahira, *Cryst. Growth Des.* **2011**,*11*, 5153-5158.
[41] T. Wakihara, R. Ichikawa, J. Tatami, A. Endo, K. Yoshida, Y. Sasaki, K. Komeya, T. Meguro, *Cryst. Growth Des.* **2011**, *11*, 955-958.
[42] A. I. Lupulescu, M. Kumar, J. D. Rimer, *J. Am. Chem. Soc.* **2013**, *135*, 6608-6617.
[43] A. Gaona-Gómez, C. H. Cheng, *Microporous Mesoporous Mater.* **2012**, *153*, 227-235.
[44] A. Gaona-Gómez, G. de Silveira, H. Doan, C. H. Cheng, *Chem. Commun.* **2011**, *47*, 5876-5878.
[45] R. Brent, A. J. W. Lobo, D. W. Lewis, M. W. Anderson, *J. Phys. Chem. C* **2010**, *114*, 18240-18246.
[46] S. Lee, D. F. Shantz, *Microporous Mesoporous Mater.* **2005**, *86*, 268-276.
[47] Y. Zhang, C. Jin, *J. Solid State Chem.* **2011**, *184*, 1-6.
[48] Z. Li, R. S. Bowman, *Environ. Sci. Technol.* **1998**, *32*, 2278-2282.
[49] F. Xu, M. Dong, W. Gou, J. Li, Z. Qin, J. Wang, W. Fan, *Microporous Mesoporous Mater.* **2012**, *163*, 192-200.
[50] J. Yao, L. Yu, L. Zhang, H. Wang, *Mater. Lett.* **2011**, *65,* 2304-2306.
[51] Y. Oumi, Y. Kakinaga, T. Kodaira, T. Teranishi, T. Sano, *J. Mater. Chem.* **2003**, *13,* 181-185.
[52] S. Jegatheeswaran, C. M. Cheng, C. H. Cheng, *Microporous Mesoporous Mater.* **2015**, *201*, 24-34.
[53] M. A. Sanhoob, O. Muraza, E. M. Al-Mutairi, N. Ullah, *Adv. Powder Technol.* **2015**, *26* 188-192.
[54] V. G. Rao, C. Banerjee, S. Ghosh, S. Mandal, J. Kuchlyan, N. Sarkar, *J. Phys. Chem. B* **2013**, *117*, 7472-7480.
[55] A. E. Persson, B. J. Schoeman, J. Sterte, J. E. Otterstedt, *Zeolites* **1994**, *14*, 557-567.
[56] T. M. Davis, T. O. Drews, H. Ramanan, C. He, J. Dong, H. Schnablegger, M. A. Katsoulakis, E. Kokkoli, A. V. McCormick, R. L. Penn, M. Tsapatsis, *Nat. Mater.* **2006**, *5*, 400-408.
[57] Z. Lai, M. Tsapatsis, J. P. Nicolich, *Adv. Funct. Mater.* **2004**, *14*, 716-729.
[58] C. H. Cheng, D. F. Shantz, *J. Phys. Chem. B* **2005**, *109*, 7266-7274.
[59] W. F. Lai, J. T. Elks, R. E. Kay, Synthesis and use of ZSM-12, US2011/0034749A1, ExxonMobil Research and Engineering Company, **2011**.

[60] W. F. Lai, I. D. Johnson, High activity small crystal ZSM-12, US 6893624B2, ExxonMobil Chemical Patents Inc., **2005**.
[61] A. Katovic, G. Giordano, J. B. Nagy, A. Fonseca, *Stud. Surf. Sci. Catal.* **1995**, *94*, 333-340.
[62] Y. Kamimura, K. Iyoki, S.P. Elangovan, K. Itabashi, A. Shimojima, T. Okubo, *Microporous Mesoporous Mater.*, 163 (2012) 282-290.
[63] K. E. Jelfs, B. Slater, D. W. Lewis, D. J. Willock, *Stud. Surf. Sci. Catal.* **2007**, *170*, 1685-1692.
[64] S. Mintova, V. Valtchev, I. Kanev, *Mol. Eng.* **1995**, *4*, 369-373.
[65] J. Cejka, G. Kosová, N. Zilková, I. Hrubá, *Stud. Surf. Sci. Catal.* **2002**, *142*, 247-254.
[66] A. S. Araujo, A. O. S. Silva, M. J. B. Souza, A. C. S. L. S. Coutinho, J. M. F. B. Aquino, J. A. Moura, A. M. G. Pedrosa, *Adsorption* **2005** *11*, 159-165.
[67] D. F. Shantz, C. Fild, H. Koller, R. F. Lobo, *J. Phys. Chem. B* **1999**, *103*, 10858-10865.
[68] Y. Kubota, T. Honda, J. Plévert, T. Yamashita, T. Okubo, Y. Sugi, *Catal. Today* **2002**, *74*, 271-279.
[69] A. Jackowski, S. I. Zones, S. J. Hwang, A. W. Burton, *J. Am. Chem. Soc.* **2009**, *131*, 1092-1100.
[70] A. Jackowski, S. I. Zones, A. W. Burton, *Stud. Surf. Sci. Catal.* **2008**, *174*, 111-116.
[71] K. Tsuji, L. W. Beck, M. E. Davis, *Microporous Mesoporous Mater.* **1999**, *28*, 519-530.
[72] D. F. Shantz, R. F. Lobo, *Chem. Mater.* **1998**, *10*, 4015-4024.
[73] M. Goepper, H. X. Li, M. E. Davis, *J. Chem. Soc., Chem. Commun.* **1992** 1665-1666.
[74] H. B. Zhu, Q. H. Xia, X. T. Guo, K. X. Su, D. Hu, X. Ma, D. Zeng, F. Deng, *Mater. Lett.* **2006**, *60*, 2161-2166.
[75] T. De Baerdemaeker, U. Müller, B. Yilmaz, *Microporous Mesoporous Mater.* **2011**, *143*, 477-481.
[76] R. García, L. Gómez-Hortigüela, F. Sánchez, J. Pérez-Pariente, *Chem. Mater.* **2010**, 22, 2276-2286.
[77] H. Lee, S. I. Zones, M. E. Davis, *Microporous Mesoporous Mater.* **2006**, *88*, 266-274.
[78] M. Sanhoob, O. Muraza, Z. H. Yamani, E. M. Al-Mutairi, T. Tago, B. Merzougui, T. Masuda, *Microporous Mesoporous Mater*. **2014**, *194*, 31-37.
[79] X. Wei, P.G. Smirniotis, *Microporous Mesoporous Mater.*, 89 (2006) 170-178.
[80] M. Kustova, K. Egeblad, C.H. Christensen, A.L. Kustov, *Stud. Surf. Sci. Catal.* **2007**, *170*, 267-275.
[81] H. Chen, J. Wydra, X. Zhang, P. S. Lee, Z. Wang, W. Fan, M. Tsapatsis, *J. Am. Chem. Soc.* **2011**, *133*, 12390-12393.
[82] Q. Li, B. Mihailova, D. Creaser, J. Sterte, *Microporous Mesoporous Mater.* **2000**, *40*, 53-62.
[83] K. E. Hamilton, E. N. Coker, A. Sacco, A. G. Dixon, R. W. Thompson, *Zeolites* **1993**, *13*, 645-653.
[84] I. Krznaric, T. Antonic, J. Bronic, B. Subotic, R. W. Thompson, *Croat. Chem. Acta.* **2003**, *76*, 7–17.
[85] M. A. Camblor, L. A. Villaescusa, M. J. Díaz-Cabañas, Top. Catal. **1999**, *9*, 59-76.
[86] A. Petushkov, S. Yoon, S. C. Larsen, *Microporous Mesoporous Mater.* **2011**, *137*, 92-100.
[87] M. M. J. Treacy, J. B. Higgins in Collection of Simulated XRD Powder Patterns for Zeolites, Elsevier, Amsterdam, Netherland, **2001**.

[88] R. F. Lobo, Introduction to the Structural Chemistry of Zeolites, in Handbook of Zeolite Science and Technology, (Eds.: S. M. Auerbach, K. A. Carrado, P. K. Dutta), Marcel Dekker, Inc., New York, USA, **2003**.
[89] L. D. Rollmann, E. W. Valyocsik, R. D. Shannon, Zeolite Molecular Sieves, in Inorganic Syntheses, (Ed.: S. L. Holt), John Wiley & Sons, Inc., Hoboken, USA, **1983**, pp. 61-68.
[90] A. Mitra, C. W. Kirby, Z. Wang, L. Huang, H. Wang, Y. Huang, Y. Yan, *Microporous Mesoporous Mater.* **2002**, *54*, 175-186.
[91] S. Mintova, V. Valtchev, *Microporous Mesoporous Mater.* **2002**, *55*, 171-179.
[92] A. V. Toktarev, K. G. Ione, *Stud. Surf. Sci. Catal.* **1997**, *105*, 333-340.
[93] R. Xu, W. Pang, J. Yu, Q. Huo, J. Chen, Chemistry of Zeolites and Related Porous Materials: Synthesis and Structure, John Wiley & Sons (Asia) Pet Ltd., Singapore, **2007**.
[94] P.A. Jacobs, J.A. Martens, Synthesis of High-Silica Aluminosilicate Zeolites, in: P.A. Jacobs, J.A. Martens (Eds.), Stud. Surf. Sci. Catal., Elsevier, Amsterdam, 1987.
[95] B. Gil, L. Mokrzycki, B. Sulikowski, Z. Olejniczak, S. Walas, *Catal. Today* **2010**, *152*, 24-32.
[96] S. Ramdas, J. Klinowski, *Nature* **1984**, *308*, 521-523.
[97] E. Bourgeat-Lami, P. Massiani, F. Di Renzo, F. Fajula, T. Courieres, *Catal. Lett.* **1990**, *5*, 265-271.
[98] K. Tsuji, M. E. Davis, *Microporous Mater.* **1997,** *11*, 53-64.
[99] P. P. E. A. de Moor, T. P. M. Beelen, R. A. van Santen, K. Tsuji, M. E. Davis, *Chem. Mate*r. **1998**, *11*, 36-43.
[100] H. Robson, Verified Synthesis of Zeolitic Materials, (Ed.: H. Robson), Elsevier, Amsterdam, Netherlands, **2001**.
[101] M. Thommes, K. Cychosz, *Adsorption* **2014**, *20*, 233-250.
[102] M. Thommes, *Stud. Surf. Sci. Catal.* **2007**, *168*, 495-523.
[103] F. Raatz, C. Marcilly, E. Freund, *Zeolites* **1985**, *5*, 329-333.
[104] D. W. Breck, Zeolite Molecular Sieves: Structure, Chemistry, and Use, Wiley, New York, USA, **1974**.

Chapter 3- Synthesis of Microporous/Mesoporous Core-Shell Materials with Crystalline Zeolitic Shell and Supported Metal Oxide Silica Core

Nima Masoumifard,[a,b,c] Kyoungsoo Kim,[d] Serge Kaliaguine,[b] Pablo M. Arnal,[e] and Freddy Kleitz*[a,c]

[a] Department of Chemistry, Université Laval, Quebec City, G1V 0A6, QC, Canada,
[b] Department of Chemical Engineering, Université Laval, Quebec City, G1V 0A6, QC, Canada,
[c] Centre de Recherche sur les Matériaux Avancés (CERMA), Université Laval, Quebec City, G1V 0A6, QC, Canada
[d] Center for Nanomaterials and Chemical Reactions, Institute for Basic Science (IBS), Daejeon 305-701, Korea
[e] Centro de Tecnología de Recursos Minerales y Cerámica (CETMIC) CIC - CONICET La Plata, Centenario y 506, B1897ZCA, M. B. Gonnet, Argentina

Published in

CrystEngComm.

Volume 18, Pages 4452- 4464

2016

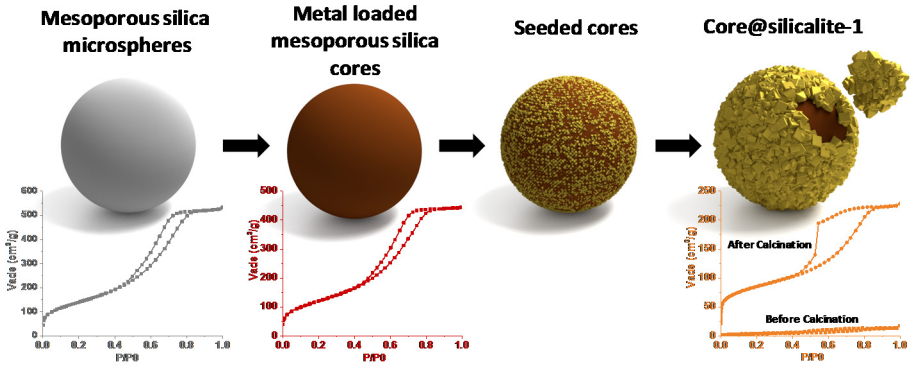

* Corresponding author:

Prof. Freddy Kleitz, E-mail: freddy.kleitz@chm.ulaval.ca, TEL: +1-418-656-7812

Résumé

Un matériau possédant une porosité hiérarchisée permettant une stéréosélectivité, a été synthétisé en plaçant une coquille microporeuse de silicalite-1 sur des microsphères de silice avec différentes espèces hôtes incorporées. Les matériaux de base ont été préparés par dispersion des espèces hôtes métalliques en quantité catalytique, incluant Co, Mn ou Ti, à l'intérieur de la structure mésoporeuse des microsphères de silice ayant des tailles de particules et de pores variables. La connectivité des réseaux micro- et méso-poreux à l'interface cœur/coquille des produits finaux, ainsi que les principaux critères de contrôle de la qualité ont été étudiés. Pour cela, les paramètres de synthèse ont été optimisés, comme par exemple les prétraitements qui incluent la modification de surface, la nucléation, les étapes de calcination ou encore le nombre de traitements hydrothermiques secondaires. En fonction de la taille du noyau/cœur mésoporeux et des espèces hôtes incorporées, l'efficacité de la nucléation se révèle être influencée par la technique de modification de surface choisie, en effet, les microsphères de silice mésoporeuses contenant des espèces métalliques nécessitent un traitement supplémentaire de fonctionnalisation chimique sur leur surface externe avec des précurseurs tels que le (3-aminopropyl) triéthoxysilane, plutôt que d'utiliser une modification de surface simple avec des polymères ioniques. Il est vraisemblable que l'utilisation d'un tel traitement chimique peut renforcer l'adhésion des noyaux à la surface du coeur en fournissant des groupes silanol supplémentaires et faciliter les interactions de type liaison hydrogène. Il est également démontré que selon la taille du coeur, de deux à quatre traitements hydrothermiques courts sont nécessaires pour transformer les cristaux de nucléation en une enveloppe entremêlée uniforme de silicalite-1 autour des microsphères de silice mésoporeuses et pour éviter l'agrégation ainsi que la dissolution des cœurs. De tels matériaux avec une enveloppe de tamis moléculaire cristallin peuvent être utilisés dans une grande variété d'applications, en particulier pour de l'adsorption et de la catalyse stéréo-sélective.

Abstract

An engineered material, possessing a hierarchical porosity in a shape-selective manner, was synthesized by placing a microporous silicalite-1 shell over silica microspheres embedded with various guest species. Core materials were prepared by dispersing catalytically important metallic species, comprising Co, Mn or Ti, within the mesoporous structure of the silica microspheres with different particle and pore sizes. The connectivity of the micro- and mesopore networks and shell integrity of the final core@shell products were studied as the main quality control criteria by varying synthesis parameters, such as core pre-treatments which include surface modification, seeding and calcination steps and by varying the number of secondary hydrothermal treatments. Depending on the core size and the presence of the guest species, the effectiveness of core seeding is found to be influenced by the chosen surface modification technique, i.e., mesoporous silica microspheres which contain guest species need an additional treatment of chemical functionalization of the external surface with species such as (3-aminopropyl)triethoxysilane, rather than using a simple surface modification with ionic polymers. It is believed that using such chemical treatment can strengthen the adhesion of the seeds to the core surface by providing some additional silanol groups and facilitating hydrogen bonding interactions. It is also shown that depending on the core size, two to four short hydrothermal treatments are required to turn the coated seed crystals into a uniform intergrown shell of silicalite-1 around the mesoporous silica microspheres and to avoid aggregation and core dissolution. Such materials with a molecular sieve crystalline shell can be used in a wide variety of applications, particularly for shape-selective adsorption and catalysis purposes.

Keywords:

Core@shell, Crystalline shell, Zeolite, Mesoporous silica, Hierarchical porosity, Metal oxide, Shape-selectivity

3.1 Introduction

Core@shell materials are quickly becoming popular in a wide variety of applications especially in the fields of adsorption and catalysis [1, 2]. In addition to profiting from the efficient combination of the inherent properties of each building block, a synergetic interaction between the core and the shell compartments could provide new desirable features to the composite entity. In this regard, a core@shell material with a crystalline zeolitic shell can benefit from all the extraordinary properties of the zeolite, including high thermal/hydrothermal stability, highly ordered pore structure, large specific surface area and micropore volume, and intrinsic chemical activity. Owing to their excellent resistance under corrosive conditions and molecular sieving property, a zeolitic shell also provides an effective protective layer under the harsh operating conditions of some reactions and processes as well as a selective barrier against impurities, poisons, and undesirable reactions. These attributes are particularly attractive to generate more durable composite catalysts with excellent activity and selectivity [3-7]. By implementing a zeolitic coating around microfibers and other macroscopic supports, a robust zeolitic-based structure can also be manufactured upon using techniques similar to those used for core@zeolite preparations. These macroscopic zeolitic assemblies (e.g., microstructured catalysts) can practically alleviate problems of using classical zeolitic catalysts, e.g., powdery crystals, microgranules or extruded pellets, in catalytic reactors by improving heat and mass transfer, low pressure drop, corrected flow pattern and avoiding the disadvantages of using inorganic binders [8-10]. Inheriting all these intrinsic properties of a zeolite by the final core@zeolite composite as well as the emergence of new synergetic features can be crucial for the core components, especially the ones which are widely used as industrial adsorbents/catalyst supports but suffer from selectivity and stability issues. In particular, high surface area and high pore volume mesoporous silica spheres with the ability of hosting various functional groups (e.g., metals, metal oxides, etc.) when finely covered with a zeolitic shell may hold considerable promise in a variety of applications [11-20].

The outstanding properties of a zeolitic core@shell are tightly related to the complete shell coverage as well as the proper communication between micro/mesopore networks of the constituents. The importance of shell integrity on the selective adsorption of small molecules from a hydrocarbon mixture containing butane, toluene, and 1,3,5-trimethylbezene was demonstrated in the pioneering work of Bouizi *et al.* [21], by using a β-zeolite@silicalite-1 material with maximum shell coverage, i.e., a triple-shell composite. Therefore, the main

objective of this study is to implement available techniques toward synthesizing an optimized zeolitic core@shell microsphere, using a mesoporous silica core, hosting various functional groups within its large pores. The desirable final products, non-aggregated core@shell microspheres, should meet a set of quality criteria including the preserved core mesoporosity during the shell formation process, complete shell coverage, pore network connectivity between constituents of the composite, and the absence of free zeolite crystals in the bulk. Although there are few examples of core@zeolite that can be produced by using a one-pot hydrothermal crystallization process[22-26], the synthesis of a great number of zeolitic core@shell materials is only viable through a multi-step synthesis route [3, 4, 9, 11, 12, 15, 21, 27-33]. The multistep synthesis route usually involves preliminary adsorption of zeolite nanocrystals onto large core particles followed by growing these nanocrystals in an appropriate synthesis gel mixture [34, 35] (Scheme 3.1). As the primary element of the final product, the properties of the core constituents, such as the core particle size and the presence of the desirable guest species, can directly impact the performance of this synthesis route and consequently the quality of the final product. In this sense, the effectiveness of the multistep technique for the synthesis of core@shell materials with mesoporous silica core in either pure form or loaded with guest species is evaluated.

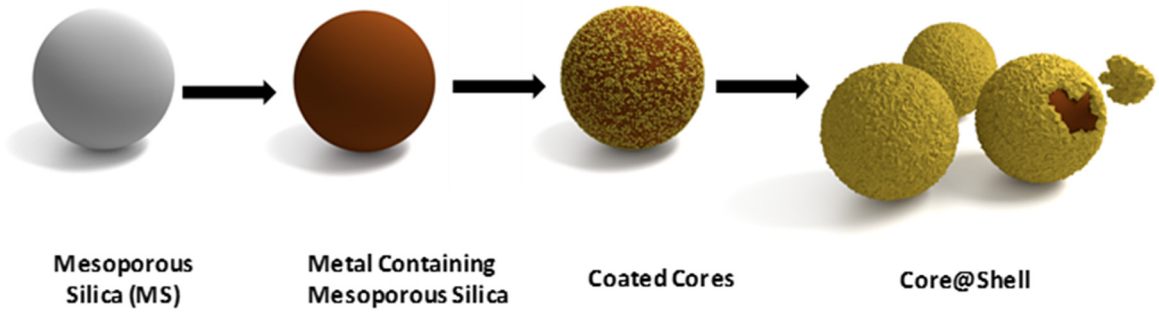

Scheme 3.1- Schematic representation of the synthesis of metal-containing mesoporous silica@silicalite-1.

3.2 Experimental

3.2.1 Pure Mesoporous Silica@Silicalite-1 Preparation

Using tetraethyl orthosilicate (TEOS) (reagent grade, 98%-Sigma-Aldrich) and tetrapropylammonium hydroxide (TPAOH) solution (1M in H_2O-Sigma-Aldrich), silicalite-1 nanocrystals with an average size of 70 nm were first synthesized from a gel with a molar composition of 9TPAOH: 25TEOS: 480H_2O: 100C_2H_5OH which was kept at 80 °C for 72 h [36]. Thoroughly washed nanocrystals were finally re-dispersed in distilled water to produce 1 wt% suspension. The pH of the suspension was adjusted to 9–10 with ammonia solution[28]. Various types of mesoporous silica spheres with different particle and pore sizes (commercial silica gel spheres; SG20: 20-45 µm and SG3: 3 µm and hexagonal mesoporous silica (HMS) spheres: ~1.5 µm) were used as core material. SG20 particles with two different average pore sizes (SG20(I): 7nm and SG20(II): 10 nm) were used. All commercial silica gel spheres were purchased from SiliCycle® Inc. Mono-dispersed HMS spheres were synthesized according to the literature [11, 37, 38]. The as-synthesized HMS particles were calcined at 550 °C for 6 h to remove the organic template from the pores.

After these preliminary steps, pure silica core@shell particles were synthesized by adopting the seeded growth method [11, 21, 27]. Around 0.2 g of mesoporous silica spheres was dispersed in 5 ml of distilled water, followed by reversing their negative surface charge upon treating with a 5 ml of 0.5 wt% aqueous solution of cationic low molecular weight poly(diallyldimethylammonium chloride) (PDADMAC) solution (20 wt% in H_2O-Sigma-Aldrich) under 20 min of stirring. Four centrifugal washings, 45 ml of water each step, were done to remove the free polyelectrolytes. Afterward, 5 ml of negatively charged silicalite-1 nanocrystals suspension was added to be adsorbed on the surface of the cores owing to electrostatic interactions. The excess nanocrystals were washed away by performing several cycles of centrifugation and re-dispersion of coated particles using a dilute NH_3-H_2O solution (pH 9.5). This intermediate product was dried in an oven at 80 °C overnight and then calcined in air at 550 °C for 5 h. The clear gel for secondary growth step was prepared according to Bouizi *et al.* [21] with the molar composition of 3 TPAOH: 25 SiO_2:1500 H_2O:100 C_2H_5OH. The coated core particles were dispersed in 10 g of the clear gel by stirring at room temperature for 15 min, followed by hydrothermal treatment at 200 °C for 45 min in a Parr Teflon-lined autoclave. After washing the product four times with distilled water, the secondary growth step was repeated several times (at least twice) to reach the desirable

shell coverage. After cooling, the product was treated with a dilute NH_3-H_2O solution (pH 9.5) using an ultrasonic bath for 10 min to remove the loosely attached silicalite-1 crystals, rinsed repeatedly with distilled water and dried at 100 °C overnight. The as-synthesized material was calcined at 550 °C for 6 h in air after reaching this temperature at a rate of 1 °C min^{-1} to remove the TPA^+ template from the zeolite pores.

3.2.2 Preparation of Metal-Containing Mesoporous Silica Microspheres

Metal ions (M= Mn and Co) were introduced into the porous network of mesoporous silica spheres (i.e., HMS, SG3 and SG20) using the incipient wetness technique. In brief, 0.3 g of mesoporous silica, previously evacuated overnight at 150 °C, was impregnated with a solution containing an appropriate amount of metal nitrate, dissolved in anhydrous ethanol, i.e., cobalt nitrate hexahydrate ($Co(II)(NO_3)_2.6H_2O$, Alfa Aesar) or manganese nitrate tetrahydrate ($Mn(II)(NO_3)_2.4H_2O$, Alfa Aesar). The concentration of the impregnation solution was adjusted to provide M/Si molar ratios between 0.05 and 0.2. Solution volumes equal to 80 % of the pore volume of the corresponding mesoporous silica spheres, as measured by N_2 physisorption, were used for each impregnation. Then, the materials were dried overnight at 40 °C and calcined at 500 °C at a 1 °C min^{-1} ramp for 3 h under air atmosphere.

Titanium- (Ti) containing mesoporous silica spheres were prepared using titanium (IV) butoxide (TNBT, reagent grade, 97%-Sigma) as the titanium precursor and acetylacetone (acac, 98%-Sigma) as a chelating ligand [39, 40]. Around 0.3 g of mesoporous silica spheres, thoroughly dried prior to use, was dispersed in 8 ml of dry toluene under inert atmosphere. The TNBT (60 µl), acac (105 µl) and 1 ml dry ethanol were quickly pre-mixed in a glass vial and then added to silica suspension in a drop-wise manner while stirring. The final mixture was stirred in an oil bath at 80 °C overnight. The solid products were recovered by centrifugation, quickly washed with 50 ml of anhydrous ethanol, and dried in air at 70 °C overnight. Finally, the yellow powder was calcined at 500 °C for 3 h.

The materials loaded with metals are referred to as M,SiO_2 where M is Co, Mn or Ti and SiO_2 is HMS, SG3, SG20(I) or SG20(II).

3.2.3 Preparation of Supported Metal Oxide Mesoporous Silica@Silicalite-1

An additional grafting of $–NH_2$ groups on the external surface of the spheres was used in order to modify the external surface of the metal- containing core particles. Typically, 0.1 g of mesoporous silica supported metal oxide, suspended in 10 ml of dry toluene, was placed in a 25 ml round bottom flask equipped with a condenser. A solution of excess amount of (3-aminopropyl)triethoxysilane (APTES, 99 %-Sigma) in 5 ml of dry toluene was added dropwise to the dispersed particles under continuous stirring. After complete addition of the organosilane precursor, the reaction mixture was kept under refluxing conditions for about 6 h in inert gas atmosphere. After cooling, the solid was washed with toluene (10 ml) and ethanol (20 ml). The final product was dispersed in 5 ml of ethanol without drying. Afterward, 5 ml of silicalite-1 nanocrystals suspension, 1 wt% in ethanol, was added and stirred for 1h at ambient temperature. The free and loosely attached nanocrystals were removed by performing several cycles of centrifugation (2000 rpm, 5 min) and re-dispersion of the coated particles in ethanol until reaching a highly clear supernatant. This intermediate product was dried in an oven at 80 °C overnight and then calcined in air at 550 °C for 5 h. Using the calcined product, supported-metal oxide mesoporous silica@silicalite-1 was synthesized following a procedure similar to the one used for pure mesoporous silica microspheres, described above.

For the sake of comparison, surface modification of the metal-containing core particles was also performed using a single layer of a cationic polyelectrolyte or multilayers of cationic/anionic polyelectrolytes. The former method, using positively charged PDADMAC solution, was performed according to a previously reported protocol [11, 21, 27] and described briefly above for pure silica core@shell preparation. As a second method, positively charged PDADMAC and anionic poly (styrenesulfonate, sodium salt) (PSS) (Sigma) solutions (0.5 wt% in water) were alternatively used to form PDADMAC/PSS/PDADMAC polyelectrolyte layers on the core particles. After each step, the particles were thoroughly washed with water (four centrifugal washings, 45 ml water each step) to remove the free polyelectrolytes. The surface modified particles obtained by either of the two methods, were coated with seeds and used to produce a core@shell material following a technique similar to that described above for pure silica core@shell preparation.

3.2.4 Materials Characterization

The powder X-ray diffraction (XRD) patterns of all samples were recorded using a Siemens powder diffractometer (40 kV, 40mA) with CuKα radiation (λ= 1.54059 Å). Scanning electron microscopy (SEM) studies were performed using a JEOL JSM-840A scanning electron microscope. High resolution scanning electron microscopy images (HRSEM) were taken with a Verios 460 (FEI) at a landing voltage of 1 kV in deceleration mode (stage bias voltage: 4 kV) (KAIST, Daejeon, Republic of Korea). Elemental mapping of the cross-section of the samples was performed using energy-dispersive X-ray spectroscopy (EDS) attached to the HRSEM instrument at 5 kV. The samples were mounted onto a SEM grid specimen holder using a carbon tape without metal coating. For cross-sectional imaging, the samples were crushed using an agate mortar and pestle before mounting on the holder. Nitrogen adsorption/desorption isotherms were measured at liquid nitrogen temperature (-196 °C), using a Quantachrome Autosorb-1 adsorption analyzer. Prior to the measurements, the noncalcined and calcined samples were evacuated at 80 °C and 200 °C, respectively, for at least 12 h, under the vacuum, provided by a turbomolecular pump. The linear part of the Brunauer-Emmett-Teller (BET) plot was used to calculate the specific surface area. The total pore volume of the micropores and mesopores was estimated from the amount of nitrogen adsorbed at P/P_0= 0.95. For advanced porosity analysis, cumulative pore volumes and pore size distributions were determined by using the non-local density functional theory (NLDFT) method applying the NLDFT metastable adsorption branch kernel and considering sorption of nitrogen at -196 °C in silica as a model adsorbent and cylindrical pores as a pore model. Micropore volumes of the zeolites and core@shell materials, as well as their pore size distributions, were determined using NLDFT method. The Quantachrome Autosorb-1 1.55 software was used for data interpretation. X-ray photoelectron spectroscopy (XPS) spectra were collected on a KRATOS Axis-Ultra electron spectrometer (UK) using a monochromatic Al Kα X-ray source at a power of 300 W. Powder was placed in a clean copper sample holder (cup). No treatment was performed on the sample other than normal vacuum pumpdown. Electrostatic charge was neutralized with the very low energy, integrated electron flood gun, the parameters of which were set to optimize energy resolution and counting rate. Survey scans were recorded with a pass energy of 160 eV and a step size of 1eV. The data were used for elemental analysis and the calculation of apparent concentration. Calculation of the apparent relative atomic concentrations was performed with the CasaXPS software.

3.3 Results and Discussion

The present contribution aims at monitoring how the parameters of the common multistep synthesis technique of the core@shell materials affect the major characteristics of the final product. The effect of surface modification techniques and the number of secondary growth steps, as the two major stages of synthesizing core@zeolite through a multistep fashion, on the quality of the resulting core@shell material are investigated using different sizes of mesoporous silica microspheres, with or without metallic guest species.

Table 3.1- Textural properties of the core@shell materials obtained by performing N_2 physisorption analysis at -196 °C.

Sample	S_{BET}[a] [$m^2\ g^{-1}$]	Micropore surface area[b] [$m^2\ g^{-1}$]	Micropore volume[c] [$cm^3\ g^{-1}$]	Pore volume[d] [$cm^3\ g^{-1}$]	Maximum mesopore size[e] [nm]
HMS (1.5 µm)	780	----	----	0.6	3.3
Silica gel (3 µm)-SG3	453	----	----	0.7	6.2
Silica gel (20-45 µm)-SG20(I)	512	----	----	0.8	6.2
Silica gel (20-45 µm)-SG20(II)	326	----	----	0.8	8
Silicalite-1 (~ 300 nm)	484	378	0.15	0.55	16
HMS@silicalite-1	430	335	0.13	0.26	3.7, 6
SG3@silicalite-1	280	166	0.08	0.25	3.5, 7.2
SG20(I)@silicalite-1	240	83	0.023	0.27	6.8
SG20(II)@silicalite-1	180	70	0.025	0.24	3.5, 7.4
Ti,HMS@silicalite-1	273	223	0.093	0.14	3.5, 5.6
Co,SG3@silicalite-1	176	115	0.046	0.186	4, 7
Co,SG20(I)@silicalite-1	287	184	0.07	0.27	6.5
Ti,SG20(I)@silicalite-1	300	124	0.043	0.35	6.5

[a] Calculated by using the BET method on relatively low-pressure region. [b] Difference between S_{BET} and NLDFT cumulative surface area for pore sizes larger than 2 nm. [c] Calculated using NLDFT cumulative pore volume for pore sizes smaller than 2 nm. [d] Calculated at P/P_0= 0.95. [e] Derived from NLDFT pore size distribution in mesopore region (pore sizes larger than 2 nm). The two values correspond to the two maxima in the pore size distribution curves.

3.3.1 Effect of Secondary Growth Repetitions Using Pure Silica Cores

The efficacy of surface modification by coating the core materials using ionic soluble polymers has been demonstrated in several research studies [28, 41]. Our previous study showed that this technique is highly efficient in providing required interactions between the nanozeolites and pure mesoporous silica spheres as used in this study [11]. Therefore, in the current section, the impact of the number of consecutive secondary growth steps, e.g., 2-4 times, on the quality of the final product is discussed. Different core particles with different sizes and textural properties, i.e., commercial silica gel spheres and hexagonal mesoporous silica microspheres (HMS), were used as core materials. Figures S 0.4a-c and S 0.5a-d (Electronic Supplementary Information) show the scanning electron microscopy (SEM) images and nitrogen physisorption isotherms (-196 °C), respectively, obtained for all the mesoporous silica cores used in the present study. Their textural properties are reported in Table 3.1. The synthesized HMS particles showed uniform size and shape with a mean diameter around 1.5 µm (Figure S 3.1a). Commercial silica gel spheres SG3 and SG20 (Silicycle Inc, Canada) showed wider particle size distributions compared to HMS, especially SG20 with a size range of 20 to 45 µm (Figure S 3.1b,c). All the mesoporous silica cores showed a type IV nitrogen adsorption/desorption isotherm, characteristic of mesoporous solids, with a significant uptake in the relative pressure region of 0.6–0.8 for silica gel and 0.2-0.3 for the HMS particles, attributed to the capillary condensation effect. The maximum point in the corresponding mono-modal pore size distribution curve, obtained from NLDFT analysis, was centered at the pore sizes of 3.3, 6, 6 and 8 nm for HMS, SG3, SG20(I) and SG20(II) with smaller and larger pores, respectively (Table 3.1). More details about their porous structure including pore size distribution curves can be found in our previous report[11].

The scanning electron microscopy images of the seeded HMS and SG particles, depicted in Figure S 3.3a-c, show that the seeding process in slightly basic condition did not irreversibly change the overall morphology of the core particles. Textural properties of the seeded cores were also evaluated by nitrogen physisorption. Figure S 3.3d,e compares the results for HMS spheres after and before seeding, as an example. Although the presence of noncalcined silicalite-1 seeds and probably of the remaining polymeric species from the coating step reduced the pore volume of the seeded cores, the shape of the isotherm and corresponding cumulative pore volume remained similar to those observed for pure HMS. The pore size distribution curve was slightly broadened which may be attributed to the

presence of polymers used for the coating and interstitial spaces between nanoparticles. However, the pore network structure of the core remained quite intact, as expected.

The shell, which was initially formed by deposited zeolite nanocrystals around the positively-charged external surfaces of the spheres using a single layer of PDADMAC polyelectrolyte, was gradually converted into a polycrystalline intergrown silicalite-1 shell through successive hydrothermal treatments of 45 min each in a gel containing TEOS and TPAOH. This repetitive quick conventional hydrothermal treatment is a crucial factor to avoid the core dissolution and aggregation of final products in comparison to longer vapor phase transport (VPT) treatment which was previously used to generate hollow zeolites using mesoporous silica spheres as the core [41, 42]. Although hollow zeolite spheres are of great importance in a variety of applications [43, 44], preserving the mesoporous silica core in a well-connected micro/mesoporous composite network can also provide several advantages including high mesopore volume and high surface area which allows having either evenly-distributed functional groups supported in a highly accessible network for reactants or high chemical/physical adsorption capacity of molecules of interest on the core surface sites. Figure 3.1 shows the SEM images of various mesoporous silica microspheres after two and four consecutive secondary growth steps. According to the literature, two successive hydrothermal treatments in the silica-containing gel are necessary for achieving an acceptable level of shell coverage over β-zeolite cores [21, 27]. We observed that the same rule holds true when mesoporous silica spheres are used, especially for the smaller ones, i.e., HMS and SG3 (Figure 3.1a,c,e). Increasing the number of secondary growth steps for the smallest cores, i.e., the HMS spheres, not only did not provide any improvements in shell coverage, but also led to the formation of highly aggregated particles and hollow spherical caps. The formation of these additional particle species is attributed to a complete dissolution of mesoporous silica from the interior region in bare spots on external surface where the initial coating of seed was not dense enough (Figure 3.1b). In contrast to small HMS core particles, SEM imaging inspection of the core@shell samples with larger SG cores did not show any aggregation or hollow bodies after repeating the hydrothermal treatments for four times (Figure 3.1c-f).

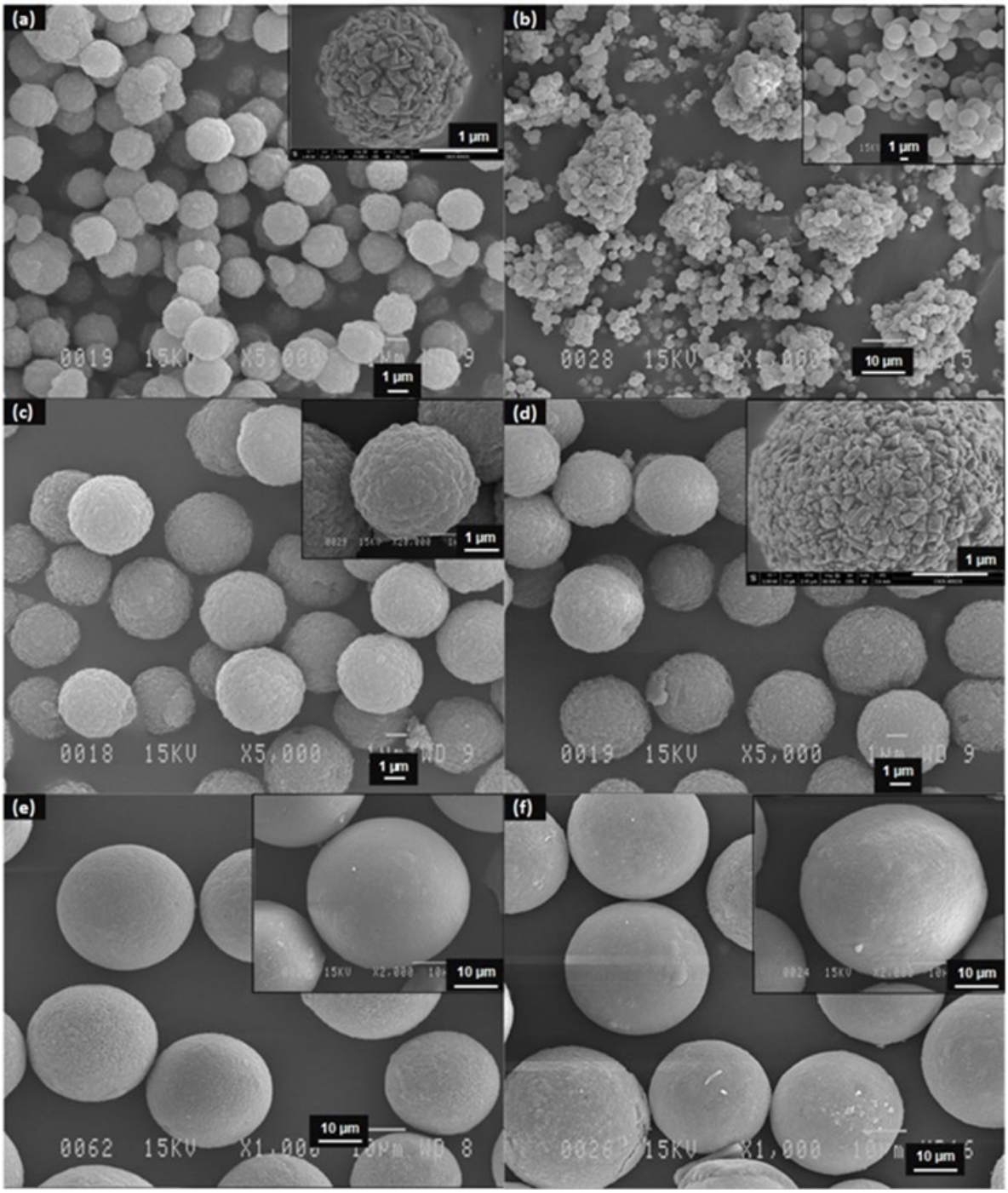

Figure 3.1- SEM images of (a,b) HMS@silicalite-1, (c,d) SG3@silicalite-1, and (e,f) SG20(II)@silicalite-1 after 2 and 4 successive secondary growth steps, respectively.

Nitrogen physisorption isotherms were measured for the core@shell products prior to the final calcination steps and used to assess the shell coverage quality and uniformity. In Figures 0.5 and S 0.7 the isotherms obtained by N_2 sorption measurements after different numbers of hydrothermal treatment steps can be compared. Since all the micropores on the shell sides are totally filled and blocked with structure-directing agent molecules, the internal porosity of noncalcined core@shell products would not be accessible, proving a perfect zeolitic shell coverage. Assuming that the mass ratio between silicalite-1 and the core for samples with different core sizes remains comparable after each secondary growth step, this property, low gas uptake by noncalcined samples, can be used to determine the number of secondary growth required for each particle. From the lowest N_2 uptake obtained for each sample (Figures 0.5 and S 0.7), it is clear that the smaller the particle is, the less hydrothermal treatments are required to achieve reasonable shell completeness, which could thus efficiently prevent N_2 to access the internal mesoporosity of the noncalcined core@shell products. For HMS particles, this is achieved after two hydrothermal treatments, while SG20 evidently needs four hydrothermal treatment sequences. SG3 particles also reached an acceptable level of shell coverage after the second hydrothermal treatment.

Nitrogen physisorption data for calcined core@shell products can be used to evaluate the pore network connectivity between the constituents. Textural properties of the final calcined core@shell materials were also evaluated for all the different core materials used and presented in Table 3.1. After calcination, the SDAs will be burned out and both core mesoporosity and shell microporosity will become accessible. In comparison to the pristine cores (Figure S 3.2), the isotherm of the calcined core@shell material (Figures 0.5 and S 0.7) showed a noticeable reduction in nitrogen uptake at higher values of P/P_0 (capillary condensation region), relative to that of the mesoporous silica spheres, showing that relative mesopore contribution in the final porosity was drastically decreased by the dense microporous silicalite-1 shell. However, capillary condensation can still be observed at high relative pressures ($P/P_0>0.6$) indicating the presence of mesopores, and it is accompanied by a complex hysteresis behavior, which we tentatively attribute to the cavitation effect [45, 46]. It is also observed that the ratio between mesoporosity and microporosity is a function of core size, with larger particles showing a higher ratio than smaller ones (Table 3.1). In other words, by using larger core particles, the contribution of micropores to the total porosity of the core@shell products decreases. This is evident by comparing the micropore volume and surface area of submicron silicalite-1 aggregates, listed in Table 3.1, with the values

reported for calcined core@shell products with different core sizes. Moreover, the large mesopores (pore sizes ~16 nm), formed upon aggregation of small crystals during drying and calcination of the silicalite-1 sample, contributing to the large total pore volume and surface area, have completely vanished in the core@shell products, confirming a tight intergrowth of nanocrystals leading to the formation of a zeolitic shell free of interstitial pores.

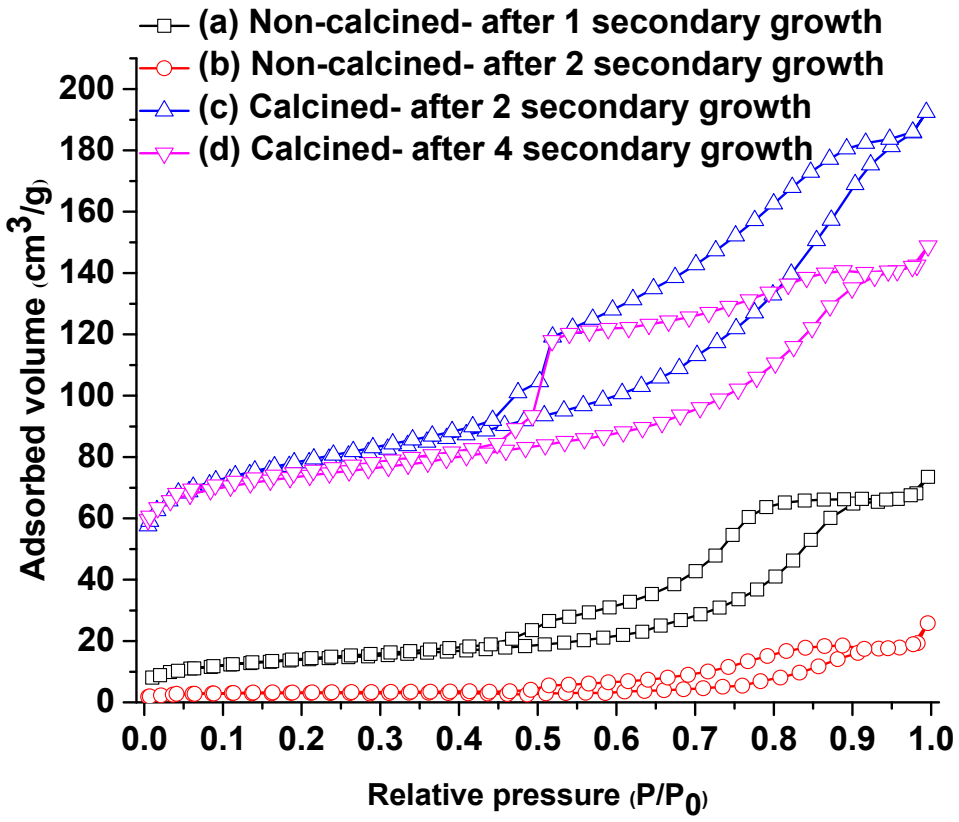

Figure 3.2- Nitrogen adsorption/desorption isotherms measured at -196 °C for synthesized SG3@silicalite-1: (a,b) noncalcined samples after one and two successive secondary hydrothermal treatments, and (c,d) calcined samples after two and four successive secondary hydrothermal treatments.

In conclusion, using pure mesoporous silica microspheres, the shell coverage and uniformity is found to be a function of the core particle size, i.e., larger particles such as SG20 benefit

from a nice and uniform shell of silicalite-1 if the secondary growth step is repeated for at least four times.

3.3.2 Effect of Surface Modifications Using Metal-Containing Cores

The results obtained for the pure silica core@shell materials can be used for synthesizing core@shell materials with guest species, e.g., metal oxides and nanoparticles, since the presence of guest species is not expected to affect the number of secondary growth steps required for the deposited nanocrystals to grow. To illustrate this feature, various metals were introduced into the pore structure of mesoporous silica spheres using impregnation techniques. Figures S 0.4d-f and S 0.5e-g (3.6 Supporting information) show the SEM images and nitrogen physisorption isotherms, respectively, obtained for some of the guest-containing mesoporous silica cores used in this study. Following exactly the same procedure as described above for synthesizing pure silica @silicalite-1 samples, the metal-containing (e.g., Co, Mn) particles were then used as the core for synthesizing metal-containing core@shell microspheres. The SEM images of the final products are shown in Figure S 3.5. Unexpectedly, in contrast to that of the pure silica @silicalite-1 samples, most of the synthesis attempts failed to provide a perfect coverage, especially for the larger particles (e.g., SG). This was probably caused by inefficient seeding of the external surface of the cores due to lack of proper interaction between the core particles and silicalite-1 nanocrystals. In other words, introducing metal oxide might change the surface properties of the particles. Surface modification is indeed crucial for preparing high-quality core@shell materials by establishing the required levels of attractive interactions between the zeolite nanocrystals and the external surface of the core, leading to high density and firm adhesion of the seeds on the surface. The low density of nanocrystals on the surface seems to spoil the possibility of forming a well-intergrown uniform shell upon hydrothermal treatment. In addition, it cannot allow the shell to play the protective role of coated seeds toward hindering the dissolution of the core or leaching of possible guest species during the course of secondary hydrothermal treatments[21]. Loose interactions between the seeds and the core surface would result in an incomplete coverage of zeolitic shell and the formation of discrete bulk crystals that would arise from detached seeds which would later grow freely inside the medium used for the secondary hydrothermal step. Complete removal of these bulk crystals, especially when their sizes are comparable to that of the core@shell product imposes some

difficulties in the purification of the final core@shell product. In addition, the growth of these bulk crystals consumes reaction nutrients required for the formation and uniform growth of the zeolitic shell.

One strategy to improve the formation of a homogeneous shell is the layer-by-layer adsorption of ionic polymers of opposite charges before seeding with nanozeolites [47-51]. Increasing the thickness of polymeric coating around the core particles can possibly enhance the interaction between negatively charged nanocrystals and positive core surfaces. Therefore, three layers of polymer in the order of PDADMAC/PSS/PDADMAC were placed around the cores. Figure S 3.6 shows that this method slightly improved the coverage; however, it led to a large number of nanocrystals formed in the bulk and irregular surface of the final product. Moreover, due to the time-consuming multistep procedure, it is often rather tedious to use this technique [52].

Alternatively, we explored the functionalization of the external surface of the particles using APTES which provides an adequate solution to this problem by increasing the zeta potential of the silica particles from highly negative toward positive values [53], improving the electrostatic interactions of nanocrystals and silica particles during the seeding step. In addition, this modification can provide amine functional groups along with some free silanol groups on the external surface which can help anchoring the seeds to the surface via hydrogen bonding and/or upon condensation during a short calcination before secondary growth. Core surface modification via functionalization of the external surface with amine moieties has previously been used for synthesizing core@shell catalysts using millimeter-size cores [13, 14, 16, 54]. Using this method, it was observed that the detachment of the seeds from the external surface was avoided leaving no bulk crystals in the as-synthesized sample after the secondary growth steps. However, reaching a large concentration of functional groups might not be possible due to the high porosity of the mesoporous cores and diffusion of the organic moieties into the pore system. Figure S 3.7 shows the results obtained when only APTES grafting was used to modify the surface of the core particles which reveals a partial coverage of silica surface even after 3-4 secondary hydrothermal steps.

Finally, a single-step surface modification with polyelectrolytes was also attempted to ensure the perfect coverage by increasing the density of nanocrystals on the core external surface. This time, Figures 0.6 and S 1.1 show a clear improvement in the zeolitic shell coverage

after adding APTES grafting and seeding steps to the method previously used for coating pure silica spheres (Scheme 3.1). The corresponding SEM images confirmed the absence of abundant silicalite-1 crystals in the bulk while all particles are entirely coated with a well-intergrown shell of silicalite-1 (Figures 0.6 and S 1.1).

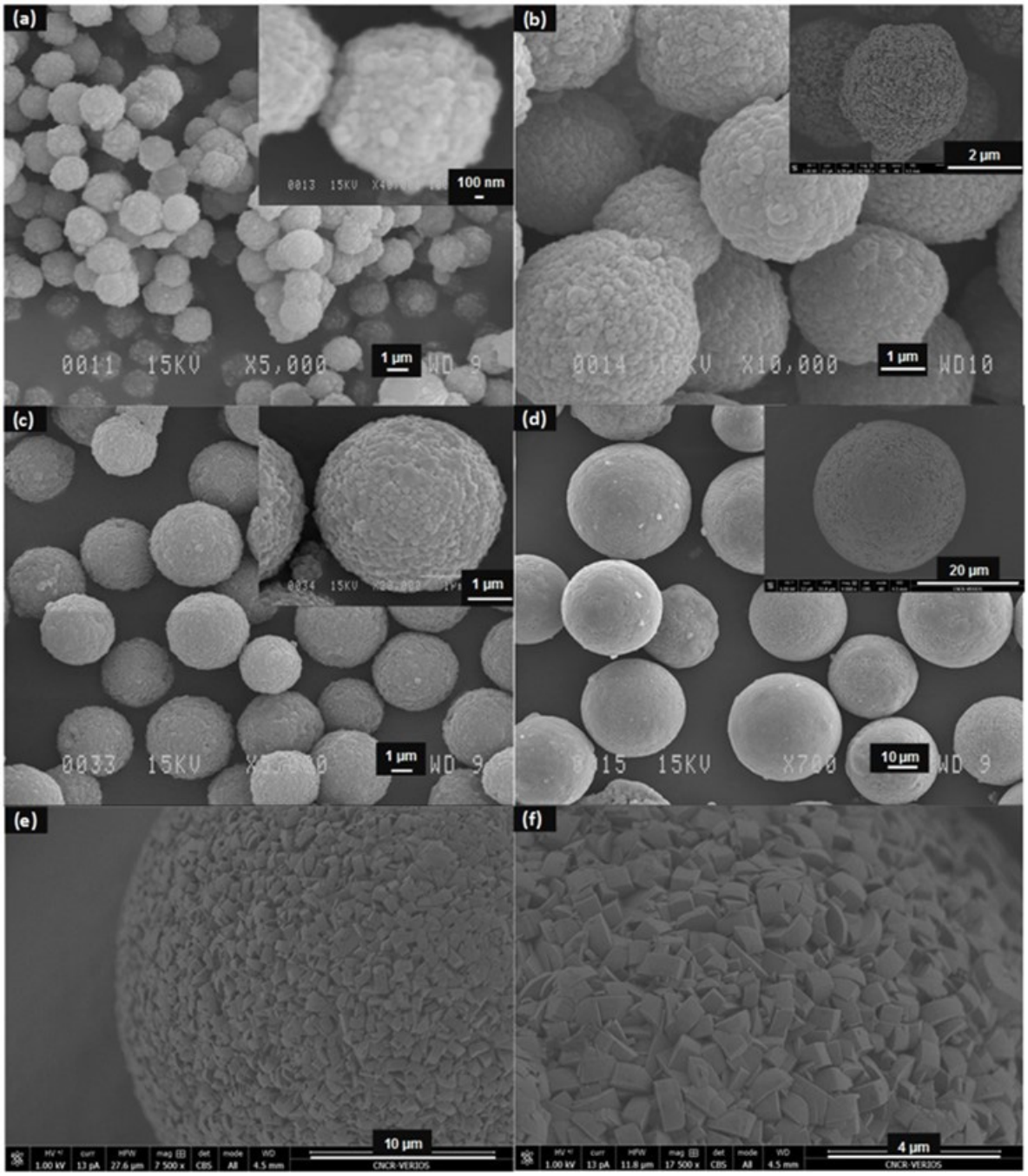

Figure 3.3- SEM images of (a) Ti,HMS@silicalite-1, (b) Co,SG3@silicalite-1, (c) Mn,SG3@silicalite-1, and (d-f) Co,SG20(I)@silicalite-1.

Moreover, the preservation of the structure of the mesoporous silica supports was studied by breaking the particles through simple mechanical grinding. The resulting SEM images (Figures 0.7a-d and S 1.2) reveal that the metal-containing core structures survived during multiple hydrothermal treatments, owing to the protective layer of silicalite-1. Figures 0.7a-d and S 1.2 clearly show the interface between the microporous crystalline shell and the mesoporous silica core. Moreover, from these images of broken particles, the shell thickness of the final product could be estimated to be smaller than about 0.5-1 µm, varying with the size of the selected core particles, i.e., larger particles allow the growth of a thicker shell. Regarding the required number of secondary growth steps, similar results were obtained as described above for pure silica core@shell materials. Nevertheless, Figure 3.4e,f shows that increasing the number of secondary growth steps can finally lead to a slight aggregation of the particles, cracking of the shell and some dissolution of the core material.

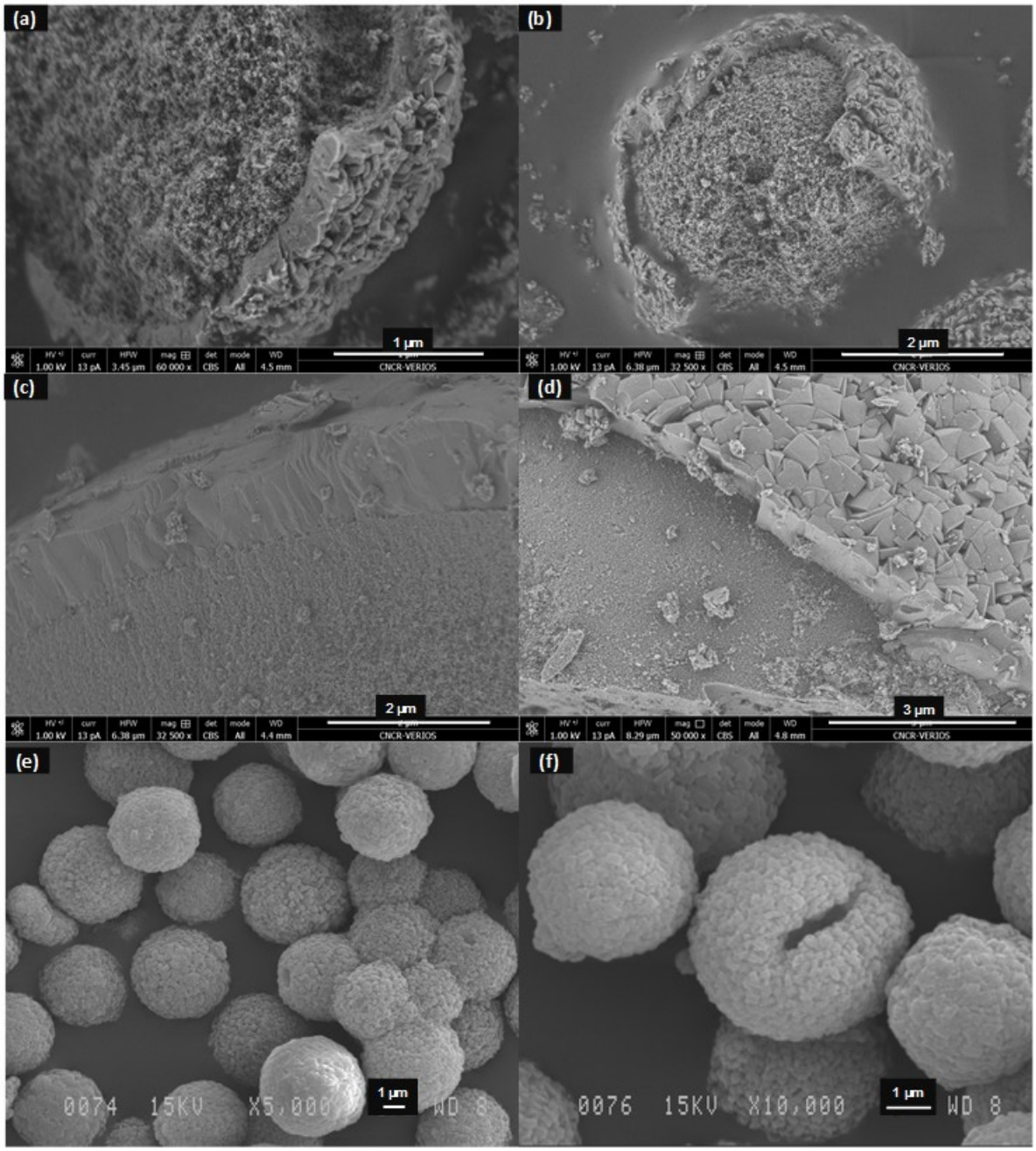

Figure 3.4- SEM images of (a,b) broken shell of Co,SG3@silicalite-1, (c,d) broken shell of Co,SG20@silicalite-1, and (e,f) Co,SG3@silicalite-1 after four secondary growth steps.

Again, nitrogen sorption measurements can be used to show that the zeolitic layer efficiently restricts the access of nitrogen molecules to the inner channels of the mesoporous silica cores. To analyze the entirety of the silicalite-1 shell, nitrogen adsorption isotherms were

obtained for the as-synthesized samples (Figures 0.8 and S 0.13). The continuity of such a zeolite shell should guarantee a shape selectivity of the final hierarchical material, however, minor deviations from the perfect shell coverage resulting from the appearance of pinholes and small cracks are not expected to prevent shape selectivity [55]. Noncalcined samples showed very little nitrogen uptake, showing that the pore-blocked zeolitic layer efficiently restricted the access of nitrogen molecules to the inner channels of the mesoporous silica core. However, upon calcination both micropores of the silicalite-1 layer and mesopores of the core are made accessible to the probe molecules. The textural properties of the different calcined core@shell spheres obtained by nitrogen physisorption measurements are summarized in Table 3.1. It should also be noted that the SG20 particles with a larger average pore size (SG20(II)) have not been used for the synthesis of metal-containing core@shell catalysts owing to their lower surface area and some mechanical stability issues.

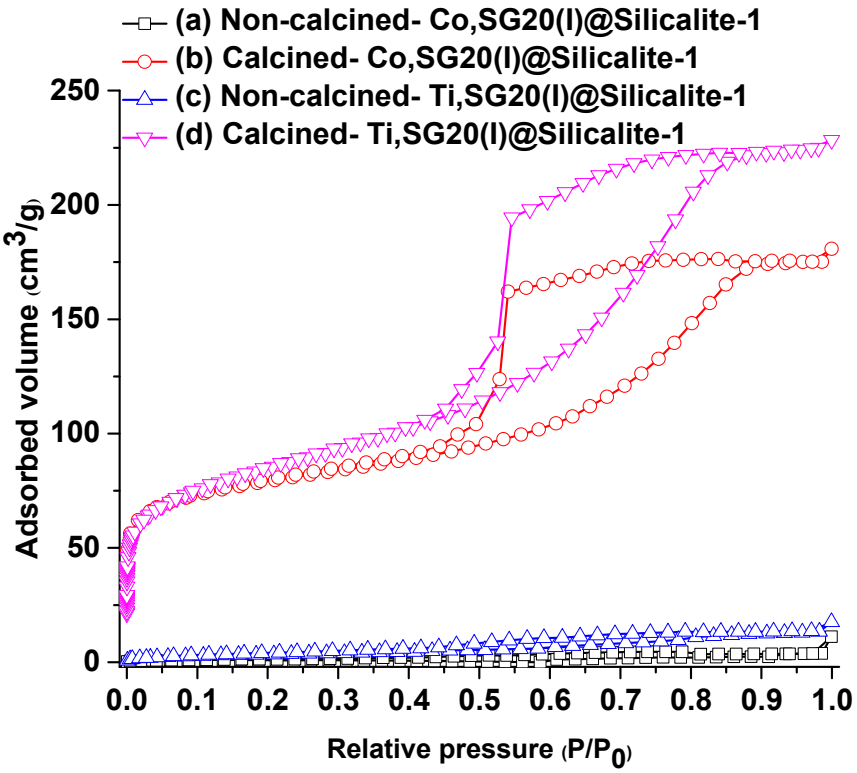

Figure 3.5- Nitrogen adsorption/desorption isotherms measured at -196 °C for (a,b) Co,SG20(I)@silicalite-1 before and after calcination, and (c,d) Ti,SG20(I)@silicalite-1 before and after calcination.

The cumulative pore volumes and pore size distributions of the pristine silica gel (SG3 and SG20(I)) and their corresponding supported-metal oxide and core@shell products were obtained by using the nonlocal density functional theory (NLDFT) method (N_2 sorption in cylindrical silica pores, adsorption branch) and are depicted in Figure 3.6. The mesoporous silica gel spheres presented the largest pore volume and a narrow pore size distribution with a maximum centered between 6 and 7 nm. Upon introducing metallic species into the pore network of silica gel particles, the total pore volume slightly decreased, without a considerable change in the pore size distribution. In contrast, the pore size distribution of the final core@shell material showed the emergence of small pores in the microporous region (pores smaller than 2 nm) which is associated to the silicalite-1 shell. Mesopores (pores larger than 2 nm) are also apparent in the pore size distribution curves which showed a wider distribution compared to the parent silica particles; however, the maximum points of the curve are still positioned between 6 and 7 nm, as observed for the silica gel particles. There is another maximum point in the mesopore region which could here be an artifact, arising from the complex pore network connectivity between the mesoporous core and microporous shell.

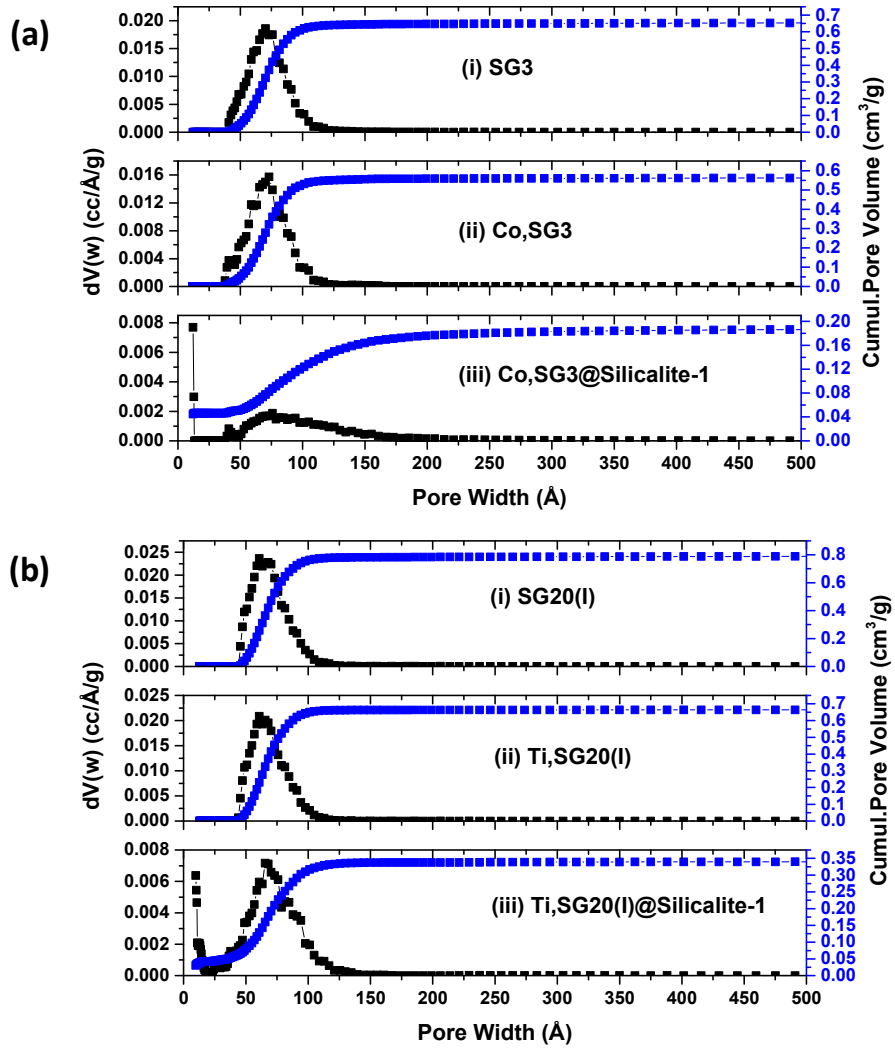

Figure 3.6- NLDFT pore size distributions and cumulative pore volumes of (a) silica gel-3 µm (SG3) (b) silica gel-20 µm (SG20(I)), in pure form, after metal insertion and after shell formation, calculated from the adsorption branch of the isotherm by using the NLDFT method.

Survey XPS spectra were used for measuring the elemental composition of the powdery samples' surfaces in the case of Co modified materials (Figure 3.7). A section of the full spectra, corresponding to the expected position for Co(2p) peaks was magnified and plotted in Figure 3.7, showing two Co2p peaks at approximately 778 eV and 793 eV for bare metal-loaded SG20(I). Although the exact determination of Co oxidation state might not be possible using these survey spectra and needs a high-resolution analysis, using this technique, the guest species which could have possibly leached out during the shell

formation steps or attached on the external surface of the un-coated particles can be detected. Apparent relative concentrations in atomic % were also estimated based on each survey spectrum and used to calculate the M/Si ratios which are presented with the corresponding spectrum in Figure 3.7. As can be seen in Figure 3.7, Co species were detected in the bare metal-containing sample and in one of the failed syntheses with partial silicalite-1 coverage. However, the core@shell products with complete zeolitic shell did not present any metal species within the Co detection limit, which was estimated to be of the order of 0.05 atomic % (Figure 3.7).

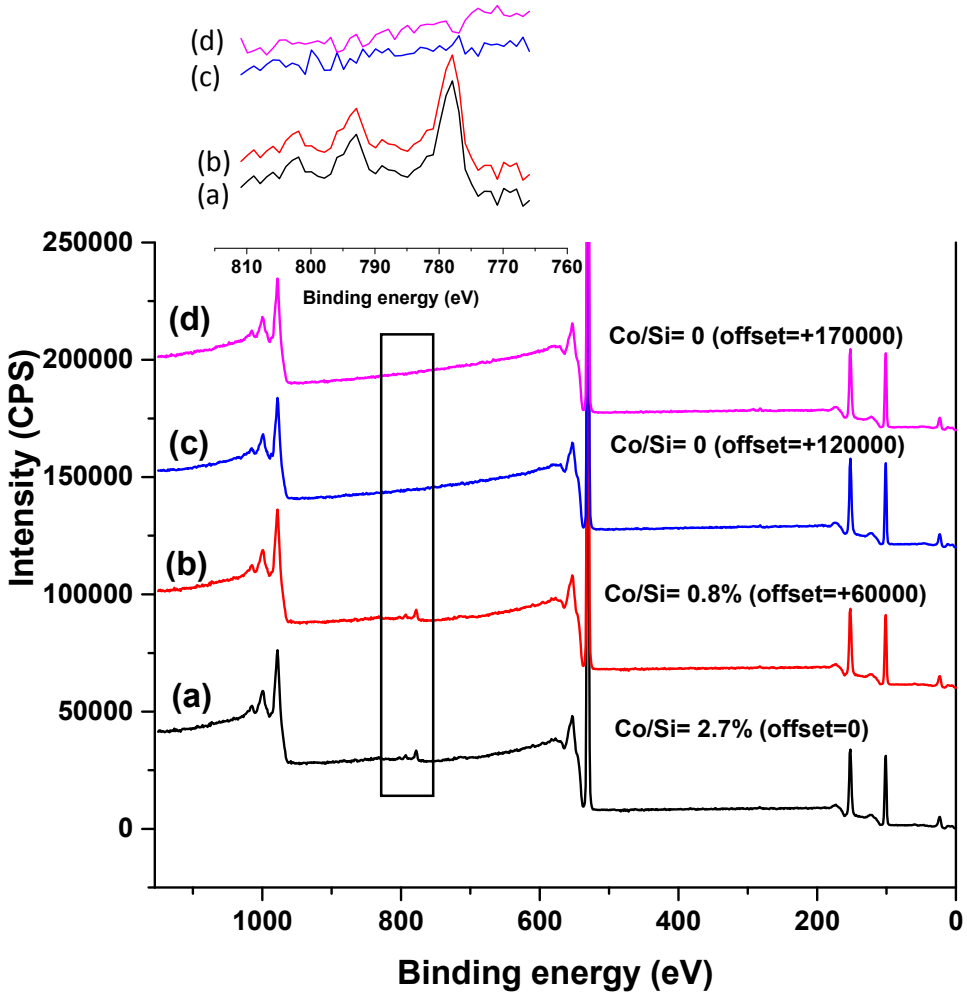

Figure 3.7- XPS survey spectra of (a) bare Co,SG20(I), (b) partially covered Co,SG3@silicalite-1, (c) fully covered Co,SG3@silicalite-1, and (d) fully covered Co,SG20(I)@silicalite-1 (survey scans were used for apparent concentrations, presented as Co/Si ratio in the graph).

The radial distribution of guest metal species was analyzed by EDS elemental mapping for two Co- containing core@shell samples at two different initial compositions (exactly the same samples which were used for XRD and XPS surface analyses). Particles were broken by simple grinding using a mortar and pestle. Figure 3.8b,d shows that the Co concentration on the core region stays constant and uniform and then drops to low quantities, close to zero, at the interface between the silicalite-1 shell and the mesoporous silica core. Grinding, as an intrusive method, could contaminate the silicalite-1 shell by pushing metal oxide traces into the shell side. It should also be noted that the sharp fluctuation at the core and shell interface, shown in Figure 3.8h, can be attributed to the gap between these two parts [30], probably caused by the destructive effect of the grinding process on the large core@shell material with SG20 microsphere as the core. The atomic metal to silicon ratio was also measured using EDS analysis as 4 and 1 % for Co,SG3@silicalite-1 and Co,SG20(I)@silicalite-1, respectively, while the XPS survey did not show any Co species on the external surface of the shell and in the bulk. The structural characteristics of these Co-containing core@shell materials were also studied using XRD (Figure S 3.11). Most of the peaks observed in XRD patterns, i.e., peaks at 2θ= 7.5–9.5, 23–24 and 30 degrees, correspond to the crystalline structure of silicalite-1 shell, as compared to simulated MFI diffractograms. Considering the low concentration of the guest species in Co,SG20(I)@silicalite-1, cobalt oxide did not appear in the powder XRD pattern, while in the case of Co,SG3@silicalite-1 with a higher concentration, a broad peak appeared on the diffractogram. The maximum point is centered at 36.9 degree which is characteristic of Co_3O_4, corresponding to 311 reflection.

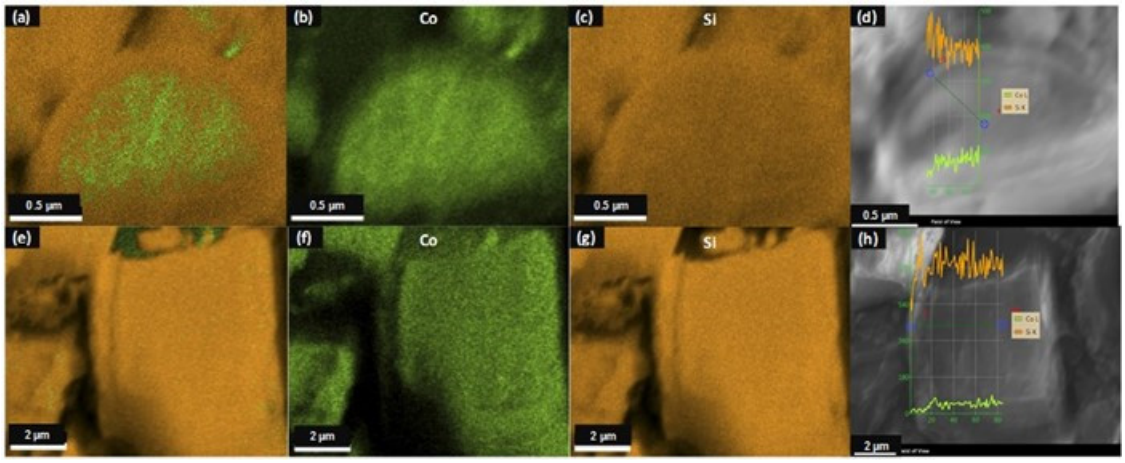

Figure 3.8- EDS elemental maps of (a-d) Co,SG3@silicalite-1 (Co/Si atomic ratio: 4%), and (e-h) Co,SG20(I)@silicalite-1 (Co/Si atomic ratio: 1%).

3.4 Conclusion

The formation of well-defined SiO_2@zeolite particles requires the ability to grow a polycrystalline, zeolitic shell around each mesoporous silica core; destruction of the spherical template and intergrowth among different particles ought to be avoided. Our work showed that SiO_2@silicalite-1 can be formed when coating mesoporous spheres with PDADMAC, adsorbing silicalite-1 nanocrystals, and then hydrothermally treating smaller microspheres (i.e., HMS and SG3) at least two times — applying more treatments leads to particle aggregation and core dissolution for HMS particles — and largest spheres (SG20) four times. Therefore, regarding these pure silica cores, the required number of secondary growth steps is directly correlated to the size of the core particles, i.e., two successive short hydrothermal treatments provide a uniform shell coverage for small microspheres like HMS particles, while larger ones may require more steps. Furthermore, when supporting metal oxides inside the mesopores of the spheres before the formation of the zeolitic shell, the creation of well-defined M,SiO_2@silicalite-1 core@shell spheres requires an additional external surface functionalization of the spheres with APTES. Accordingly, these results can be used to obtain efficient adsorbents, catalysts and zeolitic microstructures exhibiting a hierarchical architecture with various functional groups, evenly embedded within the mesoporous core compartment and protected by a shape-selective microporous zeolitic shell.

3.5 Acknowledgements

The authors acknowledge financial support from the National Science and Engineering Research Council (Canada) and the Fonds québécois de la recherche sur la nature et les technologies (FRQNT).

3.6 Supporting Information

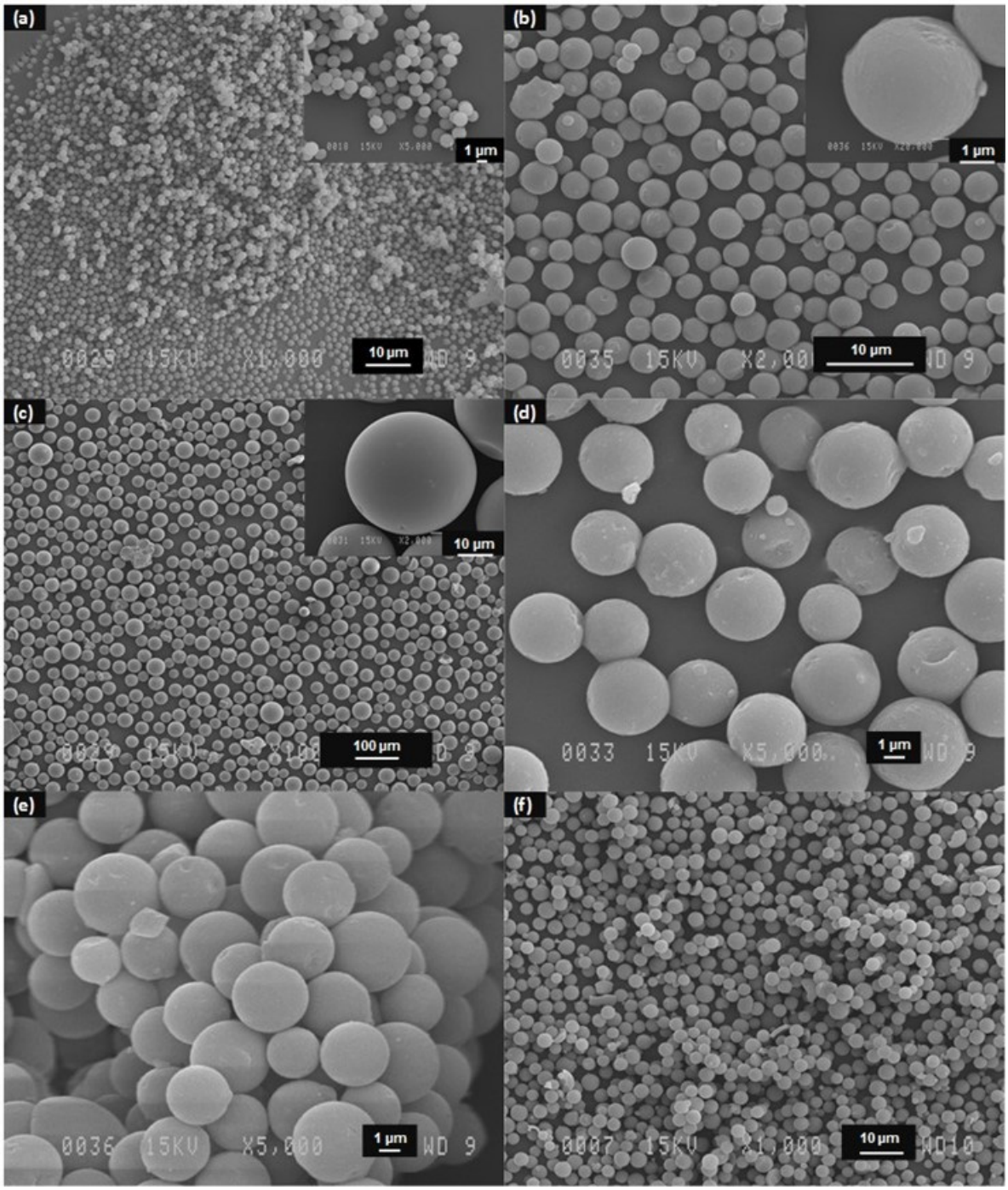

Figure S 3.1- SEM images of (a) HMS microspheres, (b) silica gel spheres 3 µm (SG3), (c) silica gel spheres 20-45 µm (SG20) and (d-f) SG3 spheres containing (d) cobalt (Co,SG3), (e) manganese (Mn,SG3), and (f) titanium (Ti,SG3).

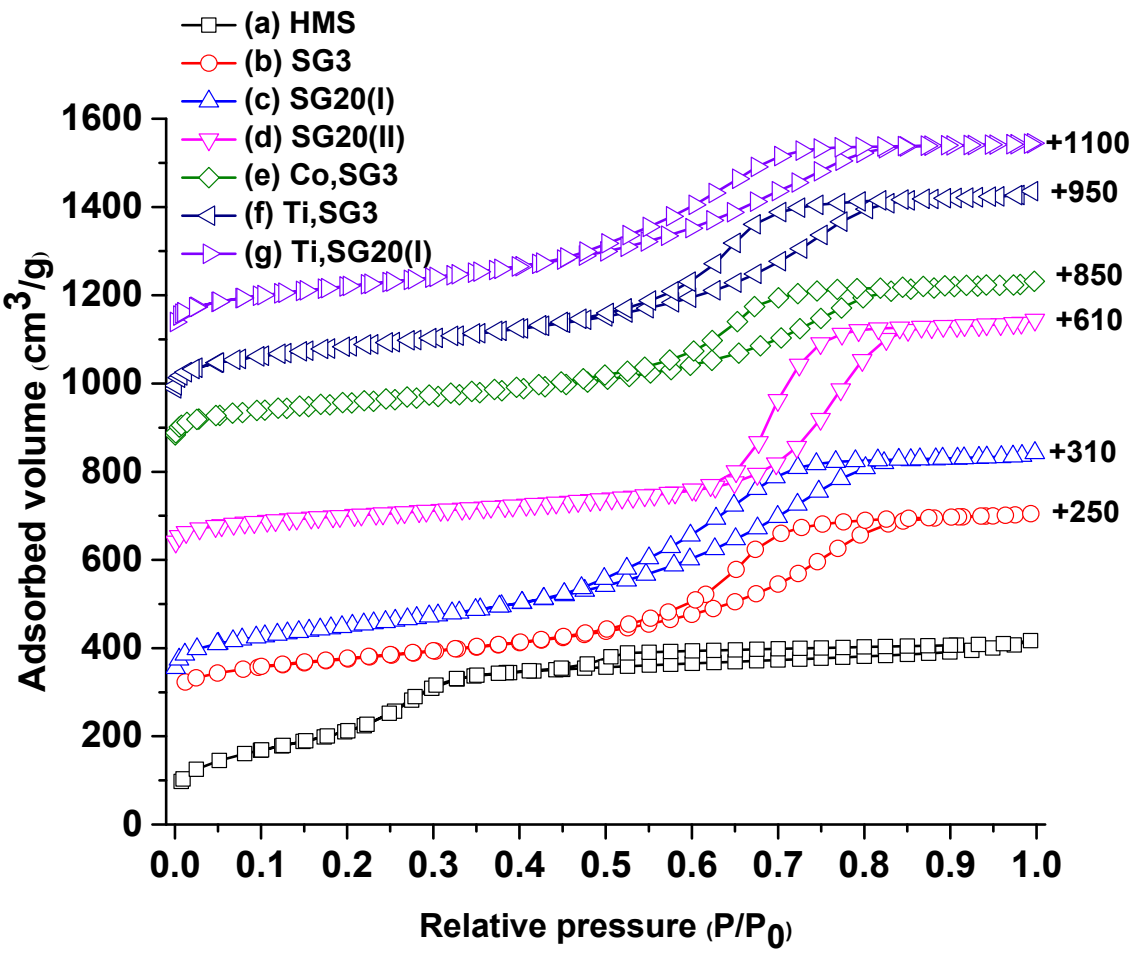

Figure S 3.2- Nitrogen adsorption/desorption isotherms measured at -196 °C for different core particles.

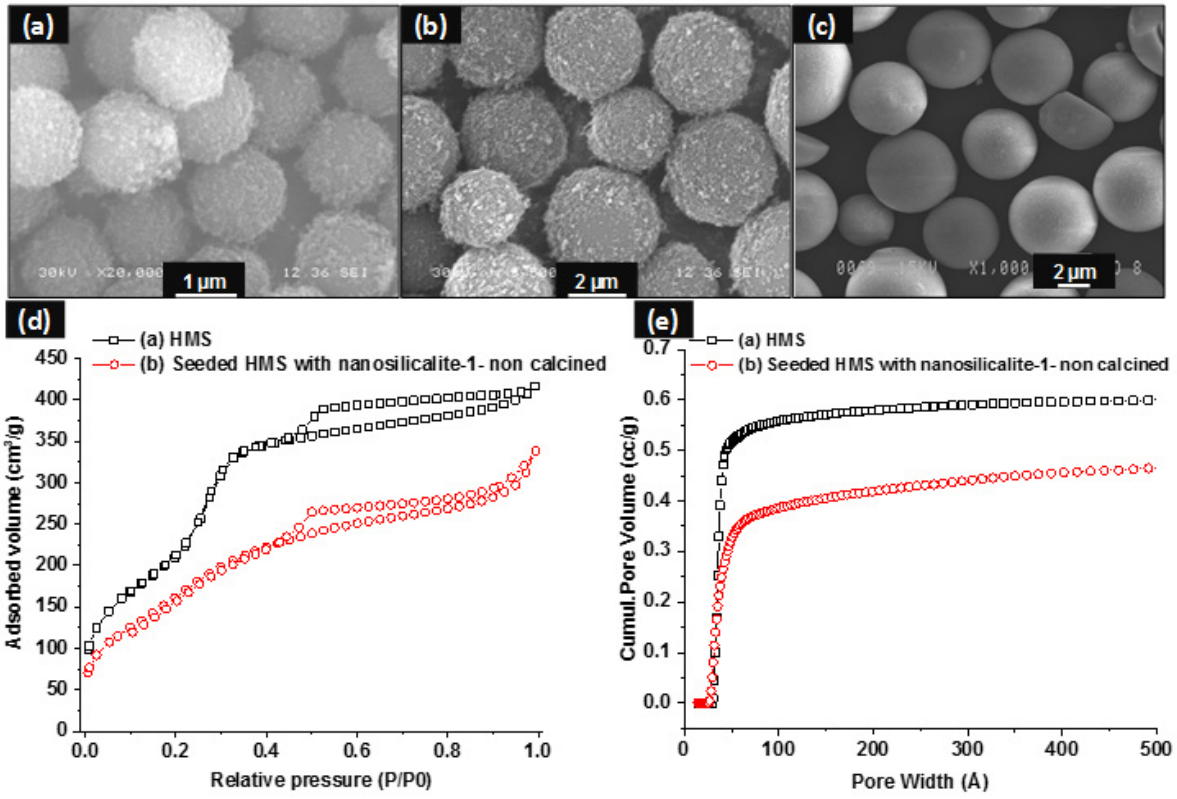

Figure S 3.3- (a-c) SEM images of HMS, SG3 and SG20 particles, covered with silicalite-1 nanocrystals, (d) nitrogen physisorption isotherms (-196 °C) and (e) NLDFT cumulative pore volume plots of pure and noncalcined seeded HMS particles.

(i)

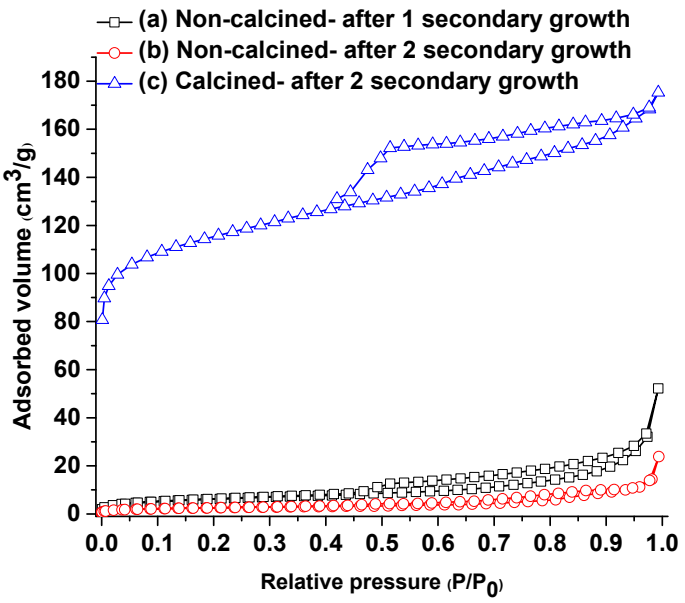

(ii)

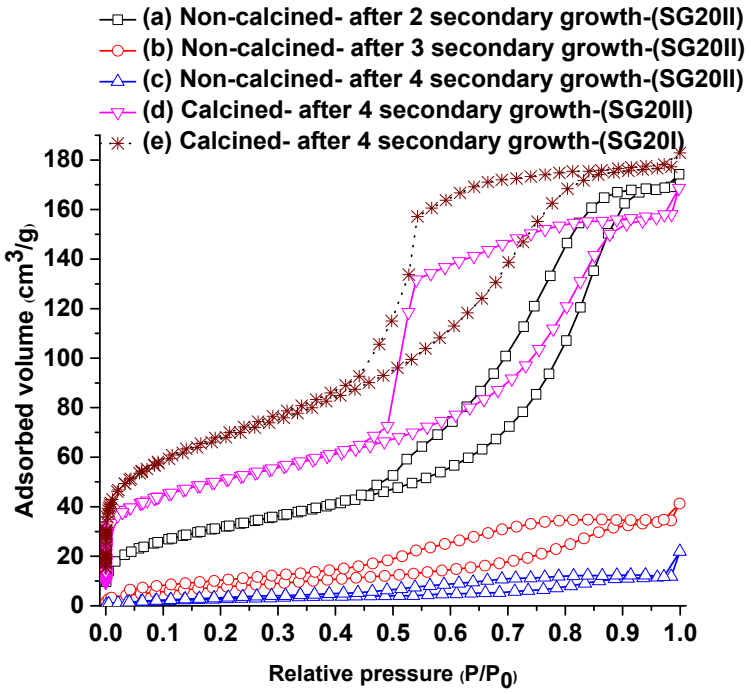

Figure S 3.4- Nitrogen adsorption/desorption isotherms measured at -196 °C (i) HMS and (ii) SG20 at different stages of the core@shell synthesis.

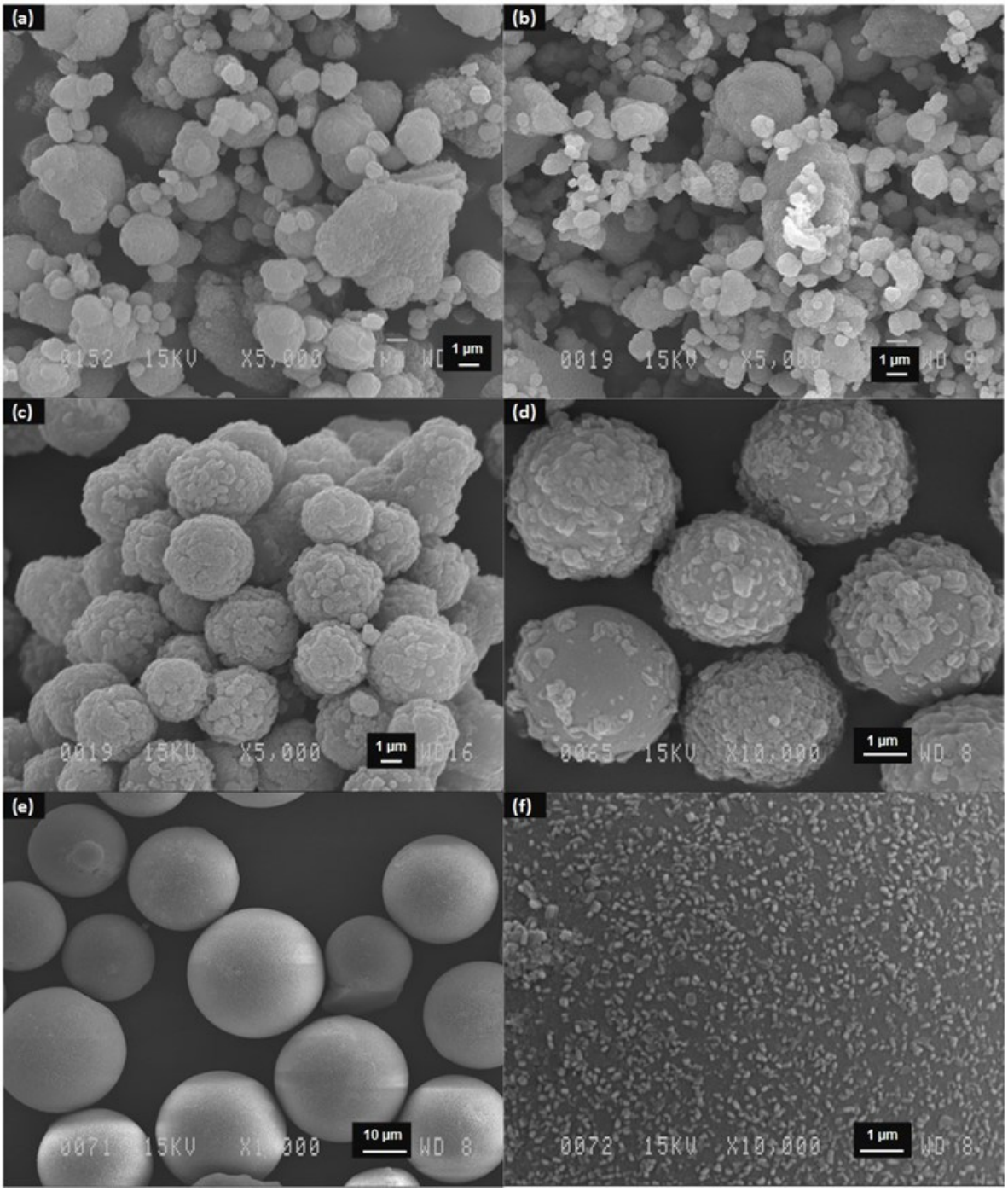

Figure S 3.5- SEM images of (a) Co,HMS@silicalite-1, (b) Co,SG3@silicalite-1, (c) Co,SG3@silicalite-1, (d) Mn,SG3@silicalite-1, (e) Co,SG20(I)@silicalite-1, and (f) Co,SG20(I)@silicalite-1 with higher magnification.

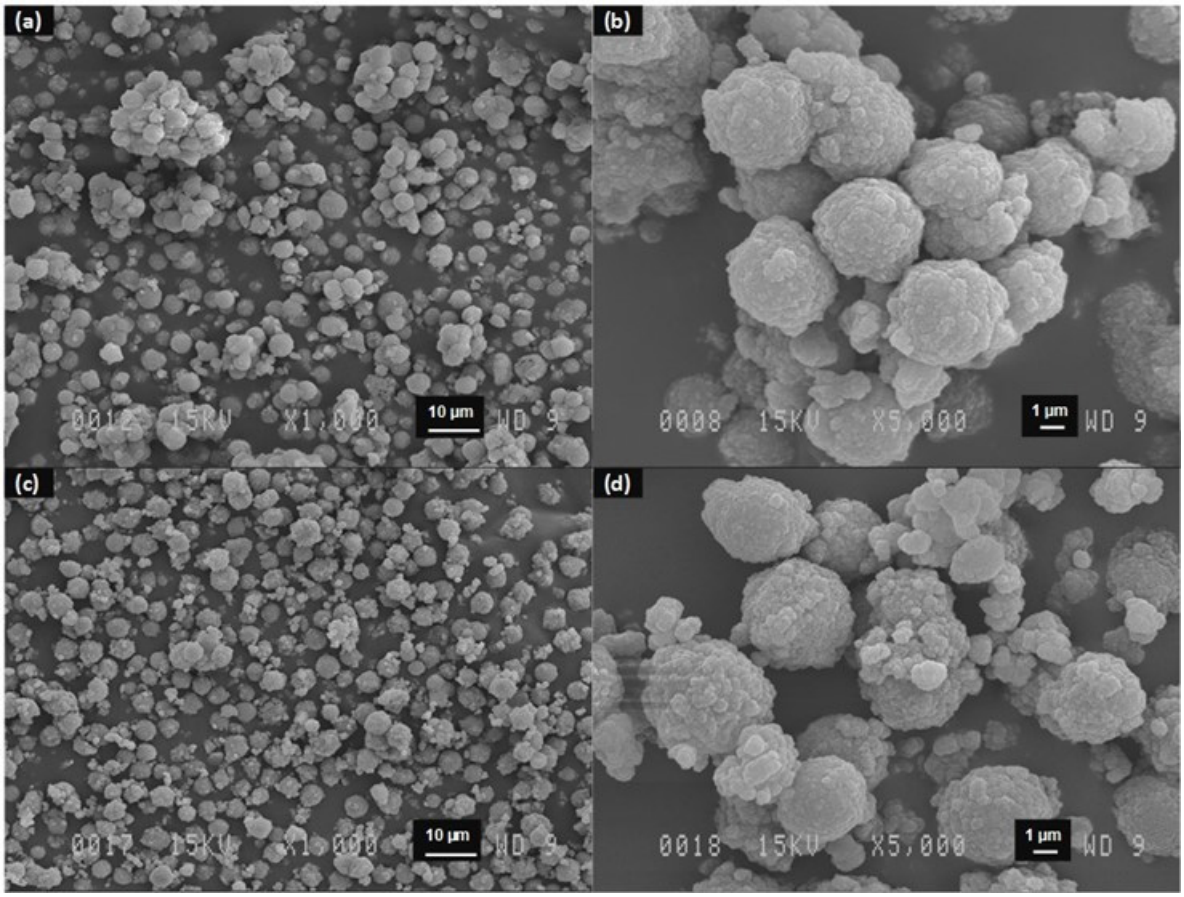

Figure S 3.6- Effect of multilayer polymer coating (PDADMAC/PSS/PDADMAC) on (a,b) SG3@silicalite-1, and (c,d) Co,SG3@silicalite-1.

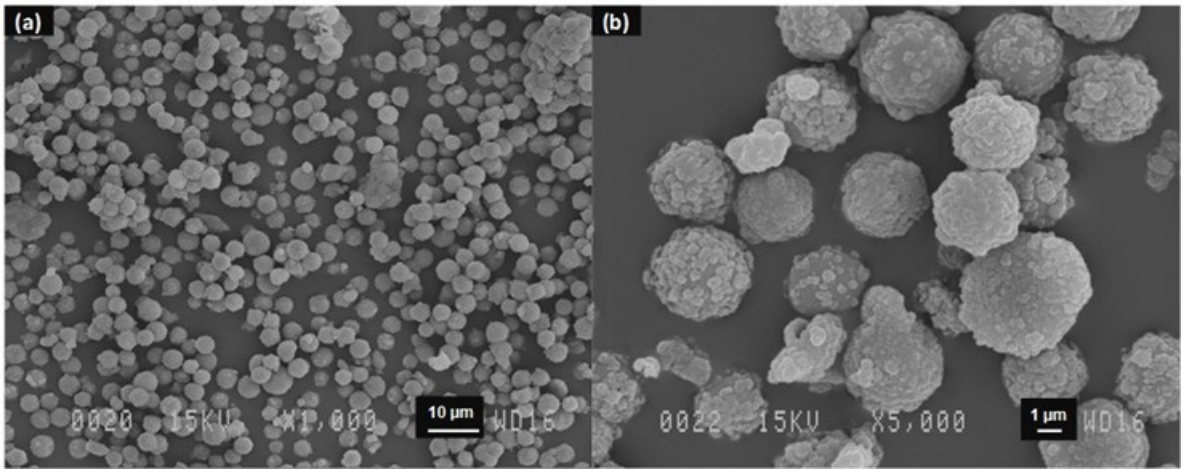

Figure S 3.7- Effect of the sole APTES modification on Mn,SG3@silicalite-1 synthesis after three secondary growth steps.

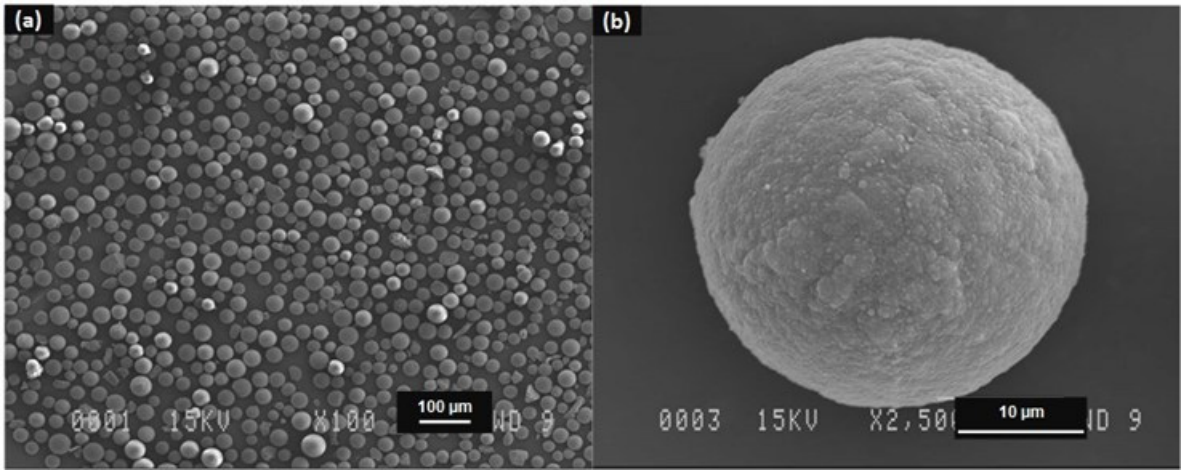

Figure S 3.8- SEM images of Ti,SG20(I)@silicalite-1 after four secondary growth steps.

Figure S 3.9- Higher magnification HRSEM image of Co,SG20(I)@silicalite-1 sample, broken using a mortar and pestle.

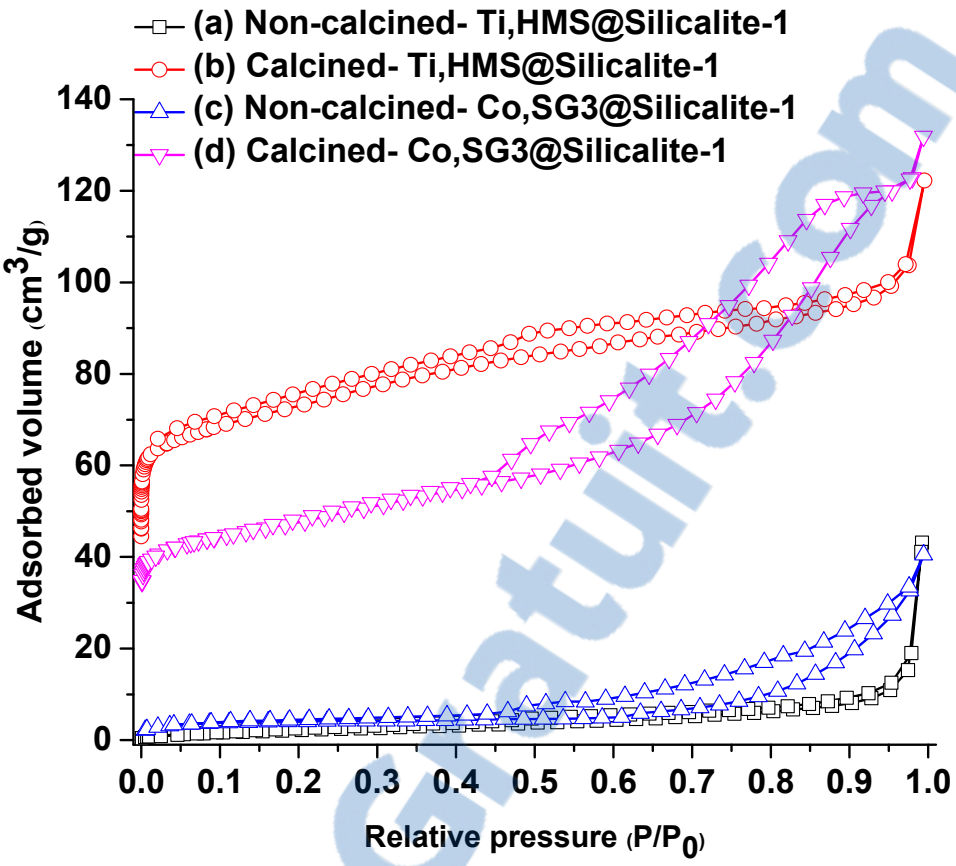

Figure S 3.10- Nitrogen adsorption/desorption isotherms measured at -196 °C for (a,b) Ti,HMS@silicalite-1 before and after calcination, and (c,d) Co,SG3@silicalite-1 before and after calcination.

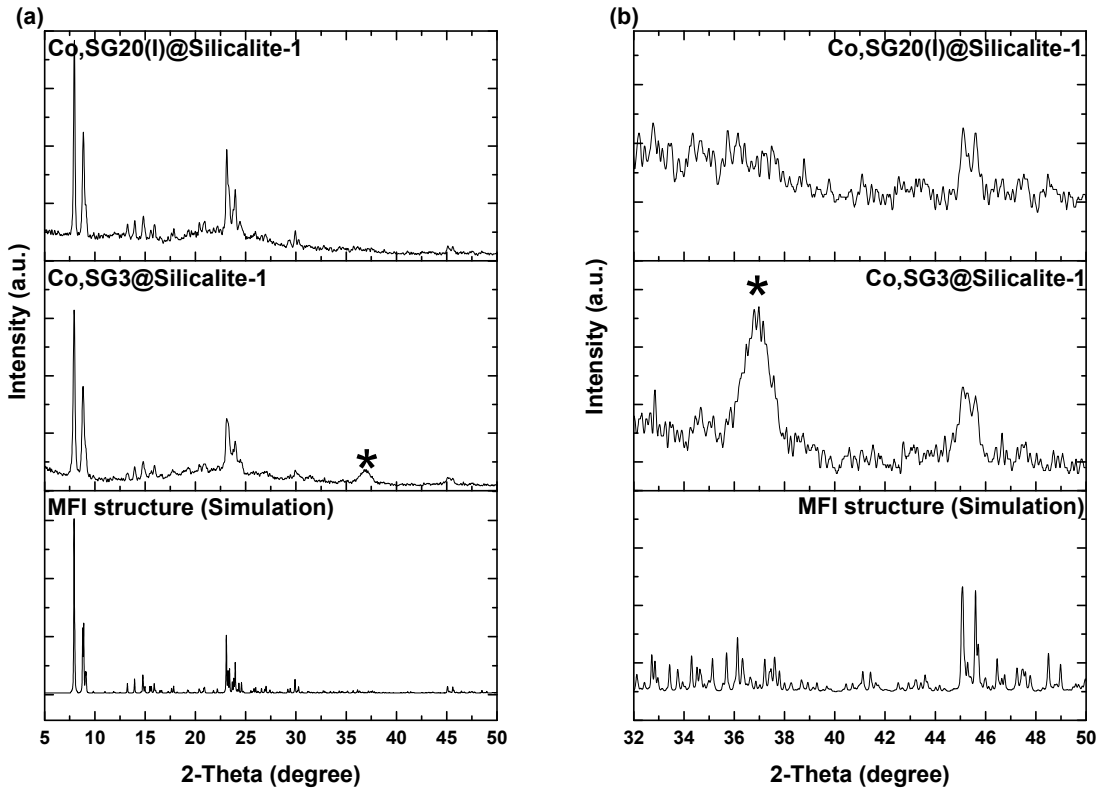

Figure S 3.11- XRD patterns of Co,SG3@silicalite-1 and Co,SG20(I)@silicalite-1. Simulations for calcined MFI structure were obtained from IZA website [56].

3.7 References

[1] R. Ghosh Chaudhuri, S. Paria, *Chem. Rev.* **2011**, *112*, 2373-2433.
[2] H. Wang, L. Chen, Y. Feng, H. Chen, *Acc. Chem. Res.* **2013**, *46*, 1636-1646.
[3] J. Zhang, T. Zhang, X. Zhang, W. Liu, H. Liu, J. Qiu, K. L. Yeung, *Catal. Today* **2014**, *236*, 34-40.
[4] A. Ghorbanpour, A. Gumidyala, L. C. Grabow, S. P. Crossley, J. D. Rimer, *ACS Nano* **2015**, *7*, 4006-4016.
[5] T. Du, H. Qu, Q. Liu, Q. Zhong, W. Ma, *Chem. Eng. J.* **2014**, *262*, 1199-1207.
[6] X. Wang, Y. Cui, Y. Wang, X. Song, J. Yu, *Inorg. Chem.* **2013**, *52*, 10708-10710.
[7] J. Wang, D. M. Do, G. K. Chuah, S. Jaenicke, *ChemCatChem* **2013**, *5*, 247-254.
[8] J. Ding, L. Han, M. Wen, G. Zhao, Y. Liu, Y. Lu, *Catal. Commun.* **2015**, *72*, 156-160.
[9] M. Wen, J. Ding, C. Wang, Y. Li, G. Zhao, Y. Liu, Y. Lu, *Microporous Mesoporous Mater.* **2016**, *221*, 187-196.
[10] X. Wang, M. Wen, C. Wang, J. Ding, Y. Sun, Y. Liu, Y. Lu, *Chem. Commun.* **2014**, *50*, 6343-6345.
[11] N. Masoumifard, P. M. Arnal, S. Kaliaguine, F. Kleitz, *ChemSusChem* **2015**, *8*, 2093-2105.
[12] E. A. Khan, A. Rajendran, Z. Lai, *Chem. Eng. Res. Bull.* **2013**, *16*, 1-15.
[13] X. Wang, X. Zhang, Y. Wang, H. Liu, J. Wang, J. Qiu, H. L. Ho, W. Han, K. L. Yeung, *Chem. Eng. J.* **2011**, *175*, 408-416.
[14] N. Jiang, G. Yang, X. Zhang, L. Wang, C. Shi, N. Tsubaki, *Catal. Commun.* **2011**, *12*, 951-954.
[15] E. A. Khan, A. Rajendran, Z. Lai, *Ind. Eng. Chem. Res.* **2010**, *49*, 12423-12428.
[16] J. Zhou, X. Zhang, J. Zhang, H. Liu, L. Zhou, K. Yeung, *Catal. Commun.* **2009**, *10*, 1804-1807.
[17] G. Yang, Y. Tan, Y. Han, J. Qiu, N. Tsubaki, *Catal. Commun.* **2008**, *9*, 2520-2524.
[18] G. Yang, J. He, Y. Zhang, Y. Yoneyama, Y. Tan, Y. Han, T. Vitidsant, N. Tsubaki, *Energy Fuels* **2008**, *22*, 1463-1468.
[19] G. Yang, J. He, Y. Yoneyama, Y. Tan, Y. Han, N. Tsubaki, *Appl. Catal., A* **2007**, *329*, 99-105.
[20] J. He, Y. Yoneyama, B. Xu, N. Nishiyama, N. Tsubaki, *Langmuir* **2005**, *21*, 1699-1702.
[21] Y. Bouizi, I. Diaz, L. Rouleau, V. Valtchev, *Adv. Funct. Mater.* **2005**, *15*, 1955-1960.
[22] A. L. Yonkeu, V. Buschmann, G. Miehe, H. Fuess, A. M. Goossens, J. A. Martens, *Cryst. Eng.* **2001**, *4*, 253-267.
[23] M. Miyamoto, T. Kamei, N. Nishiyama, Y. Egashira, K. Ueyama, *Adv. Mater.* **2005**, *17*, 1985-1988.
[24] D. He, D. Liu, *RSC Adv.* **2015**, *5*, 5438-5441.
[25] M. Okamoto, L. Huang, M. Yamano, S. Sawayama, Y. Nishimura, *Appl. Catal., A* **2013**, *455*, 122-128.
[26] Z. Jin, S. Liu, L. Qin, Z. Liu, Y. Wang, Z. Xie, X. Wang, *Appl. Catal., A* **2013**, *453*, 295-301.
[27] G. D. Pirngruber, C. Laroche, M. Maricar-Pichon, L. Rouleau, Y. Bouizi, V. Valtchev, *Microporous Mesoporous Mater.* **2013**, *169*, 212-217.
[28] V. Valtchev, S. Mintova, *Microporous Mesoporous Mater.* **2001**, *43*, 41-49.
[29] V. Valtchev, *Chem. Mater.* **2002**, *14*, 956-958.

[30] Y. Bouizi, L. Rouleau, V. P. Valtchev, *Microporous Mesoporous Mater.* **2006**, *91*, 70-77.
[31] Y. Bouizi, L. Rouleau, V. P. Valtchev, *Chem. Mater.* **2006**, *18*, 4959-4966.
[32] Y. Bouizi, G. Majano, S. Mintova, V. Valtchev, *J. Phys. Chem. C* **2007**, *111*, 4535-4542.
[33] E. A. Khan, E. Hu, Z. Lai, *Microporous Mesoporous Mater.* **2009**, *118*, 210-217.
[34] V. Valtchev, J. Hedlund, B. J. Schoeman, J. Sterte, S. Mintova, *Microporous Mater.* **1997**, *8*, 93-101.
[35] V. Valtchev, *Chem. Mater.* **2002**, *14*, 4371-4377.
[36] B. J. Schoeman, K. Higberg, J. Sterte, *Nanostruct. Mater.* **1999**, *12*, 49-54.
[37] M. Grün, G. Büchel, D. Kumar, K. Schumacher, B. Bidlingmaier, K. K. Unger, *Stud. Surf. Sci. Catal.* **2000**, *128*, 155-165.
[38] A. Dong, N. Ren, W. Yang, Y. Wang, Y. Zhang, D. Wang, J. Hu, Z. Gao, Y. Tang, *Adv. Funct. Mater.* **2003**, *13*, 943-948.
[39] F. Bérubé, B. Nohair, F. Kleitz, S. Kaliaguine, *Chem. Mater.* **2010**, *22*, 1988-2000.
[40] F. Bérubé, A. Khadraoui, J. Florek, S. Kaliaguine, F. Kleitz, *J. Colloid Interface Sci.* **2015**, *449*, 102-114.
[41] A. Dong, Y. Wang, D. Wang, W. Yang, Y. Zhang, N. Ren, Z. Gao, Y. Tang, *Microporous Mesoporous Mater.* **2003**, *64*, 69-81.
[42] R. Kanthasamy, K. Barquist, S. C. Larsen, *Microporous Mesoporous Mater.* **2008**, *113*, 554-561.
[43] B. Zornoza, O. Esekhile, W. J. Koros, C. Téllez, J. Coronas, *Sep. Purif. Technol.* **2011**, *77*, 137-145.
[44] K. Vanherck, A. Aerts, J. Martens, I. Vankelecom, *Chem. Commun.* **2010**, *46*, 2492-2494.
[45] M. Thommes, *Chem. Ing. Tech.* **2010**, *82*, 1059-1073.
[46] C. J. Rasmussen, A. Vishnyakov, M. Thommes, B. M. Smarsly, F. Kleitz, A. V. Neimark, *Langmuir* **2010**, *26*, 10147-10157.
[47] F. Caruso, R. A. Caruso, H. Möhwald, *Science* **1998**, *282*, 1111-1114.
[48] K. H. Rhodes, S. A. Davis, F. Caruso, B. Zhang, S. Mann, *Chem. Mater.* **2000**, *12*, 2832-2834.
[49] X. D. Wang, W. L. Yang, Y. Tang, Y. J. Wang, S. K. Fu, Z. Gao, *Chem. Commun.* **2000**, 2161-2162.
[50] W. Yang, X. Wang, Y. Tang, Y. Wang, C. Ke, S. Fu, *J. Macromol. Sci., Pure Appl. Chem.* **2002**, *39*, 509-526.
[51] A. Dong, Y. Wang, Y. Tang, N. Ren, Y. Zhang, Z. Gao, *Chem. Mater.* **2002**, *14*, 3217-3219.
[52] B. Sun, S. A. Mutch, R. M. Lorenz, D. T. Chiu, *Langmuir* **2005**, *21*, 10763-10769.
[53] G. E. Musso, E. Bottinelli, L. Celi, G. Magnacca, G. Berlier, *Phys. Chem. Chem. Phys.* **2015**, *17*, 13882-13894.
[54] Q. Lin, G. Yang, X. Li, Y. Yoneyama, H. Wan, N. Tsubaki, *ChemCatChem* **2013**, *5*, 3101-3106.
[55] N. van der Puil, E. W. Kuipers, H. van Bekkum, J. C. Jansen, *Stud. Surf. Sci. Catal.* **1995**, *91*, 1163-1171.
[56] http://www.iza-structure.org/databases/, **2014**.

Chapter 4- Zeolitic Core@Shell Adsorbents for the Selective Removal of Free Glycerol from Crude Biodiesel

Nima Masoumifard,[a,b,d] Pablo M. Arnal,[c] Serge Kaliaguine*[b] and Freddy Kleitz*[a,d]

[a] Department of Chemistry, Université Laval, Quebec, G1V 0A6, QC, Canada, E-mail: freddy.kleitz@chm.ulaval.ca
[b] Department of Chemical Engineering, Université Laval, Quebec, G1V 0A6, QC, Canada, E-mail: serge.kaliaguine@gch.ulaval.ca
[c] Centro de Tecnología de Recursos Minerales y Cerámica (CETMIC) CIC - CONICET La Plata, Centenario y 506, B1897ZCA, M. B. Gonnet, Argentina
[d] Centre de Recherche sur les Matériaux Avancés (CERMA), Université Laval, Quebec, G1V 0A6, QC, Canada

Published in

ChemSusChem

Volume 8, Issue 12, Pages 2093-2105

2015

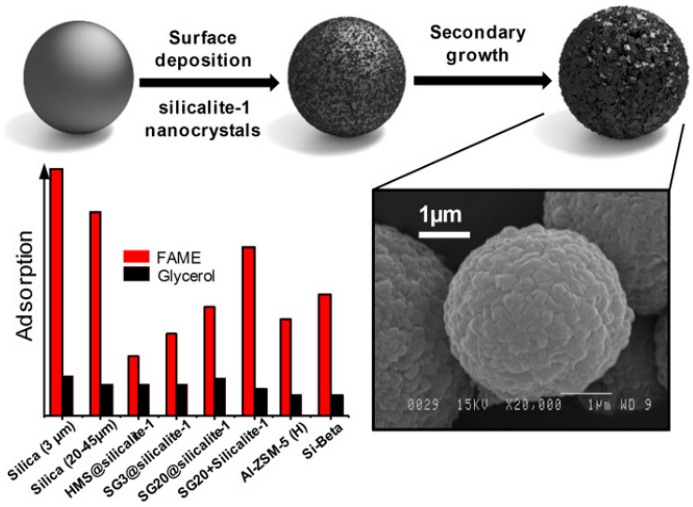

* Corresponding author:

Prof. Freddy Kleitz, E-mail: freddy.kleitz@chm.ulaval.ca, TEL: +1-418-656-7812

Prof. Serge Kaliaguine, E-mail: serge.kaliaguine@gch.ulaval.ca, TEL: +1-418-656-2708

Résumé

L’adsorption sélective du glycérol libre provenant du biodiésel brut a été réalisée à l'aide de sphères de silice mésoporeuses enrobées par une fine couche de zéolite silicalite-1 microporeuse. Une coquille polycristalline de silicalite-1 a été formée par-dessus différents types de coeurs mesoporeux, couvrant les surfaces externes avec des nanocristaux de silicalite-1, et ceci a été suivi par un court traitement hydrothermal pour assurer l'uniformité de la coquille. Des expériences d'adsorption du glycérol en conditions statiques ont été réalisées pour évaluer les capacités d’adsorption des matériaux synthétisées et les comparer à des adsorbants classiques, comme par exemple des silices mésoporeuses ou des zéolites. L’objectif est d’éliminer sélectivement le glycérol libre provenant de mélanges de biodiesel brut et de réaliser des tests à diverses températures. La fine couche de zéolite de type silicalite-1 microporeuse joue le rôle de membrane empêchant la diffusion des esters méthyliques d'acides gras dans les mésopores composant le coeur de l’adsorbant composite, tandis que le volume des mésopores du coeur permet l’adsorption du glycérol sous forme de multicouches. Finalement, ce nouveau matériau a sensiblement amélioré les performances de séparation en termes de rendement de purification et de la capacité d'adsorption.

Abstract

Selective adsorption of free glycerol from crude biodiesel was investigated by using mesoporous silica spheres coated with a thin shell of microporous silicalite-1. A polycrystalline silicalite-1 shell was formed upon first covering the external surfaces of various core templates with discrete silicalite-1 nanocrystals, and this was followed by short hydrothermal treatment to ensure shell uniformity. Batch glycerol adsorption experiments were conducted to evaluate the ability of the sorbents to remove free glycerol selectively from crude biodiesel mixtures at various temperatures, also in comparison to that of conventional sorbents, for example, bare mesoporous silica gel spheres and zeolites. The silicalite-1 shell provided a microporous membrane that hindered the diffusion of fatty acid methyl esters into the mesopores of the composite sorbent, whereas the large pore volume of the mesoporous core enabled multilayer glycerol adsorption; this ultimately substantially enhanced the performance in terms of purification yield and adsorption capacity.

Keywords: Adsorption, Biodiesel, Core@shell, Free glycerol, Zeolite

4.1 Introduction

Composite materials in a core@shell structure with inherent properties, for example, hierarchical porosity and diverse integrated functionalities, have recently attracted extensive research attention in many areas including adsorption and catalysis [1, 2]. A typical core@shell consists of two different materials in such a way that one, the shell, entirely encompasses the inner compartment, the core (Scheme 4.1). Among all types of possible building materials for such composites, crystalline zeolites seem ideal for forming the shell of a core@shell sphere owing to their high thermal/hydrothermal stability, excellent resistance under corrosive conditions, highly ordered pore structure, large specific surface area and micropore volume, shape-selectivity and intrinsic chemical activity. Over the past fifteen years, a variety of core materials, such as polymers [3-8], amorphous silica [9-12], metal oxides [13, 14] and even different types of zeolites [13, 15-19] have been used to synthesize either core@shell or hollow materials with a zeolitic shell. These materials are mostly synthesized by applying a well-known strategy, the so-called layer-by-layer technique [20], to cover the pre-synthesized solid core templates with desirable nanocrystals, which later grow through a hydrothermal treatment in a gel containing essential nutrients to strengthen the zeolitic shell and to ensure the uniform coverage [3].

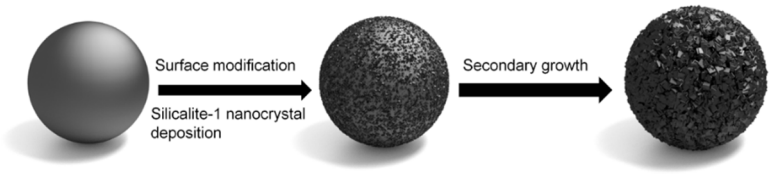

Scheme 4.1- Schematic representation of the mesoporous silica@silicalite-1 synthesis

Application of zeolitic core@shell materials began with the pioneering work of Bouizi *et al.*, [18] who illustrated the superior performance of the β-zeolite@silicalite-1 material in selective adsorption from a hydrocarbon mixture, containing butane, toluene, and 1,3,5-trimethylbezene. In contrast to smaller hydrocarbons, bulkier 1,3,5-trimethylbenze molecules are inhibited from reaching the large pores of the β-zeolite core since the silicalite-1 shell presents a smaller pore size than their kinetic diameters. Since then, core@shell materials with a zeolitic shell have been used in different applications, primarily in the field of catalysis [21-26]. The zeolitic shell provides an effective protective layer under harsh

operating conditions of the reactions as well as a selective barrier against impurities, poisons and undesirable reactions, and this enhances the catalyst activity, selectivity, and durability. The beneficial aspects of utilizing zeolitic core@shell materials in gas-phase adsorptive separation processes are also emphasized in a number of publications [27-29]. However, the performance of zeolitic core@shell materials still needs to be explored in other important liquid phase separation processes such as biodiesel purification, which involves considerable size difference between the impurities and the product molecules. Such a process is crucial for further development of sustainable chemicals and fuels.

Biodiesel, which usually refers to fatty acid methyl esters (FAMEs), is a renewable and environmentally friendly source of fuel for diesel engines. It is frequently produced on an industrial scale by the alkali-catalyzed transesterification of triglycerides from vegetable oil and animal fats with methanol. After the reaction, crude biodiesel is separated from the polar byproduct, mainly glycerol, by either centrifugation or a gravity settling process. Crude biodiesel can be neutralized at this step by adding a mineral acid to eliminate the soap from crude biodiesel. The methanol remaining in crude biodiesel which increases the solubility of glycerol, may be removed by vacuum/flash evaporation. After all these steps, crude biodiesel still contains different types of contaminants including unconverted triglycerides (TGs), diglycerides (DGs), monoglycerides (MGs), free fatty acids (FFAs), glycerol, water, catalyst, soaps, salts and others, which should be totally or partially removed. Among them, the removal of free glycerol is of a great importance for its negative effects on biodiesel storage and usage such as settling problems, fuel tank bottom deposits, injector fouling, engine durability issues and higher emission of aldehydes and acrolein. The maximum allowable concentration of free glycerol, established by ASTM D6751 and EN 14214, is 0.02 wt% in a pure finished product [30]. Traditionally, glycerol is removed through extraction with water. Despite many advantages of the water washing process, it creates a number of problems, mostly as a result of the need for large amounts of deionized water, wastewater management, biodiesel drying, significant product loss, time-consuming process, emulsion formation and corrosion [31].

There is an alternative water-free adsorption-based process for biodiesel purification known as dry washing, which is more ecofriendly and cost-effective than the traditional water washing process. Dry washing eliminates contaminants by keeping the crude biodiesel in contact with an adsorbent or an ion-exchange resin. Numerous different adsorbent materials have been previously studied for treating crude biodiesel. Relevant considerations,

similarities, and pros and cons found for all existing adsorbents are discussed in detail elsewhere [31, 32]. Among the available adsorbents, hydrophilic ones such as silica and magnesium silicate are most actively investigated for the refining of biodiesel owing to the fact that the biodiesel impurities are mostly polar compounds. Having high saturation capacity for glycerol and other polar impurities, silica gel particles are predominantly used for biodiesel purification either in a batch adsorber [33,34] or in a fixed bed [35]. Although faster diffusion of glycerol within the large pores of silica gel (pore sizes larger than 6 nm) can potentially achieve significant glycerol removal in an adsorptive separation process, it was shown that using such an adsorbent leads to a perceptible reduction in purification yields [36-38]. A part of the esters is lost during the course of purification with almost all traditional adsorbents owing to capturing of FAMEs along with unwanted impurities, which decreases the final yield [39]. This reduction becomes more significant upon applying larger doses of adsorbent.

One solution is to use adsorbents with smaller pores, for example, microporous zeolites, which, for instance, are successfully used to enhance the quality and durability of lubricant oils [40, 41]. The separation power of a zeolite strongly depends on micropore characteristics. In general, high selectivity is achieved if the pore size is comparable to the kinetic diameters of the molecules to be separated. Despite this appealing feature of zeolites, several important issues continue to limit the application of such materials as adsorbents in biodiesel purification systems. The smaller pore size is often coupled with lower adsorption capacity because of the relatively low pore volume. Moreover, intracrystalline transport limitation is another disadvantage, which imposes serious problems to process productivity, even in large pore zeolites [29].

With these considerations in mind, it was hypothesized that a novel class of composite materials, namely, core@shell architectures, consisting of high surface area, high pore volume mesoporous silica spheres covered with a shape-selective zeolite, may hold considerable promise in biodiesel purification applications with regard to selective glycerol removal in high purification yield. Therefore, the present contribution reports the synthesis of mesoporous silica@zeolite by deposition of silicalite-1 nanocrystals over mesoporous silica spheres with various particle and pore sizes followed by a secondary hydrothermal treatment step. The performance of the synthesized sorbents was evaluated under different operating conditions by conducting free glycerol removal tests from crude biodiesel.

4.2 Experimental Section

4.2.1 Preparation of Biodiesel

The biodiesel was prepared by using the procedure presented by Alves *et al.* [42] through an alkali-catalyzed transesterification reaction, by using commercial refined corn oil, purchased from a local store, and methanol (certified ACS reagent grade, Fisher Scientific) as reactants and potassium hydroxide (Sigma-Aldrich) as a catalyst. The transesterification reaction was performed in a 500 ml round-bottom flask fitted with a reflux condenser to prevent methanol loss and a magnetic stirrer to keep the mixture under constant agitation. The flask was placed in an oil bath to control the reaction temperature at 65 °C. The corn oil was preheated prior to adding the catalyst KOH pellet and methanol. The catalyst was previously dissolved into methanol until complete dissolution. This solution was also preheated at 50 °C. The oil to methanol molar ratio was (1:6), the reaction time was 1 h and the amount of catalyst in relation to the oil mass was 0.75 wt%. This mixture was then placed in a sealed separatory funnel and allowed to settle for at least 24 h, and the bottom glycerol-rich layer was removed. The produced biodiesel was used as methanol-containing crude biodiesel for adsorption tests. For methanol-free tests, the methanol was completely evaporated under 50 mmHg vacuum at 60 °C for 15 min. A simple weighing method was used to determine the methanol content of the methanol-containing crude biodiesel by recording the weights of the given amounts of crude biodiesel prior to and after evaporation. The sample weights remained constant after 15 min of evaporation under vacuum at 60 °C.

4.2.2 Synthesis of the Core@Shell Adsorbents

The core@shell adsorbents were synthesized by adopting the reported seeded growth method [18, 29]. After preparing the suspension of discrete silicalite-1 nanocrystals and mesoporous silica spheres, a multistep coating technique was used to produce nanozeolite coated cores, followed by a hydrothermal treatment to translate these coated cores into core@shell with a stable and uniform zeolitic shell (Scheme 4.1).

4.2.2.1 Preparation of Silicalite-1 Nanocrystals

The silicalite-1 nanocrystals were synthesized according to a modified procedure reported by Schoeman *et al.* [43]. For a typical synthesis of silicalite-1 nanocrystals with a size of approximately 70 nm, tetraethyl orthosilicate (TEOS) (20 g, reagent grade, 98%-Sigma-Aldrich), as silica source, was added into a tetrapropylammonium hydroxide (TPAOH) solution (40 g, 1M in H_2O-Sigma-Aldrich) with continuous stirring. By adding a certain amount of water, the molar composition of the synthesis mixture was adjusted to $TPAOH/SiO_2/H_2O/C_2H_5OH$= 9:25:480:100. After prehydrolysis by stirring at room temperature for 12 h, the clear gel was hydrothermally treated in a tightly closed propylene bottle at 80 °C for 72 h until the solution turned slightly turbid. After cooling, the obtained nanocrystals were thoroughly washed with water and recovered by using high speed centrifugation. After a series of centrifugation and resuspension in water, the nanocrystals were finally redispersed in distilled water to produce a 0.5 wt% suspension. The pH of the suspension was adjusted to 9–10 with ammonia solution, as suggested by Valtchev and Mintova [16].

4.2.2.2 Preparation of Core Materials

Mesoporous silica spheres in three different sizes (Hexagonal Mesoporous Silica (HMS) spheres: 1.5 μm and commercial silica gel spheres: 3 & 20-45 μm) were used as core materials. Monodispersed HMS spheres were synthesized according to the literature [8, 44]. In a typical procedure, hexadecylamine (2.08g, technical grade, 90%-Sigma-Aldrich) as mesoporogen, distilled water (180 ml) and 2-propanol (200 ml, fisher scientific) as solvents, and NH_3-H_2O (3.2 ml, 28%) as base catalyst were mixed together until a homogeneous solution was formed. TEOS (12 ml), as silica source, was added and the final mixture was stirred for another 1 min before it was aged overnight at room temperature. The product was recovered by filtration and washing with water. To remove organic templates from the pores, the as-synthesized material was heated in air at 550 °C for 6 h. Commercial silica gel spheres with two different particle sizes (SG20: 20-45 μm and SG3: 3 μm) were purchased from SiliCycle Inc., and were used as received without further treatment.

4.2.2.3 Preparation of Core@Shell Products

Mesoporous silica spheres (~ 0.2 g) were dispersed in distilled water (5 ml), and their negative surface charge was reversed by treatment with a 0.5 wt.% aqueous solution of cationic low molecular weight poly(diallyldimethylammonium chloride) (PDADMAC) solution (5 ml, 20 wt% in H_2O-Sigma-Aldrich) under 20 min of stirring. Afterward, the negatively charged silicalite-1 nanocrystals suspension (5 ml) was added to be adsorbed on the surface of the cores through electrostatic interactions. The excess amount of nanocrystals was washed away by performing several cycles of centrifugation and redispersion of the coated particles by using a dilute NH_3-H_2O solution (pH 9.5). This intermediate product was dried in an oven at 80 °C overnight and was then calcined in air at 550 °C for 5 h, to ensure firm adherence of the nanocrystals on the surface of the core material. The clear gel for the secondary growth step was prepared according to Bouizi *et al.* [18] with the molar composition of TPAOH/SiO_2/H_2O/C_2H_5OH= 3:25:1500:100. The coated core particles were dispersed in clear gel (10 g) by stirring at room temperature for 15 min, followed by hydrothermal treatment at 200 °C for 45 min in a Parr Teflon-lined autoclave to grow the silicalite-1 nanocrystals adsorbed on the core surfaces. After cooling the autoclave down to ambient temperature and washing the product for four times with distilled water, the secondary growth step was repeated one more time to reach a desirable shell coverage and uniformity. After cooling, the product was treated with a dilute NH_3-H_2O solution (pH 9.5) by using an ultrasonic bath for 10 min to remove the loosely attached silicalite-1 crystals, rinsed repeatedly with distilled water and dried at 100 °C overnight. The as-synthesized material was calcined at 550 °C for 6 h in air after reaching this temperature at a rate of 1 °C min^{-1} to remove the TPA^+ template from the zeolite pores.

To compare the performance of the final material in biodiesel purification, different types of conventional zeolites were also prepared including large microcrystals of pure silica β-zeolite (Si-BEA) by using the fluoride route [18], and Al-ZSM-5(H) microcrystals and submicron silicalite-1 crystals, both synthesized according to reported synthesis routes [45].

4.2.3 Material Characterization

All products, that is, core materials, nanocrystals, zeolites, and core@shell materials, were characterized by using typical characterization techniques. Powder X-ray diffraction patterns of all samples were recorded by using a Siemens powder diffractometer (40kV, 40mA) with CuK_α radiation (λ= 1.54059 Å). The transmission electron microscopy (TEM) images were recorded by using a JEOL JEM 1230 electron microscope after dispersing samples in methanol and depositing on carbon-coated nickel grids. Scanning electron microscopy (SEM) studies were performed by using a JEOL JSM-840A scanning electron microscope. To prepare the sample, a small quantity of the powder sample was placed onto the SEM sample holder and then coated two times with gold and palladium. Simultaneous thermogravimetric analysis and differential scanning calorimetry (TGA–DSC) measurements were performed by using a Netzsch STA 449C thermogravimetric analyzer. Nitrogen adsorption/desorption isotherms were measured at liquid nitrogen temperature (-196 °C), by using a Quantachrome Autosorb-1 adsorption analyzer. Prior to the measurements, the samples were evacuated at 200 °C for at least 12h, under vacuum, provided by a turbomolecular pump. The linear part of the Brunauer–Emmett–Teller (BET) equation was used to calculate the specific surface area from the adsorption data obtained, which mainly occurred at P/P_0 between 0.05 and 0.2. The total pore volume of the micropores and mesopores was estimated from the amount of nitrogen adsorbed at P/P_0= 0.95. For advanced porosity analysis, cumulative pore volumes and pore size distributions were determined by using the nonlocal density functional theory (NLDFT) method by applying the NLDFT metastable adsorption branch kernel and considering sorption of nitrogen at -196 °C in silica as a model adsorbent and cylindrical pores as a pore model. Micropore volumes of the zeolites and core@shell materials, as well as their pore size distributions, were determined by using NLDFT methods. The Quantachrome Autosorb-1 1.55 software was used for data interpretation.

4.2.4 Glycerol Adsorption Test

Crude biodiesel (with and without methanol) was purified by using different types of adsorbents, that is, mesoporous silica spheres, zeolites and core@shell particles. Prior to use, all adsorbents were dried at 150 °C in a vacuum oven overnight to eliminate free

moisture. The dry adsorbent (~ 20-30 mg) was introduced into a 5 ml glass vial containing crude biodiesel (1g) with a given initial glycerol concentration (w_0), that is, w_0= 0.065 wt% for methanol-free biodiesel and w_0= 0.22 wt% for methanol-containing biodiesel. The average methanol content of the methanol-containing biodiesel samples was measured as 0.7 wt% right before performing the adsorption tests. Freshly prepared biodiesels were used in all tests, as the glycerol concentration was found to change over time if stored owing to gradual evaporation of methanol. Samples were equilibrated for 12 h at 25 °C in an incubator while being stirred with a magnetic stirrer. Studying the temperature effect on the adsorption, all experiments were repeated at 100 °C in an oil bath. Upon equilibration, the adsorbents were separated from the purified biodiesel by sedimentation/centrifugation. Glycerol concentrations in the purified supernatant were measured after equilibration by GC-FID (FID: flame ionization detector) to quantitatively determine the initial and equilibrium concentrations in biodiesel and were used to calculate the equilibrium adsorption capacity (q_e) of dry adsorbent by using the material balance equation (Equation (1)).

$$q_e = \frac{(w_0 - w_e) \times m_{biodiesel}}{m_{adsorbent}} \times \frac{1}{100} \quad (1)$$

in which q_e is the amount of glycerol adsorbed by the adsorbent (g/g), w_0 is the initial mass percent of glycerol (g/g), w_e is the mass percent of glycerol at equilibrium (g/g), $m_{biodiesel}$ is the initial mass of biodiesel (g), and $m_{adsorbent}$ is the mass of dry adsorbent (g).

To determine the uptake of bulkier molecules, such as FAMEs, by the adsorbents, thermogravimetric experiments were performed on the used adsorbents. In a typical procedure, following the recovery of adsorbent after adsorption, the used adsorbents were quickly washed with hexane to remove the bulk molecules, and then the volatile compounds were evaporated at 35 °C for 24 h. The dried adsorbent (~ 2 mg) was placed in an alumina crucible (with no lid) of a TGA-DSC instrument and heated from 35 to 700 °C in air flow (20 ml min^{-1}) at a heating rate of 10 °C min^{-1}. The measured mass loss at high temperatures (150-550 °C) was considered as the mass of nonvolatile organic molecules that were trapped/adsorbed inside the pores of the adsorbents. The measured nonvolatile organic content was then translated into bulkier molecule uptake by the adsorbent upon subtracting the mass of adsorbed glycerol measured by GC-FID. The standard uncertainty for the uptake of glycerol and FAMEs was calculated/estimated by following the guideline provided in GUM (guide to the expression of uncertainty in measurement [46]). The corresponding

expanded uncertainties are presented with each data set by using a coverage factor *k*= *2*, which provides a level of confidence of approximately 95%.

4.2.5 Analytical Methods

Free glycerol in biodiesel was determined by using an off-line gas chromatograph, Thermo Scientific TRACE GC Ultra, equipped with a FID, automated by the TriPlus liquid autosampler. The analytical column was a nonpolar DB-5MS (30 m, 0.25 mm ID, 0.25 μm film) from Agilent technologies, Inc. Calibration was achieved by the use of 1 wt% 1,4-butanediol (Sigma-Aldrich) in pyridine (Alfa-Aesar, 99+%) as an internal standard for glycerol (ultrapure, MP Biochemicals). Transforming polar and high boiling glycerol and internal standard into more volatile silylated derivatives, they were derivatized by using the *N,O*-Bis(trimethylsilyl)trifluoroacetamide (BSTFA ≥99.0% , Fluka) derivatization reagent and pyridine as a solvent and silylation catalyst. Five calibration solutions were prepared containing glycerol and internal standard at concentrations specified in the ASTM D6584 method. The derivatization agent, BSTFA (200 μl), was added to each calibration solution in a vial. For each biodiesel sample, the homogenized sample was accurately weighed (100 mg ± 0.1 mg) in a vial; then, internal standard solution (80 μL) and BSTFA (200 μL) were added. All vials were sealed and shaken vigorously for 20 min and then aged at 60 °C for 20 min. Finally, all mixtures were dissolved in *n*-heptane (ACS grade, BDH). For analysis, an aliquot (1 μL) of the mixture was automatically injected into the GC instrument at an oven temperature of 60 °C. After an isothermal period of 1 min, the oven was heated to 230 °C at 15 °C min^{-1} and then to 300 °C at 50 °C min^{-1} (held for 5 min). Nitrogen was used as the carrier gas at a flow rate of 1 ml min^{-1}. The detector temperature was set to 350 °C. The amount of glycerol in each sample was calculated by using the calibration function derived from the glycerol calibration curve.

4.3 Results and Discussion

4.3.1 Synthesis and Characterization of the Sorbents

Microporous/mesoporous core@shell materials were synthesized by using a method similar to that described by Bouizi *et al.* for the preparation of β–zeolite@silicalite-1 composites [18]. Commercial silica gel spheres with two different sizes and HMS microspheres were used as core materials, and they were ultimately covered with a polycrystalline intergrown silicalite-1 shell (Scheme 4.1). The silicalite-1 shell could not be placed by simple one-pot hydrothermal crystallization, which is used to produce bulk crystals. Successful coverage was only possible through a multistep synthesis route involving preliminary adsorption of zeolite nanocrystals onto large core particles followed by growing these nanocrystals in an appropriate synthesis gel mixture. The chemical and hydrothermal stability of the core as well as the rapid growth of the nanocrystals were vital parameters toward the formation of the core@shell material [26, 47].

The particle size distribution and morphology of the silicalite-1 and mesoporous silica spheres were first studied by using transmission electron microscopy (TEM) and scanning electron microscopy (SEM) (Figure 4.1). Discrete silicalite-1 nanocrystals (Figure 4.1a) show a narrow crystal size distribution with a mean diameter of 70 nm and a polydispersity index of 0.025, as measured by zetasizer particle analysis (Figure S 4.1, 4.6 Supporting information). The synthesized HMS particles were quite uniform in size and shape with a mean diameter around 1.5 μm as confirmed by SEM observation (Figure 4.1b). Two commercial silica gel spheres, SG3 and SG20 (Silicycle Inc., Canada), showed wider particle size distributions than HMS, especially SG20 with a size range of 20 to 45 μm (Figure 4.1c,d). All mesoporous silica spheres provided a smooth external surface, as seen in Figure 4.1, which makes them an ideal core template for coating purposes.

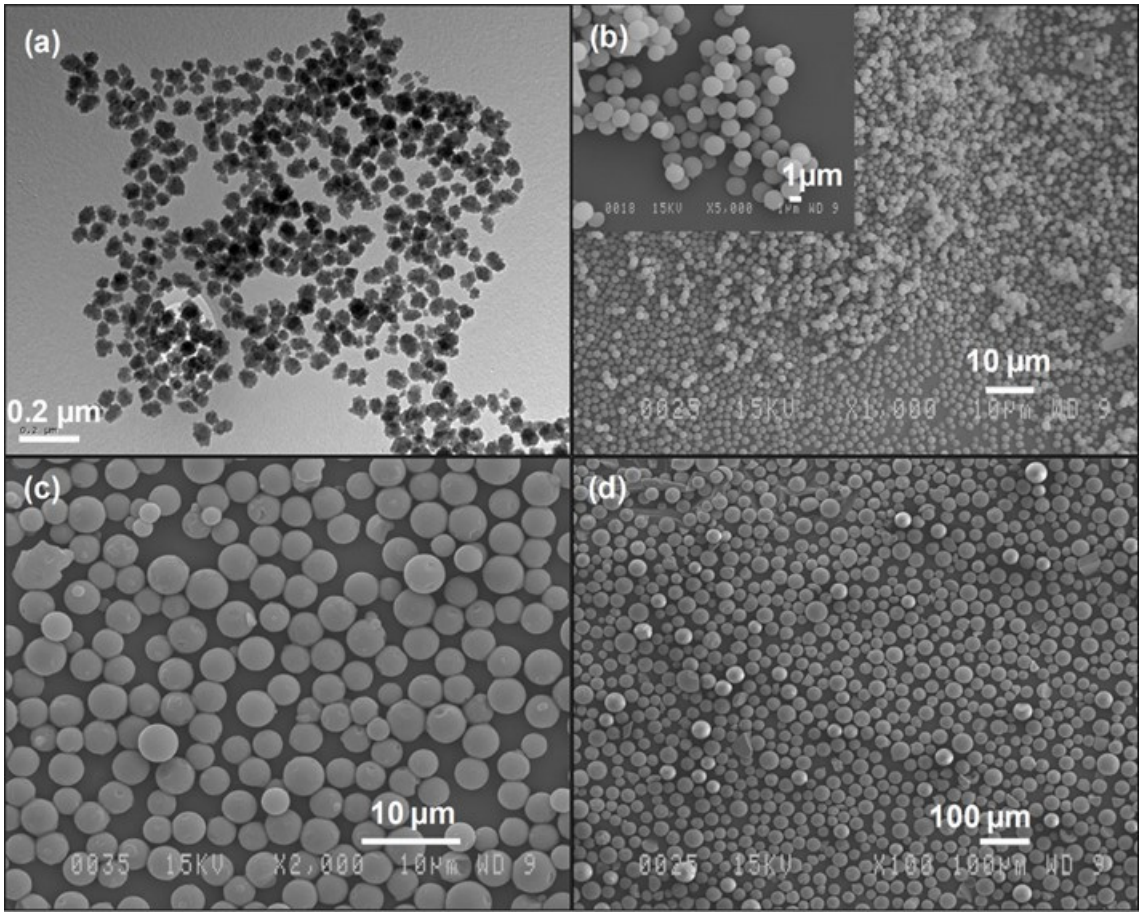

Figure 4.1- (a) TEM image of silicalite-1 nanocrystals (scale bar= 0.2 µm), and SEM images of (b) HMS microspheres (scale bar= 10 µm), (c) silica gel spheres 3 µm (SG3) (scale bar= 10 µm), and (d) silica gel spheres 20-45 µm (SG20) (scale bar= 100 µm). Inset shows a higher magnification image.

Figure 4.2 shows two different core particles after coating by a uniform and closed-packed layer of silicalite-1 nanocrystals. Following two successive hydrothermal treatments of 45 min each in TEOS/TPAOH containing gel, the shell, which is initially formed by deposited zeolite nanocrystals, became a continuous, intergrown compact layer without any visible cracks or defects on the outer surface.

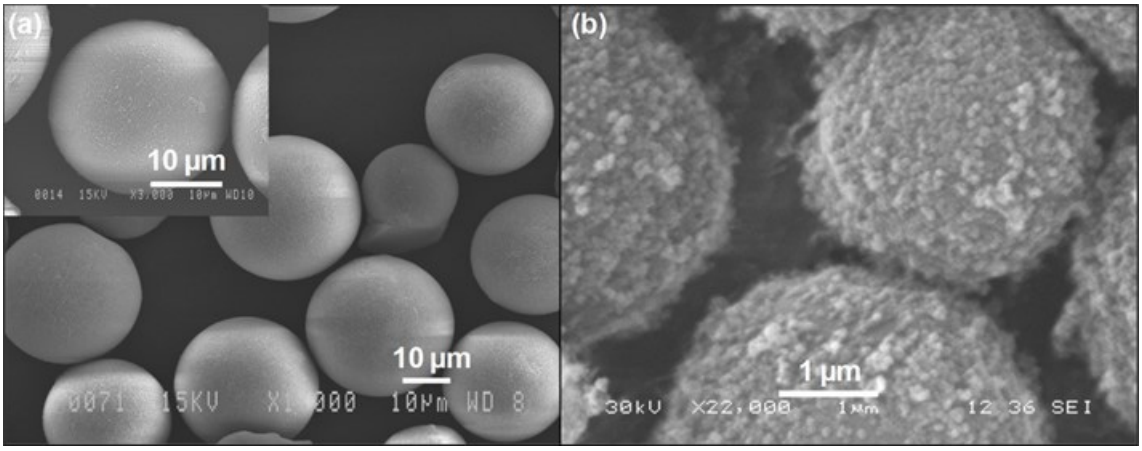

Figure 4.2- SEM images of covered (a) SG20 spheres (scale bar= 10 µm) and (b) SG3 spheres with silicalite-1 nanocrystals, by using layer-by-layer technique (scale bar= 1 µm). Inset shows corresponding higher magnification image.

Figure 4.3 shows the SEM images of core@shell particles with different core sizes. The top surface of a core@shell particle can clearly be seen from the higher magnified inset images. Subtracting the average size of the core@shell particles from the average size of the core particles, the average shell thickness could be estimated, as reported in Table 3.1, with the exception of SG20@silicalite-1 owing to the nonuniform particle size distribution of the parent particles (SG20).

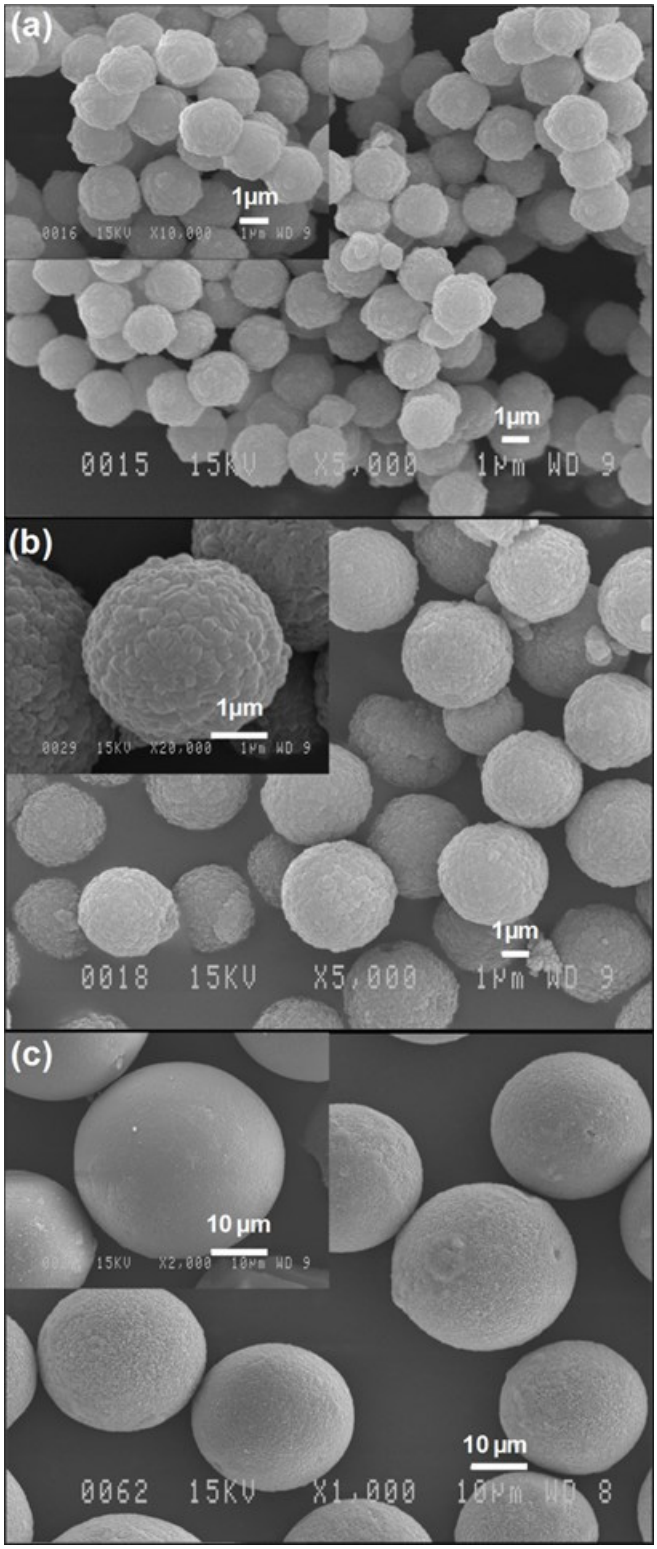

Figure 4.3- SEM images of (a) HMS@silicalite-1 (scale bar= 1 µm), (b) SG3@silicalite-1 (scale bar= 1 µm), and (c) SG20@silicalite-1 (scale bar= 10 µm). Inset shows corresponding higher magnification image.

Table 4.1- Textural properties of all the adsorbent materials obtained by performing N_2 physisorption analysis at -196 °C.

Sample	S_{BET}[a] [$m^2\ g^{-1}$]	Micropore surface area[b] [$m^2\ g^{-1}$]	Micropore volume[c] [$cm^3\ g^{-1}$]	Pore volume[d] [$cm^3\ g^{-1}$]	Maxima mesopore size[e] [nm]	Micropore size[f] [nm]	Shell thickness[g] [µm]	Shell coverage
HMS	780	----	----	0.63	3.3	----	----	----
Silica gel (3 µm)- SG3	453	----	----	0.7	6.2	----	----	----
Silica gel (20-45 µm)- SG20	326	----	----	0.79	8	----	----	----
HMS@silicalite-1- Non-calcined	8.9	----	0	0.017	----	----	----	----
HMS@silicalite-1- Calcined	430	335	0.13	0.26	3.7, 6	0.51x0.55, 0.53x0.56	0.4	99
SG3@silicalite-1- Non-calcined	11.5	----	0	0.027	----	----	----	----
SG3@silicalite-1- calcined	280	166	0.08	0.25	3.5, 7.2	0.51x0.55, 0.53x0.56	0.7	97
SG20@silicalite-1- Non-calcined	3	----	0	0.006	----	----	----	----
SG20@silicalite-1- calcined	180	70	0.025	0.24	3.5, 7.4	0.51x0.55, 0.53x0.56	----	99
Si-β-zeolite (Si-BEA)	----	608	0.24	----	----	0.66x0.67, 0.56x0.56	----	----
Al-ZSM-5(H)	----	300	0.14	----	----	0.51x0.55, 0.53x0.56	----	----
Silicalite-1	484	378	0.15	0.55	16	0.51x0.55, 0.53x0.56	----	----

[a] Calculated by using the BET method on relatively low-pressure region (P/P_0= 0.05–0.2). [b] Difference between S_{BET} and NLDFT cumulative surface area for pore sizes larger than 2 nm. [c] Calculated using NLDFT cumulative pore volume for pore sizes smaller than 2 nm. [d] Calculated at P/P_0= 0.95. [e] Derived from NLDFT pore size distribution in mesopore region (pore sizes larger than 2 nm). The two values correspond to the two maxima given by the pore size distribution curves. [f] Micropore sizes for pure zeolites and zeolitic part of the core@shell particles were derived from IZA website. [g] Estimated from SEM images.

Figure 4.4a shows the isotherms, obtained by nitrogen sorption measurements for the various materials: mesoporous silica gel-3 µm (SG3), mesoporous silica gel-3µm coated with silicalite-1 nanocrystals prior to and following the final calcination, and pure silicalite-1 submicron crystals. A large N_2 uptake and a hysteresis loop at high relative pressures (P/P_0 > 0.8) were observed for the silicalite-1 submicron crystals, which is related to adsorbate condensation in large mesopores (pore sizes ~ 16 nm) formed upon aggregation of small crystals during drying and calcination. The silica core showed a type IV nitrogen adsorption/desorption isotherm, characteristic of mesoporous solids, with an uptake in the relative pressure region of 0.6-0.8. Two successive secondary growth steps of the silicalite-1 nanocrystal layer, deposited on the external surface of the mesoporous silica spheres, led to a uniform shell of TPA^+-containing silicalite-1. This stuffed zeolitic layer efficiently restricts access of nitrogen molecules to the channels of the mesoporous silica core, as confirmed by a low N_2 uptake of the noncalcined core@shell material. The same behaviors were also observed for the bare HMS and SG20 core particles and the respective noncalcined core@shell materials (Figures S 0.8 and S 1.0, 4.6 Supporting information).

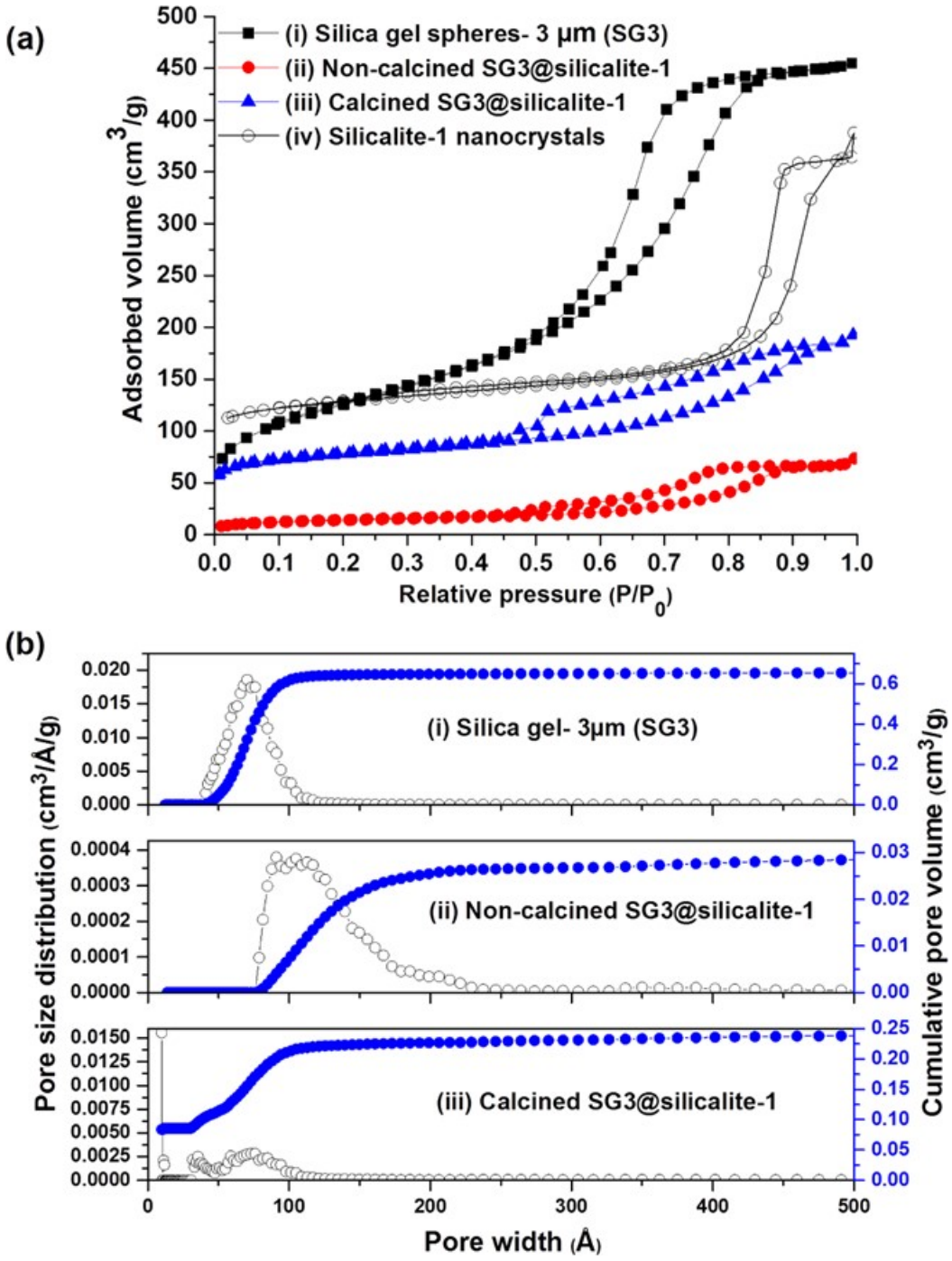

Figure 4.4- (a) Nitrogen adsorption/desorption isotherms measured at -196 °C of (i) silica gel-3µm, (ii) core@shell before calcination, (iii) core@shell with a calcined shell, and (iv) silicalite-1 submicron crystals; (b) The corresponding NLDFT pore size distributions and cumulative pore volumes of (i) silica gel-3 µm (SG3), (ii) noncalcined SG3@silicalite-1, and (iii) calcined SG3@silicalite-1, calculated from the adsorption branch of the isotherm by using the NLDFT method.

Wang *et al.* [25] showed that a reduction in N_2 uptake cannot be due to either the pore filling of the core, β-zeolite in their case, by organic TPAOH molecules used in secondary growth gel or the formation of silicalite-1 crystals as a separate phase in a mixture with the core. They obtained comparable surface area between an untreated calcined β-zeolite and a treated one under similar conditions as the secondary growth step, that is, by exposing to TPAOH-containing clear gel for a certain period of time, washing and drying. Considering this result and the fact that mesoporous silica gel (used as the core in the present study) exhibits much larger pore sizes (larger than 6 nm) than β-zeolite (around 0.65 nm), the filling of the core by organic TPAOH template molecules during secondary growth can be disregarded as a plausible cause for the observed reduction in N_2 uptake after the secondary growth step. Moreover, SEM imaging confirmed the absence of abundant silicalite-1 crystals in the bulk (Figure 4.3). All these results provide proof that the filled micropores of the shell have efficiently obstructed the path of N_2 gas toward accessing the internal porosity of noncalcined core@shell products. This phenomenon has also been used by other researchers as a way to probe the integrity of the silicalite-1 shell around a zeolitic core by calculating the ratio of surface area between the cores and the noncalcined core@shell samples [18, 19, 25, 29]. The obtained values of the BET surface area for the noncalcined sample correspond to the rough external surface of the core@shell material, as the internal pore network is not accessible. Using the same method revealed that 97% to 99% of the mesoporous silica cores are coated with a uniform silicalite-1 layer after at least two successive secondary growth steps (Table 4.1).

The presence of both micropores and mesopores along with the specific connectivity in pore networks may account for the intricate N_2 sorption behavior of the calcined sample (Figure 4.4a, see also Figures S 0.8 and S 1.0- 4.6 Supporting information). The isotherm of the core@shell material showed a noticeable reduction in nitrogen uptake at higher values of P/P_0 (capillary condensation region), relative to that of the mesoporous silica spheres, as the mesopore contribution in the final porosity was drastically decreased by the dense microporous silicalite-1 shell. However, capillary condensation can still be observed in the relative pressure region of 0.6-0.9, and it is accompanied by a complex hysteresis. This capillary condensation indicates the presence of mesopores, originating from the well-defined core mesoporosity and possible void spaces between the core and shell compartments. The hysteresis loop was built with a two-step desorption branch that shows the occurrence of normal equilibrium evaporation as well as a cavitation effect, which is clear

from a step down at relative pressures between 0.4 and 0.5 associated with hysteresis loop closure [48, 49].

The cumulative pore volumes and pore size distributions at different steps of the SG3@silicalite-1 synthesis are obtained by using the nonlocal density functional theory (NLDFT) method (N_2 sorption in cylindrical silica pores, adsorption branch) and are depicted in Figure 4.4b. The mesoporous silica gel spheres presented the largest pore volume and a narrow pore size distribution with a maximum centered between 6 and 7 nm. For noncalcined core@shell materials, the pore volume drastically decreased because the mesopores were blocked by the TPA^+-filled microporous silicalite-1 shell. However, negligible void spaces were observed which can be due to the presence of either a few uncoated silica particles or the intercrystalline spaces formed between intergrown silicalite-1 within the polycrystalline shell. Upon calcination, two different types of pores appeared in the pore size distribution contributing to the final pore volume; pores smaller than 2 nm corresponding to the microporous crystalline shell and pores larger than 2 nm which were primarily associated to the mesopore core compartment. Considering the limitation of nitrogen adsorption at -196 °C on quantitative evaluation of the microporosity, especially in the range of ultra-micropores of silicalite-1 (pore widths ~ 0.55 nm), more advanced analyses using argon as an adsorptive at -186 °C will be useful for further investigation of this system [48]. Regarding the second type of pores, that is, mesopores, a wide pore size distribution in the mesopore region was observed, and the two main peak maxima are centered at approximately around 4 nm and 7 nm. The second peak at approximately 7 nm originates from the silica gel particles as one of the main building blocks. The first peak, however, can be a feature associated with the complex pore network connectivity between the mesoporous core and microporous shell. In general, the N_2 sorption results did not fully comply with the observed mesoporosity of the parent silica particles owing to structural changes of the core during either the secondary growth or the high-temperature calcination step. Similar trends for pore size distributions of both HMS@silicalite-1 and SG20@silicalite-1 were observed, as illustrated in Figures S 0.9 and S 1.1 (4.6 Supporting information). The textural properties of the different calcined and noncalcined core@shell spheres along with the calcined mesoporous silica cores obtained by nitrogen physisorption measurements are summarized in Table 4.1. The average pore sizes of the adsorbents were derived from either N_2 sorption measurements for mesoporous materials including core@shell and silica

spheres or from tabulated data (IZA website) for microporous pure zeolitic or core@shell adsorbents [50].

The XRD patterns obtained for building materials, that is, silicalite-1 nanocrystals and HMS spheres, as well as the core@shell products before and after secondary growth steps are shown in Figure 4.5. The same patterns were recorded for other core@shell materials with silica gel-type cores and are reported in Figures S 1.2 and S 1.3 (4.6 Supporting information). Weak characteristic peaks of the silicalite-1 zeolite were observed in the XRD profile of the silica cores after depositing silicalite-1 nanocrystals (Figure 4.5b) owing to the small quantity and the size of the adsorbed nanocrystals. After hydrothermal treatment (Figure 4.5c), however, the more intense peaks of the MFI phase at 2θ= 7.5–9.58 and 23–24° emerged. Nevertheless, the preferred growth orientation could not be identified from the obtained pattern because of initial random packing of the silicalite-1 crystals over the mesoporous silica surface [47]. In addition, the peak of mesoporous silica was apparent at lower angles in the core@shell product, which confirms the silica cores were all encapsulated by zeolites, and that they survived under the harsh conditions of the secondary growth step [47]. This was also confirmed by nitrogen sorption measurements of the core@shell material. All these observations endorse the fact that the mesoporous silica@silicalite-1 structure was successfully synthesized.

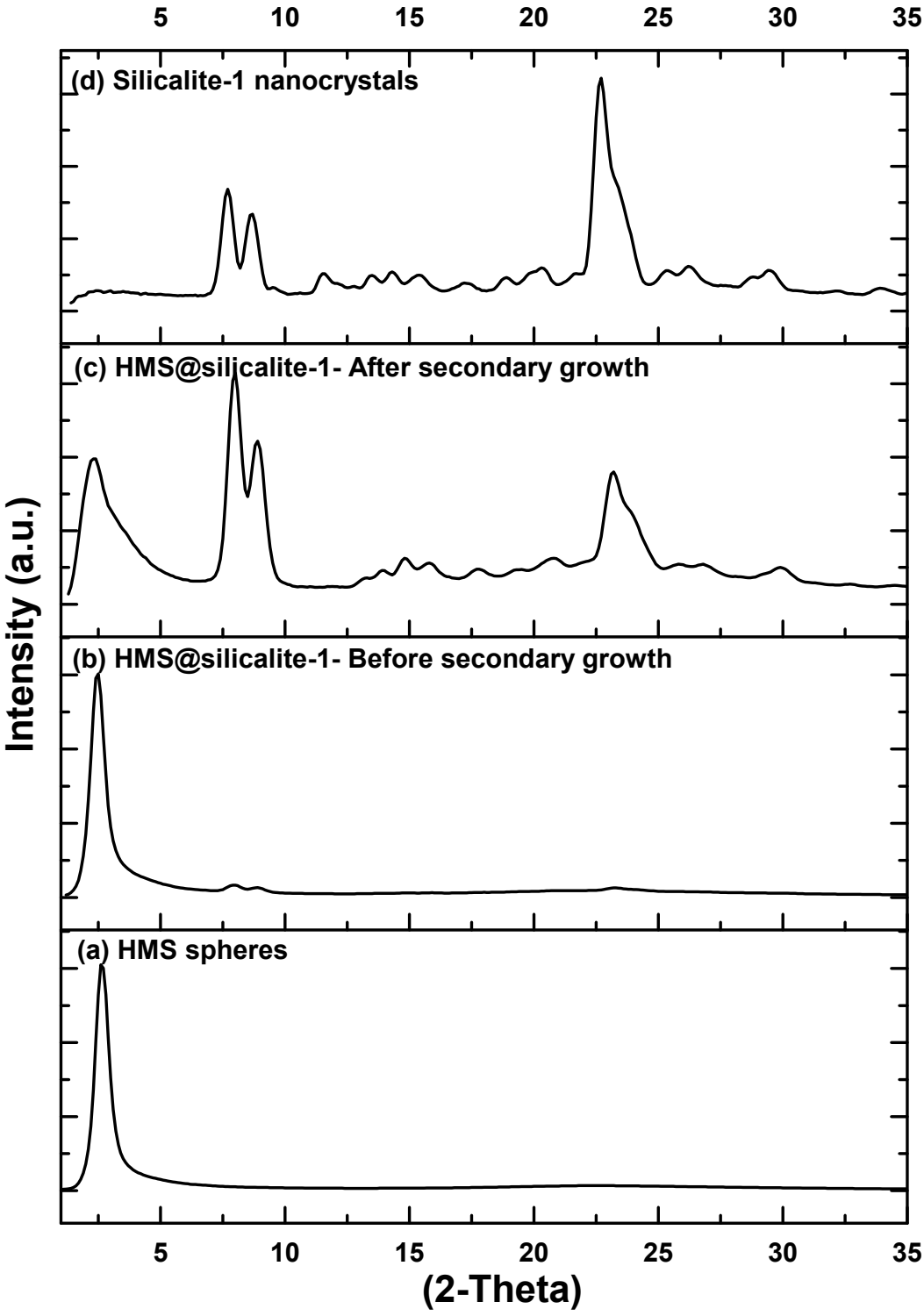

Figure 4.5- Wide-angle powder XRD patterns for (a) bare HMS, (b) coated HMS before hydrothermal treatment, (c) core@shell particles after secondary growth, and (d) silicallite-1 nanocrystals.

4.3.2 Purification of Crude Biodiesel

Table 4.1 summarizes the physical properties of all adsorbents used to remove free glycerol from crude biodiesel. These adsorbents can be categorized into three different classes of materials with regard to their pore structures:

1) Mesoporous silica with an average pore diameter of 3.5 nm for HMS spheres and larger than 6 nm for commercially-available silica gel particles, which are significantly larger than the molecular dimensions of FAMEs and glycerol. As none of these materials can provide shape selectivity for glycerol adsorption, the adsorption study with mesoporous adsorbents was performed by using the commercially available silica gel spheres.

2) Microporous zeolite crystals, that is, Si-β-zeolite (Si-BEA) and Al-ZSM-5(H) microcrystals, as shown in Figures S 0.6 and S 0.7 (4.6 Supporting information), respectively. This category provides pore sizes comparable to the dimensions of molecules present in biodiesel.

3) A core@shell material with large mesopores in the core and small micropores in the surrounding shell. The corresponding micropore entrances over the shell surface are capable of sieving molecules and allowing selective sorption from a mixture on the basis of their kinetic diameters.

To evaluate the glycerol removal ability of the adsorbents in the presence of different contaminants, crude biodiesels with two different compositions were used: first, a methanol-free biodiesel; second, a methanol-containing biodiesel (methanol content ~ 0.7 wt %). The equilibrium content of hydrophilic glycerol in biodiesel is a function of different parameters, such as temperature and other impurities, including residual methanol and amphiphilic mono- and diglycerides [34]. The free glycerol contents of methanol-free and methanol-containing biodiesels were approximately 0.065 and 0.22 wt%, respectively. The effect of temperature as one of the key parameters on biodiesel dry washing was also studied by performing the adsorption tests at 25 and 100 °C [51].

4.3.2.1 Glycerol Adsorption from Methanol-Free Biodiesel

Figure 4.6 compares the glycerol adsorption capacities at equilibrium for different adsorbents by using methanol-free biodiesel. The key role of the presence of mesopores on glycerol adsorption is clear from the glycerol uptake at equilibrium for silica gel and core@shell spheres; the one with the highest mesopore surface area, 3 μm silica gel spheres, shows the maximum glycerol adsorption capacity. In addition, the smaller silica gel spheres could probably provide better contact with the biodiesel constituents which facilitates their diffusion to reach adsorption sites within the particles. Conventional zeolites, Si-BEA and Al-ZSM-5(H) microcrystals, showed the lowest glycerol adsorption capacities with only minor differences, even though higher glycerol uptake by β-zeolite was expected because its micropore volume is higher than that of Al-ZSM-5(H). Surface chemistry provides a plausible explanation; it is known that the synthesis of zeolites by the fluoride route, for example, pure siliceous β-zeolite (Si-BEA) in this study, provides a well-defined crystalline structure with fewer framework defects (SiO^- or SiOH groups) on the surface [52]. As a consequence, the Si-BEA crystals exhibit higher hydrophobicity than the zeolite synthesized in a basic medium. In addition to the presence of more silanol groups on the surface, the synthesized ZSM-5 zeolite (Al-ZSM-5(H)) benefits from very strong acid sites owing to the presence of H^+ ions, which neutralize the surface negative charges caused by intraframework aluminum atoms. This situation provides better conditions for the adsorption of polar molecules, such as glycerol, on the surface through dipole-field interactions and hydrogen bonding. However, in contrast to mesoporous silica, the zeolite microcrystals in general suffer from a small micropore volume, a small external surface area, and a tiny pore mouth, all of which contribute to poor performance of conventional zeolites for this application. Another interesting feature of mesoporous adsorbents, such as silica gel particles, is related to the large internal pore spaces, which permit multilayer glycerol adsorption through hydrogen bonding on their silanol-rich surfaces.

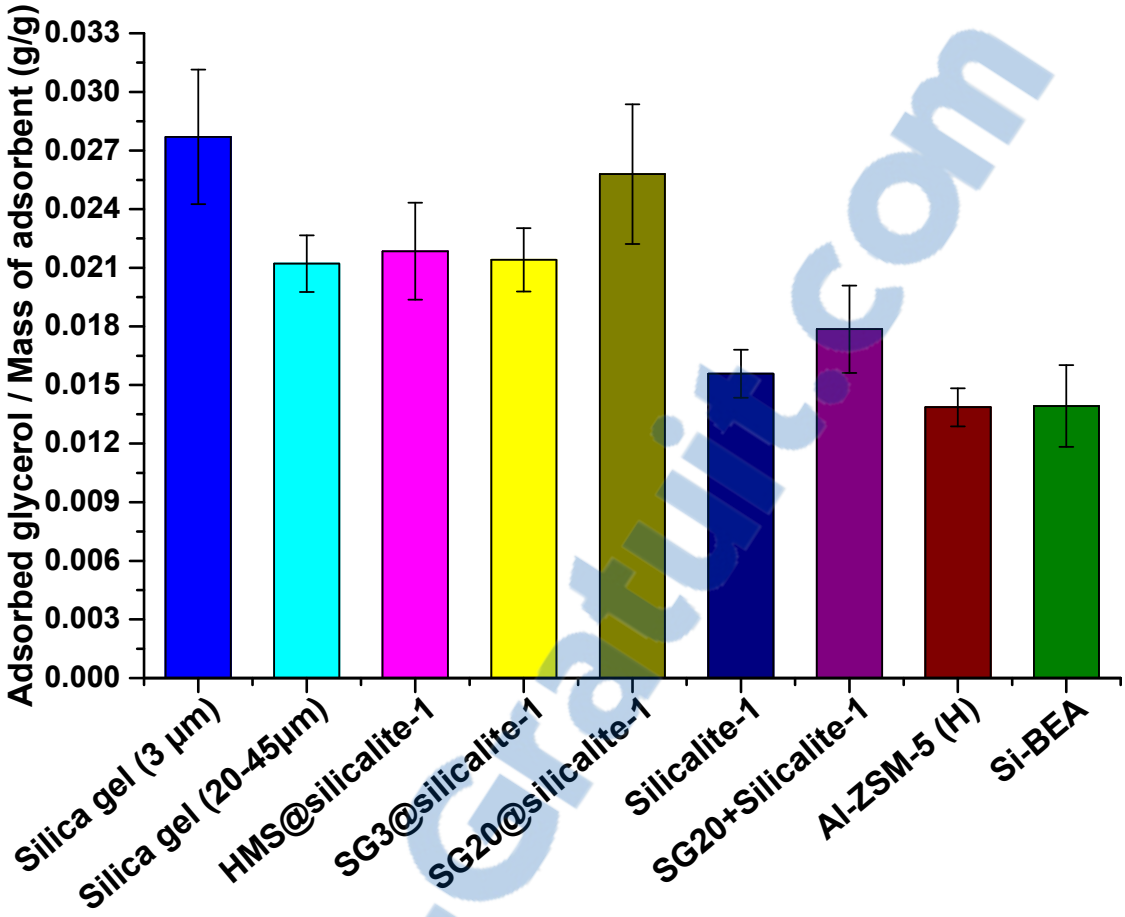

Figure 4.6- Specific adsorption loading of glycerol at equilibrium for different adsorbents by using methanol-free biodiesel at 25 °C (glycerol initial concentration in biodiesel = 0.065 wt%, adsorbent concentration= 2.3 wt%).

Covering 3 µm silica gel spheres with silicalite-1 caused a significant decrease in glycerol adsorption capacity. This could be a direct consequence of reduced mesoporosity of the core@shell materials. Therefore, the adsorption capacity may be partially restored by increasing the mesopore contribution to the total porosity of a core@shell material. One strategy is to use larger core particles. By doing so, SG20@silicalite-1 was tested, and it showed higher glycerol adsorption than other core@shell materials, and the value was even higher than that of large silica gel spheres. This can be attributed to a greater mesopore volume which is the highest among all synthesized core@shell materials. Given that the accessibility to mesopores in core@shell structures is effectively restricted by the silicalite-

1 shell, small molecules such as glycerol will diffuse faster than bulkier molecules (FAMEs, soap, MGs, DGs, and TGs) and fill the pores by multilayer adsorption. Notably, although the presence of overlapping error bars (with a 95% level of confidence), especially for SG20 and all core@shell samples, makes it difficult to presume the observed trend as statistically significant, the conclusion, that is, the larger cores improve the glycerol adsorption of core@shell materials, remains valid. Employing an equal-mixture of 20 μm silica gel spheres and silicalite-1 submicron crystals (~ 300 nm) as adsorbent resulted in no improvement in glycerol adsorption. The lower glycerol adsorption of this mixture relative to that of the core@shell adsorbents also proved that the silicalite-1 crystal shell plays a positive role as a shape-selective barrier and improves glycerol adsorption.

Total organic loadings, that is, accumulated organic molecules within the pores of each adsorbent upon termination of the purification process, were measured by running a TGA-DSC experiment over a temperature range of 35-700 °C. The TGA profiles are shown in Figure 4.7. At temperatures above 150 °C, a two-step mass loss was observed for most of the samples The first temperature-dependent mass loss with a slight slope occurred at a temperature below 300 °C, and this was attributed to vaporization of FAMEs from the outside of the pores (interparticle spaces/ external surfaces of the particles). The quite significant second mass-loss at temperatures higher than 300 °C was assigned to simultaneous volatilization/decomposition of high boiling point molecules including FAMEs, TGs, DGs, MGs, FFAs and free glycerol [53]. Even though selective adsorption of polar components should be dominant on silica surfaces, it is evidenced from Figure 4.7 that a large number of nonpolar/less polar materials enter inside the large void spaces provided by the mesopores of the bare mesoporous silica particles. On the other hand, complete displacement of air from within the pores with bulkier molecules, that is, pore intrusion, occurs alongside the adsorption of a trace amount of glycerol. FAME and FFA molecules can be adsorbed through hydrogen bonding to the surface oxygen atoms, mainly through carboxylate ions and ester carbonyl groups, respectively [54]. This phenomenon limits the effectiveness of large pore adsorbents by decreasing the glycerol adsorption capacity and the biodiesel purification yield. By subtracting the mass of adsorbed glycerol, obtained by GC-FID measurements, from the total organic loading of adsorbent obtained from the TGA experiment, the uptake of bulkier organic molecules from the biodiesel mixture can be calculated. Note that, it is assumed that quick washing with hexane right after adsorption removes all biodiesel components from the bulk without eluting adsorbed molecules within

the pores. The mass loss at temperatures higher than 150 °C was used for calculation, as the free-biodiesel molecules start to evaporate at temperatures higher than 150 °C, depending on the oil used for biodiesel production.

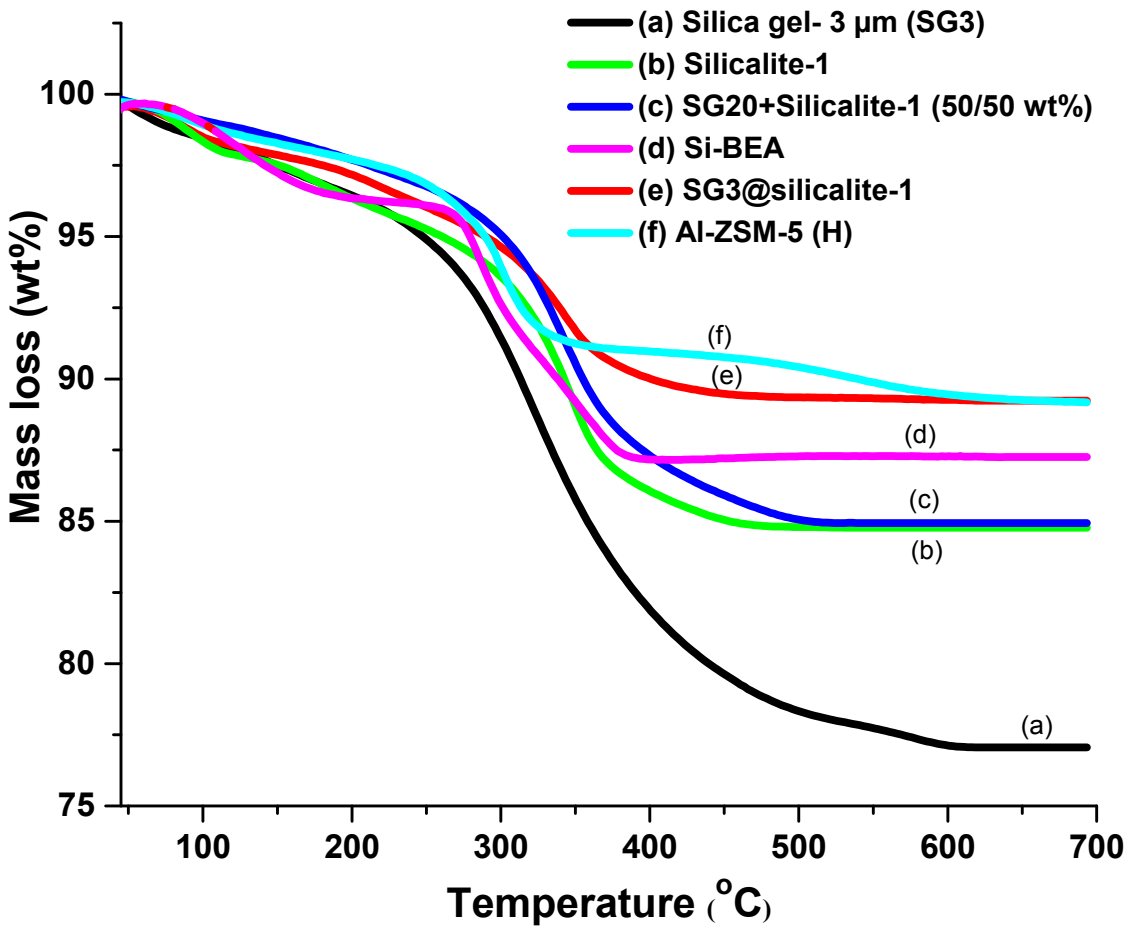

Figure 4.7- Overlay of thermogravimetric curves for the used adsorbents (glycerol initial concentration in biodiesel = 0.065 wt%, adsorbent concentration= 2.3 wt%).

The calculated uptake of FAMEs for different samples is presented in Figure 4.8. It can be seen that the silica gel particles have the highest specific loading of bulkier molecules. The fact that the cross-sectional diameters of the FAME and glycerol molecules (< 0.5 nm) are smaller than the average pore sizes of mesoporous silica spheres, listed in Table 4.1, justifies the observed behavior. Consequently, all molecules in the crude biodiesel mixture,

even the TGs, could diffuse through the extra-large pore size of the silica gel particles, and these adsorbents demonstrate no size exclusion effects, even if there is no tendency for nonpolar molecules to be adsorbed on the polar silica surface.

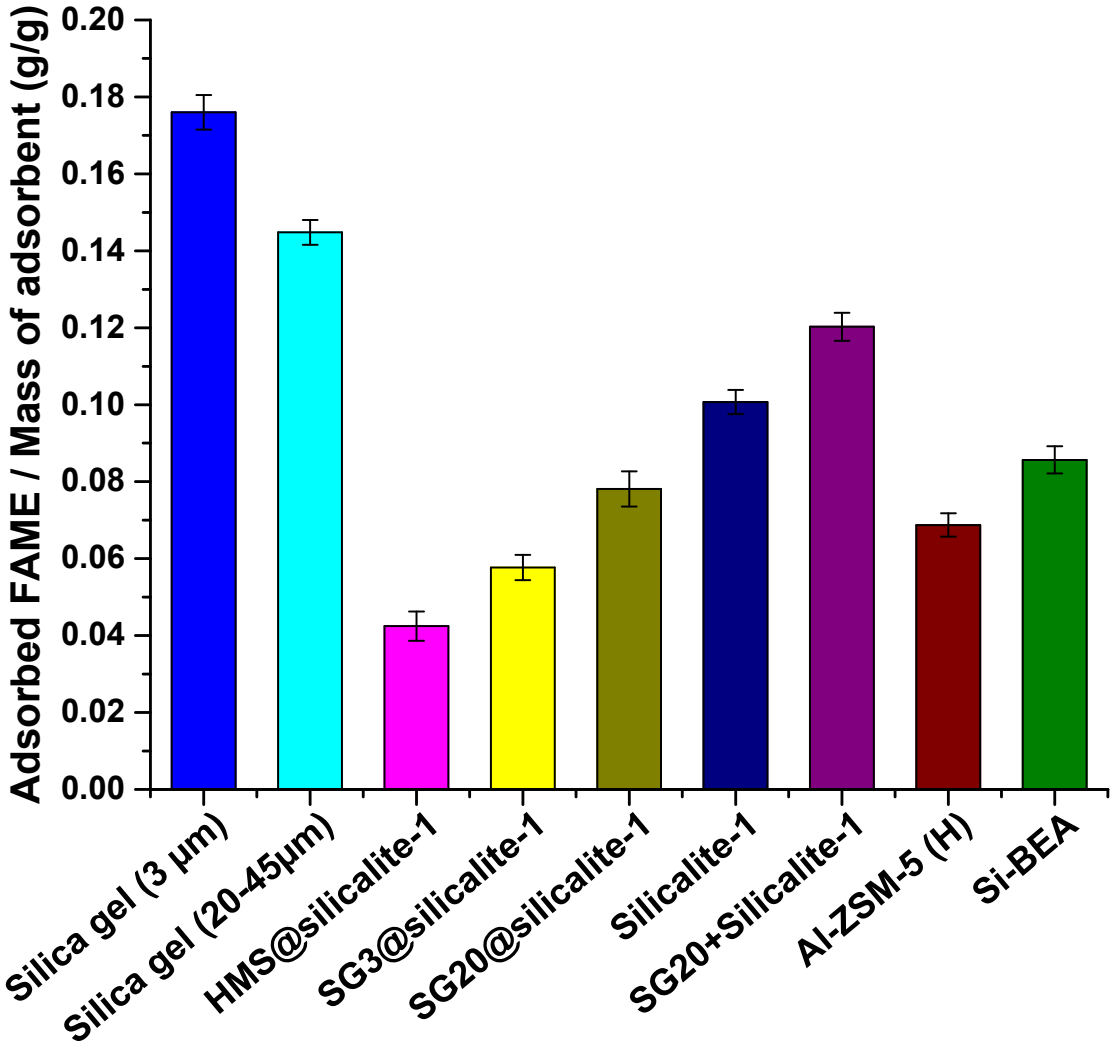

Figure 4.8- Specific uptake of FAME at equilibrium for different adsorbents using methanol-free biodiesel at 25 °C (glycerol initial concentration in biodiesel = 0.065 wt%, adsorbent concentration= 2.3 wt%).

Figure 4.8 also reveals that even conventional zeolites can accommodate large molecules such as FAMEs, possibly crawling inside. However, this would need a longer time to reach equilibration. Although FAME molecules have a very long aliphatic hydrocarbon chain, they

have a small cross-sectional molecular diameter. It was found that the effect of molecular diameter on hydrocarbon diffusion through a microporous zeolite is much more pronounced than that of the molecular length [55]. The possibility of diffusion of the FAMEs through the micropores of the zeolites is in line with a number of studies on various types of zeolites used as adsorbents for chromatographic separation of fatty acids and FAMEs from oil, or even the separation of mixtures of *cis* and *trans* geometrical isomers of mono- and polyunsaturated FAME [54, 56,57]. Looking for a zeolite that offers better sieving effect between bulky biodiesel molecules and glycerol, zeolites with MFI and BEA structures were tested. As can be seen in Figure 4.8, large pore zeolites, such as β zeolite, were not able to efficiently separate glycerol from esters of fatty acids, possibly because the pore size of these zeolites (6.5 Å) is large enough to retain the relatively large ester molecules, whereas the MFI type zeolite (5.5 Å), microcrystals Al-ZSM-5(H), was more suitable for the separation. The size of the crystals seems to have an important role as well. As can be seen in Figure 4.8, submicron silicalite-1 particles (300 nm), synthesized by secondary growth of free nanocrystals in the same gel as that used for core@shell growth, showed a very high loading of FAMEs, even higher than the loading of FAMEs on Si-BEA, which is due to the interstitial meso/macrospaces, created between aggregated small particles upon calcination. As confirmed by N_2 adsorption measurements, very large mesopores with a maximum centered at 16 nm were observed for silicalite-1 submicron crystals (Table 4.1). In contrast to this undesirable effect, silicalite-1 size reduction leads to shorter micropores and a higher external surface area, which results in a slight improvement in glycerol adsorption, as observed in Figure 4.6. The dual effect of crystal size can be exploited toward the designing of a more efficient glycerol adsorbent by simply avoiding meso/macrogaps between small particles, which is possible through secondary growth of nanocrystals while they are tightly packed on a support.

In addition to the core mesoporosity, core@silicalite-1 benefits from shorter micropores (shell thickness <1 μm as estimated by SEM imaging) without providing any interstitial spaces, susceptible to adsorption of bulkier molecules. As can be seen in Figure 4.8, the core@shell particles showed the lowest adsorption of bulkier molecules. Among the core@shell materials with different core sizes, HMS@silicalite-1 performed best with regard to the adsorption of FAMEs, owing to the microporous coverage of this material. However, the contribution of core mesoporosity to the total porosity of HMS@silicalite-1 was the lowest of the core@shell materials (Table 4.1). Notably, perceptible uptake of FAMEs still occurred

for all samples owing to the long equilibrium time of the adsorption tests. However, the uptake of FAMEs can be significantly reduced in the case of the core@shell materials, by considering the fact that glycerol enters the pores of silicalite-1 freely and moves from there to the core, but bulkier molecules, such as FAMEs, diffuse into the pores more slowly. Hence, finding an optimum contact time could significantly improve the efficiency of such core@shell materials in real practical applications.

4.3.2.2 Glycerol Adsorption from Methanol-Free Biodiesel at Elevated Temperatures

Normally, a decrease in adsorption is expected with an increase in temperature, however, in the case of biodiesel, as a multicomponent mixture of FAMEs, FFAs, TGs, DGs, MGs, and glycerol, a temperature rise will have a complicated effect. Working at higher temperature decreases the viscosity of the mixture, and thus, the diffusion rates of both glycerol and bulkier molecules into the pores of the adsorbents increase, especially for microporous materials. Figure 4.9 suggests that upon heating to 100 °C, the uptake of FAMEs in microporous silicalite-1 and the core@shell materials (equipped with a microporous shell) slightly increased, most likely because of better diffusion of bulkier molecules deep into the mesopores of the silica core. However, overlapping error bars indicate that the observed differences might not be statistically significant. The reverse behavior, a statistically significant decrease in the uptake of FAMEs, was observed for silica gel particles, which complies with the theoretical expectation.

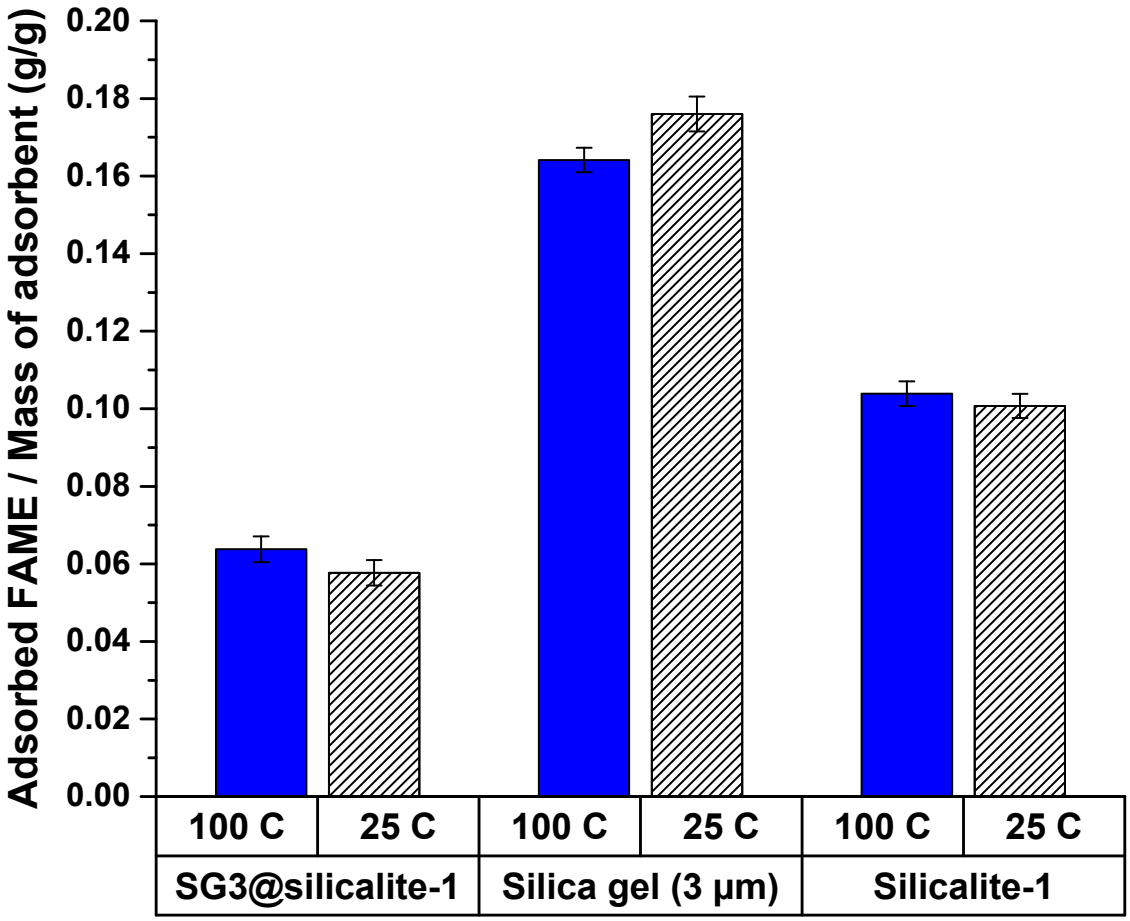

Figure 4.9- Uptake of FAMEs by different adsorbents from methanol-free biodiesel at different temperatures (glycerol initial concentration in biodiesel = 0.065 wt%, adsorbent concentration= 2.3 wt%).

Interestingly, as seen in Figure 4.10, glycerol adsorption at elevated temperatures followed the same trend as that of the uptake of FAMEs. Apparently, a temperature increase facilitates penetration of all the molecules, especially the smaller ones, and this occurs more significantly in microporous silicalite-1. This leads to desirable results for core@silicalite-1 materials by alleviating the diffusion limitations through the micropores, which thus allows multilayer adsorption inside the core compartment.

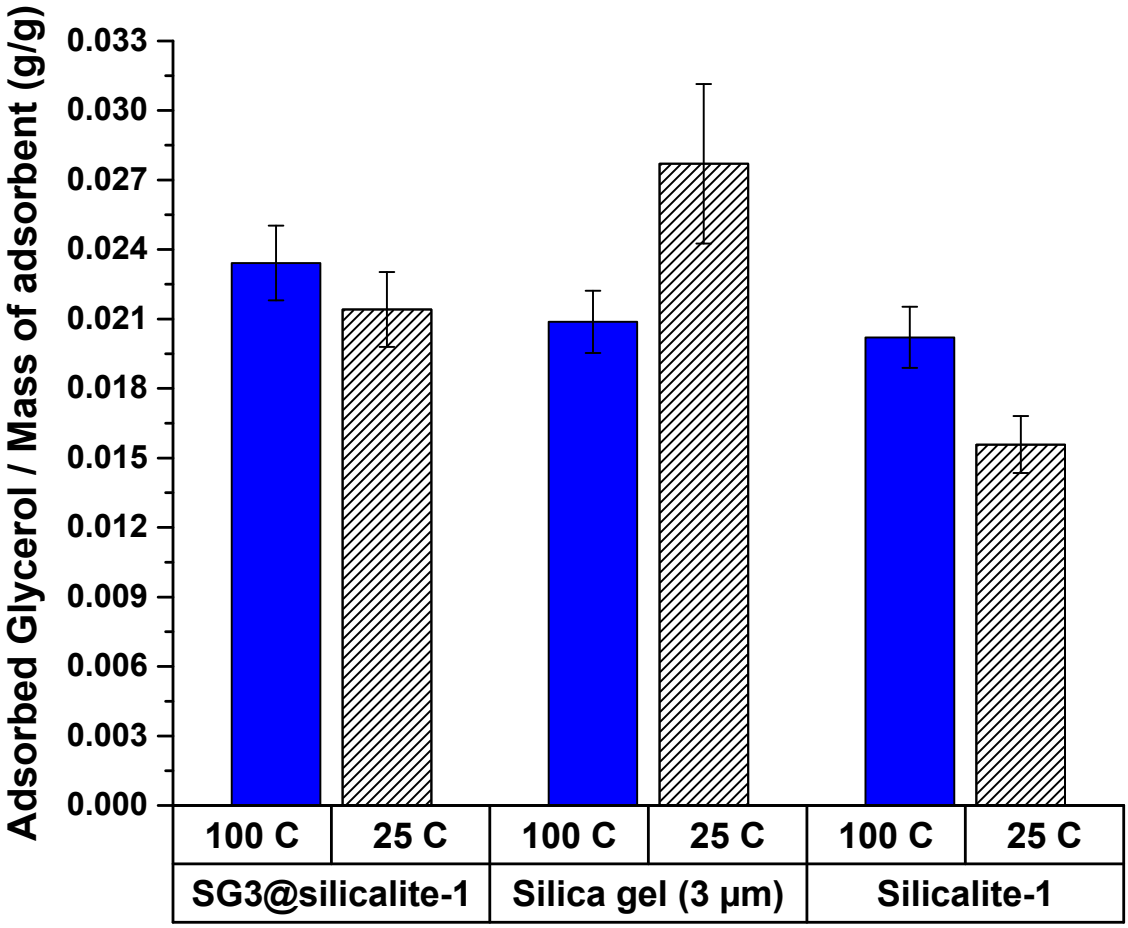

Figure 4.10- Adsorption of glycerol by different adsorbents from methanol-free biodiesel at different temperatures (glycerol initial concentration in biodiesel= 0.065 wt%, adsorbent concentration= 2.3 wt%).

4.3.2.3 Glycerol Adsorption from Methanol-Containing Biodiesel

According to the literature, methanol negatively affects the adsorption of glycerol on a silica surface because of the increased solubility of glycerol in FAMEs and because it has a higher affinity for the silica surface than glycerol [31, 34]. Although methanol has a negative effect on glycerol adsorption, it is economically and environmentally favorable to use adsorbents to purify biodiesel in its crude form right after glycerol separation by settling. Therefore, all adsorption tests were repeated for methanol-containing biodiesel, which was produced by leaving biodiesel for 24h at room temperature in a capped container after the transesterification reaction to remove the main part of glycerol byproduct by gravity

separation. Average methanol contents of 0.7 wt% were measured for the methanol-containing biodiesel samples prior to the adsorption test. Figure 4.11 shows the uptake of FAME and glycerol from a methanol-containing biodiesel for different adsorbents. The presence of methanol decreased the viscosity of the biodiesel mixture. This presumably made diffusion of the molecules easier; however, owing to a large intrinsic interaction of the inorganic adsorbents towards alcohols, the pore space was occupied by methanol and glycerol, present in much higher concentrations than in methanol-free biodiesel. Accordingly, the uptake of FAMEs dramatically decreased in all cases (compare with Figure 4.8).

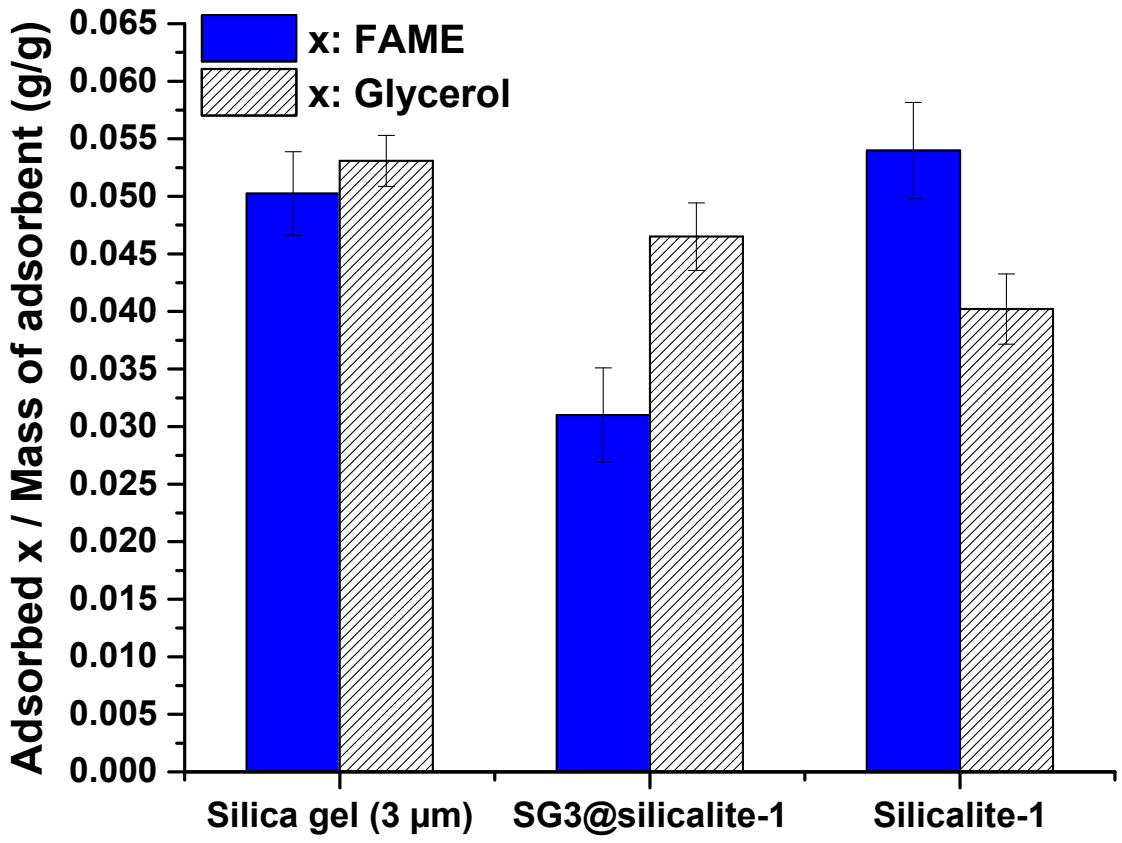

Figure 4.11- Adsorption of Glycerol and FAMEs by using different adsorbents from methanol-containing biodiesel at room temperature (glycerol initial concentration in biodiesel = 0.22 wt%, methanol content ~ 0.7 wt%, adsorbent concentration= 2.5 wt%).

Unfortunately, using all kinds of adsorbents with concentrations as high as 2.5 wt% could not decrease the glycerol content from approximately 0.22 wt% in crude biodiesel to the target ASTM limit (0.02 wt%). Under such conditions, higher adsorbent loadings or a multistep separation process should be applied to reach the standard level of free glycerol in the final product. Implementing either way could lead to a significant uptake of FAMEs by the adsorbents, especially in mesoporous silica particles. As shown above with methanol-free biodiesel purification, the loss in purification yield becomes more pronounced at lower glycerol concentrations, which would be reached in multistep purification processes.

4.3.2.4 Glycerol Adsorption from Methanol-Containing Biodiesel at Elevated Temperature

The purification tests were repeated at elevated temperature by using methanol-containing crude biodiesel, prompted by the clear improvement in glycerol adsorption by the core@shell material from methanol-free biodiesel. In contrast to purification at 25 °C, adsorption at 100 °C from methanol-containing biodiesel allowed glycerol levels well-below the standard limit (ASTM D6584) to be reached for both adsorbents (Figure 4.12). Manuale *et al.* [58, 59] also reported on the effect of increasing temperature on glycerol adsorption under vacuum. Figure 4.12 shows the significant increase in equilibrium glycerol loadings for both adsorbents, SG3 and SG3@silicalite-1 upon heating at 100 °C. To study the influence of temperature on glycerol content for a methanol-containing biodiesel, the sample was kept at 100 °C for 1 h without any adsorbents and this led to a significant reduction in glycerol concentration of the bulk from 0.22 wt% to approximately 0.07 wt%. This diminution can be attributed to the simultaneous evaporation of volatile components, such as methanol, which solubilized the main part of free glycerol in the mixture. In the presence of adsorbents, this precipitated glycerol comes into contact with the hydrophilic silica surface and is adsorbed readily. In contrast, at room temperature, this fraction of glycerol is less prone to be adsorbed on the surface owing to strong interactions between glycerol and methanol.

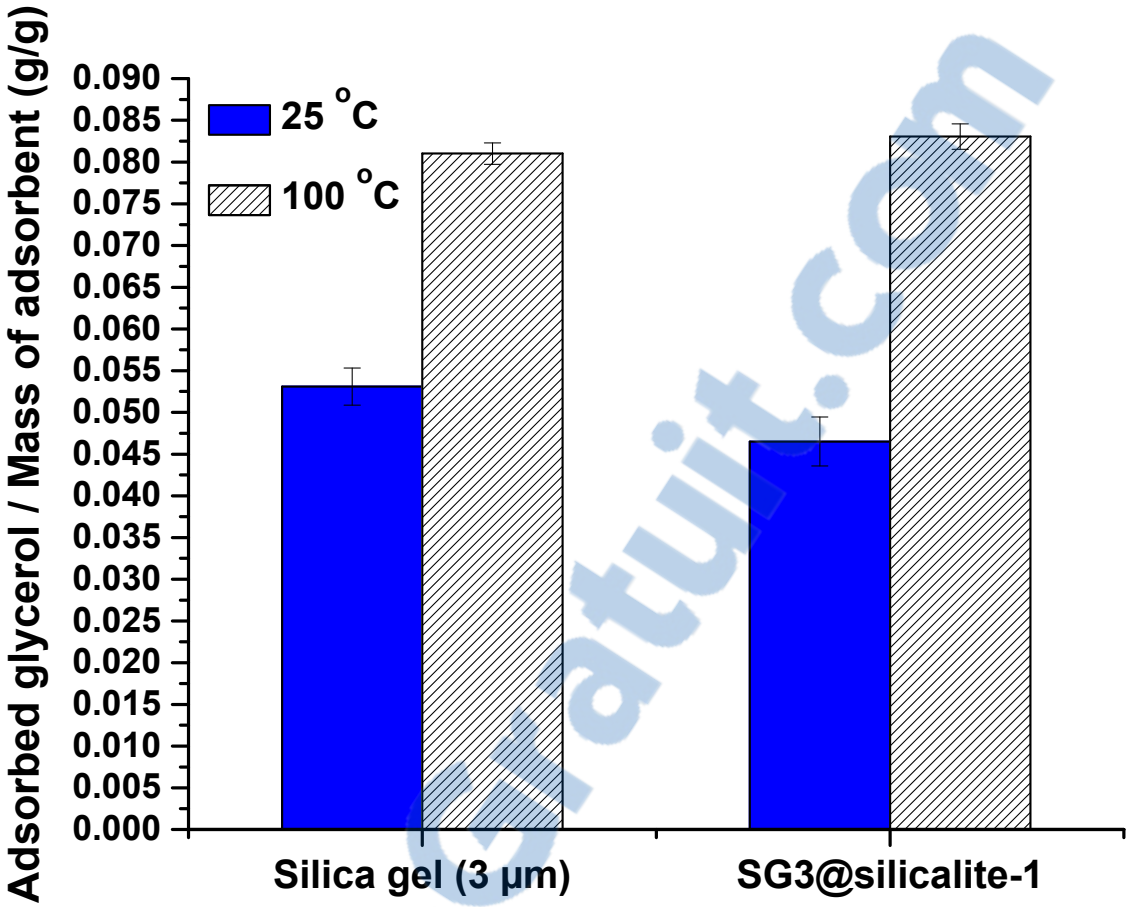

Figure 4.12- Adsorption of glycerol from methanol-containing biodiesel at different temperatures (glycerol initial concentration in biodiesel = 0.22 wt%, methanol content ~ 0.7 wt%, adsorbent concentration= 2.5 wt%).

Interestingly, these two adsorbents showed completely different behavior toward FAMEs, as revealed in Figure 4.13. A very low amount of FAMEs was taken-up upon heating the core@shell material, whereas glycerol adsorption was significantly improved. It is believed that free-glycerol in higher concentrations occupied the majority of the adsorption sites at the early stages of the process. This left no room for bulky FAME molecules to diffuse through the microporous silicalite-1 barrier. In contrast, adsorption of FAMEs by silica gel significantly increased. As previously mentioned, methanol at 25 °C was adsorbed in large quantity on the silica surface along with glycerol. Upon methanol evaporation at 100 °C, this portion of the silica gel surface was available for bulkier molecules. As the large pore size of silica gel does not impose any diffusion restriction, the FAME molecules can freely

penetrate through the pores along with glycerol. However, uptake of FAMEs from methanol-containing biodiesel was still lower than that from methanol-free biodiesel, and this is due to the difference in the initial glycerol concentration.

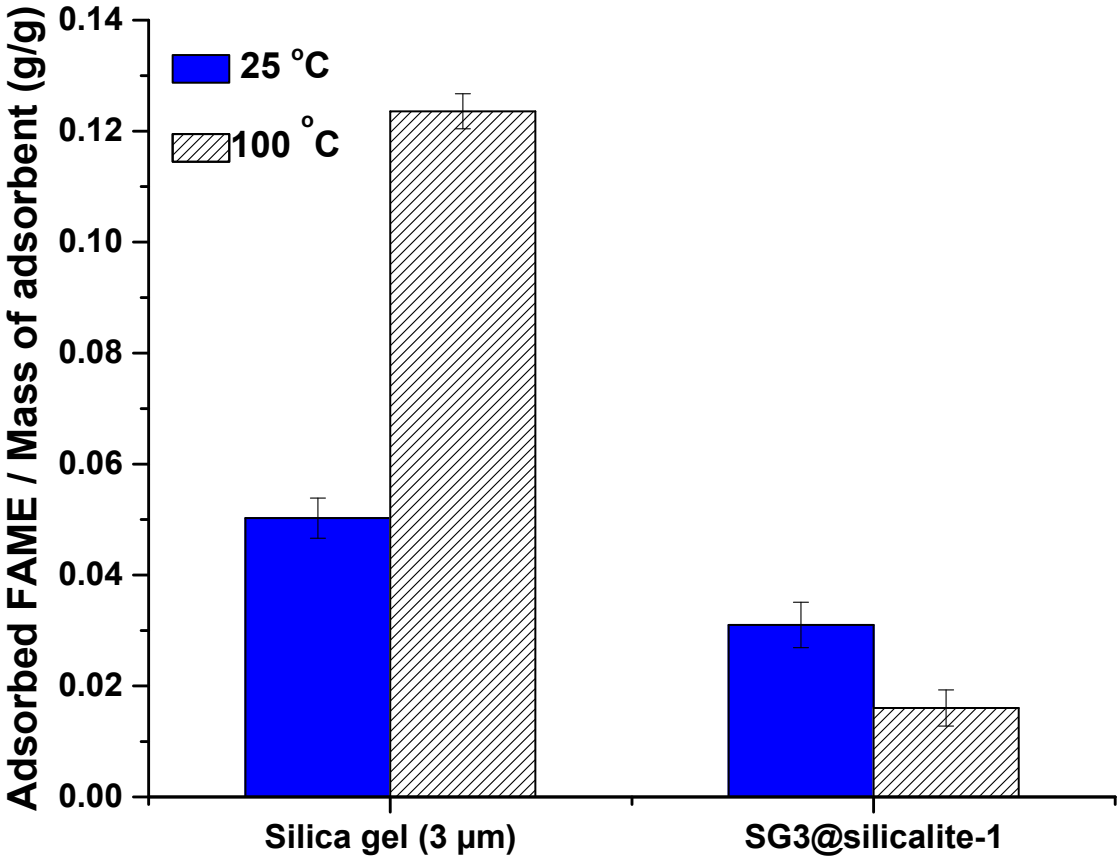

Figure 4.13- Uptake of FAMEs from methanol-containing biodiesel at different temperatures (glycerol initial concentration in biodiesel = 0.22 wt%, methanol content ~ 0.7 wt%, adsorbent concentration= 2.5 wt%).

Considering the great importance of adsorbent reusability, it is believed that the spent adsorbent could be easily restored by thermal treatment at moderate temperatures. Thermogravimetric tests of the spent adsorbents (Figure 4.7) indicated that decomposition/desorption of all adsorbed species from the core@shell sorbent was complete at temperatures well-below 550 °C, that is, the final calcination temperature used for sample preparation. Moreover, multiple eluting steps with solvents such as methanol proved to be an effective alternative means for full regeneration of the silica-based

adsorbents used in biodiesel purification [35]. Notably, the presence of the crystalline zeolitic shell significantly improves the mechanical, hydrothermal and chemical stability of the confined core, which promotes feasible regeneration and reuse of the proposed core@shell sorbent [24-26].

4.4 Conclusions

A new adsorbent for the selective removal of free glycerol from crude biodiesel mixtures was introduced; it consists of a mesoporous silica core and a microporous silicalite-1 shell. More than 97% of shell coverage was achieved by performing two successive secondary growth steps without any damage to the mesopore silica core. By using core particles with different sizes and pore textures, parameters such as shell thickness and the micropore-to-mesopore volume ratio could be adjusted. Glycerol adsorption tests revealed that, in addition to a high surface area and a large pore volume, effective adsorbents should also possess a highly size-selective pore entrance so as to maintain a larger number of adsorption sites for small molecules such as glycerol and methanol. Conventional adsorbents, for example, mesoporous silica gel, showed a high uptake of fatty acid methyl esters along with glycerol adsorption, which resulted in poorer purification yield. The synthesized core@shell composite adsorbent was proven to be a suitable alternative to address the current problems of the existing sorbents in terms of glycerol removal and purification yield. A minimized effective adsorption length resulting from shortened micropores on the shell side, possession of the sieving ability of the parent zeolite, and the core mesoporosity result in new materials with the extra ability to capture glycerol from crude biodiesel more selectively.

4.5 Acknowledgements

The authors acknowledge the financial support from the National Science and Engineering Research Council (Canada) and the Fonds québécois de la recherche sur la nature et les technologies (FRQNT).

4.6 Supporting Information

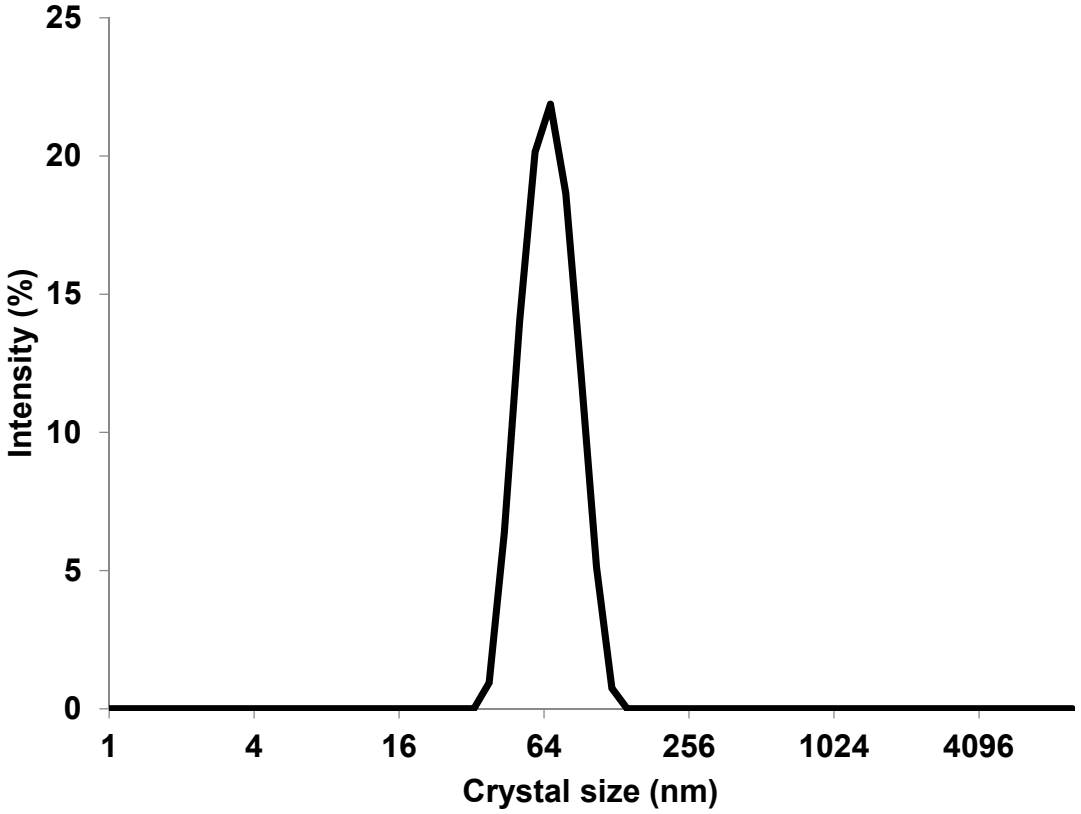

Figure S 4.1- Silicalite-1 nanocrystal size distribution by intensity (dynamic light scattering (DLS) measurements were performed using a Malvern Zetasizer Nano ZS particle analyzer (equilibration time set to 2 min; measurements repeated 3 times; only data which passed quality criteria accepted as valid results)).

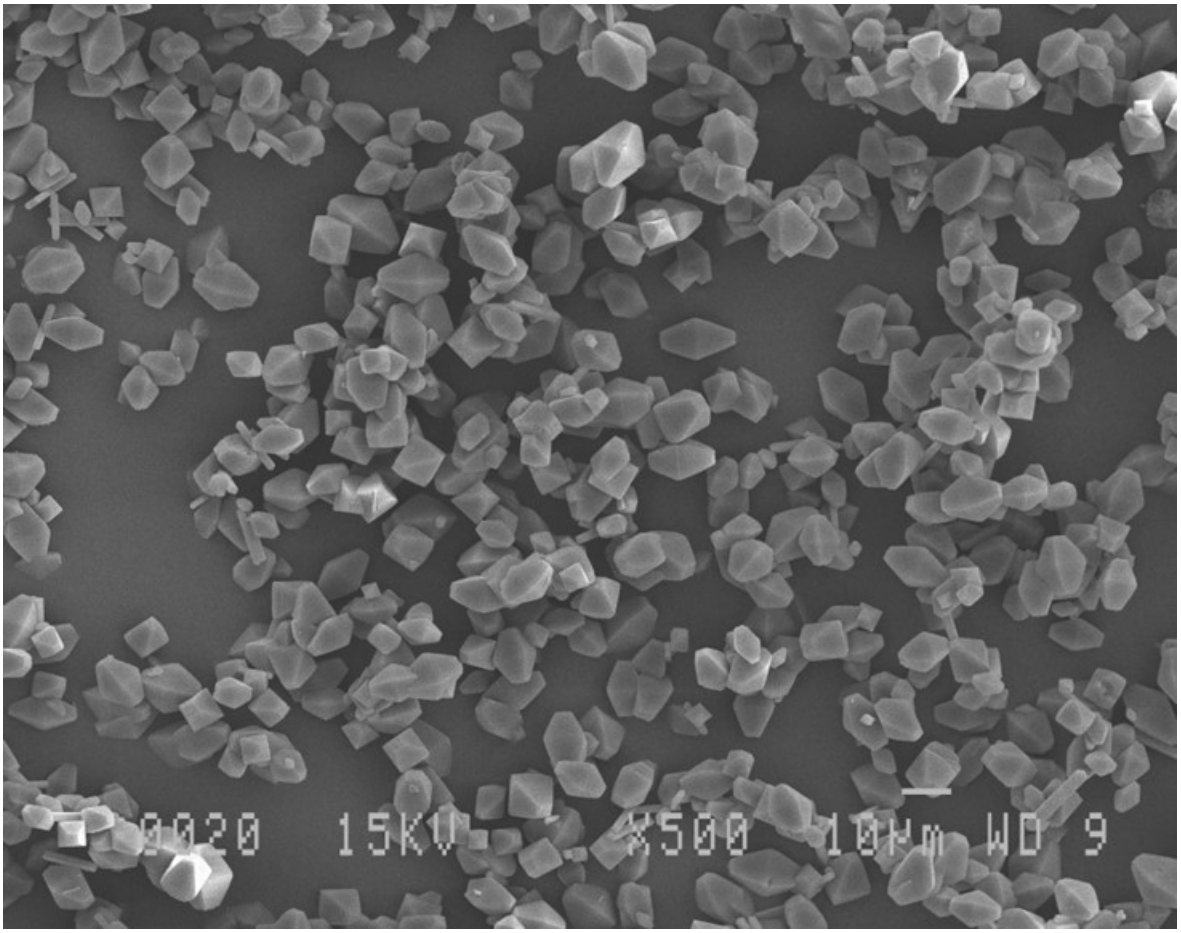

Figure S 4.2- SEM image of Si-BEA microcrystals (scale bar= 10 μm)

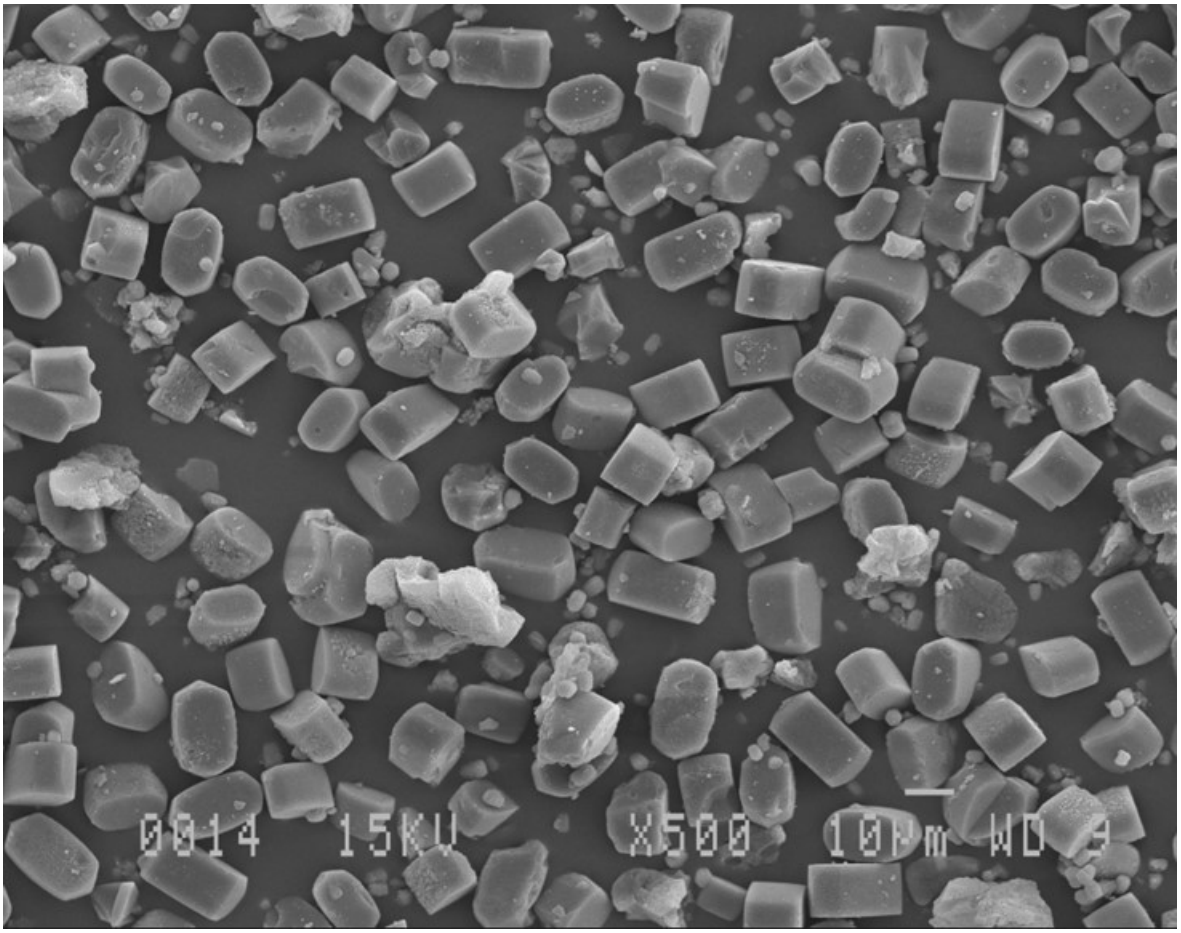

Figure S 4.3- SEM image of Al-ZSM-5(H) microcrystals (scale bar= 10 µm)

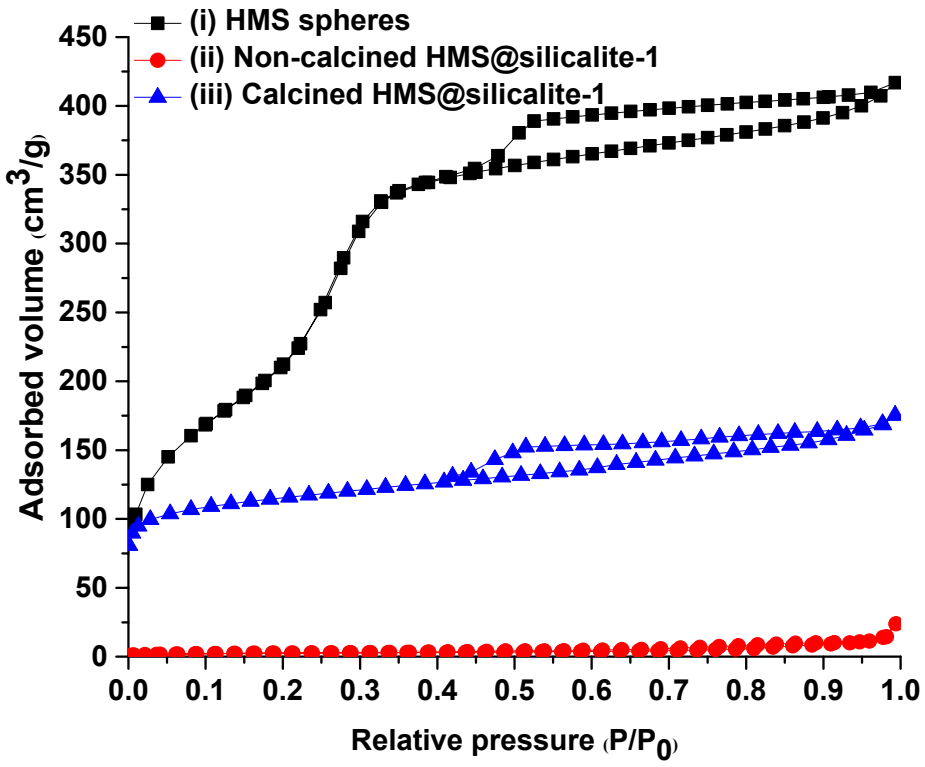

Figure S 4.4- Nitrogen adsorption/desorption isotherms measured at -196 °C of (i) HMS spheres, (ii) core@shell before calcination, and (iii) core@shell with a calcined shell

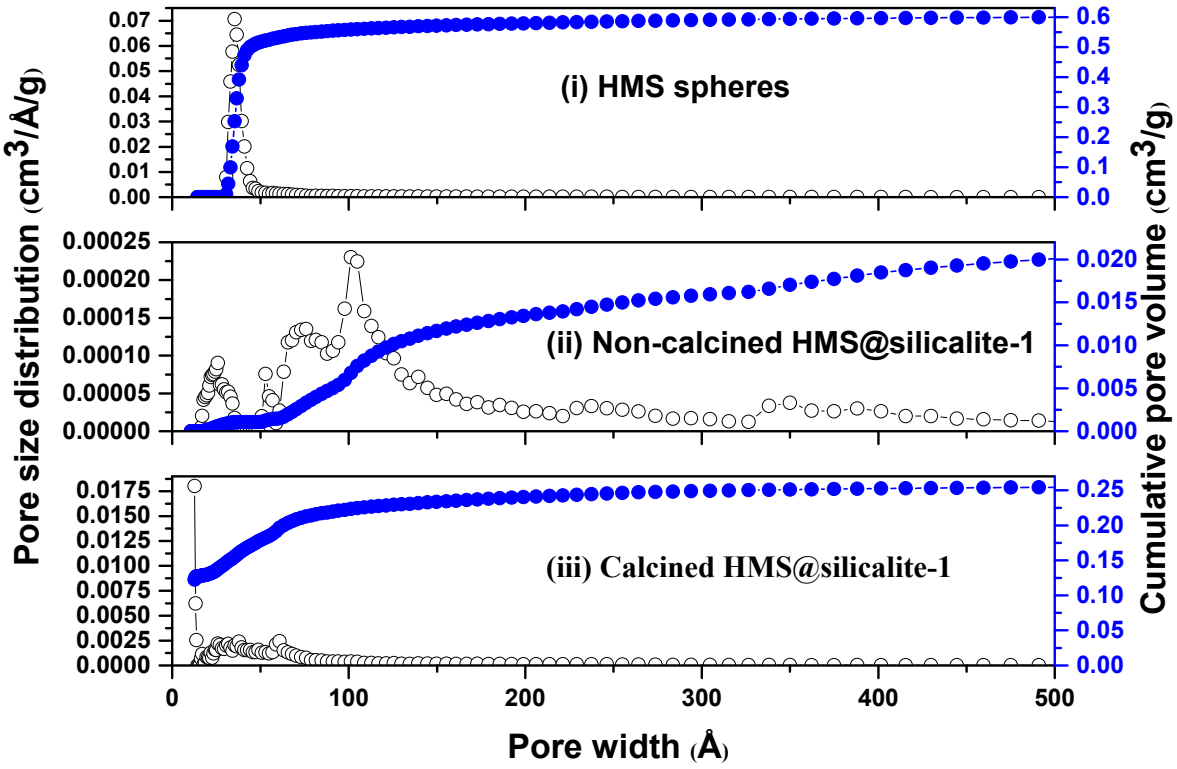

Figure S 4.5- The corresponding NLDFT pore size distributions and cumulative pore volumes of (i) HMS spheres, (ii) noncalcined HMS@silicalite-1, and (iii) calcined HMS@silicalite-1, calculated from the adsorption branch of the isotherm by using the NLDFT method.

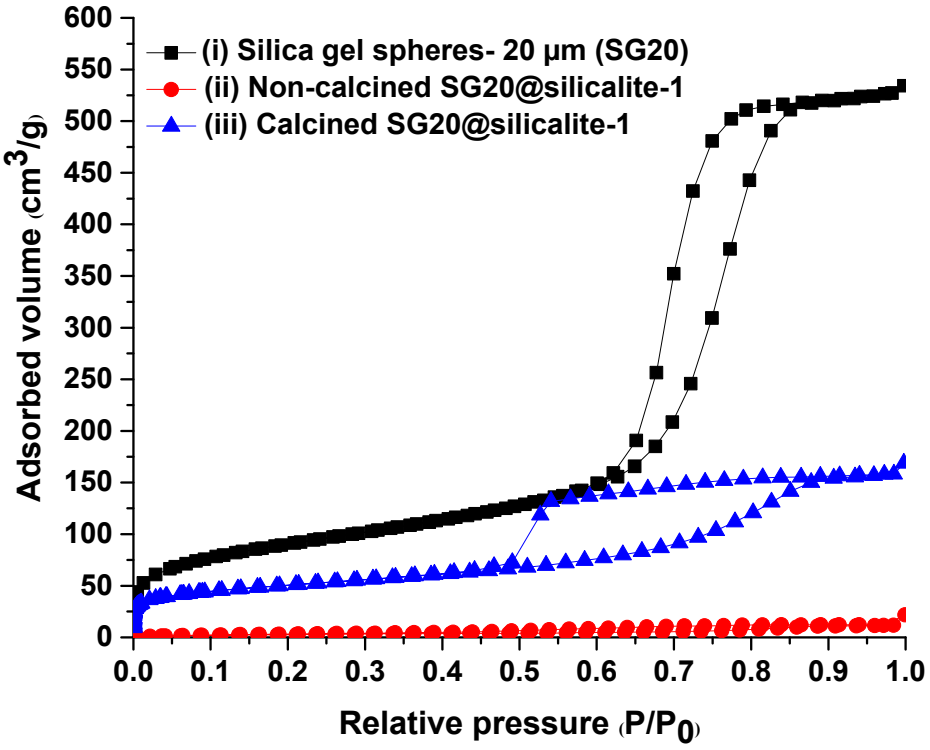

Figure S 4.6- Nitrogen adsorption/desorption isotherms measured at -196 °C of (i) silica gel-20µm, (ii) core@shell before calcination, and (iii) core@shell with a calcined shell.

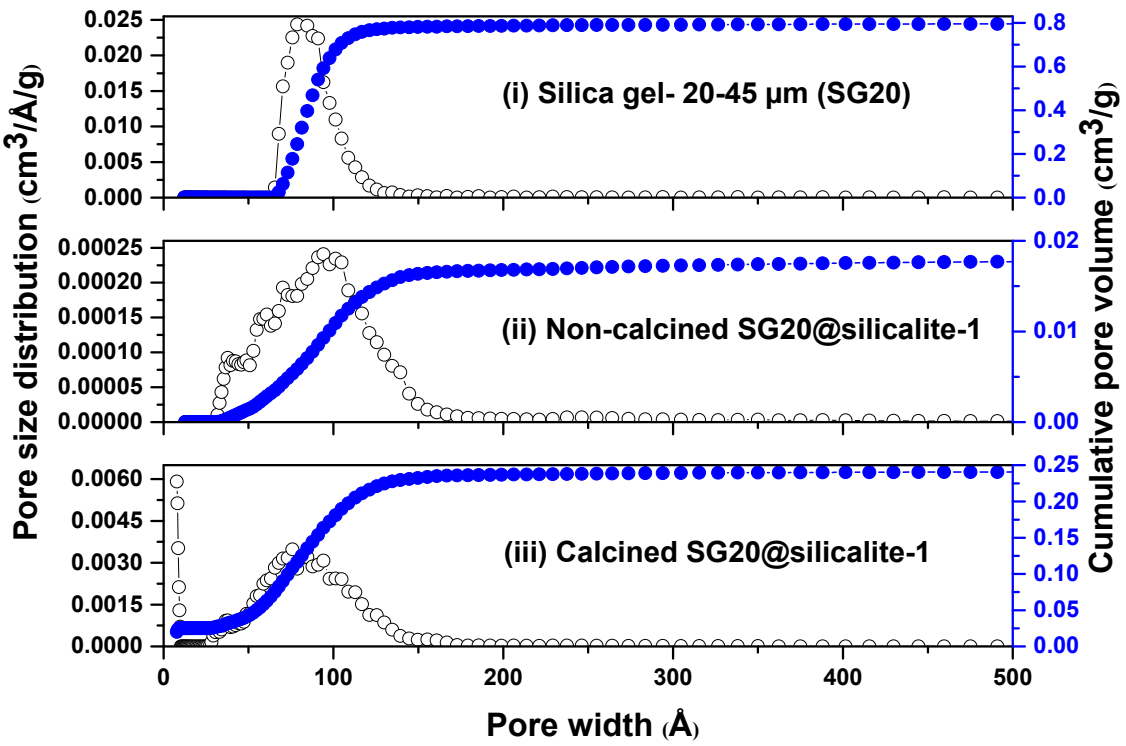

Figure S 4.7- The corresponding NLDFT pore size distributions and cumulative pore volumes of (i) Silica gel-20 µm (SG20), (ii) noncalcined SG20@silicalite-1, and (iii) calcined SG20@silicalite-1, calculated from the adsorption branch of the isotherm by using the NLDFT method.

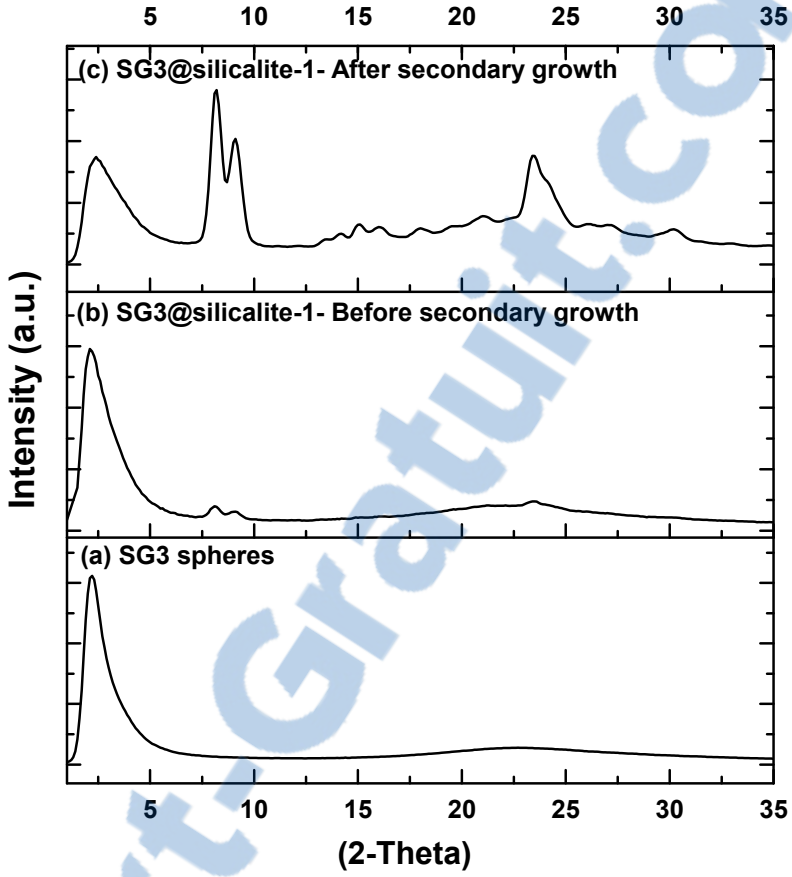

Figure S 4.8- Wide-angle powder XRD patterns for (a) bare SG3, (b) coated SG3 before hydrothermal treatment, and (c) core@shell particles after secondary growth.

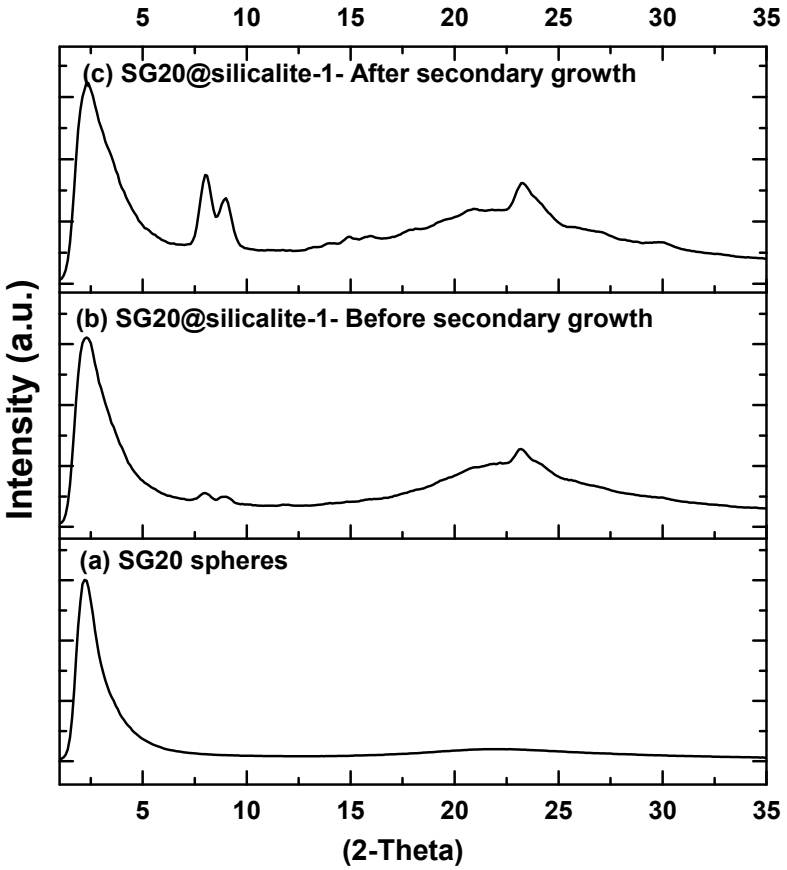

Figure S 4.9- Wide-angle powder XRD patterns for (a) bare SG20, (b) coated SG20 before hydrothermal treatment, and (c) core@shell particles after secondary growth.

4.7 References

[1] R. Ghosh Chaudhuri, S. Paria, *Chem. Rev.* **2011**, *112*, 2373-2433.
[2] H. Wang, L. Chen, Y. Feng, H. Chen, *Acc. Chem. Res.* **2013**, *46*, 1636-1646.
[3] V. Valtchev, *Chem. Mater.* **2002**, *14*, 4371-4377.
[4] V. Valtchev, *Chem. Mater.* **2002**, *14*, 956-958.
[5] W. Yang, X. Wang, Y. Tang, Y. Wang, C. Ke, S. Fu, *J. Macromol. Sci., Part A: Pure Appl. Chem.* **2002**, *39*, 509-526.
[6] X. D. Wang, W. L. Yang, Y. Tang, Y. J. Wang, S. K. Fu, Z. Gao, *Chem. Commun.* **2000**, 2161-2162.
[7] A. Dong, Y. Wang, D. Wang, W. Yang, Y. Zhang, N. Ren, Z. Gao, Y. Tang, *Microporous Mesoporous Mater.* **2003**, *64*, 69-81.
[8] A. Dong, N. Ren, W. Yang, Y. Wang, Y. Zhang, D. Wang, J. Hu, Z. Gao, Y. Tang, *Adv. Funct. Mater.* **2003**, *13*, 943-948.
[9] R. Kanthasamy, K. Barquist, S. C. Larsen, *Microporous Mesoporous Mater.* **2008**, *113*, 554-561.
[10] W. Song, R. Kanthasamy, V. H. Grassian, S. C. Larsen, *Chem. Commun.* **2004**, 1920-1921.
[11] J. C. Groen, T. Bach, U. Ziese, A. M. Paulaime-van Donk, K. P. de Jong, J. A. Moulijn, J. Pérez-Ramírez, *J. Am. Chem. Soc.* **2005**, *127*, 10792-10793.
[12] J. C. Groen, J. C. Jansen, J. A. Moulijn, J. Pérez-Ramírez, *J. Phys. Chem. B* **2004**, *108*, 13062-13065.
[13] Y. Deng, C. Deng, D. Qi, C. Liu, J. Liu, X. Zhang, D. Zhao, *Adv. Mater.* **2009**, *21*, 1377-1382.
[14] J. Zheng, Q. Zeng, J. Ma, X. Zhang, W. Sun, R. Li, *Chem. Lett.* **2010**, *39*, 330-331.
[15] J. Zheng, Q. Zeng, Y. Zhang, Y. Wang, J. Ma, X. Zhang, W. Sun, R. Li, *Chem. Mater.* **2010**, *22*, 6065-6074.
[16] V. Valtchev, S. Mintova, *Microporous Mesoporous Mater.* **2001**, *43*, 41-49.
[17] Y. Bouizi, G. Majano, S. Mintova, V. Valtchev, *J. Phys. Chem. C* **2007**, *111*, 4535-4542.
[18] Y. Bouizi, I. Diaz, L. Rouleau, V. Valtchev, *Adv. Funct. Mater.* **2005**, *15*, 1955-1960.
[19] Y. Bouizi, L. Rouleau, V. P. Valtchev, *Chem. Mater.* **2006**, *18*, 4959-4966.
[20] F. Caruso, R. A. Caruso, H. Möhwald, *Science* **1998**, *282*, 1111-1114.
[21] J. Zhang, T. Zhang, X. Zhang, W. Liu, H. Liu, J. Qiu, K. L. Yeung, *Catal. Today* **2014**, *236*, 34-40.
[22] Y. Yoneyama, X. San, T. Iwai, N. Tsubaki, *Energy Fuels* **2008**, *22*, 2873-2876.
[23] N. Jiang, G. Yang, X. Zhang, L. Wang, C. Shi, N. Tsubaki, *Catal. Commun.* **2011**, *12*, 951-954.
[24] X. Wang, Y. Cui, Y. Wang, X. Song, J. Yu, *Inorg. Chem.* **2013**, *52*, 10708-10710.
[25] J. Wang, D. M. Do, G. K. Chuah, S. Jaenicke, *ChemCatChem* **2013**, *5*, 247-254.
[26] E. A. Khan, A. Rajendran, Z. Lai, *Ind. Eng. Chem. Res.* **2010**, *49*, 12423-12428.
[27] C. Casado, J. Bosque, N. Navascués, C. Téllez, J. Coronas, *Microporous Mesoporous Mater.* **2009**, *120*, 69-75.
[28] E. A. Khan, A. Rajendran, Z. Lai, *Chem. Eng. Res. Bull.* **2013**, *16*, 1-15.
[29] G. D. Pirngruber, C. Laroche, M. Maricar-Pichon, L. Rouleau, Y. Bouizi, V. Valtchev, *Microporous Mesoporous Mater.* **2013**, *169*, 212–217.

[30] A. Carrero, Á. Pérez, in *Advances in Biodiesel Production: Processes and Technologies* (Eds.: R. Luque, J. A. Melero), Woodhead Publishing Series in Energy, Cambridge, UK, **2012**, pp. 91-130.
[31] I. J. Stojković, O. S. Stamenković, D. S. Povrenović, V. B. Veljković, *Renew. Sustainable Energy Rev.* **2014**, *32*, 1-15.
[32] M. Berrios, R. L. Skelton, *Chem. Eng. J.* **2008**, *144*, 459-465.
[33] S. L. Dmytryshyn, A. K. Dalai, S. T. Chaudhari, H. K. Mishra, M. J. Reaney, *Bioresour. Technol.* **2004**, *92*, 55-64.
[34] V. A. Mazzieri, C. R. Vera, J. C. Yori, *Energy Fuels* **2008**, *22*, 4281-4284.
[35] J. C. Yori, S. A. D'Ippolito, C. L. Pieck, C. R. Vera, *Energy Fuels* **2006**, *21*, 347-353.
[36] S. Özgül-Yücel, S. Türkay, *J. Am. Oil Chem. Soc.* **2003**, *80*, 373-376.
[37] Z. J. Predojević, *Fuel* **2008**, *87*, 3522-3528.
[38] A. L. M. T. Pighinelli, R. A. Ferrari, A. M. R. O. Miguelb, K. J. Parka, *Grasas Aceites* **2011**, *62*, 171-180.
[39] K. Mis Solval, S. Sathivel, *J. Am. Oil Chem. Soc.* **2012**, *89*, 1713-1721.
[40] E. P. Ng, L. Delmotte, S. Mintova, *ChemSusChem.* **2009**, *2*, 255-260.
[41] G. Majano, E. P. Ng, L. Lakiss, S. Mintova, *Green Chem.* **2011**, *13*, 2435-2440.
[42] M. J. Alves, S. M. Nascimento, I. G. Pereira, M. I. Martins, V. L. Cardoso, M. Reis, *Renew. Energy* **2013**, *58*, 15-20.
[43] B. J. Schoeman, K. Higberg, J. Sterte, *Nanostruct. Mater.* **1999**, *12*, 49-54.
[44] M. Grün, G. Büchel, D. Kumar, K. Schumacher, B. Bidlingmaier, K. K. Unger, **2000**, *128*, 155-165.
[45] H. Robson, *Verified Synthesis of Zeolitic Materials*, (Ed.: H. Robson), Elsevier, Amsterdam, Netherlands **2001**.
[46] BIPM, IEC, IFCC, ILAC, IUPAC, IUPAP and OIML, Evaluation of measurement data-guide to the expression of uncertainty in measurement, GUM 1995 with minor corrections Joint Committee for Guides in Metrology (JCGM) 100 **2008**
[47] E. A. Khan, E. Hu, Z. Lai, *Microporous Mesoporous Mater.* **2009**, *118*, 210-217.
[48] M. Thommes, *Chem. Ing. Tech.* **2010**, *82*, 1059-1073.
[49] C. J. Rasmussen, A. Vishnyakov, M. Thommes, B. M. Smarsly, F. Kleitz, A. V. Neimark, *Langmuir* **2010**, *26*, 10147-10157.
[50] http://www.iza-structure.org/databases/, **2014**.
[51] M. B. Carlos Vera, J. Yori, G. Torres, D. Manuale, S. Canavese, J. Sepúlveda in Biodiesel: Feedstocks and Processing Technologies, (Ed.: M. Stoytcheva), InTech, Rijeka, Croatia, **2011**, pp. 427-458.
[52] D. P. Serrano, R. Van Grieken, P. Sánchez, R. Sanz, L. Rodríguez, *Microporous Mesoporous Mater.* **2001**, *46*, 35-46.
[53] P. Chand, C. V. Reddy, J. G. Verkade, T. Wang, D. Grewell, *Energy Fuels* **2009**, *23*, 989-992.
[54] G. Üstün, *J. Am. Oil Chem. Soc.* **1996**, *73*, 203-210.
[55] J. Xiao, J. Wei, *Chem. Eng. Sci.* **1992**, *47*, 1143-1159.
[56] S. Kulprathipanja, R. B. James, in *Zeolites in Industrial Separation and Catalysis*, (Ed.: S. Kulprathipanja), Wiley-VCH Verlag GmbH & Co. KGaA, Weinheim, Germany, **2010**, pp. 173-202.
[57] I. N. Lykakis, C. Ferreri, S. A. Grabovskiy, C. Chatgilialoglu, *Tetrahedron* **2010**, *66*, 2203-2209.
[58] D. L. Manuale, E. Greco, A. Clementz, G. C. Torres, C. R. Vera, J. C. Yori, *Chem. Eng. J.* **2014**, *256,* 372-379.

[59] D. L. Manuale, V. M. Mazzieri, G. Torres, C. R. Vera, J. C. Yori, *Fuel* **2011**, *90*, 1188-1196.

Chapter 5- General Conclusions and Perspectives

Making more efficient zeolitic materials demands proper manipulation of their intrinsic properties such as shape selectivity, acidity, pore size, etc. Depending on the framework type of the zeolite, the road toward bringing such efficient materials into reality might be obstructed by many issues and challenges. The initial objective of this study was to address some of these matters (i.e., lack of proper control over crystal size and morphology), which hindered improving the performance of a promising zeolite, i.e., ZSM-12. Two commercially available organic templates, supplying tetraethylammonium (TEA^+) and methyltriethylammonium ($MTEA^+$) cations in the synthesis mixture, were used for synthesizing ZSM-12 zeolite using the conventional hydrothermal treatment method. In the first part, the crystallization behavior of ZSM-12 within a gel containing TEAOH, the most common organic template used for this framework type, and organic chemical sources of Si and Al, i.e., TEOS and $Al(O\text{-}i\text{-}Pr)_3$, were investigated. The results showed that using these chemical sources mainly led to severe gelation of the synthesis mixture and the formation of amorphous materials rather than crystalline ZSM-12. Higher initial water content was found to be necessary to prepare an initial water-clear solution. It was also learned that the water and sodium hydroxide contents of the gel had to be carefully adjusted in order to reach pure-phase ZSM-12 crystals. Although at the end of the crystallization period, a highly pure-phase ZSM-12 was produced, the proposed synthesis condition could not provide sufficient control over the nucleation and crystal growth processes toward reaching single crystals with smaller sizes, preferably nanocrystals.

Repeating similar synthesis conditions, i.e., using TEOS and $Al(O\text{-}i\text{-}Pr)_3$, except for the use of MTEAOH as the organic template, pure ZSM-12 zeolite could not be formed. Using colloidal silica source, however, led to the formation of mono-sized ZSM-12 single crystals. When using MTEAOH organic template, hydroxide ion and Na^+ contents and the type of Al source were found to be playing major roles toward nucleation and growth of ZSM-12 crystals. Although the ultimate goal of the current study, i.e., the formation of nano-ZSM-12 crystals, has not been fully actualized by using MTEAOH organic template, the proposed synthesis has provided some advantages over TEAOH-based method, such as faster crystallization, high purity, controlled size and morphology and formation of pure ZSM-12 single crystals over a wide range of Si/Al ratio.

Aiming to synthesize zeolitic materials with improved properties and diverse capabilities, mesoporous silica@zeolite core-shell materials were synthesized in the next part of the study. In general, mesoporous silica spheres have numerous interesting properties such as high specific surface area and pore volume, tunable particle and pore sizes, etc., and more importantly, the possibility of making highly efficient hybrid materials, simply by hosting a large number of functional groups very effectively within their highly accessible pore system. In this regard, among all possible candidates, mesoporous silica microspheres, in their pure form, were initially chosen to serve as core compartment to generate a zeolitic core@shell composite. Various types of mesoporous silica spheres with different sizes (commercial silica gel spheres: 20-45 μm and 3 μm and HMS spheres: ~1.5 μm) were used. A polycrystalline silicalite-1 shell was formed by first covering the external surface of the modified core templates with discrete silicalite-1 nanocrystals via electrostatic attractions, followed by multiple short hydrothermal treatments in Si/TPAOH-containing gel to ensure the shell coverage and uniformity. The study showed that modifying the surface of these spheres with a cationic polymer (PDADMAC) provides attractive forces, strong enough to properly fix nanoparticles on the surface of the cores. However, the minimum number of secondary growth steps was governed by the size of the cores, i.e., smaller microspheres (i.e., HMS and SG3) needed at least two times and largest spheres (SG20) four times. The optimum number of secondary growth steps has to be found experimentally since excess treatments can potentially lead to particle aggregation and core dissolution.

After establishing a synthesis procedure for synthesizing pure silica@shell composites, the possibility of generalizing the synthesis technique for metal-containing mesoporous silica@silicalite-1 was investigated. M,SiO_2@silicalite-1 materials with a complete microporous shell can be used as micron-sized membrane reactors for many reactions which seek for protection from harsh reaction conditions, shape selectivity or controlling the overall rate of the reaction by imposing a diffusion barrier, etc. The study showed that simple surface modification using cationic polymers did not provide adequate interactions for the firm attachment of the seeds to the core surface. Therefore, an additional external surface functionalization of the spheres with APTES was used. Finally, well-defined M,SiO_2@silicalite-1 core@shell spheres (M: Ti, Co and Mn) were successfully synthesized which can be used in a wide variety of applications, particularly for shape-selective adsorption and catalysis.

In the last part of the study, the performance of these zeolitic core@shell materials was evaluated. As a model application process, the ability of the synthesized core@shell material (pure silica mesoporous core and a microporous silicalite-1 shell) in selective removal of free glycerol from crude biodiesel mixture was assessed. Free glycerol is traditionally removed through extraction with water. Due to numerous problems, caused by this technique, dry washing technique was alternatively introduced in which the contaminants, such as free glycerol, are eliminated, in an eco-friendly manner, by keeping the crude biodiesel in contact with an adsorbent such as silica gel or an ion-exchange resin. Using these traditional adsorbents along with the core@shell ones revealed that although bare silica gel achieved significant glycerol removal, it has also simultaneously captured a large number of the molecules of the desirable product. In contrast, core@shell material consisting of high surface area, high pore volume mesoporous silica spheres covered with a shape-selective zeolite has succeeded to selectively remove small molecules such as glycerol, leading to higher purification yields (Figure 5.1).

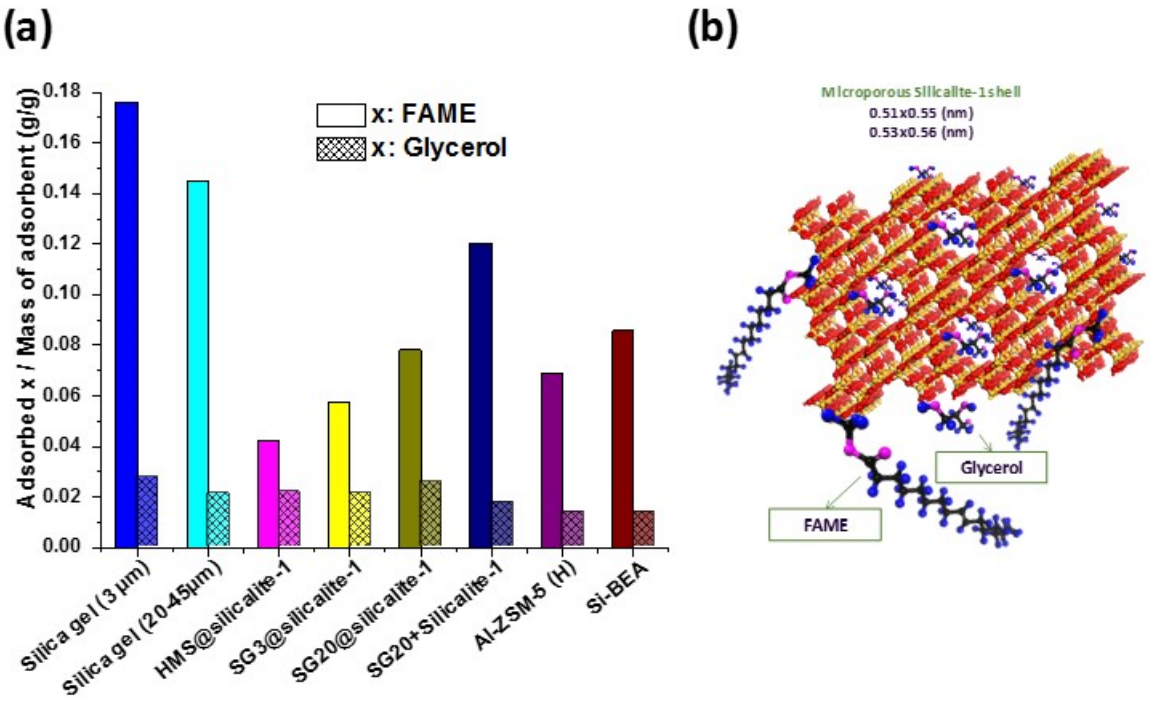

Figure 5.1- (a) Specific uptake of FAME and glycerol at equilibrium for different adsorbents using methanol-free biodiesel at 25 °C (glycerol initial concentration in biodiesel = 0.065 wt%, adsorbent concentration= 2.3 wt%). (b) Schematic representation of selective adsorption of glycerol by diffusing through the microporous silicalite-1 shell.

5.1 Future Work

In Chapter two, we have tried to synthesize ZSM-12 zeolite with controlled size and morphology in a shorter time period than what was previously reported. Despite the improvements made by using non-expensive and commercially-available organic templates, further modifications are highly desirable. Currently, the preparation of nanozeolites is one of the biggest challenges in the field of zeolite synthesis. Several methods were already developed, however, many of them cannot be easily extended to synthesize nanozeolites of different framework types, especially high-silica zeolite ZSM-12. Since ZSM-12 possess a 1D micropore channel system, such an achievement can significantly enhance its performance in many applications. Moreover, it would allow designing highly efficient structured zeolites using ZSM-12 as a building block.

Chapter three reports the synthesis of a microscopic core@shell with an entirely microporous shell. Achieving such a fully microporous shell by using multistep seeded growth technique was realized to be rather cumbersome, even in the case of a widely-studied zeolite such as silicalite-1. In addition to the demanding synthesis procedure, one of the main drawbacks of this technique is the lack of flexibility toward fine adjustment of the final product properties such as shell thickness and micropore orientation. Therefore, developing new easy-to-implement techniques which allow more efficient control over tuning these properties would be highly desirable at this stage. Moreover, the applicability of the new synthesis techniques for the preparation of core@shell materials with other framework types than silicalite-1 should also be taken into consideration. The new framework types can equip the composite with various functionalities such as acidity or ion-exchange possibilities, etc., on the shell side. For instance, having a 1D zeolitic shell, e.g., ZSM-12 shell, with radially-oriented micropores can possibly be one of the most desirable materials for many applications which demand efficient storage, encapsulation, controlled release, etc.

As shown in Chapter three, a final calcination step is mandatory to remove the organic templates from the micropores of the zeolitic shell. Such high-temperature treatment prohibits the possibility of integrating organic functional groups, grafted on the internal mesopore surface of the core. Eliminating the usage of such organic materials by developing an organic template-free secondary growth technique or using recyclable SDAs, would enable the synthesis of a core@shell material with much more diverse functionalities. This could also facilitate the use of cores with organic nature, such as polymers or carbons.

Novel zeolitic frameworks, composites and structures have growingly been the subject of numerous research studies with the end goal of developing more robust and efficient materials, rationally designed for catalyzing various reactions. Here, the performance of synthesized materials including ZSM-12 and metal-containing core@shell particles remains to be explored, especially for the processes and reactions which are looking for a finely-controlled rate of reaction, shape-selectivity, bi-functionality, etc.

Appendix - Hexagonal Mesoporous Silica Spheres (HMS)

Ordered mesoporous silica materials, their discovery and diverse types were briefly discussed in Chapter one where relevant references were also mentioned. The MCM-41 as the first member of OMM family with hexagonally arranged uniform mesopores was successfully synthesized using an ionic surfactant as the template. Shortly after, researchers in Prof. Pinnavaia's group [1-3] introduced new classes of mesoporous silica materials (HMS and MSU) using neutral and non-ionic organic templates, e.g., long chain n-alkylamines and polymeric surfactants. Compared to M41S family, these materials mainly showed disordered pore structures.

HMS mesoporous silica with a 3D disordered wormhole-like structure which is used in our study was first synthesized under neutral conditions using n-alkylamines templates. This condition promoted the formation of the mesophase via hydrogen-bonding interactions and self-assembly between the neutral primary amine micelles (S^0) and neutral inorganic silicate precursors (I^0), the so-called S^0I^0 route (Figure App 1) [1, 3]. A detailed description of various cooperative inorganic–organic interactions within different synthesis media can be found elsewhere [4]. Although rapid condensation of silicate species in neutral synthesis environment (pH ~ 7) led to a disordered porous structure, the final product benefited from a highly uniform pore size distribution, similar to what obtained for MCM-41 types. In addition, the HMS possess thicker walls than MCM-41 which improves thermal and hydrothermal stability [1]. The textural properties including surface area, pore volume and size can be tuned using templates with different alkyl chain length [3]. Owing to weak organic-inorganic assembly forces, in contrast to strong electrostatic interactions provided by ionic templates used in M41S synthesis, the template can be easily extracted/washed out from the porous network with washing with solvents [5]. This facilitates the recycling of the organic template through a simple and an environmentally benign route.

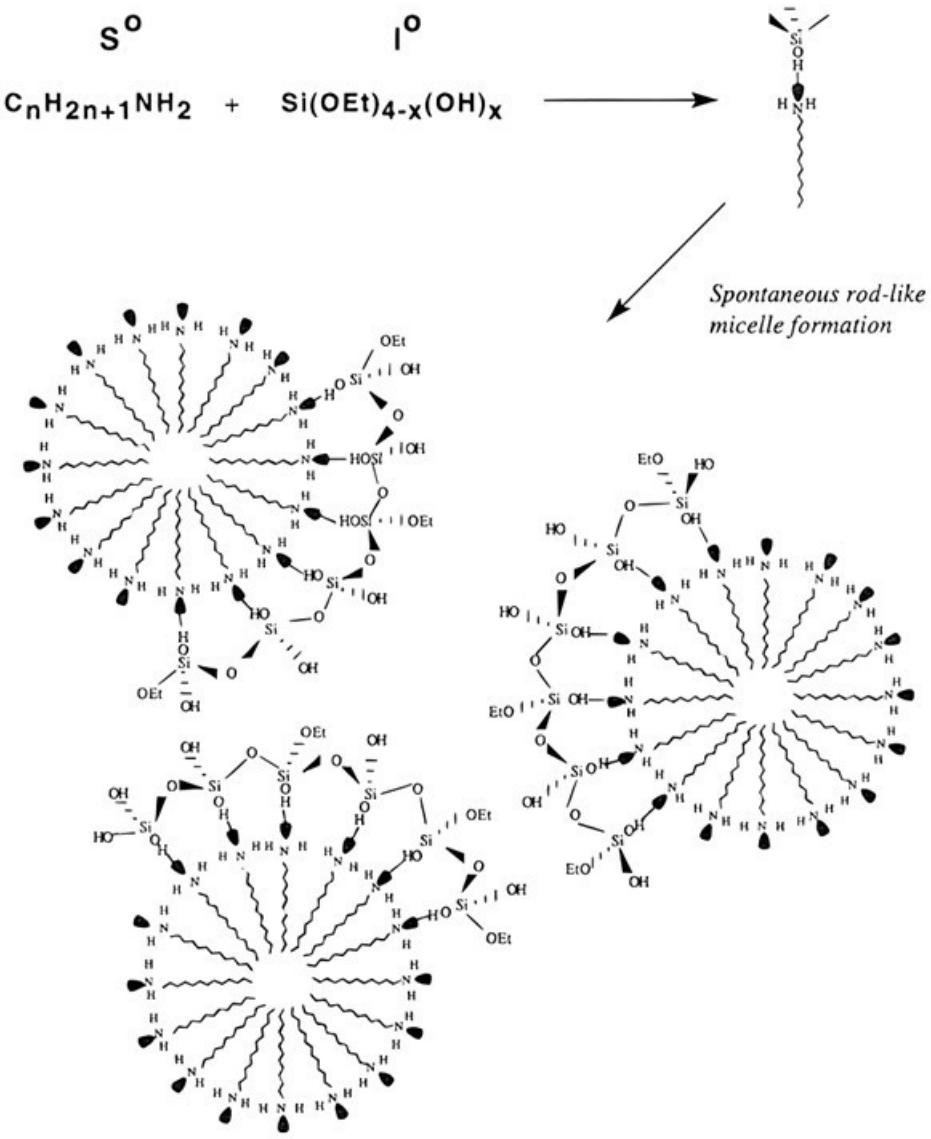

Figure App 1- Schematic representation of the S^0I^0 templating mechanism of formation of HMS (Reprinted with permission from [3]. Copyright 1996 ACS.).

Morphology Control

Mesoporous materials with defined morphologies, especially the spherical ones, are of particular interest and importance in many applications. The control of size and morphology of HMS particles toward producing microspheres were thoroughly studied by Grün *et al.* [6]. The original synthesis technique of HMS material was modified using the Stöber process

which is widely-used for synthesizing non-porous silica micro- and sub-microspheres [7]. The type of the co-solvent and the presence of ammonia were the main differences with the original synthesis method. Co-solvent makes the synthesis mixture homogeneous while ammonia act as a morphological catalyst. Ethanol was used as the co-solvent in the original synthesis whereas 2-propanol was used in the modified synthesis technique.

Optimized Synthesis Method

Mono-dispersed HMS spheres were synthesized according to methods in the literature [6, 8]. In a typical producer, 2.08 g of hexadecylamine (technical grade, 90%-Sigma-Aldrich) as mesoporogen, 180 ml of distilled water and 200 ml of 2-propanol (Fisher scientific) as solvents were mixed in a 1L polypropylene beaker. The mixture was magnetically stirred at constant temperature 35 °C in an incubator until reaching a water-clear solution. Then, the temperature was stabilized at 25 °C, followed by addition of 3.2 ml of NH_3-H_2O (28%). 12 ml of TEOS as silica source was added in one-shot and the final mixture stirred for another 1 min before aging overnight at 25 °C. The product was recovered by filtration and washing with water and ethanol. For removing the organic template from the pores, the as-synthesized material was heated in air at 550 °C for 6 h.

References

[1] P.T. Tanev, T.J. Pinnavaia, *Science* **1995**, *267*, 865-867.
[2] S.A. Bagshaw, E. Prouzet, T.J. Pinnavaia, *Science* **1995**, *269*, 1242-1244.
[3] P.T. Tanev, T.J. Pinnavaia, *Chem. Mater.* **1996**, *8*, 2068-2079.
[4] F. Kleitz, Ordered Mesoporous Materials, Handbook of Heterogeneous Catalysis, Wiley-VCH Verlag GmbH & Co. KGaA, **2008,** pp. 178-219.
[5] U. Ciesla, F. Schüth, *Microporous Mesoporous Mater.* **1999**, *27*, 131-149.
[6] M. Grün, G. Büchel, D. Kumar, K. Schumacher, B. Bidlingmaier, K.K. Unger, Rational design, tailored synthesis and characterisation of ordered mesoporous silicas in the micron and submicron size range, in: G.K. K.K. Unger, J.P. Baselt (Eds.) Studies in Surface Science and Catalysis, Elsevier, **2000,** pp. 155-165.
[7] W. Stöber, A. Fink, E. Bohn, *J. Colloid Interface Sci.* **1968**, *26*, 62-69.
[8] A. Dong, N. Ren, W. Yang, Y. Wang, Y. Zhang, D. Wang, J. Hu, Z. Gao, Y. Tang, *Adv. Funct. Mater.* **2003**, *13*, 943-948.